DEVELOPMENT AND APPLICATION OF NEW MODEL ALGORITHMS OF THE BIOLOGICAL CARBON PUMP IN THE NORTH ATLANTIC: A STUDY ON PARTICLE EXPORT, SINKING AND DECOMPOSITION

A THESIS SUBMITTED TO
THE GRADUATE SCHOOL OF MARINE SCIENCES
OF
MIDDLE EAST TECHNICAL UNIVERSITY

VELİ ÇAĞLAR YUMRUKTEPE

IN PARTIAL FULFILLMENT OF THE REQUIREMENTS
FOR
THE DEGREE OF DOCTOR OF PHILOSOPHY
IN
OCEANOGRAPHY

DECEMBER 2016

Approval of the thesis:

DEVELOPMENT AND APPLICATION OF NEW MODEL ALGORITHMS OF THE BIOLOGICAL CARBON PUMP IN THE NORTH ATLANTIC: A STUDY ON PARTICLE EXPORT, SINKING AND DECOMPOSITION

submitted by **VELİ ÇAĞLAR YUMRUKTEPE** in partial fulfillment of the requirements for the degree of **Doctor of Philosophy in Oceanography Department, Middle East Technical University** by,

Assoc. Prof. Dr. Barış Salihoğlu _____

Director, Graduate School of **Marine Sciences**

Prof. Dr. Süleyman Tuğrul _____

Head of Department, **Oceanography**

Assoc. Prof. Dr. Barış Salihoğlu _____

Supervisor, **Oceanography Department, METU**

Examining Committee Members:

Prof. Dr. Zahit Uysal _____

Marine Biology and Fisheries Department, METU

Assoc. Prof. Dr. Barış Salihoğlu _____

Oceanography Department, METU

Assoc. Prof. Dr. Bettina A. Fach Salihoğlu _____

Oceanography Department, METU

Prof. Dr. Susanne Neuer _____

School of Life Sciences, Arizona State University, USA

Dr. Adrian P. Martin _____

National Oceanography Center, UK

Date: _____

I hereby declare that all information in this document has been obtained and presented in accordance with academic rules and ethical conduct. I also declare that, as required by these rules and conduct, I have fully cited and referenced all material and results that are not original to this work.

Name, Last Name : VELİ ÇAĞLAR YUMRUKTEPE

Signature :

ABSTRACT

DEVELOPMENT AND APPLICATION OF NEW MODEL ALGORITHMS OF THE BIOLOGICAL CARBON PUMP IN THE NORTH ATLANTIC: A STUDY ON PARTICLE EXPORT, SINKING AND DECOMPOSITION

VELİ ÇAĞLAR YUMRUKTEPE

Ph. D., Department of Oceanography

Supervisor : Assoc. Prof. Dr. Barış Salihoğlu

December 2016, 151 pages

A 1D lower trophic level pelagic ecosystem model, NAGEM, was developed to investigate processes moderating productivity, algal community structure and resulting carbon export at BATS, ESTOC and PAP time-series stations in the North Atlantic. At each site, the relative effects of community structure, sinking rates, physical and biological aggregation, mineral ballasting and diel vertical migration on carbon export were explored. Simulated carbon export rates were evaluated using in situ sediment trap data collected at the 3 time series stations and model algorithms were modified in order to best represent observed differences in export rates between stations. The observed 3-4 fold difference in carbon export between BATS and ESTOC is partially explained by differences in hydrographic conditions. The deeper and more prolonged vertical mixing at BATS results in efficient particle transport, whereas slower particle sinking at ESTOC results in a relatively higher

remineralization pressure. This work highlighted the benefits of adequately describing plankton community structure in models to define the magnitude and structure of particle export and nutrient decoupling. Modelled carbon export was highly sensitive to changes in particle sinking rates, although these changes did not introduce variability in export. Temporal and spatial variability was achieved when specific sinking rates were assigned to detritus from each community. This resulted in relatively higher export efficiency at the PAP site due to the presence of larger plankton. Further improvements to model performance were achieved through adjusting aggregation, mineral ballasting, community specific remineralization rates and diel vertical migration of zooplankton.

Keywords: Carbon export; BATS; ESTOC; PAP; model algorithms; detritus feeding; bacterial remineralization; subtropical gyre; the North Atlantic

ÖZ

BİYOLOJİK KARBON POMPASI MODEL ALGORİTMALARININ GELİŞTİRİLMESİ VE KUZEY ATLANTİK BASENİNE UYARLANMASI: PARÇACIK GÖNDERİMİ, ÇÖKMESİ VE AYRIŞMASI ÜZERİNE

VELİ ÇAĞLAR YUMRUKTEPE

Doktora, Oşinografi Anabilim Dalı

Tez Yöneticisi : Doç. Dr. Barış Salihoğlu

Aralık 2016, 151 sayfa

Kuzey Atlantik'te bulunan BATS, ESTOC ve PAP zaman serisi istasyonlarındaki üretimi, tür dağılımını ve gerçekleşen karbon dikey gönderimlerini yöneten prosesleri incelemek amacıyla NAGEM 1D alt trofik pelajik ekosistem modeli geliştirilmiştir. Her bir istasyon için tür dağılımının, parçacık çökme hızlarının, fiziksel ve biyolojik yığışımın, mineral balastın ve günlük dikey göçün karbon gönderimine etkileri araştırılmıştır. Simüle edilen karbon gönderimleri, istasyonlarda bulunan veri setleri ile karşılaştırılmış, ve model algoritmaları istasyonlardaki değişkenlikleri temsil edecek şekilde uyarlanmıştır. BATS ve ESTOC istasyonlarındaki 3-4 kat karbon gönderimi farkı, kısmi olarak istasyonlardaki farklı fiziki yapılar ile açıklanabilmektedir. BATS'taki görece daha derin ve uzun süreli dikey karışım verimli gönderime neden olmakta olup, ESTOC'taki yavaş çökelme mekanizmaları parçacıkların daha fazla ayrışma baskısı altında kalmasına neden olmaktadır. Model, tür dağılımının parçacık gönderiminin miktarına ve yapısına, inorganik besin tuzları bağlaşımının kesilmesinin tür dağılımına etkisini

vurgulamıştır. Simüle edilen karbon gönderiminin parçacık hızlarındaki değişimlere çok hassas olduğu belirlenmiş olduğu halde sonuçlarda değişebilirlik düşük seviyelerde kalmıştır. Zamansal değişebilirlik, parçacık çökme hızlarının tür dağılımı etkileşimi ile gerçekleştirilebilmiştir. Tür dağılımı etkileşimleri sayesinde modelde zamansal ve bölgesel değişebilirlik elde edilmiş olup, görece büyük fitoplankton türlerini barındırabilen PAP istasyonunda artan parçacık gönderimine neden olmuştur. Parçacık yığışımı, mineral balast etkisi, tür dağılımı etkileşimi içeren ayrışma mekanizmaları ve günlük dikey göç, modelin gözlemelere daha iyi uymasını sağlamıştır.

Anahtar kelimeler: Karbon gönderimi; BATS; ESTOC; PAP; model algoritmaları; parçacık beslenimi; bacteriyel ayrışma; subtropik döngü; Kuzey Atlantik

.

To Heather, Ela Amelia and my family

ACKNOWLEDGMENTS

I would like to begin by thanking my supervisor Dr. Barış Salihoğlu for his supervision and support through the course of this work. I would also like to express my gratitude to Dr. Sinan Arkın, Dr. Bettina Fach Salihoğlu, Dr. Zahit Uysal, Dr. Susanne Neuer and Dr. Adrian Martin for their guidance in progressing and finalising this thesis work.

I thank Dr. Susanne Neuer in particular for her support in preparation of the papers associated with this thesis work.

I also express my gratitude to Dr. Adrian Martin in particular for his support during my 3 month fellowship in Southampton, UK.

I would like to thank Yasin Tuna for the time he spent in preparation of the hard copy of this thesis.

Many thanks to all my colleagues and friends in IMS. My professional scientific career has evolved to this point during my stay in IMS through their scientific and social contribution to my life.

My family has always supported me in any moment of my life and in any decision I made. I am truly lucky to have them with me.

Finally and most importantly, I cannot express how grateful I am to have Heather with me. She has been my biggest support in every aspect of my life. Now we have Ela Amelia with us and I am very excited for the years to live together.

This work has been part of and scientifically supported by EU FP7 EUROBASIN project.

My doctorate study has been financially supported by TÜBİTAK (Türkiye Bilimsel ve Teknolojik Araştırma Kurumu) (The Scientific and Technological Research Council of Turkey) under the fellowship program towards scientific prior areas, 2211-C.

TABLE OF CONTENTS

LIST OF TABLES

LIST OF FIGURES

LIST OF ABBREVIATIONS

BCP – The Biological Carbon Pump

BATS – Bermuda Atlantic Timeseries Study

ESTOC – European Station for Time series in the Ocean, Canary Islands

PAP – Porcupine Abyssal Plain

DVM – Diel vertical migration

DCM – Deep chlorophyll maxima

EZ – Euphotic zone

MLD – Mixed layer depth

NSTD – Normalized standard deviation

CHAPTER

1. THESIS INTRODUCTION

The principal objective of this thesis work is to explore the dynamics of the biological carbon pump in marine ecosystems, and the possibilities in representing its internal processes in 1D/3D biogeochemical models.

Improved parameterization of carbon sequestration within the ecosystem models is currently one of the major areas in global carbon cycle studies. The necessity of including detailed components of the "biological carbon pump (BCP)" in ecosystem models lies in BCP's importance in regulating the global carbon cycle. Since 1750, which is the beginning of the industrial era, the atmospheric carbon dioxide (CO_2) concentration has increased from 277 parts per million (ppm) (Joos and Spahni, 2008) to 400.72 ppm in April 2015 and to 404.08 ppm in April 2016 (Dlugokencky and Tans, 2016). The ~ 220 ppm increase in CO_2 concentrations occurred in nearly 260 years, which is an increase of an order of magnitude higher compared to any change estimated for the past 22,000 years till the industrial era. With the addition of CH_4 and N_2O to the estimations, the average rate of increase in the radiative forcing of the greenhouse gases that is available for comparison is larger during the industrial era compared to the last 16,000 years. The anthropogenic forcing implied global climate change is under a rapid progress which has never been occurred before for the last 22,000 years (Joos and Spahni, 2008).

For the last decade (2005 – 2014), CO_2 emissions from fossil fuels and industry (9.0 ± 0.5 Gt C yr^{-1}), land use (0.9 ± 0.5 Gt C yr^{-1}) have resulted in atmospheric CO_2 rate of growth of 4.4 ± 0.1 Gt C yr^{-1}. Oceanic CO_2 sink was estimated to be 2.9 ± 0.5 Gt C yr^{-1} and 3.0 ± 0.8 Gt C yr^{-1} for the terrestrial component (Le Quéré *et al.*, 2015). In terms of partitioning, these

rates suggest that 91% of the total emissions were fossil fuel and industry origin, and 44% of the total emissions accumulated in the atmosphere, 26% in the oceans and 30% in land. Since 1960's, every decade witnessed an average fossil fuel emission increase of 3.1 ± 0.2 Gt C yr^{-1}. In line with these emissions, the atmospheric CO_2 growth rate increased from 1.7 ± 0.1 Gt C yr^{-1} in the 1960's to 4.4 ± 0.1 Gt C yr^{-1} during 2005 – 2014. Again, in line with the increase in atmospheric accumulation, the oceanic CO_2 sink increased from 1.1 ± 0.5 Gt C yr^{-1} in the 1960's to 2.6 ± 0.5 Gt C yr^{-1} during 2005 – 2014.

Steady rise in CO_2 levels has reached a new era. By the time of writing this section (June 2016), National Oceanic and Atmospheric Administration (NOAA) has announced that South Pole Observatory has reached the 400 ppm symbolic threshold CO_2 concentration for the first time in 4 million years (NOAA, 2016), in which this station was the last station below 400 ppm records in the world. Another remote station, Mauna Loa, Hawaii, has reached an annual mean CO_2 concentration of 400.9 ppm in 2015, first in its recording period, and the global levels are likely to stay above the 400 ppm threshold in our lifetimes (Betts *et al.*, 2016).

These dramatic changes have major impacts on the climate systems. According to the recently published Intergovernmental Panel on Climate Change Fifth Assessment Report (IPCC, 2014), last 3 decades have been successively warmer than any preceding decade since 1850. This 3 decade period (1983 – 2012) was possibly the warmest 30-year period within the last 1400 years in the Northern Hemisphere. Since 1880, globally averaged combined land and ocean surface temperature show a warming of 0.85 ^{o}C. The oceans absorbed 90% of the energy accumulated between 1971 and 2010, with upper 75 m temperature increased by 0.11 ^{o}C per decade since 1971. Possibly, regions of high salinity have become more saline, and those of low salinity have become fresher since 1950s. The pH of the ocean surface has decreased by 0.1 since the beginning of the industrial era. Per decade, annual mean Arctic sea-ice extent has decreased by 3.5 to 4.1%. This decrease happened in every season and every successive decade since 1979. Since 1900s, global mean sea level rose by 0.19 meters, a rate that was unprecedented during the previous two millennia.

Unfortunately, the future projected changes in the climate system are not optimistic either. Again referencing IPCC 2014, all assessed scenarios project rise (0.3 – 4.8 ^{o}C under

different scenarios by the end of the 21st century compared to 1986 – 2005 period) in surface temperature. More frequent, with longer duration heat wave events will occur, extreme precipitation events will become more intense. The oceans will continue to warm and acidify (pH decrease of 0.06 to 0.32 under different scenarios by the end of the 21st century), along with the rise in mean sea level (0.26 – 0.82 m). The impacts will likely to continue for centuries even if anthropogenic emissions of greenhouse gases stop.

In light of these estimations and predictions, the BCP becomes a key mechanism to counteract the effects of the accumulating greenhouse gases in the atmosphere and in turn the oceans. It is estimated that the oceans fix 40 – 50 GT C yr^{-1} by primary production (Falkowski *et al.*, 1998, Field *et al.*, 1998). Of this fixed carbon, through BCP processes, 5 – 15 GT C yr-1 (Boyd and Trull, 2007; Henson *et al.*, 2011) are transferred below the euphotic zone. This estimation is actually a comparable amount to the anthropogenic related emissions given in Le Quéré *et al.* (2015). In the absence of the BCP, the atmospheric CO_2 concentration would be 200 ppm higher than todays observed levels (Parekh *et al.*, 2006). Therefore, understanding the dynamics of the BCP is vital. In a changing climate, better predictions of the strength and magnitude of the BCP will enable the scientists and the stakeholders to take necessary actions and shed light on an unknown future.

The definition of the biological carbon pump is simple. It is the combined processes that begin with inorganic carbon conversion to organic carbon through photosynthesis and its subsequent transformation within the foodweb processes, physical mixing, transport and gravitational settling (Ducklow *et al.*, 2001). However, each of these processes has many sub-processes and numerous dependents. Many of these processes are physically and biologically controlled and are highly restricted to environmental constraints, and their magnitude and attenuation with depth will greatly vary within different regions and seasons (Buesseler and Boyd, 2009). To understand these dynamics and especially the particle export at depth, measurements at time-series stations have been operating for decades at various locations in the world oceans (i.e. Bermuda Atlantic Time Series Study, European Station for Time Series in the Ocean, Porcupine Abyssal Plain Sustained Observatory). All of these time-series stations have similarities and dissimilarities that regulate the extent of the carbon sequestration (Neuer *et al.*, 2002; Cianca *et al.*, 2007; Helmke *et al.*, 2010; Lampitt *et al.*, 2010). However, physical, experimental, lack of knowledge, and economical constraints limit our efforts in understanding these dynamics. At this point, models emerge as a tool to fill these gaps.

Numerical models transfer empirical knowledge into quantitative descriptions and as such provide tools that can be used to improve understanding of ecosystem dynamics. There is an increasing need for more systematic understanding of the processes of the biological carbon pump, and these topics should be incorporated in novel algorithms in order to be included in global models. This kind of approach will provide dynamic definitions to models and will exempt the models from empirical definitions limited to few dataset and lacking the functionality representing different locations and past and future conditions. Unfortunately, the algorithms used by the modelling community have not evolved much from the classical NPZD (nutrient-phytoplankton-zooplankton-detritus) models, or they are based on empirical datasets limited to few observations in a certain region (Martin *et al.*, 1987). There are many modelling groups that are trying to go beyond simple NPZD models, and divide the plankton into functional groups (Hood *et al.*, 2006), which distinguish silica producers (diatoms) and calcifiers, N-fixers. Some groups increase the functioning of the ecosystem algorithms by including explicit bacterial compartments (Blackford *et al.*, 2004), redefining the assimilation capacity of grazers (Mitra, 2006), adding complex physical aggregation processes (Kriest, 2002, Aumont *et al.*, 2015), introducing density dependent sinking via interactions with mineral presence (Yool *et al.*, 2011), or dividing the "detritus" compartment into size based suspended and sinking particles and lability based dissolved organic compartments.

Through learning more about key processes controlling carbon sequestration by field, laboratory and mesocosm experiments, it has become clear that adding certain complexities to the models is necessary for improved representations of the global carbon cycle. However, such efforts in return also introduce the problem of dysfunctionality to the models (Anderson and Mitra, 2010). Incorporating new compartments to the models with the aim of increasing complexity requires the introduction of increasing number of parameters, and those parameters have to be tuned in order to fit the observations. The problem with such parameter tuning is that, the complex models due to extensive tuning may begin to fit the uncertainties in the observational data in place of the functional relationships they aim at representing. Another issue that emerges with complexity is that different functions may lead to a correct answer with the wrong reason, which in turn the predictive capacities of the models would be less than those simple models (Hood *et al.*, 2006).

Thus, functionality is a must in models, so is the cost. Even if the parameters are carefully tuned and even if they will theoretically lead to the reality, the cost of such a modeling framework might be so high that the reality would be undesirable. So, what is the extent of detail in the models? These are necessary and hard questions to be answered by the modeling community.

The North Atlantic is a major carbon sink region among the world oceans (Takahashi *et al.*, 2009), and it is estimated that the NA exports ~ 0.55 – 1.94 GT C yr^{-1} (Sanders *et al.*, 2014), which makes the NA a valuable study area for model purposes. This study is designed to aid in advancing our understanding on the variability, potential impacts, and feedbacks of global change and anthropogenic forcing on the structure, function and dynamics of the North Atlantic and associated shelf sea ecosystems as well as the key species influencing carbon sequestration and ecosystem functioning. However, there is a significant lack of information at a mechanistic level about how the atmospheric and the anthropogenic forcing impacts marine populations and how impending climate changes may alter the ecology and biogeochemical cycling of the basin. Consequently, there is pressing requirement to better understand the functioning of our ecosystems. At this point, the importance of modelling studies emerges, where such studies fill in the gaps of field and laboratory observations.

In order to realistically simulate our ecosystems, a novel set of algorithms has to be constructed and be incorporated into models that are running on basin scale and globally. The list of topics to be evaluated, such as aggregate formation, ballasting effects, phytoplankton functional groups, zooplankton life cycle effects, bacterial production and decomposition are key elements that scientists consider when defining the functioning of the fate of carbon and its sequestration (Sanders *et al.*, 2014).

To address the questions and requirements above, a 1D lower trophic pelagic ecosystem model was designed and implemented at 3 time-series stations in the North Atlantic (BATS, ESTOC and PAP). Chapter 2 of this thesis introduces the time-series stations and their background internal dynamics. The data retrieved and the model forcing applied are described in this chapter. Chapter 3 applies the 1D model NAGEM (The North Atlantic Generic Ecosystem Model) at BATS and ESTOC stations. An extensive model validation and discussion follows, comparing the model data to the observed data from BATS and ESTOC. The model is tuned to represent detritus consumption by zooplankton, and in this

chapter, the extent of the removal of detritus by zooplankton is evaluated. The detritus consumption is intensified by increasing the remineralization applied by implicit bacteria. In summary, this chapter along with the model validation, explains the extent of the detritus recycling, and attempts to investigate reasons behind the 3 – 4 fold difference in carbon export observed at these stations. Furthermore, detailed examination of the plankton functional types and their influence on the magnitude and timing of carbon export is done. The complete evaluation of the model is finalized by analyzing the sensitivity analyses on decoupling C:N:P:Si ratios forced in the model. Chapter 4 discusses the algorithms related to the carbon export mechanisms, and through sensitivity analyses, the influence of the new additions is evaluated regarding the magnitude, strength and timing of the primary production and carbon export processes. Algorithms cover a wide range from aggregation coupled to physics and fecal pellet production, to mineral ballast effect, variable particle settling rates and diel vertical migration of zooplankton. Again a comparison between BATS and ESTOC stations are made. Chapter 5 investigates the algorithms applied at PAP station, which is further north in the Atlantic Ocean andhas deeper mixing events and less available light for primary production. Finally, a conclusive chapter is given to summarize the work done in this thesis, addressing future work.

CHAPTER

2. THE STRUCTURE OF THE TIME SERIES STATIONS AND THE MODEL SETUP

Given the North Atlantic Ocean as a major element in regulating the global carbon cycle, understanding its dynamics and the structure of the carbon cycle within becomes a vital issue. To understand these dynamics and especially the particle export at depth, measurements at time-series stations have been operating for decades at various locations in the world oceans. As such, understanding of biogeochemical processes in the NA has benefited greatly from the maintenance of the long-term monitoring stations (BATS (Bermuda Atlantic Time-series Study 31.7^{o} N–64.2^{o} W), ESTOC (European Station for Time series in the Ocean, Canary Islands, 29.16^{o} N–15.5^{o} W) and PAP (Porcupine Abyssal Plain, 49 ^{o} N–16.5 ^{o} W)) (Figure 1). From the model development point of view, these time-series stations become valuable assets for model initialization, evaluation and validation because of their coverage of deep reaches of the oceans and their weekly to seasonal temporal coverage of ecosystem dynamics. The time-series data from these stations have been used extensively in this study. For this reason, this chapter is dedicated to the brief description of these time-series stations, and the data used for modeling purposes, i.e. model initialization, forcing and evaluation.

2.1. Hydrography and biological characteristics of the time-series stations, BATS, ESTOC and PAP

BATS is located in the western part of the North Atlantic Subtropical Gyre (31.7^{o} N–64.2^{o} W) or the Sargasso Sea, in between the Gulf Stream on the west and northwest and the

equatorial current on the south (Figure 1) and is still operating since 1988 with monthly and biweekly basis with the strategy resolving seasonal patterns and interannual variability. During the cruises, hydrography, nutrients, particle flux, pigments and primary production, bacterioplankton abundance and production measurements were made. Significant seasonal and interannual variability in phytoplankton and bactrioplankton biomass exist with the dominance of the prokaryotic picoplankton community (Steinberg *et al.*, 2001). Diatom blooms are rare but occur periodically.

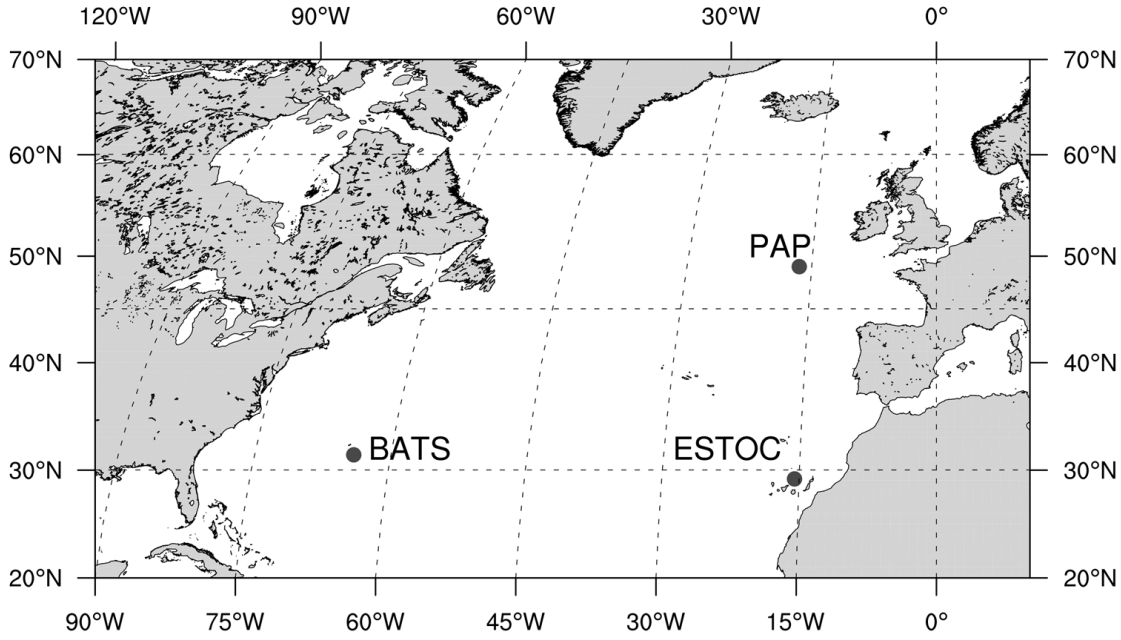

Figure 1) – Locations of the time-series stations that the 1D model NAGEM was implemented.

The hydrography and biogeochemical characteristics of the Sargasso Sea has been well documented, and is characterized by deep winter mixing and strong summer stratification, with significant mesoscale eddy structure (Menzel and Ryther, 1959; Michaels *et al.*, 1994; Michaels and Knap, 1996; McGillicuddy and Robinson, 1997; McGillicuddy *et al.*, 1998; Siegel *et al.*, 1999). The interannual variability is defined by the strength of the surface heating, wind stress, the strength of the winter mixing and the formation of the 18ºC mode water. Strong stratification starts from April and continue to October, with winter mixing depths below 200 m depth (Figure 2a). The biology is strongly linked to the physical dynamics and the inorganic nutrients (Figure 3) are replenished in the EZ due to the mixing and mesoscale events followed by increases in primary production, chlorophyll biomass, suspended organic matter (Steinberg *et al.*, 2001; Cianca *et al.*, 2007). Located in the subtropical gyre, BATS show oligotrophic characteristics with inorganic nutrients being depleted in the EZ. Furthermore, BATS nutrient ratios yield N:P higher than the Redfield

ratio of 16:1, and is reported to be severely P-limited (Cavender-Bares *et al.*, 2001; Mather *et al.*, 2008, Lomas *et al.*, 2010).

ESTOC is located at the eastern part of the North Atlantic Subtropical Gyre (29.16^{o} N–15.5^{o} W), at a similar latitude to BATS (Figure 1), in the Canary Current, the weak eastern boundary current. ESTOC is well located away from the African coast, which exhibit an open ocean oligotrophic gyre characteristics (Davenport *et al.*, 2002; Neuer *et al.*, 2002a). The station hydrography shows a distinct seasonal cycles with intense mixing above 90 m to more than 200 m in Janury to March period, and a stratified period starts from June (Figure 2b). A parallel increase in the strength of the trade winds in summer prevent the stratification to be as high as BATS, with mixed layer depths located in the 40 – 50 m at the surface (Neuer *et al.*, 2007). Similar to BATS, biochemical parameters also respond to the physical events with highest chlorophyll values coincide with the deep mixing events, indicating that the phytoplankton communities are rather nutrient limited than light. On the contrary to BATS which has a high N:P ratio, ESTOC yield a good match with the 16:1 Redfield ratio (Neuer *et al.*, 2002a). With the onset of the stratification, surface waters of ESTOC become nutrient limited with nitrate plus nitrite values are generally low or not measurable (Figure 4). Interestingly, there is a distinct difference in inorganic nutrient concentrations below the nutriclines between BATS and ESTOC, such that ESTOC has nearly the double amount of available nutrients for production. This is due to the presence of 18^{o}C mode water at BATS which is consumed of its inorganic nutrients. This feature between the two sites have major impacts on the comparative biogeochemistry of the two sites which will be mentioned in the following chapters.

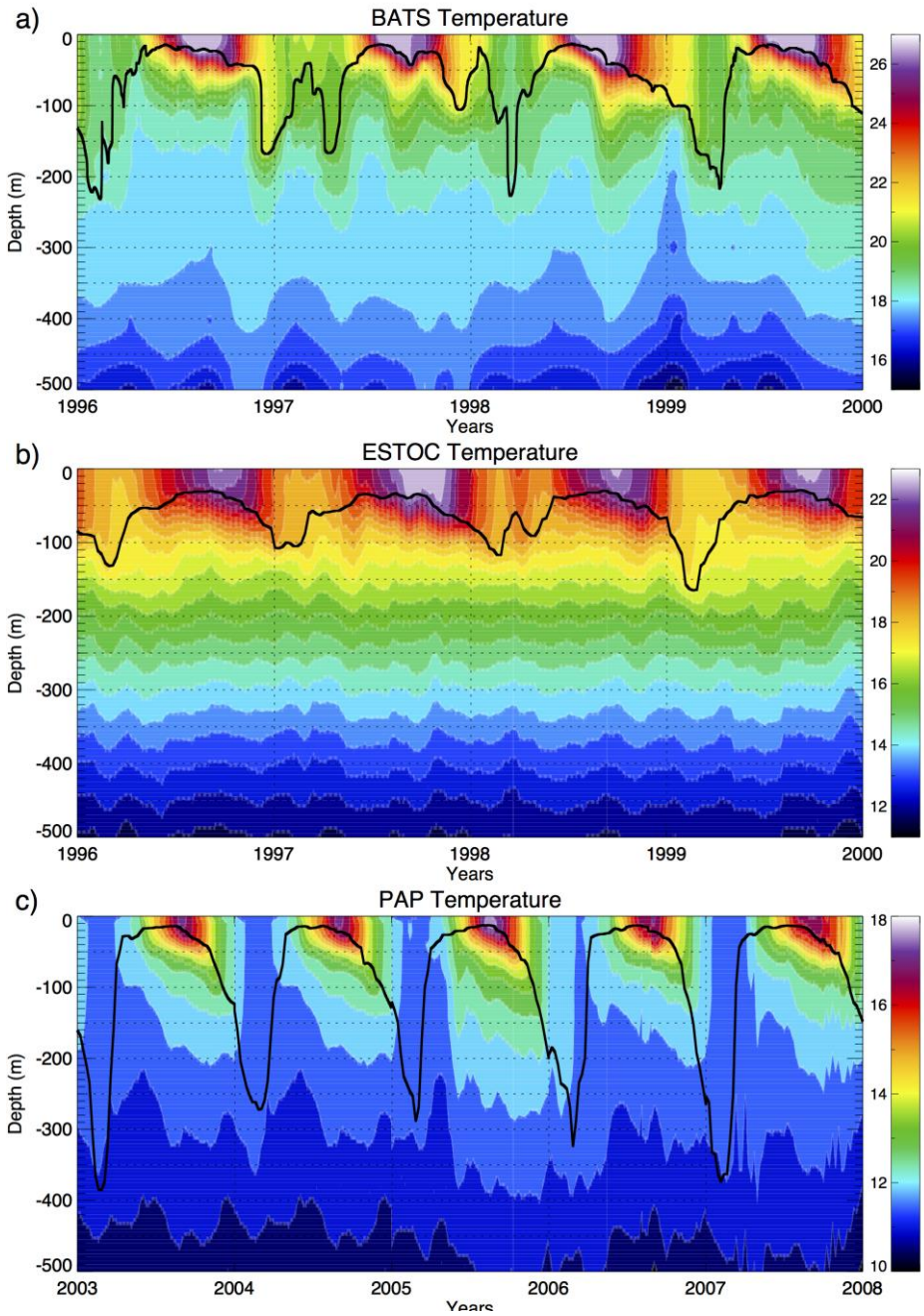

Figure 2) - *In-situ* temperature fields. **a)** BATS, **b)** ESTOC and **c)** PAP. The black lines in the figures denote the MLD estimated using a 0.5 ^{o}C difference from the surface temperature. The BATS data was retrieved from www.bats.bios.edu indicating the monthly sampling. ESTOC and PAP data were retrieved from ARGO database gridded dataset for the North Atlantic. For the simulations, data down to 3000 m was used. Only the upper 500 m was shown here to mimic the differences between the sites and the variabilities.

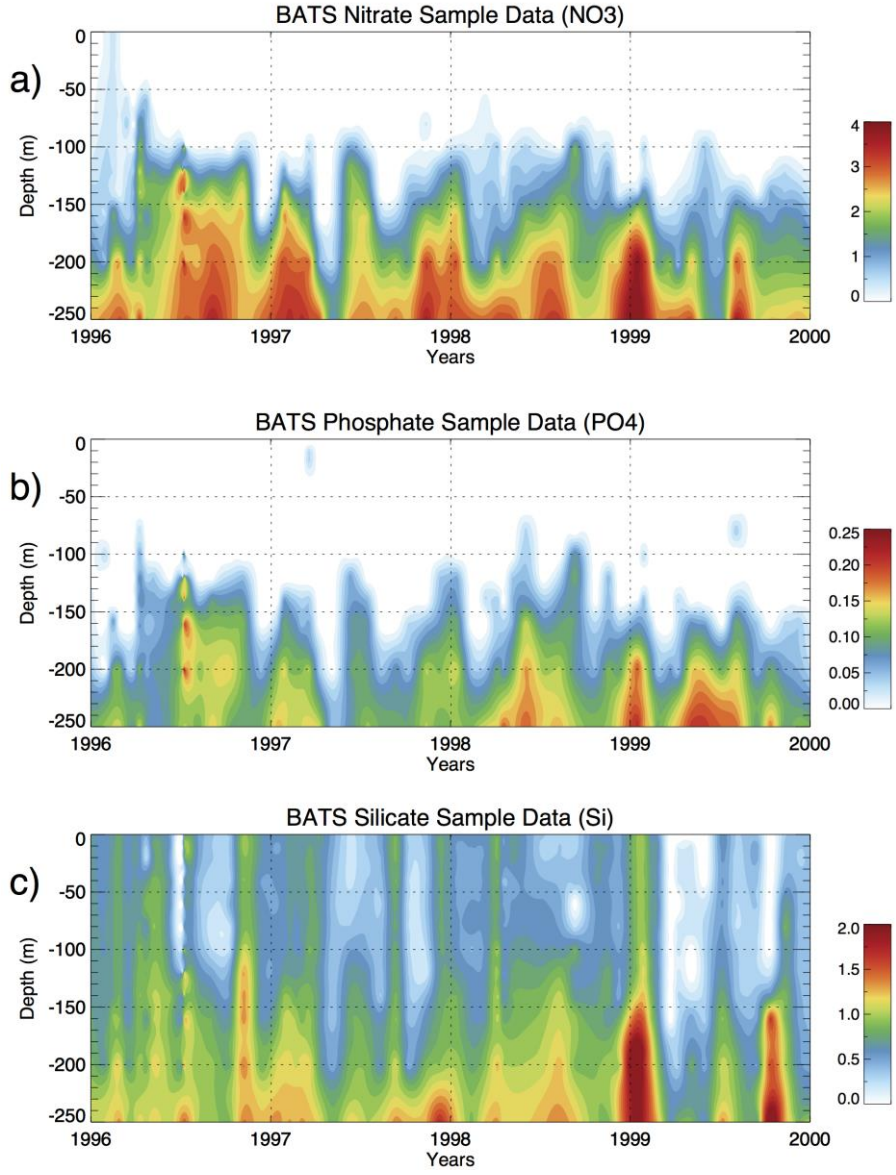

Figure 3) - Time-series of the inorganic nutrients collected in BATS monthly cruises. Data was retrieved from BATS website (bats.bios.edu). a) Nitrate, b) Phosphate and c) Silicate (Si)

PAP is, unlike BATS and ESTOC, is located in the far north at the southeast of the Subpolar Gyre (49 º N–16.5 º W), and is being operated for more than 20 years now. The location of the PAP site is chosen such that it is in minor influence of the processes of the continental shelves, with weak currents, low lateral advection speeds (but can still have significant influence on the site), negligible particle advection and with either rare or stationary for long periods of time eddy activity (Weaver *et al.*, 2000; Lampitt *et al.*, 2001; Chelton *et al.*, 2007; Hartman *et al.*, 2010; Lampitt *et al.*, 2010). Unfortunately, a continuous record of water column nutrients available like those at BATS and ESTOC is absent in the case of PAP. The nitrate and chlorophyll sensors located at the nominal depth of 35 m provide the only continuous inorganic nutrient data (Figure 5). Clear seasonal signals are also the case at PAP

site, where deep MLD's (as deep as 400 m in winter) are accompanied by high nitrate concentrations, and as the seasons progress, a decrease in nitrate and increase in chlorophyll levels are observed.

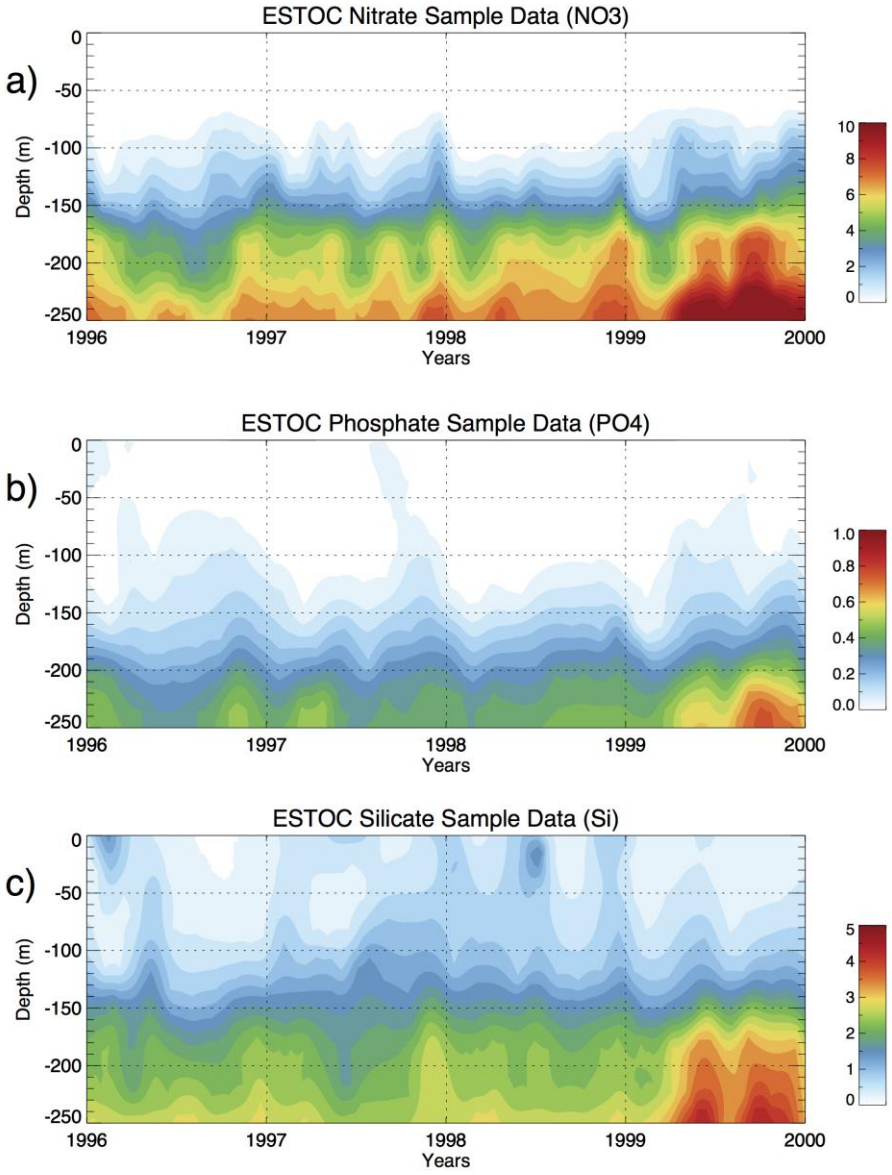

Figure 4) - Time-series of the inorganic nutrients collected in ESTOC cruises. Data was retrieved from Neuer *et al.* (2007) a) Nitrate, b) Phosphate and c) Silicate (Si)

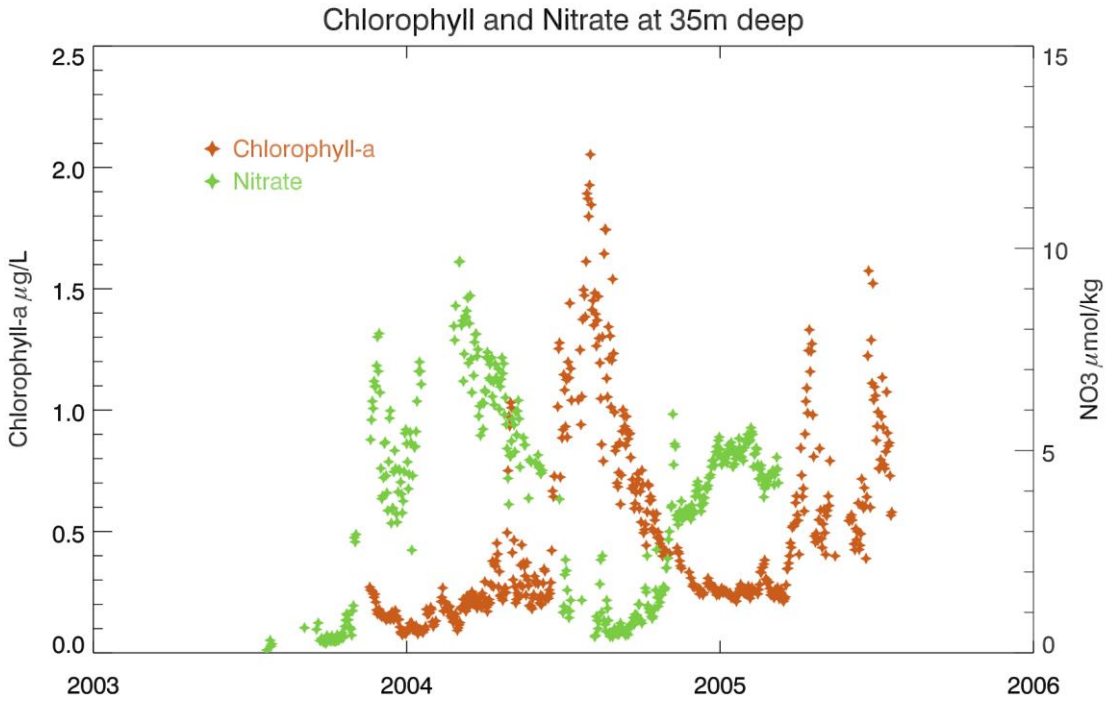

Figure 5) – Timeseries of PAP site chlorophyll-a (µmol L^{-1}) and nitrate (µmol kg^{-1}) located at 35 m depth. Data was retrieved from the Eurosites webpage (http://www.eurosites.info/pap/data.php).

2.2.Model initialization and forcing

Extensive comparative studies of the biogeochemistry of BATS and ESTOC are available in the literature for the 1996 – 1999 period (Neuer *et al.*, 2002b; Cianca *et al.*, 2007; Helmke *et al.*, 2010). For this reason, the BATS and ESTOC simulations in this thesis are based on these years, so that (i) there is more available *in-situ* data from the sites, (ii) those data were already evaluated in the literature and various questions arose to be answered in which models possibly could explain. Unfortunately, the data coverage at PAP for that period is not as high as the subtropical counterparts. It would have been a good opportunity to compare all the three sites in parallel, but the extensive evaluation of biogeochemistry is covered for the years 2003 – 2005 (Hartman *et al.*, 2010), and sediment trap measurements continue to operate beyond that period. For this reason, the PAP simulations are set for the years 2003 – 2008.

NAGEM requires temperature as the main forcing. Temperature is both required to calculate the mixed layer depths (MLD's), where the state variables are homogenously mixed within, and the biological process rates are temperature dependent, i.e. higher temperatures dictate

faster growth, faster remineralization. Since a homogenous distribution is applied within the MLD, vertical mixing is the dominant physical forcing at the surface, and as mentioned above and shown in Figure 2c, this force can be effective even at depths below 400 m. Several threshold criteria based on temperature and density exist in literature for the calculation of MLDs (see Table1 in de Boyer Montegut *et al.*, 2004). The time varying MLD was chosen in this study to be the depth where a difference of 0.5 ^{o}C was observed from the surface temperature value (Spall *et al.*, 2000) for BATS and ESTOC, and 0.03 kg m^{-3} density difference from 10 m depth (Cole, 2013) was used for PAP site.

Below the MLD, diffusion is the only driving force impacting the distribution of state variables between vertical layers. Within the MLD, the vertical diffusion coefficient (K_v) was set to 100 cm^2 s^{-1}, and it was 1 cm^2 s^{-1} elsewhere to parameterize turbulent transport. These values are an order of magnitude higher than the observed values (Ledwell *et al.*, 1998), however, similar modeling studies (e.g. Hood *et al.*, 2001; Dadou *et al.*, 2004) have shown that the values given in Ledwell *et al.* (1998) underestimate the nutrient concentrations. Hood *et al.* (2001) point out that isopycnal and mesoscale processes are possibly reflected by using high K_v values. Application of a high value accelerates nutrient intrusion to the surface layers and sustains production representing overall turbulent transport. The only other physical forcing applied is the settling of detritus, zooplankton and large diatoms.

A 1 hour model time step was chosen in this study. This time period is sufficient enough for the diurnal variability of the biological processes. Vertical layers of the model are 1 meter each and for all of the stations, model vertical domain extend down to 3000 m. Temperature initial conditions for January 1st, 1996 for BATS is taken from the bottle samples (see Section 2.1) and for ESTOC and PAP, from the ARGO database (Cabanes *et al.*, 2013). For PAP, the initial conditions are from January 1st, 2001. Temperature profiles obtained are linearly interpolated to every layer down to 3000 m. At the temporal scale, temperature data are bilinearly interpolated to 1 meters depth levels and 1 hour time intervals to cover 1996 – 2000 at BATS and ESTOC, and 2001 – 2006 at PAP. Figure 2 is directly plotted from the bilinearly interpolated model temperature forcing data.

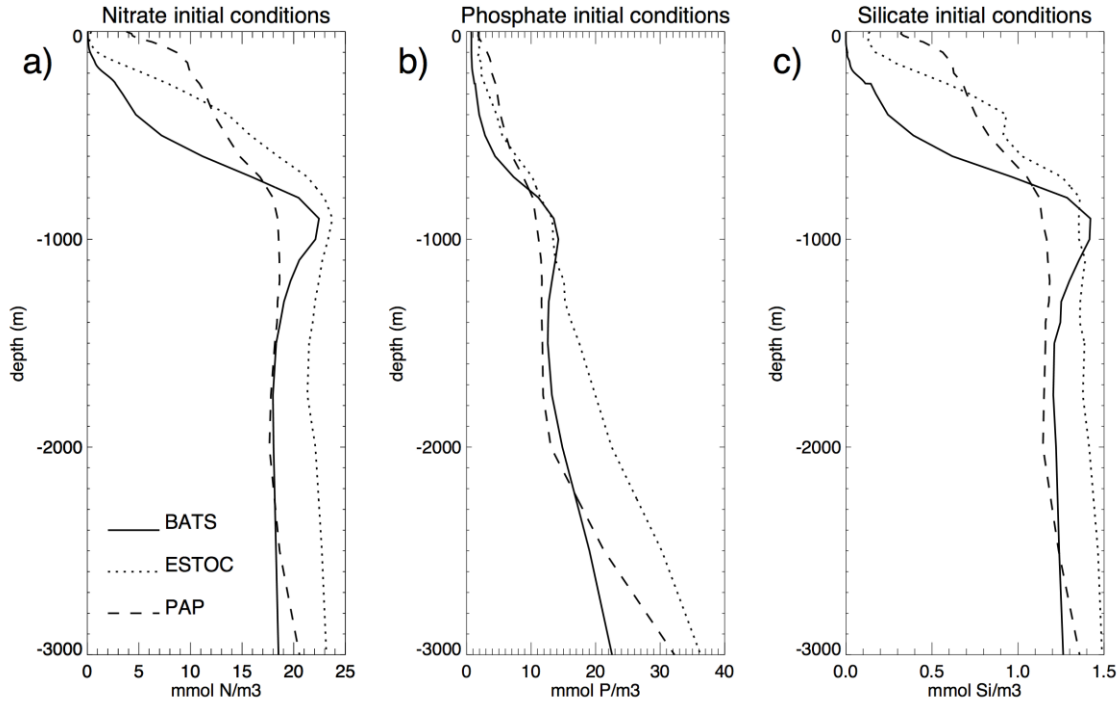

Figure 6) – Depth varying initial conditions set for the simulations corresponding to January 1st, 1996 for BATS and ESTOC, January 1st, 2001 for PAP site. Upper water column BATS data were retrieved from the stations website (http://www.bats.bios.edu), ESTOC data from PLOCAN database (http://data.plocan.eu/thredds/), and the remaining depths down to 3000 m including the PAP site water column data from WOA database (Garcia *et al.*, 2014). a) nitrate, b) phosphate, c) silicate.

For the simulations, nutrient forcing was only used at locations in the water column, except nitrate for BATS where nitrogen fixation processes were simplified as direct nitrate inputs from the surface. At 3000 m, inorganic nutrient (nitrate, phosphate and silicate) concentrations were taken from WOA'13 database (Garcia *et al.*, 2014), and linearly interpolated to 1 hour intervals to fit the model time-step. The other location in the water column that the model was assigned inorganic nutrient forcing are 250 m's for BATS and ESTOC, and 400 m for PAP site (Figure 7). These depths were chosen such that they are above the MLD's assigned for physical forcing. The reason behind such an application was to include the temporal changes in the nutrient concentrations due to lateral interactions or mesoscale activity, since NAGEM uses only vertical physical dynamics. Any changes in the observations due to interactions in the spatial scale was partly represented this way.

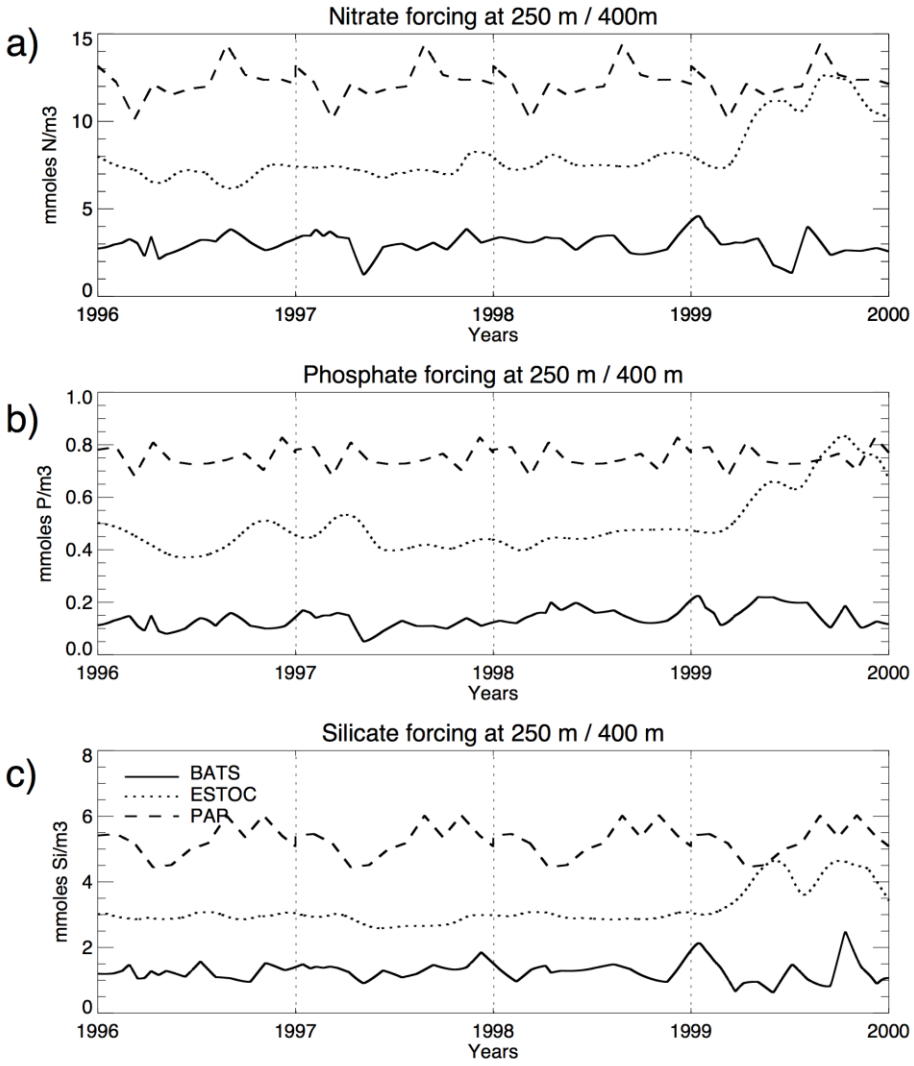

Figure 7) – Inorganic nutrient forcing applied at depth: 250 m for BATS and ESTOC, and 400 m for PAP. BATS data were retrieved from the stations website (http://www.bats.bios.edu), ESTOC data from PLOCAN database (http://data.plocan.eu/thredds/), and the remaining depths down to 3000 m including the PAP site water column data from WOA database (Garcia *et al.*, 2014). a) nitrate, b) phosphate, c) silicate.

Final forcing the model uses was the radiation at the surface. The model calculates at each time-step and depth the radiation penetrates the water column. The surface light field was retrieved from the ECMWF ERA-INTERIM reanalysis (Dee *et al.*, 2011). The specific variable used was the 'surface net solar radiation' (W m^{-2}) at 3 h intervals. The retrieved data were linearly interpolated to 1 h intervals and converted to µmol quanta m^{-2} s^{-1}, which the model uses to calculate the light limited growth rate of the phytoplankton.

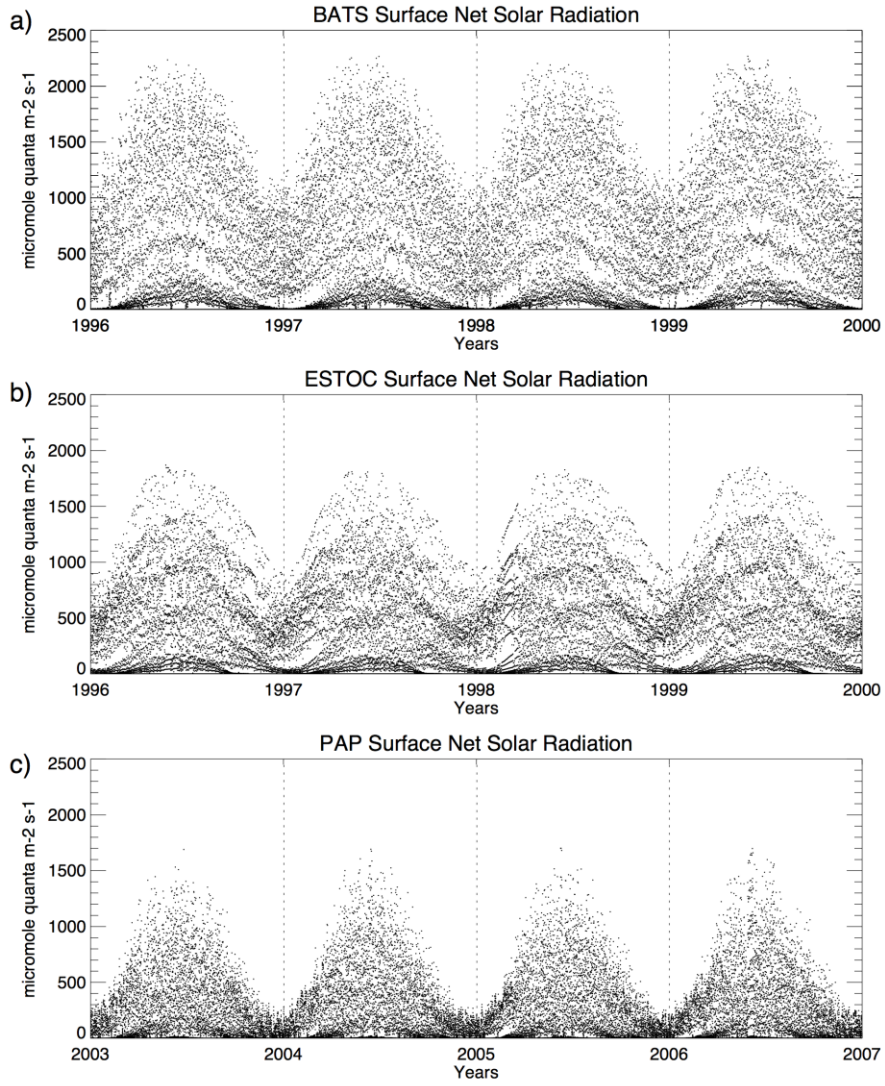

Figure 8) – Surface net solar radiation forcing at the model surface. The surface light field was retrieved from the ECMWF ERA-INTERIM reanalysis (Dee *et al.*, 2011) and converted to µmol quanta m^{-2} s^{-1}. a) BATS, b) ESTOC and c) PAP.

Overall, this study covers 3 different time-series stations in the North Atlantic with different physical and biochemical backgrounds. Using the same modeling tool with the same parameterization and with different forcing among the 3 sites would enable a good comparative study of the algorithms applied in the model, and would shed light on the source of the reasons for the differences observed. For instance, at first sight, BATS has the highest temperature records among the 3 (> 26 ^{o}C) and a wide depth range of the 18 ^{o}C mode water, whereas ESTOC has milder temperatures in summer (~22 ^{o}C) with a gradual decrease in the water column. Even at 500 m, BATS temperature is ~5 ^{o}C higher than ESTOC (Figure 2). PAP is much colder. Degrees above 18 ^{o}C is rarely seen, and surface winter temperatures are ~10 - 12 ^{o}C, which can penetrate through the 500 m water column. Winter convection, thus, is much stronger at PAP where MLD's can be seen as deep as 400

m, where BATS witnesses MLD's ~200 m, and ESTOC rarely exceeding 150 m. The depth of the MLD's and the origin of the watermasses have huge impact on the nutrient levels, such that BATS has the lowest inorganic nutrient levels at the surface, and lower than ESTOC in the mesopelagic due to the presence of wider 18 ^{o}C low nutrient mode water. The nutricline is much deeper at BATS due to deeper mixing. Continuous depth varying nutrient data is absent at PAP, but sensor data indicate an intense intrusion of nutrients to the EZ due to strong vertical mixing. The location of the 3 sites also determine the temporal progress of the biochemistry. Located in the subtropical gyre, BATS and ESTOC receive more light at the surface, especially in the winter. Timing of the light availability determines the timing of the bloom, and in turn the timing of the carbon export. It is important to understand these differences because, ultimately, these are the key elements in forcing the model dynamics to different productivities, community compositions and export rates. Algorithms, regardless of complexity, will fail to function unless these elements are properly supplied to the simulations.

2.3. The list of common parameters used in this study

To pursue the aims of this study, it was necessary for the model to share a common set of parameterization among the different time-series stations. The reason behind is to address the ultimate goal of this work which is to provide a successive set of algorithms and parameterizations that are generic enough to be adopted to various regions with different physical and ecological backgrounds. This way, the experience gained with this work would be passed onto the 3D global modeling studies. For this reason, the lower trophic ecosystem model parameter's definitions and values are listed in Table 1, Table 2 and Table 3, which will be used referred in Chapter 3, 4 and 5.

Table 1) Definitions and the units of the parameters used in the equations that derive phytoplankton dynamics.

Symbol	Definition	Units
μ_{ll_i}	Light-limited carbon-specific growth rate	h^{-1}
μ_{nul_i}	Nutrient-limited carbon-specific growth rate	h^{-1}
α_i	Photosynthetic efficiency	(μmole quanta m^{-2})$^{-1}$
rad_comp_i	Compensation light flux	μmole quanta m^{-2} s^{-1}
rad_inh_i	Inhibiting light flux	μmole quanta m^{-2} s^{-1}
dr_i	Light limitation coefficient	μmole quanta $^{-1}$
θopt_i	Optimal C / Chlorophyll	(g g^{-1})
θint_i	Irradiance vs θopt_i intercept	(g g^{-1})
S_i	Slope of irradiance vs θopt_i	-
m_i	Phytoplankton-specific death rate	d^{-1}
μ_{mi}	Maximum, 24 h, carbon-specific growth rate at 27 ºC	d^{-1}
μ_{mt_i}	Maximum, temperature-dependent carbon-specific growth rate	h^{-1}
μ_i	Growth rate at maximum cellular nutrient concentrations	d^{-1}
g_{AG_i}	Phytoplankton-specific grazing coefficient	d^{-1}
Λ	Ivlev coefficient of grazing	(mmol C m^{-3})$^{-1}$
$\rho_{NO_3^-}i$	Absolute nitrate transport flux	μmol N L^{-1} d^{-1}
$\rho_{NH_4^+}i$	Absolute ammonium transport flux	μmol N L^{-1} d^{-1}
$\rho_{PO_4^{3-}}i$	Absolute phosphate transport flux	μmol P L^{-1} d^{-1}
ρ_{Si_5}	Absolute silicate transport flux	μmol Si L^{-1} d^{-1}
$K_{sNO_3^-}i$	Half saturation constant for nitrate uptake	μmol N L^{-1}
$K_{sNH_4^+}i$	Half saturation constant for ammonium uptake	μmol N L^{-1}
$K_{sPO_4^{3-}}i$	Half saturation constant for phosphate uptake	μmol P L^{-1}
K_{sSi}	Half saturation constant for silicate uptake	μmol Si L^{-1}
K_{QN_i}	Subsistence quota for nitrogen-limited growth	μmol N (μmol C)$^{-1}$
K_{QP_i}	Subsistence quota for phosphorus-limited growth	μmol P (μmol C)$^{-1}$
K_{QSi_5}	Subsistence quota for silicate-limited growth	μmol Si (μmol C)$^{-1}$
Q_{N_i}	Cellular nitrogen status of the algal group	μmol N (μmol C)$^{-1}$
Q_{P_i}	Cellular phosphorus status of the algal group	μmol P (μmol C)$^{-1}$
Q_{Si_5}	Cellular silicate status of the algal group	μmol Si (μmol C)$^{-1}$
QN_{max_i}	Maximum allowed nitrogen to carbon ratio in each algal group	μmol N (μmol C)$^{-1}$
QP_{max_i}	Maximum allowed phosphorus to carbon ratio in each algal group	μmol P (μmol C)$^{-1}$
QSi_{max_5}	Maximum allowed silicate to carbon ratio in each algal group	μmol Si (μmol C)$^{-1}$

Table 2) Values of the parameters defined in Table 1 for each algal group.

Parameter	AG1	AG2	AG3	AG4	AG5
m	0.05[1]	0.05[1]	0.05[1]	0.05[1]	0.05[1]
μ_{mi}	1.35[2,3,4,5,*]	1.35[2,3,4,5,*]	2.25[2,3,4,5,*]	2.88[7,*]	2.07[6,*]
g_{AG_i}	4.0[8,9]	4.0[8,9]	6.5[8,9]	4.0[8,9]	5.0[10,11]
$K_{sNO_3^-}i$	0.1[12,13]	0.1[12,13]	0.167[12,13]	0.417[13]	2.29[14]
$K_{sNH_4^+}i$	0.05[12,13]	0.05[12,13]	0.083[12,13]	0.208[13]	2.18[14]
$K_{sPO_4^{3-}}i$	0.00625[15]	0.00625[15]	0.01[15]	0.026[16]	0.143[13]
K_{sSi}	-	-	-	-	1.2[17]
K_{QN_i}	7.4[-1 5]	7.4[-1 5]	7.4[-1 5]	11.0[-1 12,18,19,20]	13[-1 21]
K_{QP_i}	464[-1 22]	464[-1 22]	464[-1 22]	128[-1 23]	110[-1 24,25]
K_{QSi_5}	-	-	-	-	0.18[26]
QN_{max_i}	5.2[-1 5]	5.2[-1 5]	5.2[-1 5]	5.5[-1 12,18,19,20]	5.25[-1 21]
QP_{max_i}	151[-1 22]	151[-1 22]	206[-1 22]	27[-1 23]	50[-1 24,25]
QSi_{max_5}	-	-	-	-	0.315[26]
α_i	1.2E[-6]	1.2E[-6]	1.2E[-6]	1.2E[-6]	1.2E[-6]
rad_comp_i	12	15	15	17	17
rad_inh_i					
dr_i	0.1	0.001	0	0	0
θint_i	25	20	35	30	35
S_i	1.8	0.675	0.225	0.27	0.15

Superscripts refer to the sources of the parameter values used with citations as follows: [1]Leonard *et al.* (1999); [2]Moore *et al.* (1995); [3]Partensky *et al.* (1993); [4]Cuhel and Waterbury (1984); [5]Kana and Glibert (1987); [6]Sunda and Huntsman (1995); [7]Moran (2007); [8]Landry *et al.* (1995); [9]Verity *et al.* (1996); [10]Dam *et al.* (1995); [11]Roman and Gauzens (1997); [12]Harrison *et al.* (1996); [13]Salihoglu *et al.* (2008); [14]Zhang and Zou (1997); [15]Timmermans and *et al.* (2005); [16]Parpais *et al.* (1996); [17]Nelson and Treguer (1992); [18]Laws and Bannister (1980); [19]Sakshaug *et al.* (1989); [20]Flynn *et al.* (1994); [21]Geider *et al.* (1998); [22]Bertilsson *et al.* (2003); [23]Geider and La Roche (2002); [24]Ho *et al.* (2003); [25]Leonardos and Geider (2004); [26]Takeda (1998);

* see text for the reasoning of the higher than the reference values used

Table 3) Definitions, values and units of the parameters used in the zooplankton, nutrient and detritus equations.

Symbol	Definition	Value	Units
Λ	Ivlev coefficient of grazing	1[1]	(mmol C m^{-3})$^{-1}$
exc_{micro}	Microzooplankton excretion rate	0.1[2,3,4]	d^{-1}
$m_{Z_{micro}}$	Microzooplankton death rate	0.5[7]	d^{-1}
exc_{meso}	Mesozooplankton excretion rate	0.1[2,3,4]	d^{-1}
$m_{Z_{meso}}$	Mesozooplankton death rate	0.5[7]	d^{-1}
λ	Zooplankton assimilation efficiency	0.7[1]	-
$g_{Z_{micro}}$	Mesozooplankton specific grazing coefficient	15[5,6]	d^{-1}
$nitr$	Nitrification rate of ammonium to nitrate	0.05[7]	d^{-1}
FN	Aeolian nitrogen deposition at the surface	Estimated[7]	μmol N m^{-2} d^{-1}
$Nfix$	Nitrogen fixation	Estimated[7]	μmol N m^{-2} d^{-1}
c_a	Remineralization rate of DON to ammonium	0.02[8]	d^{-1}
c_p	Remineralization rate of DOP to phosphate	0.02[8,9,10]	d^{-1}
c_{Si}	Dissolution rate of detritus to silicate	0.1[11]	d^{-1}
c_{DON}	Remineralization rate of detritus to DON	0.2[8,12]	d^{-1}
c_{DOP}	Remineralization rate of detritus to DOP	0.2[8,9,10]	d^{-1}
$sink_{slow}^{det}$	Slow detritus sinking rate	5[14]	m d^{-1}
$sink_{fast}^{det}$	Fast detritus sinking rate	24[14]	m d^{-1}
agg	Aggregation rate of slow detritus to fast detritus	0.01[13]	d^{-1}
c_{cslow}	Remineralization rate of slow detritus to carbon	0.2[8]	d^{-1}
c_{cfast}	Remineralization rate of fast detritus to carbon	0.16[8]	d^{-1}

Superscripts refer to the sources of the parameter values used with citations as follows: [1]Leonard *et al.* (1999); [2]Landry *et al.* (1996); [3]Hutchins and Bruland (1995); [4]Steinberg *et al.* (2000); [5]Dam *et al.* (1995); [6]Roman *et al.* (2002); [7]Salihoglu *et al.* (2008); [8]Laws *et al.* (2000); [9]Karl and Bjorkman (2002); [10]Benitez-Nelson (2000); [11]Nelson *et al.* (1995); [12]Bronk (2002); [13]Jackson and Burd (1998); [14]Turner (2015).

CHAPTER

3. A NUMERICAL STUDY OF BIOPHYSICAL CONTROLS ON PRODUCTIVITY AND CARBON EXPORT RATES IN THE SUBTROPICAL NORTH ATLANTIC

3.1. Introduction

The subtropical gyres of the world's oceans occupy 40% of the surface area of the earth. They are characterized by strong seasonal stratification, low input of nutrients into the euphotic zone and low productivity and biomass, thus dominated by the regenerated production (Fasham, 2003; Brix *et al.*, 2006). Such oligotrophy has led scientist to describe these regions as oceanic deserts. Carbon flux related studies (Emerson *et al.*, 1997 and 2001) have, however, demonstrated that the subtropical gyres make a large contribution to the export of biogenic carbon, knowledge of which is critical to understanding the influence of the oceans on global CO_2 regulation.

Understanding of biogeochemical processes in the NA subtropical gyre has benefited greatly from the maintenance of two long term monitoring stations (BATS (Bermuda Atlantic Time-series Study 31.7^o N–64.2^o W) and ESTOC (European Station for Time series in the Ocean, Canary Islands, 29.16^o N–15.5^o W). The ecosystem of the subtropical gyres have been described as being relatively uniform in space and time. Comparative studies have, however, revealed considerable dissimilarities between the western and eastern boundaries of the North Atlantic subtropical gyre (NASG) (Neuer *et al.*, 2002; Cianca *et al.*, 2007 and 2012; Helmke *et al.*, 2010). These studies investigated how differences in hydrography

influenced biogeochemical processes at BATS and ESTOC. BATS is strongly affected by mesoscale processes resulting from the recirculation of the Gulf Stream. ESTOC is indirectly influenced by the Canary current upwelling system, via the Ekman transport of nutrients and organic matter towards the center of the gyre (Álvarez-Salgado *et al.*, 2007; Pelegrí *et al.*, 2005). ESTOC is far removed from the immediate upwelling region, however, and is oligotrophic in character, exhibiting nutrient scarcity and low production rates (Davenport *et al.*, 2002). Thus, BATS and ESTOC are both oligotrophic in character and exhibit similar rates of primary production and similar phytoplankton biomass. Estimates of carbon export from sediment trap measurements, however, revealed that ESTOC has 3 to 4 times lower export ratios at 200 m than BATS (Neuer, 2002; Helmke *et al.*, 2010). Various hypotheses were proposed to explain this unresolved phenomena in the past, analyzing observed physical and the biogeochemical processes.

It has been proposed that mesoscale activity at BATS leads to enhanced nutrient input into the euphotic zone, increasing new and export production observed at this site (Siegel *et al*, 1999). This hypothesis was tested in a comparative study between BATS and ESTOC by Cianca *et al.* (2007), who demonstrated using 10 years of satellite altimetry data that the mean sea level anomaly at BATS was twice that at ESTOC. These authors found that the higher mesoscale activity constituted a significantly greater source of new nutrients at BATS compared to ESTOC. BATS also has deeper mixed layer depths which enable nutrient poor surface layers to interact with the deeper layers of higher nutrient concentrations. The main new nutrient supply at ESTOC was caused by winter convection. Although shallower mixing events are observed at ESTOC, the shallower nutricline partly compensates for the weaker mixing activity, leading to similar primary production at both sites. They estimated that ESTOC received 75% of BATS' nutrients available for new production (statistically not significant because of the interannual variability), and concluded that BATS primarily received new nutrients via eddy pumping and ESTOC via wintertime convection. The passage of eddies was shown to enhance or diminish particular bloom events (Sweeney *et al.*, 2003), with eddy/wind induced interactions influencing upwelling at the center of the eddies (McGillicuddy *et al.*, 2007), suggesting a complex physical and biological interplay.

Biogeochemical processes themselves, for example nitrogen fixation may provide a significant source of new nitrogen in oligotrophic waters (Hansell *et al.*, 2004; Capone *et al.*, 2005). However Neuer *et al.* (2002) reported evidence that nitrogen fixation is less important at ESTOC compared to BATS. Differences in organic matter remineralization

rates might further contribute to the 3-4 fold difference in export rate between BATS and ESTOC, as higher oxygen consumption rates were reported in the eastern part of the Atlantic (Mouriño-Carballido and Neuer, 2008). Additionally, increased bacterial activity in response to atmospheric dust deposition (with no response seen in phytoplankton) has been demonstrated between the 30 ºN and 30 ºS band in the Atlantic Ocean (Marañón *et al.*, 2010). Due to the strong response of bacterial respiration to atmospheric deposition, Pulido-Villena *et al.* (2008) suggest differences in bacterial activity may also contribute to the discrepancy in export rates. Although they point to higher remineralization rates at shallower depths at ESTOC, Fernández-Castro *et al.* (2012) conclude that higher new production and differences in remineralization rates do not fully explain the observed difference in export rates between BATS and ESTOC, as they emphasize the potential importance of horizontal processes. Helmke *et al.* (2010) suggested that differences in plankton community structure may also play a role. Intense mixing events may cause episodic blooms, during which non-calcifying plankton such as diatoms escape grazing control, leading to episodes of high export near the surface. Such episodic primary production may result in the production of more labile organic matter and intense mesopelagic attenuation activity (Henson *et al.*, 2012; Le Moigne *et al.*, 2012), resulting in faster removal of organic matter in the mesopelagic.

There still much remains unknown about the biogeochemistry of the subtropical gyres particularly on the biogeochemical budgets of carbon and nutrients. Numerical models transfer empirical knowledge into quantitative descriptions and as such provide tools that can be used to improve understanding of ecosystem dynamics. This thesis introduces a 1D pelagic lower trophic ecosystem model that distinguishes limiting nutrients (N, P, Si) within the state variables and introduces separate algal communities with variable growth dependencies to investigate the relationship between physics and the ecosystem dynamics, and the effect of remineralization rates. By evaluating and comparing the model results, the content of carbon export and export rates were quantified and the links between the export and the physical processes were shown. Following the initial simulations, the model was modified to mimic the effect of different remineralization rates suggested in the literature. In particular, the impact of variable bacterial remineralization rates and detritus consumption by zooplankton on carbon export, and investigate the response from the two sites were explored.

The first part of the chapter describes the model structure, and demonstrates through comparison with observations the capabilities and limitations of the model in describing observed seasonality in primary production, the seasonal succession of plankton functional types, and carbon export at these two locations. The model structure was designed with flexibility to accommodate new algorithms derived from recent experimental studies, or algorithms that are used in various other ecosystems model into the numerical code. Direct application of new algorithms in complex 3D coupled hydrodynamic-ecosystem models is difficult and costly. Thus, the model details presented here are used to facilitate algorithm testing and development, and are expected to inform new algorithms into 3D coupled ecosystem models. The second part of this chapter shows how the model is used to explore the drivers of similarities and dissimilarities in primary production and carbon export at BATS and ESTOC.

3.2.Material and Methods

3.2.1. The ecosystem model

A one-dimensional lower trophic level pelagic ecosystem model has been developed for this study referred to hereinafter as NAGEM (North Atlantic Generic Ecosystem Model). The schematic description of NAGEM is given in Figure 9. NAGEM is based on the modeling tools developed for the Equatorial Pacific (Salihoglu and Hofmann, 2007) and the Subtropical North Atlantic (Salihoglu *et al.*, 2008). The adapted model has been re-coded in FORTRAN90 and was modified to better simulate carbon export, with the goal to establish a generic modeling tool and a parameterization set suitable for application to the entire North Atlantic. The equations are described in detail in Section 3.2.4.

NAGEM includes separate state variables for nitrate, ammonium, phosphate, and silicate. This way, the model resolves possible multiple nutrient limitation in the environment, and each algal group can utilize ammonium, nitrate and phosphate. Diatoms can further utilize silicate. NAGEM includes 5 algal groups (AG) representing different size classes and process rates. AG's are classified as prokaryotes (3 subgroups), autotrophic eukaryotes (pico and nano sizes represented together) and large diatoms. The phytoplankton functional groups included in NAGEM represent the dominant autotrophic biomass in the Sargasso Sea (see discussion in 3.2.4.1) determined from pigment and size fractional studies (DuRand *et*

al., 2001; Steinberg *et al.*, 2001; Casey *et al.*, 2013; Lomas *et al.*, 2013). Prokaryotes are divided into low and high light adapted *Prochlorococcus* and *Synechococcus*. The model takes into account the minimum of light- and nutrient-limited growth rates when dictating the actual growth rate of each phytoplankton. The nutrient-limited growth rate is calculated by a quota based approach (Droop, 1973), such that, each AG has separate cellular carbon, nitrogen, phosphorus compartments, and AG5 has an extra silicate compartment. Separate growth rates for nitrogen, phosphorus and silicate are estimated when calculating uptake rates of nutrients in reference to cellular nutrient contents, which result in variable cellular carbon-to-nutrient ratios. The nutrient-limited growth rate is the combination of these separate nutrient based growth rates. The light limited-growth rate for each algal group is governed by a hyperbolic tangent function (Jassby and Platt, 1976). Light attenuation is a function of the absorption and backscattering of seawater and chlorophyll *a*. Variable chlorophyll-to-carbon ratios for each AG are also included in the model following the procedure given in Bissett *et al.* (1997) determined by the carbon content, irradiance and growth for each AG at each time step.

Two zooplankton functional groups were included in the model. The microzooplankton group theoretically includes phagotrophic protists, and animals smaller than 200 µm (Landry *et al.*, 1995). The larger zooplankton group, mesozooplankton are those that are between 200 to 2000 µm in size (classified as copepods) (Dam *et al.*, 1995; Madin *et al.*, 2001) (see discussion in 3.2.4.1). Microzooplankton graze on the smaller size fraction of the autotrophs in NAGEM (AG1-4). Mesozooplankton graze on diatoms (AG5) and microzooplankton. The grazing of phytoplankton is of the form of a non-saturating function with a prey refuge at low concentrations following Franks *et al.* (1986). Organic matter is recycled through detritus and dissolved organic matter. Detritus is divided into two main compartments with slow and fast sinking rates, and those are divided into 4 sub-compartments representing C, N, P and Si content. DOM is represented by separate DON and DOP compartments. DOC is resolved implicitly, as the model does not assume carbon as a limiting factor.

3.2.2. Model physics and setup

NAGEM is run offline and is not coupled to an external physical model. The main driving physical force in the model is the mixing in the surface layers. Within the mixed layer depth (MLD), all the state variables are homogeneously distributed. Below the MLD, vertical

diffusion and particle settling are the only physical forces acting on the state variables. The vertical coordinates were set at 1 meter and the time resolution at 1 hour intervals for all simulations. A 1 h time interval is sufficient to resolve the diurnal dynamics in phytoplankton growth kinetics. A 4 year simulation period was chosen, extending from 1996 to 2000. The mismatch and discontinuity of the initial conditions were implicitly removed by performing a 10 year spin-up run before the model results were stored as model outputs. For the spin-up, forcing from 1996 was applied repeatedly for 10 years. The spin-up, enabled a stable seasonal cycle prior to beginning the numerical experiments. The model outputs presented here are thus the results from the 10^{th} to 14^{th} year simulation years.

Temperature, MLD and *Kv* are derived directly from the available observations. Observed temperature profiles at both sites were interpolated onto 1 m depth (extends down to 3000 m) and 1 h time intervals mapped onto the model coordinates. Temperature data from the field surveys at BATS (monthly-bimonthly) and from the ARGO database (Cabanes *et al.*, 2013) at ESTOC were used. MLDs were calculated following the interpolation. Several threshold criteria based on temperature and density exist the literature for the calculation of MLDs (see Table1 in de Boyer Montegut *et al.*, 2004). The time varying MLD was chosen in this study to be the depth where a difference of 0.5 ^{o}C was observed from the surface temperature value (Spall *et al.*, 2000).

Below the MLD, diffusion is the only driving force impacting the distribution of state variables between vertical layers. Within the MLD, the vertical diffusion coefficient (K_v) was set to 100 $cm^2\ s^{-1}$, and it was 1 $cm^2\ s^{-1}$ elsewhere to parameterize turbulent transport. These values are an order of magnitude higher than the observed values (Ledwell *et al.*, 1998), however, similar modeling studies (e.g. Hood *et al.*, 2001; Dadou *et al.*, 2004) have shown that the values given in Ledwell *et al.* (1998) leads to an underestimation of the nutrient concentrations. Hood *et al.* (2001) point out that isopycnal and mesoscale processes are better reflected by using high K_v values. Application of a high value accelerates nutrient intrusion to the surface layers, representing overall turbulent transport, and sustains production. The only other physical forcing applied is the settling of detritus, zooplankton and large diatoms.

The surface light field was retrieved from the ECMWF ERA-INTERIM reanalysis (Dee *et al.*, 2011). The specific variable used was the 'surface net solar radiation' (W m^{-2}) at 3 h

intervals. The retrieved data were linearly interpolated to 1 h intervals and converted to µmol quanta m^{-2} s^{-1}. For irradiance at depth, the non-spectral version of the bio-optical model used in Salihoglu, (2005) was applied. Light attenuation was represented as a function of the absorption and backscattering of the seawater and particulate material. The amount of particulate material in the water column was estimated from the pigment concentrations estimated for each algal group.

3.2.3. Biogeochemical data

The biogeochemical data available from observations at BATS and ESTOC have provided values of many of the state variables used for setting up of the initial and boundary conditions for the simulations. The available data was also used to evaluate the model's success in representing spatial and temporal variability in ecosystem dynamics at both sites. Field data for BATS were retrieved from the BATS website (bats.bios.edu). Further details can be seen in Lomas *et al.* (2013). For ESTOC, inorganic nutrient and chlorophyll data at the surface (0–200m) were retrieved from the PLOCAN database (http://data.plocan.eu/thredds/). Sediment trap data for both of the stations are available both on the BATS website and PANGEA (Neuer *et al.*, 2002; Torres Valdés *et al.*, 2014) database.

Surface boundary conditions were set as no flux conditions for all state variables, with the exception of nitrate at BATS. A daily nitrate atmospheric flux and fixation was forced at the surface boundary in µmol N m^{-2} d^{-1}. The forcing is only applied to the uppermost layer, where nitrate is assumed to rapidly distribute vertically through mixing and diffusion. Inorganic nutrients (nitrate, phosphate and silicate) were also forced in two locations in the water column, at 250 m depth and at the bottom layer. The 250 m data used were retrieved from BATS and ESTOC cruise data, and for the bottom conditions at 3000 m, data were obtained from World Ocean Atlas 2013 (WOA) climatology (Garcia *et al.*, 2014), and both were linearly interpolated to 1 h intervals. The forcing at 250 m represents the nutrient variability that may not be resolved with the physical forcing we use in the model. This way, seasonal and annual variability was introduced to the model. The Neumann boundary condition ($\delta X / \delta z = 0$) was applied for phytoplankton and zooplankton compartments at the bottom layer. Large diatoms, zooplankton and slow and fast sinking detritus were allowed to sink through vertical layers. Initial conditions of the ecosystem state variables were derived

from the observations where available. The closest available data to January 1996 was used to set the initial conditions. The missing data at depth (i.e. > 200 m) was retrieved from the WOA'13 climatology for January. All state variables were linearly interpolated from the surface down to 3000 m at 1 m depth intervals.

3.2.4. Model Formulation

3.2.4.1. Plankton Dynamics

The state equations of the physics and biological compartments were solved numerically using the Crank-Nicholson scheme (Crank, 1956). Within the parameter ranges used in this study, this scheme is unconditionally stable. The schematic description of the model compartments and currency flow are shown in Figure 9. The values used in parameterization of NAGEM are listed in TableTable **1**,Table **2** and Table **3**, where further detail can be found in Salihoglu and Hofmann (2007) and Salihoglu *et al.* (2008).

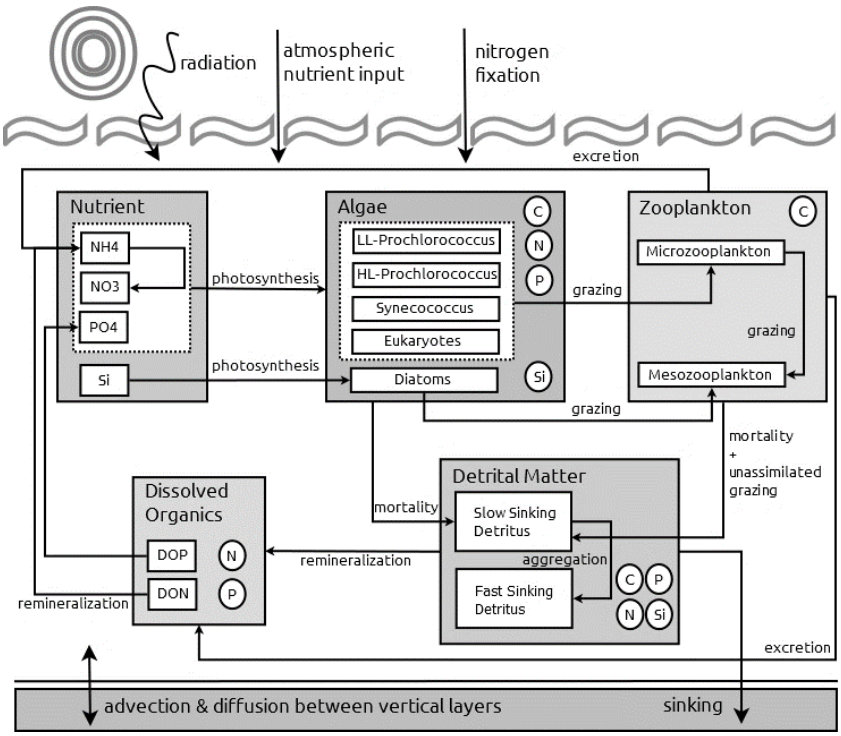

Figure 9) Structure of NAGEM. Shaded rectangles indicate trophic levels, and internal compartments are indicated within. The small circles within the trophic levels indicate the internal nutrient composition. Arrows represent the direction of transfer between the state variables. Abbreviations used are: C - carbon, N - nitrogen, P - phosphate, Si - silicate, DON - dissolved organic nitrogen, and DOP - dissolved organic phosphorus.

State equations for the algal growth and grazing follow

$$\frac{\partial AG_i}{\partial t} + w\frac{\partial AG_i}{\partial z} - \frac{\partial}{\partial z}Kv\frac{\partial AG_i}{\partial z} = \left[min\left(\mu_{ll_i}, \mu_{nul_i}\right)\right]AG_i - m_i AG_i - I_{AG_i}Z \quad \text{for i=1,5} \tag{3.1}$$

$$\frac{\partial Z_{micro}}{\partial t} = \sum_{i=1}^{4} \lambda\, I_{AG_i} Z_{micro} - I_{Z_{micro}} Z_{meso} - exc_{micro} Z_{micro} - m_{Z_{micro}} Z_{micro} \tag{3.2}$$

$$\frac{\partial Z_{meso}}{\partial t} = \lambda\, I_{AG_5} Z_{meso} + \lambda\, I_{Z_{micro}} Z_{meso} - exc_{meso} Z_{meso} - m_{Z_{meso}} Z_{meso} \tag{3.3}$$

$$I_{AG_i} = g_{AG_i}\, \Lambda\, [AG_i]\left(1 - e^{-\Lambda\,(AG_i)}\right) \tag{3.4}$$

$$I_{Z_{micro}} = g_{Z_{micro}}\, \Lambda\, [Z_{micro}]\left(1 - e^{-\Lambda\,(Z_{micro})}\right) \tag{3.5}$$

where the terms on the LHS of Eq.(1) represent the changes in algal group *AG* in time *t* at any location, *z* is depth, w is vertical advection and *Kv* is the vertical diffusive flux. The RHS terms are the biological source and sink terms which include light- (μ_{ll_i}) and nutrient- (μ_{nul_i}) limited growth that are temperature corrected for each time step, natural mortality (m_i) and losses due to grazing activity (I_{AG_i}) of micro- and mesozooplankton. $g_{AG,Z}$ denotes maximum grazing rate on each AG and microzooplankton. The terms *exc* and *m* denote excretion and natural mortality rates. λ denotes zooplankton assimilation efficiency and Λ represents the Ivlev (1955) coefficient for zooplankton grazing.

The *Prochlorococcus* (AG1 and 2) represent the smallest (~0.7 µm) size groups in NAGEM. They have been shown to account for a significant proportion of the carbon biomass in the Sargasso Sea (~12 - 50%; DuRand *et al.*, 2001; Steinberg *et al.*, 2001). *Prochlorococcus* have better photoacclimation capacity than *Synechococcus*, but are strongly affected by N limitation, thus they often bloom in deeper layers in the euphotic zone closer to the nitracline (Olson *et al*, 1990; Moore *et al.*, 1995; Partensky *et al.*, 1999; Casey *et al.*, 2007). Such behavior is represented in the model by including a low light adapted *Prochlorococcus* (LL-*Prochlorococcus*), which are adapted to maintain growth at low light levels, and strongly restricting the N uptake of AG1 and 2 from NO_3 (Moore *et al.*, 2002). With their competitive uptake capacity, *Prochlorococcus* dominate the phytoplankton biomass during the stratified summer months.

Synechococcus (AG3), are slightly larger (~1 µm). Their biomass in the Sargasso Sea was reported to be ~9 - 23% (DuRand *et al.*, 2001) and is most abundant in the upper 80 m of the water column, just above the depths dominated by *Prochlorococcus* (Casey *et al.*, 2013). *Synechococcus* biomass is most abundant in spring, decreasing towards the summer months. Together, prokaryotic picoplankton carbon at BATS forms ~ 20-58% of the total phytoplankton carbon. Autotrophic picoeukaryotes (AG4) (non-coccolithophore) biomass reaches a maximum around spring season each year (35 - 73% of the total phytoplankton carbon; DuRand *et al.*, 2001). Eukaryotes maintain growth at reduced levels throughout the year, and the spring bloom is followed by prokaryotic succession (Steinberg *et al.*, 2001). Eukaryotic phytoplankton is resilient to the changes in physical forcing around BATS (Goericke, 1998). Large diatoms (AG5) only contribute ~6-7% to the total chlorophyll *a* concentration, although this number may occasionally reach ~34% at BATS during bloom events (Steinberg *et al.*, 2001).

Heterotrophic carbon biomass at BATS is dominated by bacteria and nanozooplankton (protozoa), with the latter accounting for ~ 70% of the heterotrophic carbon (Caron *et al.*, 1995; Roman *et al.*, 1995). Zooplankton dynamics show the highest biomass in spring (March/April) following the phytoplanktonic bloom, with 3 times high biomass compared to August in the upper 200 m of the water column. Micro-, meso-, and macrozooplankton in total constitute ~30 % of the integrated heterotrophic carbon biomass in spring and summer at BATS (Roman *et al.*, 1993; Madin *et al.*, 2001). Compared to BATS, we have much less information about the structure and the seasonal development of the plankton community at ESTOC. DNA-based molecular fingerprinting of eukaryotic protists and cyanobacteria (Amacher *et al.*, 2009) reveal that Dinoflagellates were the most abundant in both water column and in trap material at 150 m, with much less contribution of diatoms. Small eukaryotes, *Prochlorococcus* and *Synechococcus* were also present and could be identified from the trap material.

3.2.4.2. Nutrient dynamics

N and P are reported to limit primary production in the subtropical North Atlantic (Fanning, 1992; Wu *et al.*, 2000; Lomas *et al.*, 2004), and silicate may limit diatom growth (Brzezinski and Nelson, 1996; Lima and Doney, 2004). The model resolves possible multiple nutrient limitation in the environment, and each algal group can utilize ammonium, nitrate and phosphate, and diatoms can further utilize silicate. *Prochlorococcus* was initially thought

from culture studies to use only ammonium for growth (Moore *et al.*, 2002), but both Casey *et al.* (2007) and Martiny *et al.* (2009) found that some ecotypes present in the ocean that were not included in the culture study can assimilate nitrate. Thus, every algal group in NAGEM can uptake nitrate, however, *Prochlorococcus* are highly limited in nitrate utilization.

Each AG has separate cellular carbon, nitrogen, phosphorus, and AG5 has an extra silicate compartment. Separate growth rates for nitrogen, phosphorus and silicate are estimated through calculating uptake rates of nutrients in reference to cellular nutrient contents. Variable chlorophyll *a* to carbon ratios for each AG are also included in the model. Carbon content, irradiance and growth rates are coupled to estimate chlorophyll *a* to carbon ratios for each AG at each time step.

Nutrient state equations follow:

$$\frac{\partial NO_3^-}{\partial t} = -\sum_{i=1}^{5} \rho_{NO_3^- i} + nitr + \delta(z)[FN + Nfix] \qquad \begin{matrix}\delta(z=0)=1\\ \delta(z>0)=0\end{matrix} \tag{3.6}$$

$$\frac{\partial NH_4^+}{\partial t} = -\sum_{i=1}^{5} \rho_{NH_4^+ i} - nitr + 0.5 exc_{micro} Z_{micro} \left(\frac{N}{C}\right)_{Z_{micro}} + 0.5 exc_{meso} Z_{meso} \left(\frac{N}{C}\right)_{Z_{meso}} + c_a DON \tag{3.7}$$

$$\frac{\partial PO_4^{3-}}{\partial t} = -\sum_{i=1}^{5} \rho_{PO_4^{3-} i} + c_p DOP \tag{3.8}$$

$$\frac{\partial Si}{\partial t} = -\rho_{Si_5} + c_{Si} DetSi \tag{3.9}$$

where, ρ denote the nutrient and AG specific uptake rates, *nitr* represent the nitrification of ammonium to nitrate, *FN* and *Nfix* are extra sources of nitrogen from the surface boundary layer in the form of atmospheric (aeolian) deposition of nitrate and nitrogen fixation respectively. N/C terms denote the internal zooplankton nitrogen:carbon ratios. C_x terms represent the remineralization rates applied to DON, DOP and detrital silicon.

The uptake (ρ) for nutrients are calculated via a Monod function applied to the ambient nutrient concentration, and are stored in phytoplankton as a separate state variable. All nutrients follow the same equation, phosphate is given as an example here:

$$\frac{\partial AGP_i}{\partial t} = \rho_{PO_4^{3-}i} - m_i AGP_i - I_{AGP_i}\left[Z_{micro}\left(\frac{P}{C}\right)_{Z_{micro}} + Z_{meso}\left(\frac{P}{C}\right)_{Z_{meso}}\right] \tag{3.10}$$

$$\rho_{PO_4^{3-}i}(z,t) = \mu_{mt_i}(z,t) AGP_i\left[\frac{PO_4^{3-}}{K_{sPO_4^{3-}i} + PO_4^{3-}}\right] \tag{3.11}$$

where $\mu_{mt_i}(z,t)$ is the temperature dependent specific growth rate of each AG, and $K_{sPO_4^{3-}}$is the half saturation constant for phosphate uptake. Note that internal P content (AGP) is also included in the equations, and zooplankton carbon content is converted to nutrient equivalents. μ_{mt_i} (temperature (*T*) corrected growth rate using specific growth relationship given by Eppley (1972), determines the maximum growth rate an AG can achieve under nutrient saturated conditions as:

$$\mu_{mti}(z,t) = \mu_{mi}(z,t) exp^{0.0633(T(z)-27)} \tag{3.12}$$

$$\mu_i(z,t) = \mu_{mt_i}(z,t)\left[1 - \frac{K_{QN_i}}{QN_{max_i}}\right]^{-1}\left[1 - \frac{K_{QP_i}}{QP_{max_i}}\right]^{-1}\left[1 - \frac{K_{QSi_5}}{QSi_{max_5}}\right]^{-1} \tag{3.13}$$

where $QN, QP\ and\ QSi$ are the algal group internal nitrogen to carbon ratios ($AGN_i : AG_i$), phosphorus to carbon ratios ($AGP_i : AG_i$) and silicate to carbon ratio ($AGSi_5 : AG_5$). Higher maximum growth rates are assigned for AG's compared to Salihoglu and Hoffman (2007) and Salihoglu *et al.* (2008) to reach the observed productivity at BATS and ESTOC (Table 2). *A max* subscript denotes the maximum attainable nutrient to carbon ratios. K_{QN_i}, K_{QP_i} and K_{QSi_5} denote the minimum allowed nutrient to carbon ratios, where the zero growth rate occurs. Following the maximum growth rate under temperature corrected conditions, the actual nutrient-limited growth rate (μ_{nul_i}) is calculated by the nutrient to carbon ratios (*Q*):

$$\mu_{nul_i}(z,t) = \mu_i(z,t)\left[1 - \frac{K_{QN_i}}{Q_{N_i}(z,t)}\right]\left[1 - \frac{K_{QP_i}}{Q_{P_i}(z,t)}\right]\left[1 - \frac{K_{QSi_5}}{Q_{Si_5}(z,t)}\right] \tag{3.14}$$

The light-limited growth rate (μ_{ll_i}) is calculated by a hyperbolic tangent function, which takes into account the irradiance at depth (*rad(z,t)*), phytoplankton compensation light flux where growth stops below (rad_comp_i) and an exponential light inhibition term as follows:

$$\mu_{ll_i}(z,t) = tanh\left[\frac{\alpha_i(rad(z,t) - rad\_comp_i)}{\mu_{mti}(z,t)}\right]\mu_{mti}(z,t)\ exp^{-dr_i(rad(z,t)-rad\_inh_i)} \quad (3.15)$$

Carbon to chlorophyll ratios are estimated at each time-step and depth by:

$$\theta opt_i(z,t) = \theta int_i + S_i * rad(z,t) \quad (3.16)$$

3.2.4.3. Organic matter dynamics

Rapid recycling of dissolved organic matter (DOM) in the marine environment results in the release of nutrients (Pomeroy, 1974; Azam and Hudson, 1977) through several processes including phytoplankton exudation, bacterial release, viral lysis, zooplankton excretion and grazing (Carlson, 2002), and mechanical breakdown and subsequent dissolution of detritus and fecal pellets (Jumars *et al.*, 1989; Lampitt *et al.*, 1990; Strom *et al.*, 1997). DOM dynamics are included in NAGEM, and breakdown by bacteria is parameterized implicitly as a function of temperature, following:

$$\frac{\partial DON}{\partial t} = 0.5exc_{micro}Z_{micro}\left(\frac{N}{C}\right)_{Z_{micro}} + 0.5exc_{meso}Z_{meso}\left(\frac{N}{C}\right)_{Z_{meso}} + c_{DON}DetSlow_N + c_{DON}DetFast_N - c_aDON \quad (3.17)$$

DOP state equations are exactly the same, except all excreted P are sent to the DOP pool, rather than distributing half to the inorganic PO_4^{3-} pool.

NAGEM has the capacity to differentiate plankton sources and detrital size classes. It resolves suspended and slow sinking particles under the "Slow Sinking Detritus" state variable in NAGEM. This compartment is labile and since its sinking speed is slow, it is prone to high rates of recycling within the surface layers. Since detritus forms a major

compartment in recycling of matter in NAGEM, complete flushing out of detritus from the euphotic zone was prevented by defining a low settling rate for the slow detritus (5 m d^{-1}) and a moderate one for the fast detritus (24 m d^{-1}) (Alldredge and Gotschalk, 1988), consistent with preserving the continuity in the numerical solver. Non-grazing phytoplankton mortality, zooplankton mortality and unassimilated grazed fraction are the sources of the Slow Detritus compartment. Aggregation leads to the formation of the Fast Detritus compartment (Jackson and Burd, 1998). Slow and fast sinking detritus are defined by their sinking and remineralization rates. Breakdown of detritus is parameterized through remineralization to DON and DOP. Detritus equations are:

$$\frac{\partial DetSlow}{\partial t} + \left(w + sink_{slow}^{det}\right)\frac{\partial DetSlow}{\partial z} - \frac{\partial}{\partial z}Kz\frac{\partial DetSlow}{\partial z} = \sum_{i=1}^{4}\left[m_i AG_i + (1-\lambda)I_{AG_i}Z_{micro}\right] + m_5 AG_5 + m_{Z_{micro}}Z_{micro} + (1-\lambda)\left(I_{AG_5} + I_{Z_{micro}}\right)Z_{meso} + m_{Z_{meso}}Z_{meso} - c_{cslow}DetSlow - aggDetSlow \quad (3.18)$$

$$\frac{\partial DetFast}{\partial t} + \left(w + sink_{fast}^{det}\right)\frac{\partial DetFast}{\partial z} - \frac{\partial}{\partial z}Kz\frac{\partial DetFast}{\partial z} = aggDetSlow - c_{cfast}DetFast \quad (3.19)$$

where C_x terms represent the remineralization rates applied on DetSlow and DetFast. Aggregation rate is applied under the *agg* terms and $sink_{slow}^{det}$ and $sink_{fast}^{det}$ are the sinking rates of the detritus state variables.

3.2.5. Model Experiments

3.2.5.1. The reference simulation (M-REF)

The results section reports a validation of an initial simulation set, referred to hereinafter as the reference simulations (M-REF), followed by two additional experiments designed to investigate the role played by zooplankton grazing on detritus and bacterial remineralization rates on carbon export. The effect of nutrient additions from the surface layer was also investigated in a separate set of simulations. Below, the modifications made on the

formulations are described. The acronyms and short description of the simulations are summarized in Table 4. The model formulation and parameterization set given in Section 3.2.4 form the reference simulation (M-REF).

Table 4) Definitions and the units of the parameters used in the equations that derive phytoplankton dynamics

Simulation	Definition
M-REF	The reference simulation summarized in Figure 9. Detritus is only consumed by implicit bacterial actvity
M-ZOO	Zooplankton consumption of detritus added to M-REF simulation
M-REM	M-ZOO simulation implicit bacterial activity rates are increased by 40%.
Nutrient additions	See Table 5

3.2.5.2. Detritus consumption by zooplankton (M-ZOO)

In the reference simulation (M-REF), the remineralization of detritus was defined as a function of temperature (Eppley, 1972). This is an implicit way of resolving the bacterial degradation of organic matter. The same mechanism was also applied to the dissolved organic components, meaning that remineralization was the only biological sink term on "non-living organic matter". However, microbial degradation is not the only mechanism by which organic matter such as fecal pellets become removed from the water column, rather, a combination of microbial degradation and zooplankton mediated processes such as fragmentation of fecal pellets (Svensen *et al.*, 2012) are important, and as much as half of the fast-sinking particles are ingested and fragmented by zooplankton (Giering *et al.*, 2014). Many sediment trap studies have revealed that POC in the form of fecal pellets remained near the epipelagic zone and did not sink to deeper layers (Viitasalo *et al.*, 1999; Wexels Riser *et al.*, 2006). Furthermore, fecal pellets can sink fast enough (at a rate of hundreds of meters per day) to escape microbial remineralization (Turner, 2002), suggesting that zooplankter play an important role in the retention of fecal pellets in the upper layers of the water column. The activities involved are complete ingestion of the fecal pellets, breaking of pellets into smaller particles, or partial dispersal of the fecal material. Ultimately, these activities transform the larger fast sinking particles into smaller, slow sinking or suspended particles.

The zooplankters responsible for the retention of fecal pellets within the epipelagic zone are primarily copepods (Gonzales and Smatacek, 1994). However, Poulsen and Kiørboe (2006) suggested that microzooplankton of <200 micrometer in size are also important in degrading fecal pellets. This was further confirmed by Poulsen an Iversen (2008) and Poulsen *et al.* (2011). However, copepods grazing on protozooplanktons make them indirectly involved in the process. Thus, degradation of particulate matter by zooplankton activities, combined with the microbial remineralization are important factors regulating carbon export mechanisms at depth. Our reference simulation included only the latter process. For this reason, in a second set of simulations, we introduced zooplankton consuming detrital matter in order to represent the zooplankton mediated breakdown of fecal pellets. These simulations are referred to hereinafter as M-ZOO, and are intended to help understand the extent to which consumption of detritus by zooplankton moderates carbon export, and whether this can explain any of the observed differences in exported carbon between BATS and ESTOC.

In order to prevent over-grazing on phytoplankton, rather than modifying the existing microzooplankton compartment, a third zooplankton compartment was added (Z_{det}). After inclusion of Z_{det}, microzooplankton feeds on primary producers (AG1-4), Z_{det} feeds on detritus and mesozooplankton feeds on diatoms (AG5), microzooplankton and Z_{det}. The preference of food for Z_{det} was mainly (90%) given to the fast sinking detritus component so that the removal of fecal pellets was represented. The grazing pressure of Z_{det} on detritus was calculated in the same way as for the other zooplankton compartments, only the food source was modified to include the fast and slow sinking detritus. Detritus feeding additions to the state equations follow:

$$\frac{\partial Z_{det}}{\partial t} = \lambda\, I_{det_{slow}} Z_{det} + \lambda\, I_{det_{fast}} Z_{det} - I_{Z_{det}} Z_{meso} - exc_{det} Z_{det} - m_{Z_{det}} Z_{det} \quad (3.17)$$

$$I_{det} = g_{det}\, \Lambda\, [det] \left(1 - e^{-\Lambda\,(\mathrm{det})}\right) \quad (3.18)$$

3.2.5.3. Increased bacterial remineralization

In order to investigate the impact of remineralization rates on carbon export, a third set of simulations were conducted using a higher remineralization rate (referred to hereinafter as

M-REM). In order to investigate the bacterial effects resolved implicitly, we increased the remineralization rate of DetSlow by 40% of the slow sinking detritus. In order to balance the excess removal of detritus, the remineralization rate of DetFast compartment was decreased by 25%. These multipliers were chosen within a limited range in order to keep the productivity levels as realistic as possible. This way, Fast Detritus was subject to an increase in the rate of breakdown by zooplankton (M-ZOO simulation), and Slow Detritus was subject to an increase in the rate of breakdown by bacterial processes. For the M-REM simulations, modifications were made on the M-ZOO model set-up, thus the M-REM simulations also include grazing of detritus by zooplankton.

3.2.6. Nutrient additions

In order to evaluate the response of the production and the community composition on the availability of the limiting nutrients, a series of sensitivity analyses in the form of NH4, NO3 and PO4 additions were made. Injecting the nutrients to the intermediate layers was avoided for any circumvention caused by the variability in model physics. Therefore, the additions were made at the top layer, and were assumed to be immediately distributed within the MLD. The nutrient addition simulations mimicked the nutrient decoupling imposed by external pressure, and the resulting community structure and primary productivity was investigated. Since the additions were done at the top layer, the simulations could possibly mimic increases in atmospheric nutrient depositions. For simplicity, constant values were chosen from the values reported in Zamora *et al.* (2013). In order to test the high end of the additions, for the N additions, high end values reported in Zamora *et al.* (2013) were used for both BATS and ESTOC. The PO_4 ranges given in Zamora *et al.* (2013) were too low to evaluate any response, therefore PO_4 additions were designed to follow a 16:1 N/P ratio representing the Redfield ratio. The values used and the scenario names are given in Table 5.

Table 5) Summary of the nutrient addition sensitivity analyses. Units of the additions are µmoles N m^{-2} $hour^{-1}$ for NH_4 and µmoles P m^{-2} $hour^{-1}$ for PO_4.

Scenario	N001	N005	N01	P001	P005	P01
NH_4 addition	0.001	0.005	0.01	-	-	-
PO_4 addition	-	-	-	0.001/16	0.005/16	0.01/16

3.3. Results

3.3.1. Model evaluation

First, the results from the M-REF runs are presented, and the success of the model's initial parameterization and setup in representing the physical environment, primary productivity, the seasonal succession of plankton functional types, nutrient levels and resulting export rates are evaluated. The magnitude and annual/seasonal variability in each state variable and compare them with the available observations are reported. In the following sections, the results from the sensitivity analyses of M-ZOO, M-REF and nutrient additions are presented. The model statistic of validation for all the simulations are provided in the supplementary section of the paper.

3.3.1.1. Primary production, chlorophyll and algal distributions

Model - data comparisons of chlorophyll *a* levels (Figure 10) demonstrate that mixing events, mainly in winter, increase nutrient input to the surface layers and enhance productivity leading to an increase in chlorophyll *a* concentration to levels of > 0.3 µg/L throughout the euphotic zone. Following the onset of seasonal stratification, chlorophyll a concentration in the upper layers zone fall to ~0.1 µmoles/L at both stations. Enhanced production commences at the end of December or the beginning of January during each year and continues until early spring. Enhanced chlorophyll levels (> 0.3 µmoles/L) are sustained throughout the year at depths of 90 m and 100 m at ESTOC and BATS respectively, forming the Deep Chlorophyll Maximum (DCM). The model reproduces observed seasonal variability, and depth profiles of chlorophyll-a.

The observed chlorophyll *a* distributions of the individual algal groups also compare well with the model results (Figure 11). The percent contributions to the integrated total chlorophyll *a* of each algal group represents the seasonality in the observed data, with the exception of *Synechococcus*. The model captures the blooming of pico- nanoeukaryote and diatom chlorophyll *a* in winter and spring months, followed by LL and HL *Prochlorococcus* in the summer months.

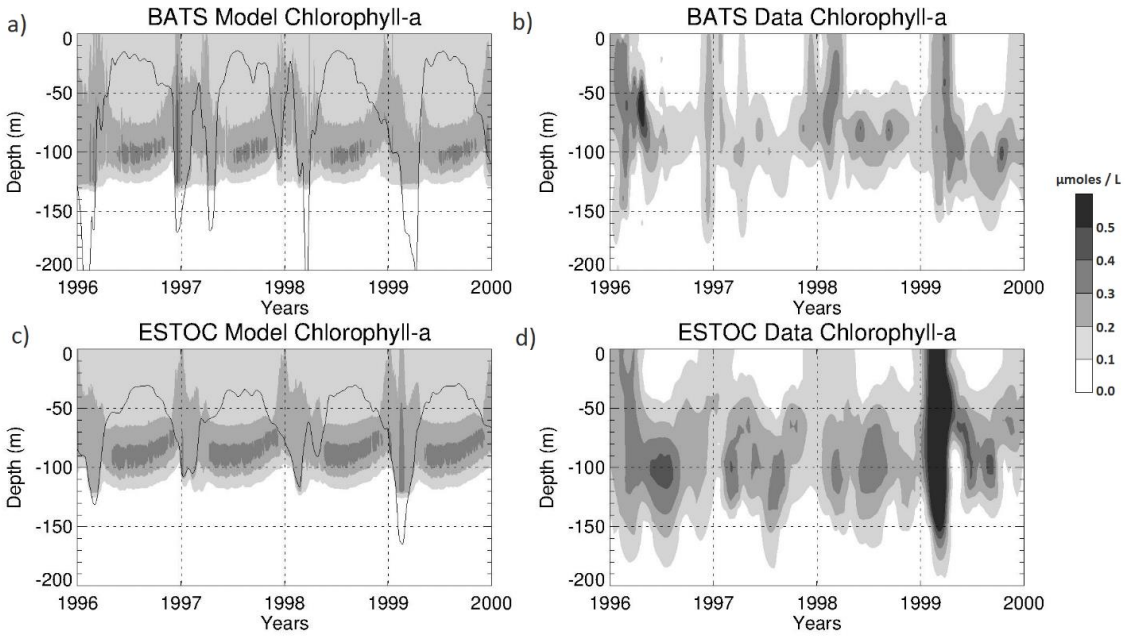

Figure 10) Chlorophyll *a* concentration (micromoles/L). **a)** simulated at BATS, **b)** observed at BATS, **c)** simulated at ESTOC and **d)** observed at ESTOC.

Simulated primary productivity shows distinct seasonality, dictated by the timing of deep mixing events (Figure 12). Simulated four-year averaged depth integrated productivities are 13.12 mol C m-2 y-1 and 11.12 mol C m-2 y-1 at BATS and ESTOC respectively, ranging from an annual minimum of 10.84 mol C m-2 y-1 in 1997 to an annual maximum of 12.66 mol C m-2 y-1 in 1999 at ESTOC, and from an annual minimum of 12.46 mol C m-2 y-1 in 1998 to an annual maximum of 13.7 mol C m-2 y-1 in 1999 at BATS. Thus, the model simulates slightly lower productivity values at ESTOC compared to BATS. There is considerable evidence that the primary productivities at both stations are very similar in terms of magnitude (Helmke *et al.* 2010). Given the background nutrient levels below the EZ, and the vertical mixing estimated from temperature measurements, the model is able to estimate similar primary productivity values to those reported in the literature. Reported primary productivities for BATS are 13.33 mol C m-2 y-1 (Menzel and Ryther, 1960), 12.83 mol C m-2 y-1 (Steinberg *et al*, 2001), 13.08 mol C m-2 y-1 (Lomas *et al*, 2013), 11.56 mol C m-2 y-1 (Helmke *et al*, 2010) and are slightly lower than previously reported values at ESTOC of 13.66 mol C m-2 y-1 (Davenport *et al.*, 2002) and 13.38 mol C m-2 y-1 (Helmke *et al*, 2010). The model captures the timing of the winter blooms at both sites correctly (Figure 12). Multiple peaks in productivity during the winter and spring intervals at BATS (Figure 12a & b) are reflected in the results.

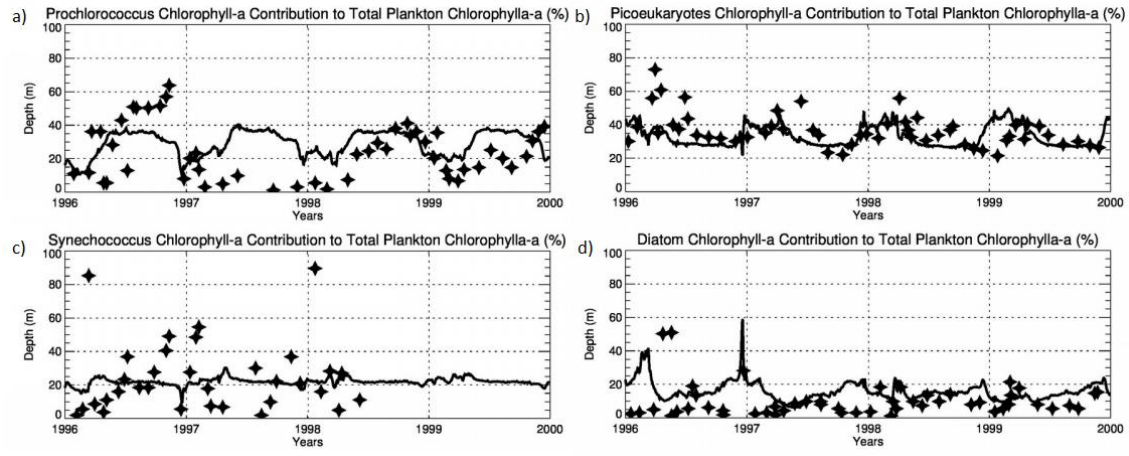

Figure 11) Contribution of each simulated algal group chlorophyll *a* content to the total simulated chlorophyll *a* (%). Stars indicate observed values (Lomas *et al*, 2013). **a)** *Prochlorococcus*, **b)** *Synechococcus*, **c)** picoeukaryotes and **d)** diatoms.

When AG's 1, 2 and 3 (Figure 13a-c) are combined into a total cyanobacteria group, their contribution to the total biomass adds up to 45 - 46 %, making the prokaryotes the dominant algal groups at both stations. This is agreement with the findings (20 – 58%) of DuRand *et al.* (2001) and Steinberg *et al.* (2001). Individual depth distributions of each AG reveal at both stations that autotrophic eukaryotes (Figure 13d) are the dominant individual groups with a contribution of 25 - 26 % to the total biomass. Diatoms (Figure 13e) had the lowest contribution to total biomass with up to 10 - 11 %. Within the spring bloom, pico-nanoeukaryote is the dominant algal group forming up to 40 % of total biomass. Diatoms form 10 - 12 % of the total winter/spring bloom biomass. Microzooplankton (Figure 13f) groups at both stations are the dominant grazers (consuming ~16% of the total plankton biomass) due to their diverse choice of prey which includes AG 1-4. Mesozooplankton (Figure 13g), feeding only on diatoms and microzooplankton, only consumed ~0.03% of the total plankton biomass.

The vertical and temporal distributions of individual plankton groups show distinct characteristics. Prokaryotes (AG's 1-3), which are less dependent on available limiting nutrients, bloom at depths near the surface. The partitioning between the *Prochlorococcus* (AG1 & 2) and *Synechococcus* (AG3) was captured by the model dynamics. DuRand *et al.* (2001) point out that these two communities have opposite seasonal patterns with *Synechococcus* slightly dominant during the spring bloom and *Prochlorococcus* exceeding *Synechococcus* in summer. The results of Casey *et al.* (2013) demonstrate a similar seasonal succession of phytoplankton to that shown in Durand *et al.* (2001) and further demonstrate

the niche partitioning, with *Synechococcus* dominating the upper 80 m, directly above the *Prochlorococcus* abundance maxima. Model results show that LL and HL *Prochlorococcus* are most prolific during the late spring and summer seasons when they form ~25% of the total biomass. *Synechococcus* has comparable annual mean biomass to *Prochlorococcus*, but blooms during spring seasons when it forms ~20 % of total biomass (Figure 13h). Within the *Prochlorococcus* groups, LL *Prochlorococcus* with its low light adaptive capacity, sustained its highest biomass below HL *Prochlorococcus*, at depths of ~90-100 m. Due to their higher dependency on available nutrients and high growth rates, pico- nanoeukaryotes dominated the winter and spring blooms at both stations at all depths in the EZ, forming > 45% of the total biomass. pico- nanoeukaryotes also sustained growth near the surface throughout the summer months, but its dominant contribution was to the DCM at depths of ~100 m. The pico- nanoeukaryote contribution to the DCM was also noted by Casey *et al.* (2013) at BATS.

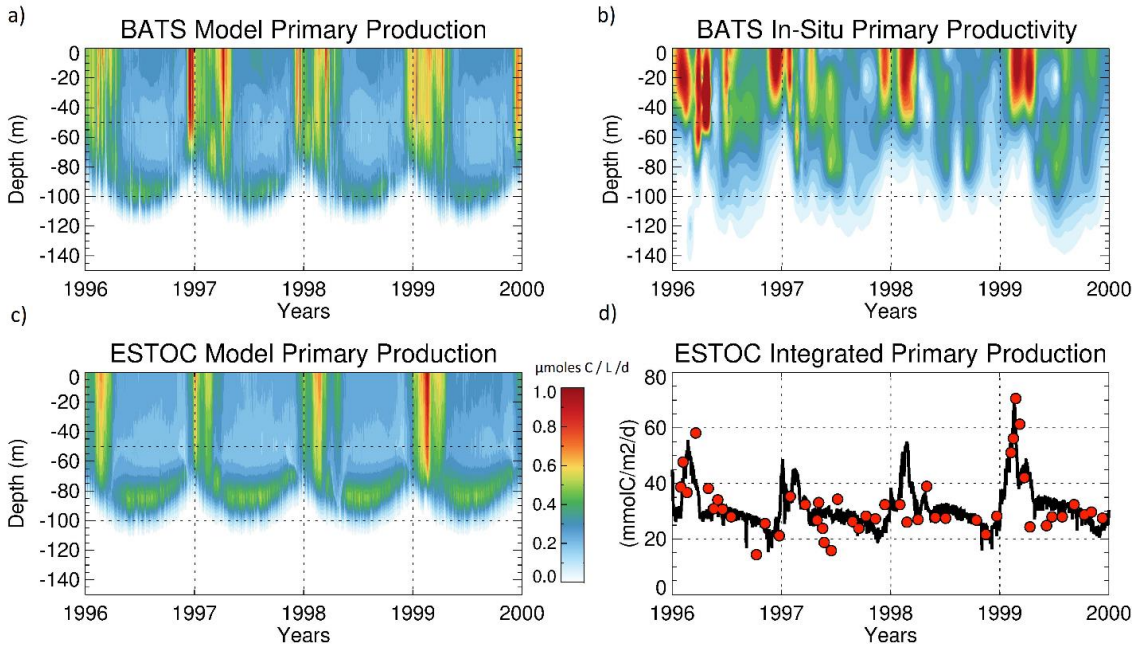

Figure 12) Hovmoeller plots of **s**imulated and observed primary productivity (µmoles C/L/d). **a)** Simulated at BATS, **b)** Observed at BATS, **c)** Simulated at ESTOC and **d)** Simulated depth integrated primary productivity at ESTOC station (mmol C/m2/d) . In (d), red marks indicate the satellite estimated integrated primary productivities (Neuer *et al.*, 2007).

Diatoms had a minor contribution to the total annual phytoplankton biomass. Their production was, however, significant (> 40% of total biomass) during winter/spring bloom episodes at both stations. All of the AG's contributed to the winter/spring blooms to variable extents, and also to the DCM chlorophyll content. These findings are in agreement with previous works at BATS (Durand *et al.*, 2001; Steinberg *et al*, 2001). Model results also

suggest that the annual mean chlorophyll a contribution of *Prochlorococcus* exceeded that of *Synechococcus*. Pulses of diatom lasted for short periods (5 – 15 days), episodes of diatom growth constituted up to 40% of the total biomass, locally supported by enhanced new nitrogen from deeper layers. Observations have revealed similar pulses of diatoms, showing them to form 16 – 40 % of the annual new production in the region (Nelson and Brzezinski, 1997; Krause *et al.*, 2009). In the case of ESTOC, we do not have the time-series of AGs to compare with the model results, but Amacher *et al.* (2009) reported that the diatoms accounted for the three quarters of the analyzed clones at the 150 m DCM layer using molecular techniques. Their sampling time was March 2005, which does not correspond to our simulation period, but high diatom contribution is possible in with a well mixed period around 150 m depth (Figure 13e). Thus, the model community distribution is well described and the model is suitable for testing the hypothesis posed in this study.

3.3.1.2. Nutrient dynamics

Simulated nitrate, phosphate and silicate concentrations (Figure 14a,c,e) agree well with observations at BATS (Figure 14b,d, f). Phosphorus within the EZ is depleted throughout the year including during deep winter mixing events at both stations (Figure 14c). This is in accordance with observations which reveal that phosphorus is depleted within the upper 200 m throughout winter mixing events and within the upper 100 – 150 m during summer. Both the simulations and the observations locate the phosphocline at ~125 m. Nitrate is also depleted in the surface layers in both model results and observations (Figure 14a), with the nitracline located at 100 – 110 m depth. There is a significant difference in the depths of the nitracline and the phophocline (~20 m). Within the winter mixing period, the model overestimates nitrate levels compared to observations by 1 μmoles N L^{-1}, although nitrate is depleted during deep mixing events according to the observations. Model results also overestimate the silicate levels (Figure 14e) in the surface layers, suggesting silicate consumption by diatoms may be underrepresented (although diatom biomass in the simulations agrees well with the observations). It should also be noted that the minor accumulation of nitrate, phosphate and ammonium at depths of 150 – 200 m is a result of direct input through remineralization, the process which represents implicitly resolved bacterial decomposition of organic matter.

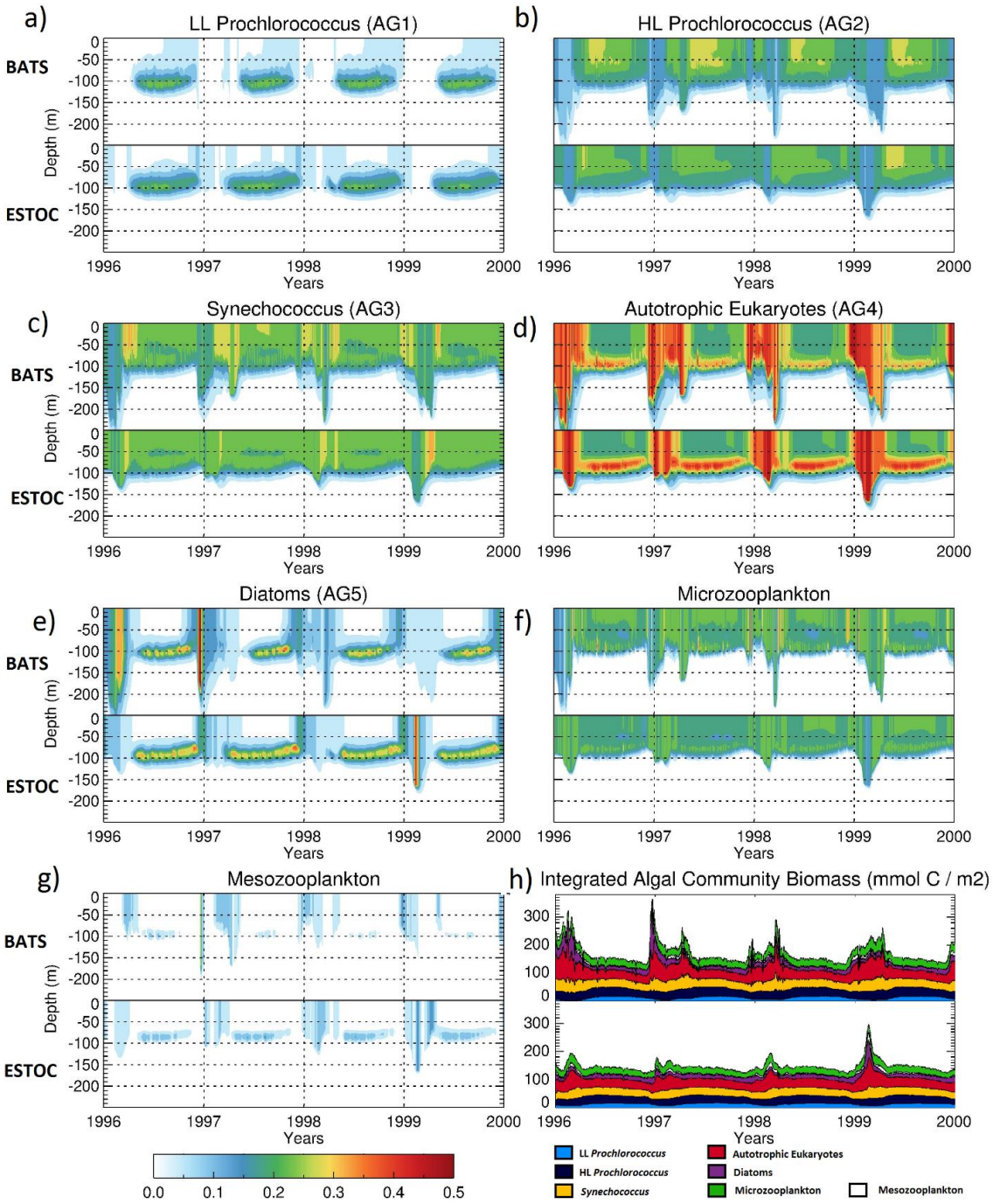

Figure 13) Hovmoller plots of simulated plankton community distributions (µmoles C L^{-1} d^{-1}). Each plot is subdivided into two panels, where the upper panels correspond to BATS, and the lower correspond to ESTOC simulations respectively, for **a)** LL *Prochlorococcus*, **b)** HL *Prochlorococcus*, **c)** *Synechococcus*, **d)** Autotrophic eukaryotes, **e)** Diatoms, **f)** Microzooplankton, **g)** Mesozooplankton. Plot **h** represent the cumulative integrated biomasses of algal groups (mmoles C m^{-2}).

Simulated nitrate, phosphate and silicate concentrations at ESTOC (Figure 14a,c, and e) are also similar to observations (Figure 14b,d and f). The surface to 100 m depth range is the nutrient limited zone in both simulations and observations. However, the model overestimates nitrate and phosphate concentrations within the 100 m to 200 depth range. In

reference to the physical forcing used in the ESTOC simulations, the mixed layer is limited to the upper 100 m of the water column, with the exception of winter 1999. Below 100 m, the water column is more stable, thus slow sinking detritus and dissolved organics tend to accumulate at that depth range, resulting in remineralization which enhances inorganic nutrient levels. This feature was also noted for the BATS simulations. A lack of silicate removal (Figure 14e) from the surface layers is also an issue for the ESTOC runs. The simulations suggest an accumulation of DOM at ~100 m, due to the remineralization of detrital matter.

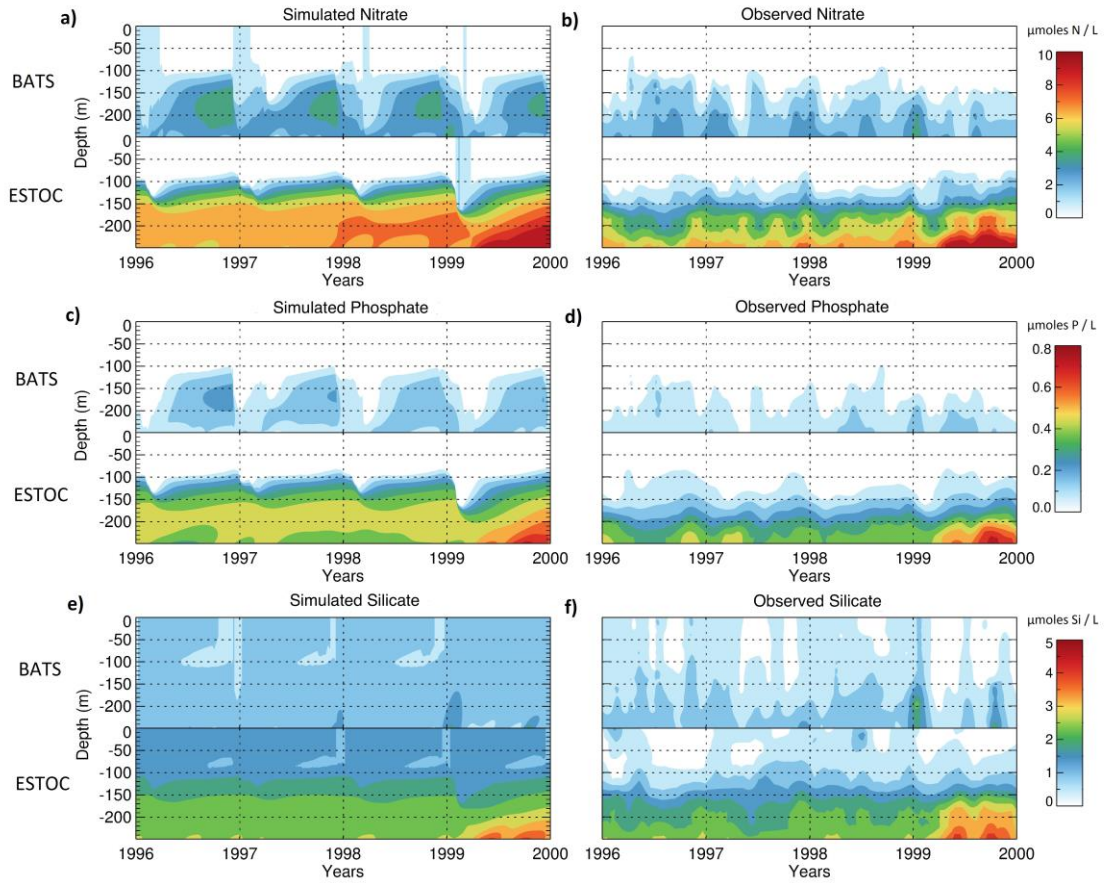

Figure 14) Hovmoller plots of simulated and observed inorganic nutrients (µmoles L^{-1}). Each plot is subdivided into two panels, where the upper panels correspond to BATS, and the lower correspond to ESTOC simulations, respectively, for **a)** simulated nitrate, **b)** observed nitrate, **c)** simulated phosphate, **d)** observed phosphate, **e)** simulated silicate, **f)** observed silicate.

The subtropical gyre of the Sargasso Sea is reported to be severely P-limited (Cavender-Bares *et al.*, 2001; Mather *et al.*, 2008, Lomas *et al.*, 2010a). Phosphate limitation is also evident in the model results. The winter mixed layer at BATS is depleted in phosphorus (< 0.02 µmoles P L^{-1}), whereas nitrate levels remain between 0.5 – 1.5 µmoles P L^{-1}. This

suggests that the phosphorus in the water column becomes completely depleted, leaving the nitrate partly consumed. BATS is also reported to exhibit non-Redfield nutrient ratios (Michaels and Knap, 1996; Cotner *et al.*, 1997), consistently exceeding the N:P ratio of 16 in the upper thermocline. Model results agree with these studies suggesting an average ratio of 24 within the upper 250 m in the water column at BATS. At ESTOC, the modelled ratio was 15.8, very close to the Redfield ratio of 16:1, which is in agreement with the findings of Neuer *et al.* (2002).

3.3.1.3. Carbon export

Simulations suggest enhanced concentrations of slow detritus during the winter/spring bloom periods. Enhanced detritus production continues within the DCM region (~100 m depth) throughout the year. The seasonal distribution of fast sinking detritus follows the pattern of the slow sinking detritus, with pronounced higher concentrations following the winter/spring blooms and removal from the DCM layers throughout the year. Comparison of the in-situ particulate organic carbon (POC) with the model POC (Figure 15) demonstrates that the magnitude and the seasonal patterns are captured by the model. The model results are in agreement with the pronounced peaks in the observed concentrations, with the peaks seen in the upper 100 m, with extensions down below 200 m depth.

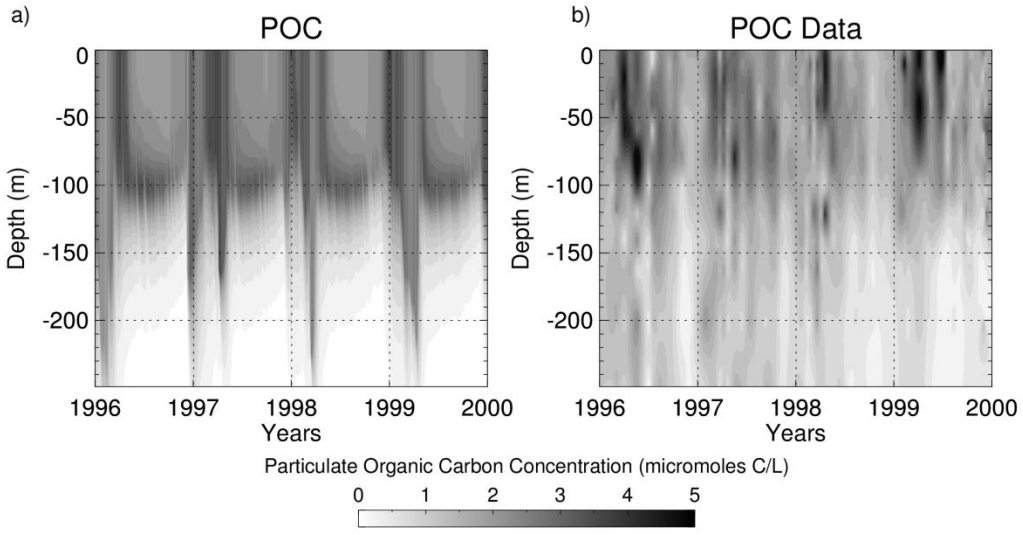

Figure 15) BATS water column POC. **a)** Simulated (upper 250 m shown) and **b)** observed particulate organic carbon values (µmoles C L^{-1}).

Carbon export at BATS showed high seasonality at all depths and the maxima were located in the late winter and early spring periods, and the minima towards the end of summer. Annually averaged organic carbon export at 150 m was 67.39 mg C m^{-2} d^{-1} (ranging from 33.2 to 166.7 mg C m^{-2} d^{-1}), at 200 m was 39.9 mg C m^{-2} d^{-1} (ranging from 18 to 119 mg C m^{-2} d^{-1}), and at 300 m was 17.68 mg C m^{-2} d^{-1} (ranging from 9.42 - 47.74 mg C m^{-2} d^{-1}). When compared with the observed export at BATS (Figure 16a-d, depicted in black solid lines), the model captures the timing of the peaks in export. The second peak simulated in 1997 was not observed in the sediment trap data (shown in grey colored markers in Figure 16) although primary productivity showed an increase during that period (Figure 12b). Simulated averaged carbon flux peaks at ~ 100 m depth. Below that depth, there is an exponential decrease in the export rates (Figure 16e). The periodic increase in export rates due to intense mixing events can be observed even at depths below 200 m, as indicated by the line of maximum export.

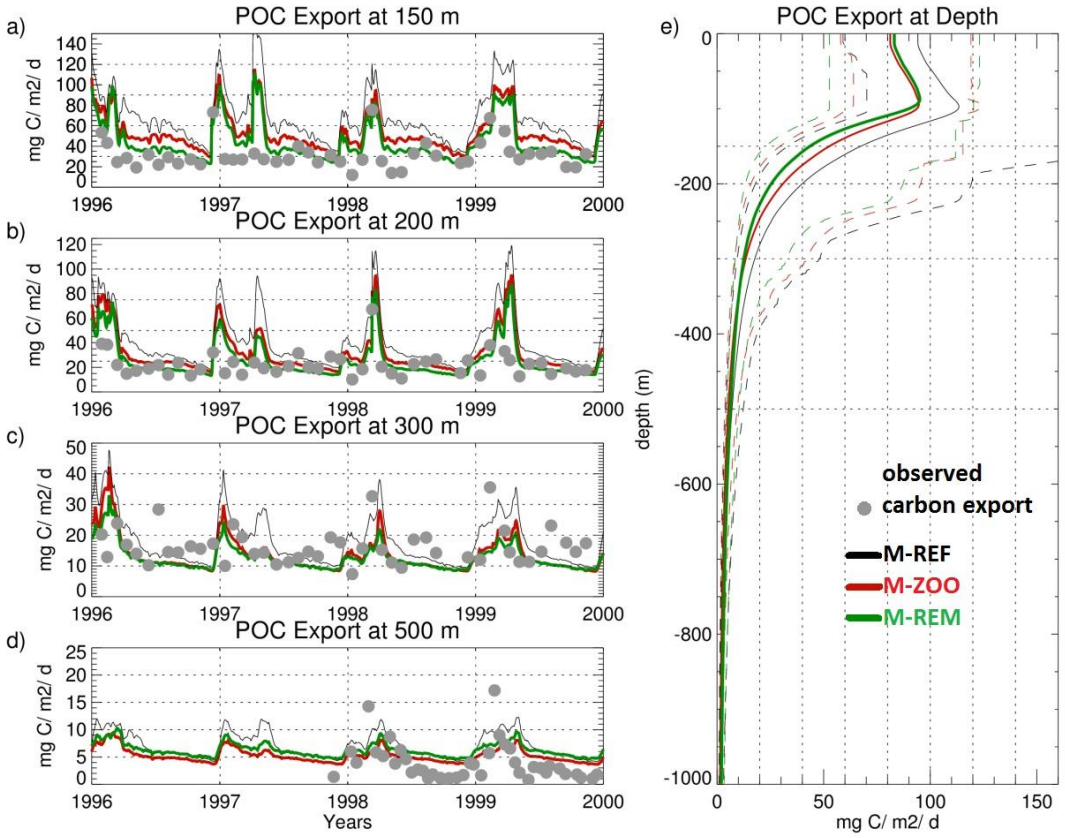

Figure 16) Simulated carbon export at BATS (mg C m^{-2} d^{-1}) at **a)** 150 m **b)** 200 m **c)** 300 m, and **d)** 500 m depth. Grey dots indicate the observed exported carbon from the surface tethered drifting traps for a, b, c, and moored traps at Bermuda (OFP Site) for d. **e)** Simulated averaged (4 years) carbon export at BATS vs depth. Dashed lines indicate the minimum and maximum values of the simulated period for that depth. Black lines are the M-REF simulation results. Red lines indicate the M-ZOO simulations, and the green lines represent the M-REM simulations.

ESTOC simulations yield similar detrital matter distributions to those at BATS. Enhanced slow sinking detritus is seen during winter, with continuous accumulation within the DCM layer (~90 - 100 m). However, as ESTOC is less dynamic, enhanced levels of slow sinking detritus are limited to the upper 150 m depth range. Simulated annually averaged organic carbon export at 150 m was 60 mg C m^{-2} d^{-1} (ranging from 32.3 - 175.65 mg C m^{-2} d^{-1}), at 200 m was 32.67 mg C m^{-2} d^{-1} (ranging from 18.72 - 105 mg C m^{-2} d^{-1}), and at 300 m was 16.5 mg C m^{-2} d^{-1} (ranging from 10.22 - 37.46 mg C m^{-2} d^{-1}). When compared with BATS simulations, the averaged export values are lower at ESTOC. Further analyses of model-data comparisons (Figure 17) show that the model estimations improve in deeper regions. The gap between the model results and the observations decreases to nearly 2-fold at 500 - 600 m depth, and is within the range of the observations (0 – 8 mg C m^{-2} d^{-1}) at 800 - 900 m depth.

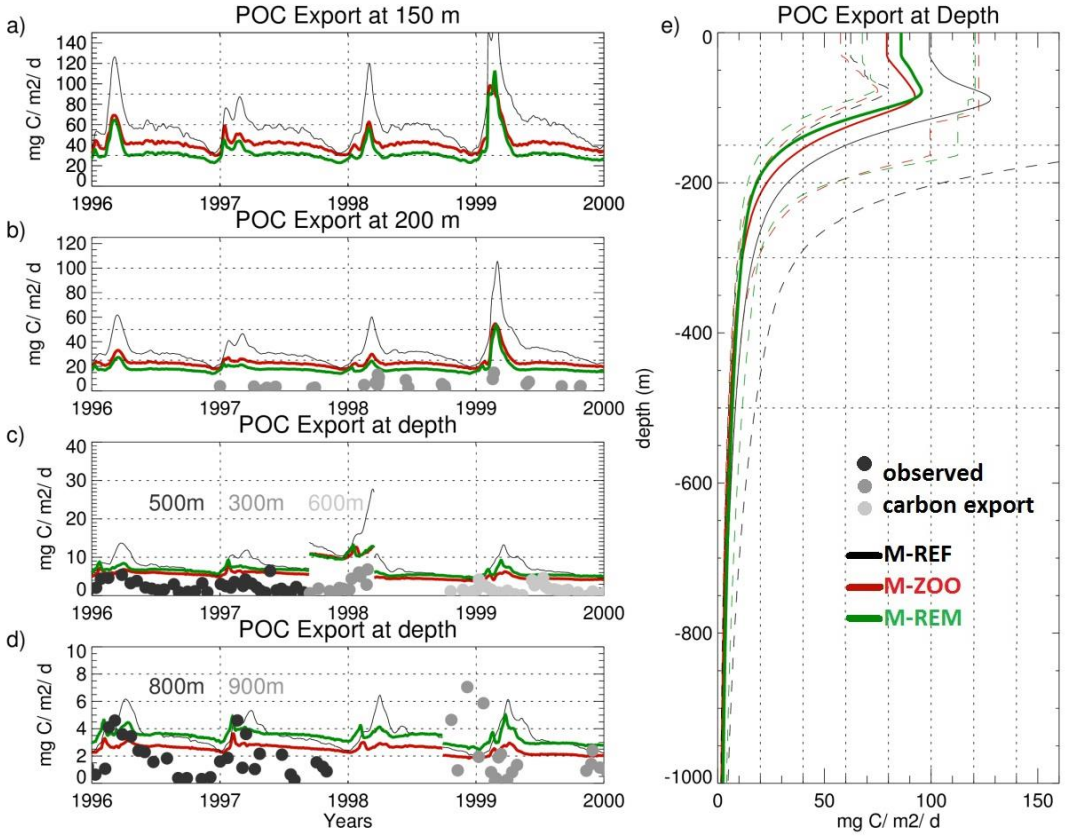

Figure 17) Simulated carbon export at ESTOC (mg C m^{-2} d^{-1}). **a)** 150 m **b)** 200 m **c)** 500-300-600 m **d)** 800-900 m. Grey dots indicate the observed exported carbon from the surface tethered drifting traps for a, and moored traps at ESTOC for b,c, and d. **e)** Simulation averaged (4 years) carbon export at ESTOC vs depth. Dashed lines indicate the minimum and maximum values of the simulated period for that depth. Black lines are the M-REF simulation results. Red lines indicate the M-ZOO simulations, and the green lines represent the M-REM simulations.

Simulated export ratios were calculated by dividing carbon export fluxes at 200 m by the integrated primary productivity (Figure 18). f-ratios are calculated by dividing the total nitrate uptake by the total nitrogen uptake (nitrate + ammonium) from the simulations. Thus, this ratio represents the production as a result of direct input of nitrate from external sources to the EZ (new production). For the calculations, the effect of nitrification was subtracted. The average export ratio of 0.1 (Figure 18a) and an f-ratio of 0.138 was calculated for BATS with the highest values occurring during winter/spring deep mixing events. Values of *f*-ratios as high as 0.5 are reached during these events, implying half of the production was sustained by new nutrient input during these months. At BATS, observed *f*-ratios were 0.06 and 0.059 (Steinberg et al., 2001; Helmke et al., 2010) and modelled were 0.071 (Salihoglu et al., 2008). The export ratio at 200 m at ESTOC was 0.086 (Figure 18b), in comparison to 0.02 reported for ESTOC by Neuer *et al.* (2007). The modelled value is slightly lower than that at BATS (0.1), and the *f*-ratio is 0.122, again slightly lower than BATS (0.138). Neuer *et al.* (2007) reported f-ratios between 0.06 – 0.17 for the 1996 – 2000 period for ESTOC. When export ratios are compared, the BATS export ratio is 15% higher than that at ESTOC, a much smaller difference than the 3-4 fold difference derived from observations (Helmke *et al.*, 2010).

The resulting total annual export at 200 m at BATS was 12.22 g C m^{-2} y^{-1} and 9.86 g C m^{-2} y^{-1} at ESTOC. At both stations, microzooplankton originated sinking carbon (simulated through mortality and unassimilated prey) constituted nearly 60% of the sinking carbon, followed by 10% each originating from both mesozooplankton and pico- nanoeukaryotes at BATS, 14.5 % from mesozooplankton and 9% from pico- nanoeukaryotes at ESTOC. The magnitude and percentage contribution of each algal group also varied by season (Figure 19). This variability was more pronounced at BATS where, although, the annual mean contribution of microzooplankton was 59.5%, seasonally, it ranged between ~ 45 and 70%. At times when there was a decrease in sinking carbon originating from microzooplankton, there was typically an increase in the mesozooplankton contribution at BATS, in agreement with the increased grazing pressure of meso- on microzooplankton. At times of picoeukaryotes and diatom blooms, mainly coinciding with the deepening of the MLD's, both pico- nanoeukaryote and diatom contributions increased to ~15 - 20% of total export. On the contrary, prokaryotic contribution is highest from summer till the end of the year. Their relative contributions are in total as high as ~20%. ESTOC showed less variability in the contribution of different communities. Throughout the 4-year simulation period, their

export contribution was around 60% except during the abnormally productive year of 1999. During this year their contribution decreased down to ~50%, while the mesozooplankton contribution increased to as much as ~30%. Likewise at ESTOC, the prokaryotic contribution was as high as ~20% in summer months and decreased during the bloom periods related to winter convection.

3.3.2. Results from model experiments

In this section, I attempt to investigate the possible mechanisms leading to the differences in export ratios at BATS and ESTOC, and why ESTOC has a much lower observed export ratio compared to its f-ratio. The M-REF simulation was inadequate to represent these differences, and in this section I evaluate additional detritus removal mechanisms to the model.

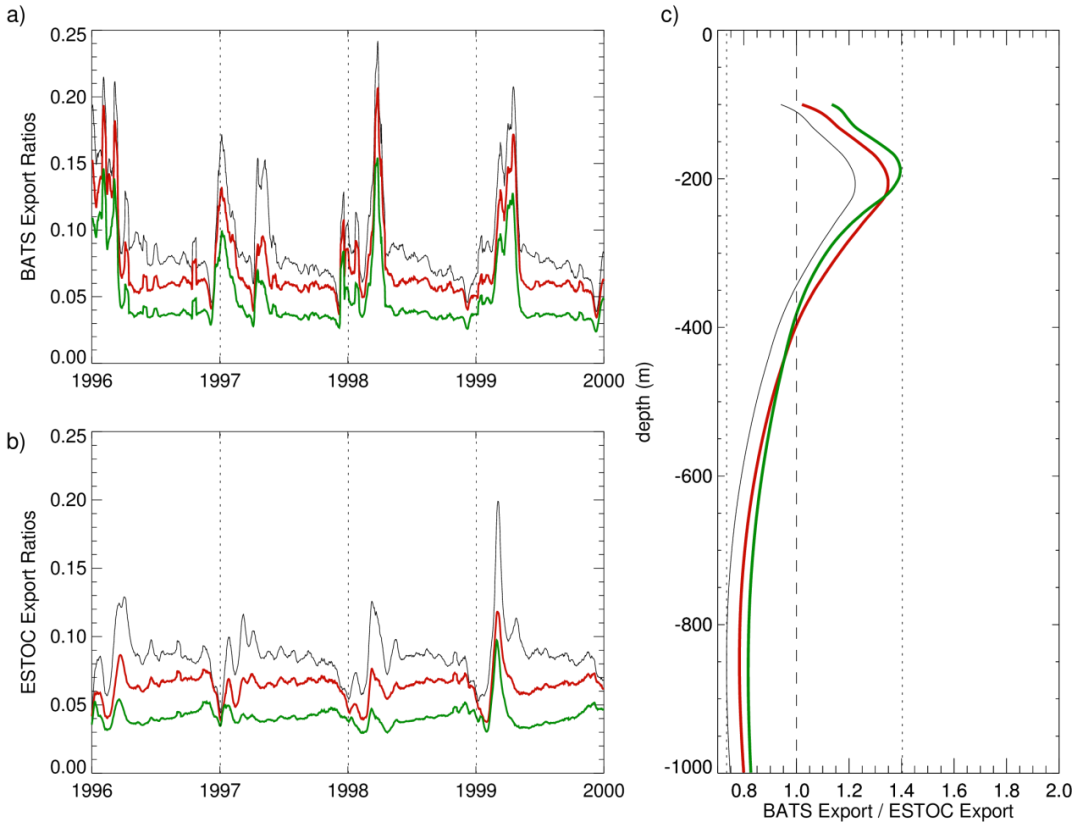

Figure 18) Simulated export ratios (Carbon export at 200 m normalized to the integrated primary productivity **a)** at BATS **b)** at ESTOC **c)** Comparison of the ratios of the export ratios at depth (BATS/ESTOC)). Black lines are the M-REF simulation results. Red lines indicate the M-ZOO simulations, and the green lines represent the M-REM simulations. Dotted lines in c) represent the maximum and minimum ratio of export rates of all simulations. The dashed line denotes the 1-to-1 ratio.

3.3.2.1. Detritus consumption by zooplankton (M-ZOO)

The first sensitivity test considers the role of zooplankton feeding on detritus in moderating export, and whether this process explains discrepancies between simulated and observed export rates in the upper water column. The export rates at all depths at both stations decreased by 25-30% (Figure 16 and Figure **17**). Such a decrease is anticipated because Zdet dominantly consume "DetFast" which is the main sinking carbon below 200 – 300 m resulted in our simulations. In accordance with the decrease in export rates, export ratios dropped by ~20% at BATS (0.072 compared to 0.1) and ~ 25% at ESTOC (0.064 compared to 0.086). Simulated BATS export ratio at 200 m is now within the observed ranges reported as 0.06 and 0.059 (Steinberg *et al.*, 2001; Helmke *et al.*, 2010) and modelled (0.071) values (Salihoglu *et al.*, 2008). Although minor, the ESTOC simulation improved as well, but was still higher than the reported 0.02 export ratio (Neuer *et al.*, 2002). Observed carbon flux during winter/spring bloom periods at BATS was still higher at 150 and 200 m than the observed trap data. When deeper layers are considered, simulated export was within range of the observations, exhibiting pronounced seasonality with higher rates in winter/spring periods. Similarly at ESTOC, winter convective periods resulted in higher export rates. Regardless of seasonality, simulated export rates remained higher than observations throughout the simulation. However, improvements in model performance were attained as the smaller modelled export decreased towards the observed values. Results reveal a difference in the percent changes of export rates of 25 % and 30 %, and export ratios of 20 % and 25 % at BATS and ESTOC respectively. This difference is due to the 10 % decrease in simulated primary production in M-ZOO simulations. Our analyses suggest that additional detritus (DetSlow & DetFast) consumption, and their accumulation in Zdet biomass leads to a lesser extent in the amount remineralized nutrients, therefore slowing down the primary production.

3.3.2.2. Increased bacterial remineralization (M-REM)

The M-ZOO results revealed that the carbon export at both sites is very sensitive to detritus removal by zooplankton. To completely test the sensitivity of the export to heterotrophy, in M-REM simulations, remineralization rates were increased for Slow Detritus. Remineralization rate modifications lead to an increased supply of recycled inorganic

nutrients. PP increased by 18% (15.96 mol C m-2 y-1) at BATS and by 16% (13.26 mol C m-2 y-1) at ESTOC. On the contrary, upper water column export decreased further (green lines in Figure 16 and Figure **17**). Export ratios decreased by 48% to 0.049 (former values of M-REF = 0.1, M-ZOO = 0.072) at BATS and by 52% to 0.042 (former values of M-REF = 0.086, M-ZOO = 0.064) at ESTOC. Although lower in M-REM compared to M-ZOO in the upper layers, carbon flux in the mesopelagic and below (mainly below 500 m) was higher in M-REM simulation (Figure 16d, Figure **17**c, Figure **17**d and Figure **18**c). This shift was due to the slower remineralization rates applied to Fast Detritus (see 3.2.5.3). These changes emphasize the importance of the remineralization used in the model. The introduction of community specific remineralization rates (i.e. labile organic matter production by diatoms (Henson *et al.*, 2012; LeMoigne *et al*, 2012) to the model may provide better representations of seasonal and interannual carbon flux at depth. Both experiments decreased export rates at ESTOC more than at BATS (Figure 18c). The largest changes were seen in the upper layers (<400 m depth). Although the same modifications were applied, ESTOC responded more, thus the ratio between the export rates of the two stations increased. As the retention time of particulate matter at ESTOC was higher (cf. Section 3.4.1), there was a larger decrease in export rates at ESTOC.

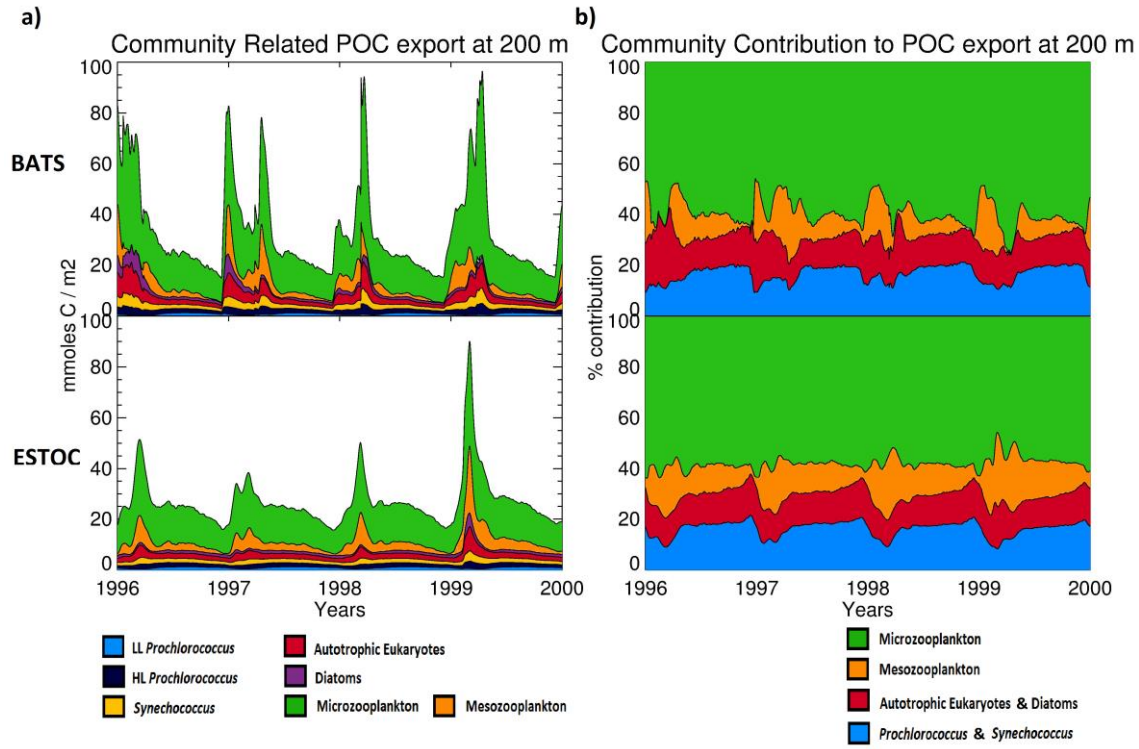

Figure 19) Community contribution to sinking detritus at 200 m depth. Phytoplankton contribute through mortality terms, whereas zooplankton contribute through mortality and unassimilated grazing **a)** (mmoles C m^{-2}). **b)** Percent contribution to detritus at 200 m. Prokaryotes (AG 1 – 3) are merged and depicted in color blue, as well as autotrophic eukaryotes (AG 4 and 5) depicted in red.

The bacterial activity sensitivity to temperature was also mimicked below the EZ. When M-REF, M-ZOO and M-REM simulation BATS / ESTOC export ratios are compared (Figure 18c), both M-REF and M-ZOO simulations follow parallel attenuation curves at depth. At the band between ~ 250 – 450 m depths, M-REM simulation deviates from a similar curve with a lower ratio at this range, and higher at the remaining depths. This occurred due to the temperature differences between the two stations at those depths, which was also hypothesized by Helmke *et al.* (2010). Mesopelagic waters at BATS are under the influence of thick layers (200 – 500 m depth) of mode water of temperature ranging between 17 – 19 ^{o}C. At ESTOC, the water temperature at that depth ranges from 12 – 16 ^{o}C. While particles sink (with a 24 m d^{-1} sinking speed applied) within this depth range, they are more prone to bacterial breakdown at the BATS site, since the applied remineralization rates are temperature dependent (higher temperatures result in higher remineralization). Because the model was modified to have an increased level of remineralization, bacterial breakdown became more eminent compared to M-REF and M-ZOO simulations, in which differences in temperature fueled the bacterial activity and resulted in a relative decrease in BATS export rates at ~ 300 m. These results have important implications for future, warmer oceans.

3.3.3. Carbon flow between the state variables in the model

The carbon flux between each state variable is given in Figure 20. The reader is reminded here that the content of detritus produced by zooplankton was not distinguished, but the total amount produced due to zooplankter activities were given, that the original sources are the individual phytoplankton groups in the model. The results highlight that, with flow of unassimilated prey in addition to mortality, microzooplankton were, thus, the major source of detritus carbon, with a flux of 21.2 mmol C m^{-2} d^{-1} at BATS and 19.0 mmol C m^{-2} d^{-1} at ESTOC. These fluxes were followed by total phytoplankton flux (dominated by pico-nanoeukaryotes) of 6.9 mmol C m^{-2} d^{-1} and 5.9 mmol C m^{-2} d^{-1} respectively mimicking the importance of small phytoplankton contribution to carbon export (see Section 3.1.3 for further details). The reason for such high microzooplankton input to detrtius was due to (1) being the dominant grazer, (2) high mortality rates assigned to zooplankton. Zooplankton mortality is the closure term for the carbon cycle in NAGEM and zooplankton mortality rate was 10 times higher than phytoplankton mortality rate (0.5 vs 0.05 d^{-1}). Such a relatively high mortality rate thus represents all of the sources of carbon from the higher trophic levels

in addition to the zooplankton in NAGEM. Ultimately, this leads to the zooplankton being the major source to the detritus in the model.

The advantage of the modeling study was exploited when comparing the attained differences after an additional diet to zooplankton. With the addition of Z_{det} (detritus consumers) to the model (M-ZOO simulation), a major shift (~5 mmol C m^{-2} d^{-1}) of the carbon pathway from "slow detritus to DOC" to "slow detritus to detritus consumers" was simulated, as a result, separate links were formed from detritus consumers to DOC (excretion) and to mesozooplankton (grazing). In reference to the given carbon export rates and modifications applied (Figure 16 and Figure **17**), these changes were reflected in the decrease of carbon export at 200 m depth. We have also received changes in the N-cycle of the system. NH_4 centered N flow between living and non-living compartments (Figure 20) also indicate major changes. Around 0.5 mmol N m^{-2} d^{-1} extra nitrogen is sent to the NH_4 pool through excretion by detritus feeders. This increase is reflected by the HL *Prochlorococcus*, *Synechococcus* and pico- nanoeukaryote between 10 - 75 %. In the form of carbon, only HL *Prochlorococcus* witnessed a biomass increase (15 - 33%), where pico- nanoeukaryote and diatom biomass for BATS and *Synechococcus* as well for ESTOC experienced a decrease (8 – 22%).

The extent of the community response to the changes in inorganic nutrient availability was further investigated by performing model experiments mimicking the decoupling of C/N/P ratios. The results are listed in detail in (Table 5) The high dependence of *Prochlorococcus*, and partly *Synechococcus* on NH4 dictates a clear response in primary productivity of these algal groups. As the NH4 addition increases, the response of HL *Prochlorococcus* is highest at both stations. The N01 scenario yields an increase of 23% in HL *Prochlorococcus* primary productivity at BATS, and 57.7% at ESTOC. Relatively smaller increases (5.3 – 29.8) in *Synechococcus* and pico- nanoeukaryote primary productivities were simulated. Although heavily dependent on NH4 for growth, LL *Prochlorococcus* did not respond to the NH4 additions. It should be noted that these additions were made from the surface layer, and LL *Prochlorococcus* was more competitive at the bottom of the EZ (Figure 13).

Pico- nanoeukaryotes were also competitive species as defined in NAGEM. This was reflected in their increase in productivity to the NH4 additions, although relatively lower compared to prokaryotic production. Diatoms were negatively affected by the NH4

additions as they require high NO3 and PO4 concentrations for optimal growth. Therefore, they responded by a decrease in primary productivity by ~11 % in the N01 scenario at both stations. Simulations indicated a different picture to the PO4 additions. Both pico-nanoeukaryotes and diatoms were more dependent on PO4 compared to the prokaryotes. Therefore, P additions resulted in increase in pico- nanoeukaryote productivity by 14% and 15% at BAT and ESTOC, and diatom productivity by 20 % and 28 % again at BATS and ESTOC, respectively. In fact, the prokaryote response to P additions was very low (~1 %). Both stations responded similarly to PO4 addition in terms of total production (6.5 – 7 % increase). In the case of NH4 additions, increase in productivity at ESTOC was nearly threefold that at BATS (9.3 vs 29.9 %), suggesting ESTOC's high dependency on inorganic nitrogen.

Table 6) Response of each AG to the addition of NH_4 and PO_4 from the surface layer. PP1-5 indicate the 250 m integrated daily mean primary productivity (mmole C m^{-2} d^{-1}) of AG1-5 respectively. Total PP's indicate the total of the primary productivity of all AG's. "%" indicate the percent change with respect to the M-REF simulation value.

BATS	**M-REF**	**N001**	**%**	**N005**	**%**	**N01**	**%**
PP1	1.41	1.41	0.0	1.41	0.2	1.41	0.7
PP2	7.17	7.35	2.6	7.99	11.6	8.83	23.2
PP3	12.64	12.83	1.5	13.30	5.2	13.76	8.9
PP4	13.31	13.46	1.1	13.77	3.4	14.02	5.3
PP5	1.42	1.40	-1.9	1.33	-6.4	1.27	-10.9
Total PP	35.95	36.45	1.4	37.80	5.2	39.29	9.3
ESTOC	**M-REF**	**N001**	**%**	**N005**	**%**	**N01**	**%**
PP1	1.56	1.55	-0.6	1.54	-1.0	1.54	-0.9
PP2	6.28	6.71	6.8	8.19	30.4	9.90	57.7
PP3	10.96	11.57	5.6	13.24	20.8	14.22	29.8
PP4	11.31	11.86	4.8	13.17	16.4	14.03	24.0
PP5	1.41	1.37	-2.8	1.28	-9.4	1.25	-11.5
Total PP	31.52	33.06	4.9	37.42	18.7	40.95	29.9
BATS	**M-REF**	**P001**	**%**	**P005**	**%**	**P01**	**%**
PP1	1.41	1.40	-0.3	1.40	-0.7	1.39	-1.0
PP2	7.17	7.18	0.3	7.22	0.8	7.26	1.3
PP3	12.64	12.72	0.6	12.79	1.2	12.77	1.0
PP4	13.31	13.65	2.5	14.47	8.7	15.34	15.2
PP5	1.42	1.45	1.6	1.54	8.5	1.72	20.6
Total PP	35.95	36.40	1.3	37.42	4.1	38.47	7.0
ESTOC	**M-REF**	**P001**	**%**	**P005**	**%**	**P01**	**%**
PP1	1.56	1.55	-0.2	1.55	-0.2	1.56	0.0
PP2	6.28	6.27	-0.1	6.30	0.2	6.33	0.7
PP3	10.96	10.91	-0.5	10.86	-0.9	10.98	0.2
PP4	11.31	11.74	3.8	12.53	10.7	12.89	14.0
PP5	1.41	1.48	4.4	1.65	16.7	1.82	28.8
Total PP	31.52	31.95	1.3	32.88	4.3	33.58	6.5

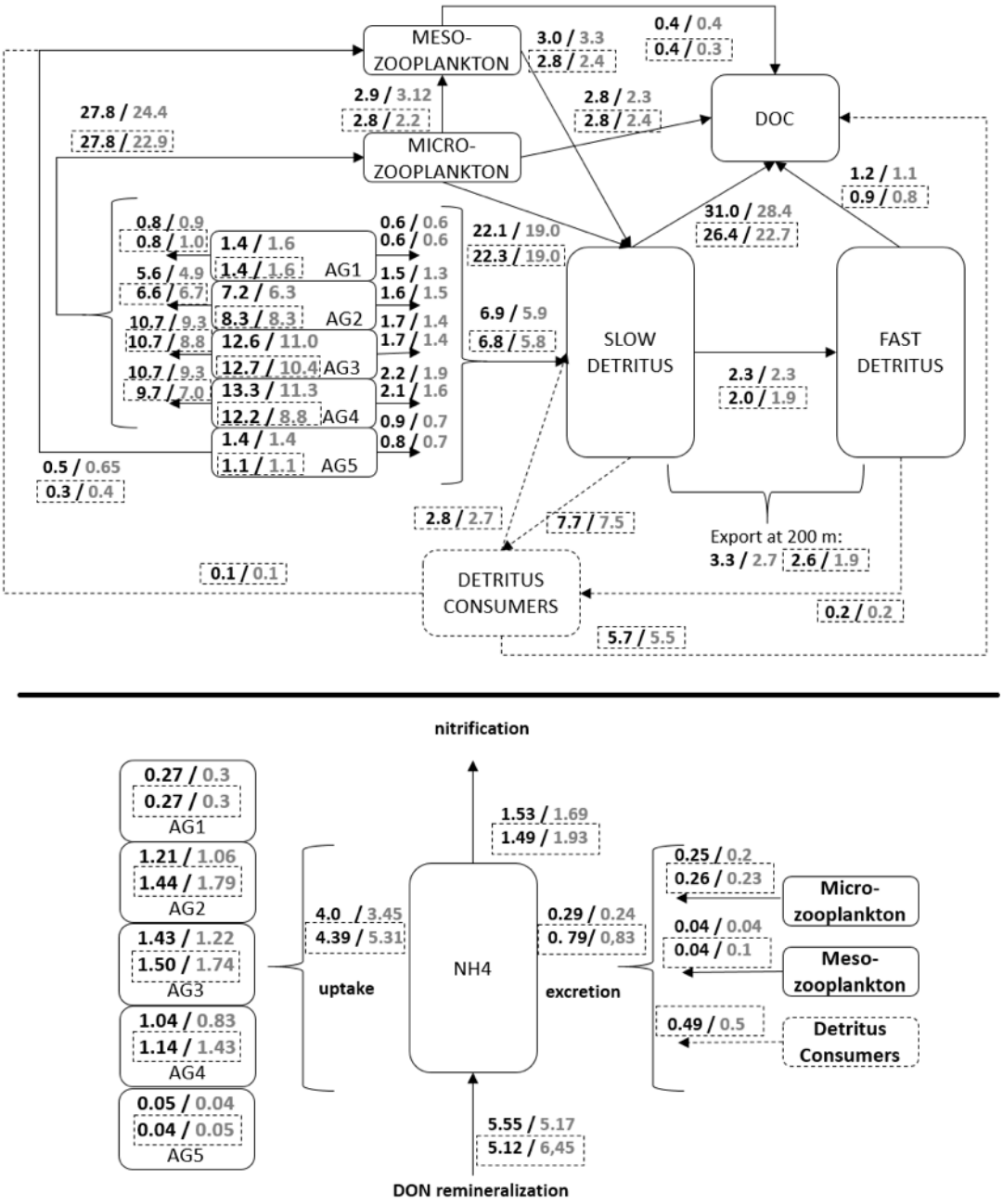

Figure 20) Flowchart of the simulated carbon budget (upper panel) (mmoles C m^{-2} d^{-1}) and gains and sinks for NH_4 (lower panel) (mmoles N m^{-2} d^{-1}) obtained for NAGEM. Arrows indicate the direction of carbon transfer between model compartments. The ecosystem variables are daily averaged over the euphotic zone (0–200 m). The numbers in the algal groups are the mean daily primary production for each AG. Arrows between algal groups and zooplankton compartments and the arrows between microzooplankton, detritus consumers and mesozooplankton compartments indicate net daily grazing. Phytoplankton to slow detritus arrows indicate mortality, and for zooplankton they additionally indicate unassimilated grazing. Arrows between the detritus compartments and the dissolved organic carbon (DOC, which is not tracked in the model) indicate the loss of carbon from the detritus compartments by remineralization. The link between the zooplankton and the DOC are the excretion rates. From Slow to Fast detritus, the link is the aggregation rate. The gain terms for NH_4 are excretion from zooplankton and remineralization from DON. The loss terms are the uptake of phytoplankton and nitrification to NO_3. For both of the panels, the state variables, arrows and fluxes given in dashed lines represent the M-ZOO scenario. Flux values given in black denote BATS fluxes, and the ones in gray are the ESTOC fluxes.

3.3.4. The model performance and statistics

In order to analyze the magnitude, timing and drivers of carbon export and attenuation, the model has to be successful in representing the productivity of algal groups and their community composition and concentration levels of all the compartments. These are the key elements in the production of particulate organic matter, which in turn drive the carbon export. Modelled depth integrated annual mean primary productivity agree well with reported observations (see Section 3.3.1.1), and reproduces observed high productivity values in winter and early spring at both stations. Occasional multiple blooms (BATS winter 1998 and 1999) and abnormal highs in primary productivity (ESTOC winter 1999) were successfully captured (Figure 12a and b).

The simulations also show discrepancies from the observations once the comparisons were scaled down to specific time periods. For example, at BATS, the model skill is poorer in capturing the increases in productivity during late spring and summer months (Figure 12a and b). Observations also show increases in production in late spring and summer months which the model fails to reproduce. These discrepancies may be a result of the underrepresentation of the mesoscale structure, which was reported to be important at BATS (Cianca *et al.*, 2007; Helmke *et al*, 2010), where simulations point to a higher correlation between the primary productivity and winter convection at both sites. This may be due to winter convection, and in turn the supply of nutrients from below is captured by the model, but the mesoscale eddy induced supply of nutrients in summer months may not have been resolved due to the low resolution (30 days) of the physical forcing data. In the case of ESTOC simulations, it has been reported that the eddy fueled primary production is less compared to that at BATS (Cianca *et al.*, 2007) and winter convection is the main nutrient source for primary producers. Thus, these results support the conclusion that the model can better perform when high variability events (e.g. eddies) are of lesser importance in estimating the timing and the magnitude of production (Figure 12c and d). The model performance could be improved with higher resolution physical forcing.

The reference model export at 200 m during bloom periods was nearly twice the observed values (~30 – 50 vs ~ 80 – 120 mg C m^{-2} d^{-1}) as shown in Figure 16, but the 300 m results were very close to the reported values (mean value of 16.3 mg C m^{-2} d^{-1}) at BATS. It should be noted that 200 m depth lies within the estimated MLD's for our simulations. As the model

homogeneously distributes state variables within the MLD, overestimation of export rates within the lower reaches of the mixed layer is anticipated. High peaks in POC flux correlating with the periods where convective mixing exceeds the trap depth is a known issue (Steinberg *et al.*, 2001). High peaks in export corresponding to deep convective mixing events and have been recorded during recent studies at BATS (Owens *et al*, 2013). Overall at 300 m, the model's skill in describing export rates is high. The model represents BATS export rates at 500 m well, although slightly overestimates the export during summer periods for the years 1998 and 1999. On the contrary, the reported values of export at ESTOC (Helmke *et al.*, 2010) show distinct differences in export with depth, such that at 200 m export was 4.5 mg C m^{-2} d^{-1} and at 300 m export was 3.0 mg C m^{-2} d^{-1} on average, whereas the model estimates 20 – 30 mg C m^{-2} d^{-1} at 200 m and 10 – 15 mg C m^{-2} d^{-1} at 300 m for M-REF, M-ZOO and M-REM, although results get relatively better in the latter two simulations.

The slightly higher than previously reported *f*-ratios at BATS (see Section 3.3.1.3) could partly be due to the depth of export ratio calculations, such that 200 m depth can stay within the MLD's for the BATS simulations. When the export ratio from 250 m depth was calculated, on average, the resulting ratio was 0.061 which is within the range of reported values. When export ratios were compared, the BATS export ratio is 15% higher than at ESTOC, a much smaller difference than the 3-4 fold difference derived from observations (Helmke *et al.*, 2010). Considering these, the gap between the observed and simulated export at ESTOC suggests that there are mechanisms yet to be represented in the model formulation.

The reference model (M-REF) and the modified version's (M-ZOO & M-REM) results were evaluated statistically with their standard deviations normalized to observation's standard deviations (NSTD), correlation coefficients (r) and percent biases from the observations. These statistics are summarized in Figure 21 using a Taylor diagram (Taylor, 2001). Most of the assessed model outputs were significantly correlated to the observations. The weaker correlations ($0.2 < r < 0.5$) were seen in BATS export at 300 m and ESTOC export at 500 – 900 m. Upper layer export (200 m) correlations for both stations ranged from 0.5-0.7 indicating the response of carbon export to upper layer dynamics such as mixing and productivity. Regarding chlorophyll a, primary productivity and nutrient concentration, for both of the stations, model-data correlations are >0.5, suggesting a successful representation of the observed data. Regarding the standard deviations, variability in primary productivity

and chlorophyll a concentrations at BATS were underestimated with a lower than normalized standard deviation of 1, but still higher than 0.5. Similar results were seen in ESTOC primary productivity, but chlorophyll a standard deviations were close to 1. Although highly correlated, variability in nutrient concentrations were overestimated for both of the stations (norm. std > 1).

The Taylor diagram makes it easy to compare the relative performance of the different simulations. Results show that there are improvements in carbon export at BATS at 150 – 200 m in M-ZOO and M-REM. The normalized standard deviation of export at 150 m export reached nearly 1, and at 200 m to 1.25 - 1.5. Export at BATS at 300 m export showed a reduced response to the variability with the changes. Although not in the range of the diagram, ESTOC export at 200 m variability improved with decreased NSTD's from 4.15 to 1.95 switchin from M-REF to M-ZOO and M-REM. These finding indicate that the increased recycling at both stations had positive effects on the export simulation in the upper layers. The NSTD's were reduced with the modifications (decreased from 1.5 to 0.75) at ESTOC at 500 – 600 m, but relatively improved getting closer to NSTD=1 in M-ZOO and M-REM. The export at 800 – 900 m at ESTOC decreased in variability (NSTD's 0.24 and 0.29) after M-ZOO and M-REM application. For both stations, simulations exhibited weak variability in silicate levels, although silicate at ESTOC was highly correlated with the observations. This lack of response in silicate concentrations and diatom dynamics were mentioned in Section 3.3.1.2. The percent biases (% differences from the observed mean values) were also represented in the diagram. Overall, export rates near the surface (150 – 200 m) are still higher than observations. Slight improvements were seen in BATS 300 m export. As mentioned in the text, high biases in ESTOC export are represented here as well. Overall, the model performance is good in the upper water column with significant correlations and similar variability to the observations. Further improvements are necessary however to simulate the carbon export dynamics.

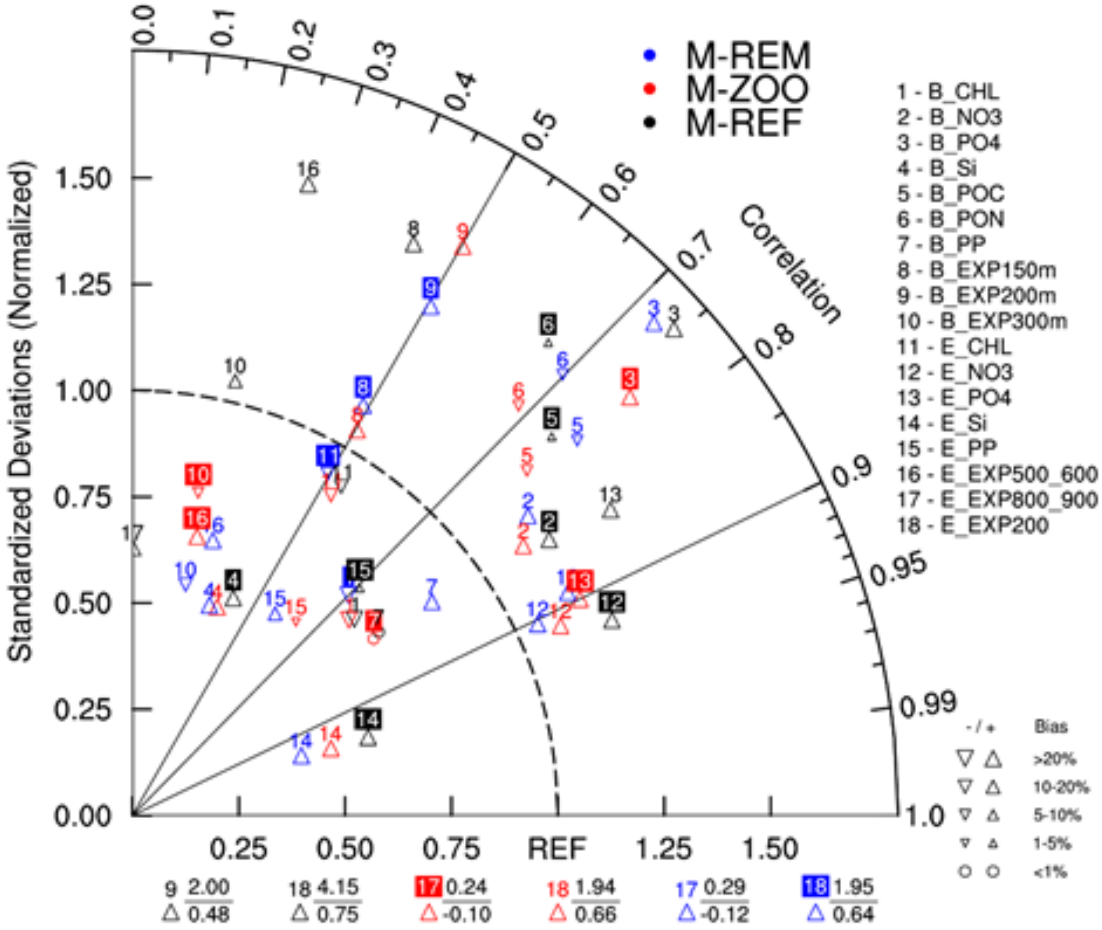

Figure 21) Model statistics shown on a Taylor diagram. The x- and y-axis denote the standard deviations of the model data normalized to standard deviations of the observed data. The REF on the x-axis is the observed data standard deviation. The radial axis represents the model data to observed data correlation coefficients (r). Statistically, the success of model in representing the observations increases towards the REF point on the x-axis, with 1-to-1 standard deviation and with the r equal to 1. Percent biases are also represented with triangles. Upper triangles indicate that model has a positive bias, and down triangles indicate negative bias. The percent intervals are represented with the triangle size. Model data standard deviations outside the x- and y-axis range are shown below the diagram. Black marks represent the M-REF, red marks represent the M-ZOO and blue marks represent the M-REM simulations. The evaluated state variables are represented by numbers on the plot, where B and E initials stand for BATS and ESTOC respectively.

3.4.Discussions

A 4-year (1996-2000) hindcast of the lower trophic ecosystem dynamics and the resulting export rates at BATS and ESTOC stations in the Subtropical North Atlantic was performed. The modeling suite presented here was successful in representing the ecosystems at both stations from physical background to nutrient dynamics to productivity. Model result of community composition agreed with the BATS observations, however seasonally resolved

observations of community composition are lacking at ESTOC. The model successfully provided the tools to understand the insights of the processes leading to production and export, and additional detritus consumption mechanisms lead to decreases in export at both stations, effecting ESTOC export relatively more than BATS export. In this section, the possible mechanisms leading to such de-coupling in carbon export between these stations, and exploit the use and effect of community structure on export rates is discussed.

3.4.1. Mixing, productivity and export

Simulations help to elucidate the extent to which the upward transfer of nutrients due to vertical mixing drives the seasonal cycle of productivity. The response to mixing (forced by homogenous mixing and increased diffusivity within MLD) is seen within the chlorophyll *a* (Figure 10a and c), plankton functional type (Figure 13), and inorganic nutrient (Figure 14) concentrations. As the inorganic nutrient concentrations increase in the EZ, productivity increases in winter/spring periods (Figure 12), which is in turn reflected in the carbon export rates (Figure 16 and Figure 17). High correlation is hence expected between the depth of the mixed layer and primary production (0.66 and 0.73 at BATS and ESTOC respectively). Likewise, high correlation between primary production and export rates at 200 m is also expected. The highest correlation (0.72) was found on applying an 11 day time lag to the model export data at BATS, similar to findings (1 week lag) in Steinberg *et al.* (2001). Steinberg *et al.* (2001) assumed particle sinking rates of 50-100 m d^{-1} (our model assumes sinking rate of 24 m d^{-1}), and estimated a 1-week lag for the POC to reach trap depths. At ESTOC the highest correlation between the model primary productivity and the POC flux (0,9) was obtained after applying a 17 day time lag. The time lag between production and export is directly influenced by the sinking speeds (5-24 m d^{-1}) applied in the model. At these sinking speeds, carbon is expected to reach 200 m within 11 - 17 days. A 6 day time – difference in the export lag between BATS and ESTOC can also be explained by ESTOCS's shallower MLD's. The average annual maximum MLD at BATS was ~ 200 m and at ESTOC ~ 120 m. Away from the influence of direct mixing, cross correlations between the MLD's and the export rates (at 300 m) are 0.86 (lag of 17 days) and 0.84 (lag of 31 days) for BATS and ESTOC respectively. This highlights the importance of the shallower MLD's (due to the less dynamic regime) at ESTOC, which results in a prolonged settling duration of organic carbon in the upper layers. This has important implications for the recycling of matter, as discussed in detail in the following sections.

Both BATS and ESTOC are scarce in inorganic nutrients within the EZ. Productivity is thus dependent on nutrient input from the deeper layers. The relationship between the intensity of mixing, primary productivity and export rates is evident when timing and magnitude of the positive anomalies in export rates and productivities are compared with the deep mixing (MLD deeper than EZ depth) events, where increased pulses of integrated primary productivity and export rates are related to the deep mixing events (Figure 22). The intensity of mixing is represented here by the difference between the MLD and the EZ depth. The higher the difference, the more readily available nutrients will be mixed into the EZ, sustaining new production. At both stations each intense mixing period is accompanied by a positive anomaly in primary productivity (Figure 22). At ESTOC and during 1997 at BATS, positive export anomalies at 200 m follow positive anomalies in primary productivity with the lags mentioned above. The higher lag time at ESTOC (17 days vs 11 days at BATS) is also visible in Figure 22. For the years 1996, 1998 and 1999 at BATS, intense mixing is accompanied by positive anomalies in export rates, whose timing exactly matches each other. Those are the years when MLD exceeds 200 m, the point of flux estimations, and when export ratios at BATS (Figure 18) were 1.5-2 fold that of the year 1997. The implications of this are two fold, (1) productivity and export rate anomalies follow intense mixing periods, with the peak in export rates showing relative lags, (2) if the mixing is intense enough to exceed the depth of flux recording, export rate anomalies will be in phase with the mixing period. This indicates a mechanism where organic carbon is flushed out of the EZ due to deep mixing within the days of production regardless of the magnitude of the production, much faster compared to the time lags of (11-17 days) mentioned above. This has major impacts on the productivity and export dynamics of both stations. Figure 12 indicates the dynamic nature of BATS, with more intense mixing events. Over the 4-year simulation period, the total number of days where the MLD exceeded the EZ depth was 236 days at BATS and 90 days at ESTOC, a difference of nearly 250%. Hence, although the background inorganic nutrient concentrations at ESTOC are nearly double that at BATS (Figure 3 and Figure **4**), BATS can sustain similar annual productivity to ESTOC due to the enhanced upward transfer of nutrients into the EZ. Cianca *et al.* (2007) attribute this to greater eddy activity at BATS resulting in more nutrients available for new production, with ESTOC receiving 75% of that received at BATS. The deeper mixing at BATS enhances POC export with much faster sinking velocity (> 200 m d^{-1}), showing seasonal peaks in export rates. Even though more dynamic physics at BATS and slower sinking mechanism explains the timing and magnitude in export upto an extent, the model is still not capable of capturing the observed 3 - 4 fold (Helmke *et al.*, 2010; Neuer *et al.*, 2002) difference in export rates.

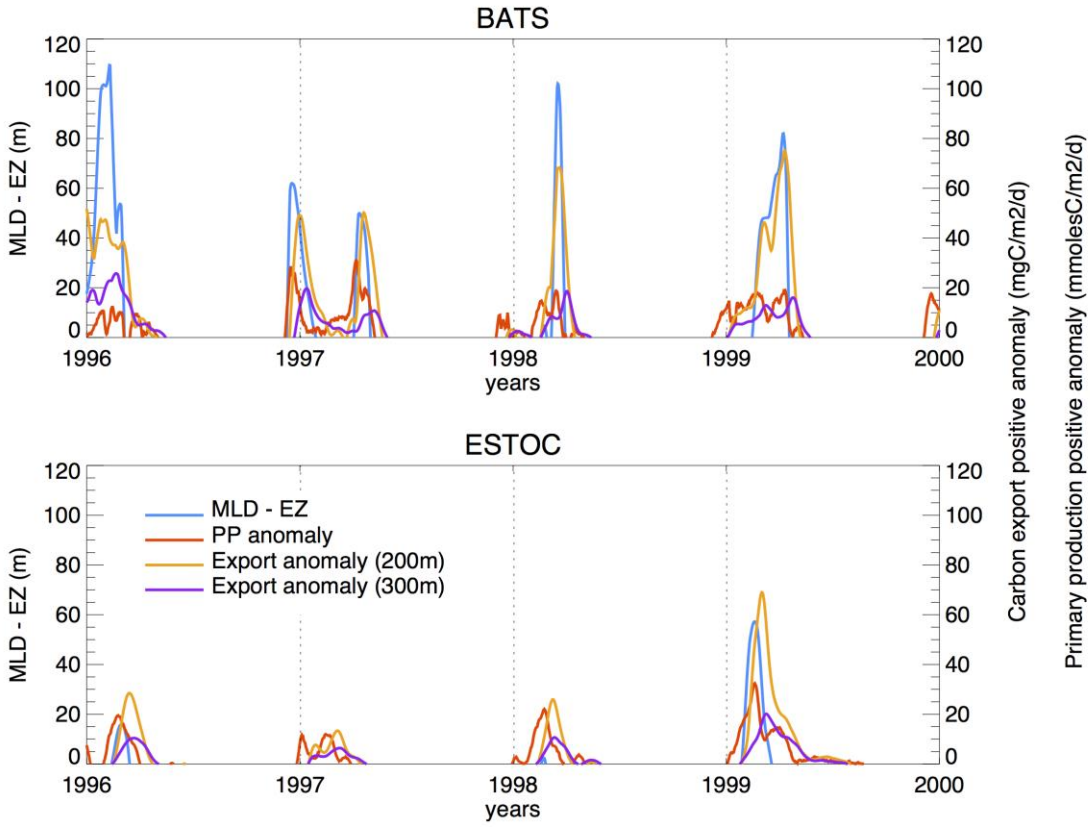

Figure 22) Comparison of MLD, export and productivity **a)** BATS and **b)** ESTOC simulations. Black lines denote the MLD difference from the EZ depth (MLD - EZdepth). Blue lines denote the positive anomalies in export rates (μgr L^{-1} d^{-1}) at 200 m and red lines at 300 m. Green lines denote the integrated primary productivity positive anomalies (μmoles C L^{-1} d^{-1}).

To understand how the relatively dynamic physical conditions at BATS impacts productivity and export rates, modelled and observed new production were compared, estimated from nitrate uptake. The remaining N-uptake (ammonium uptake) was considered as the regenerated production, as the sources of ammonium in the model derive from the remineralized organic matter (POM & DOM) and excretion of zooplankton. According to the M-REF simulations, new production at BATS was 0.69 moles N m^{-2} y^{-1} and 0.465 moles N m^{-2} y^{-1} at ESTOC (hence new production at ESTOC is ~33% less than at BATS). BATS results are in agreement with the literature. Experimental, modeling and remote sensing studies suggest new production ranges between 0.39 - 0.7 moles N m^{-2} y^{-1} (with ~ 0.15 moles N m^{-2} y^{-1} average uncertainty) at BATS (Jenkins and Goldman, 1985; Spitzer and Jenkins, 1989; Jenkins, 1998; Siegel *et al.*, 1999; McGillicuddy *et al.*, 2003), whereas Neuer *et al.* (2007) report an average of 0.24 moles N m^{-2} y^{-1} for ESTOC for the 1994 – 2000 period (C based new production is converted to N with a C/N ratio of 6.6).

Although simulations demonstrate the strong relationship between vertical mixing, the supply of nutrients to the upper layers, and primary productivity, our physical forcing was mainly limited to the mixing within the MLD. The secondary physical force was the vertical diffusivity. The low temporal resolution (monthly) of the temperature observations means mesoscale features (having a time scale of days) are not fully represented by the model, as the model uses observed temperatures to estimate MLDs. The importance of mesoscale activity in supplying nutrients to the EZ has been highlighted by various studies (McGillicuddy *et al.*, 1998; Siegel *et al.*, 1999; McGillicuddy *et al.*, 2003; Cianca *et al.*, 2007). On the contrary, Oschlies *et al.* (2000) demonstrate the importance of convective mixing in winter by using an eddy-permitting model, and Oschlies (2002) support this result further and suggest horizontal injections of nutrients are secondary to vertical processes. Processes potentially leading to the supply of nutrients through horizontal processes include Ekman transport (Williams and Follows, 1998), atmospheric deposition (Prospero *et al.*, 1996), and nitrogen fixation (Capone *et al.*, 2005). Atmospheric deposition at BATS were represented in our model. A high constant diffusivity coefficient was used to represent diffusive transport throughout the simulation period (see Section 3.2.2 for the vertical diffusion forcing). This by default leads to underrepresentation of the variability in turbulence dynamics, and in turn the nutrient pulses to the EZ. Our additional approach was to force the model nutrient concentrations at 250 m directly from the observations at both stations. Thus, our model represents the variability in background nutrient levels and the influence of the mesoscale activity is partly represented by the nutrient observations. These two approaches can be inconclusive if the sampling frequency was inadequate to capture shifts in eddy structure, which may well be possible considering the monthly sample collection frequency. Considering the successful representation of the primary productivity at both sites, our model suggest that convective mixing is the main source of nutrients in the EZ.

3.4.2. Controls of detritus grazing and recycling on carbon export

Helmke *et al.* (2010) pointed out the importance of investigating the retention efficiency and remineralization time scales. Our M-REF results showed that the primary productivities and carbon export rates at both stations were similar in magnitude as shown in Section 3.3.1.1 and 3.3.1.3. The importance of mesopelagic consumers on the utilization of the primary and export production was addressed by Banse (1990), Ducklow *et al.* (2001) and Steinberg *et al.* (2008). The grazers may cause changes in the exponent in the Martin decay function

(Martin *et al.*, 1987) of organic matter by consuming smaller sinking or suspended particles and producing dense and faster sinking fecal pellets. Our model at this stage does not distinguish dense fecal pellet formation. Faster sinking particles are formed through aggregation of the slow sinking particles. In the M-REF simulations, BATS export ratios (at 200 m) were only ~7% difference higher that at ESTOC, hence, the reference simulation did not resolve the processes leading to the observed difference in export efficiency between BATS and ESTOC. The M-ZOO simulations showed a 13% higher export ratio at BATS. This number increased to 17% with the additional recycling in the M-REM simulations. It should be noted that although the modelled differences between the two stations are still relatively low compared to observations, the modifications made to the model for the M-ZOO and M-REM simulations resulted in a significant decline in export ratios at both stations (20% at BATS and 25% at ESTOC in the M-ZOO simulation and 48% at BATS and 52% at ESTOC in the M-REM simulation).

These results demonstrate the importance of the recycling mechanisms at these two stations, and point to the control of micrograzing and bacterial pressure on the export of organic matter. It is vital to understand the underlying mechanisms in the mesopelagic and the implications of the variability and the long term permanent changes in climate. For instance, Lomas *et al.* (2010b) emphasized that the Sargasso Sea ecosystem is not as static as it has been thought. During the 1996 – 2007 period, they reported an increase in integrated autotrophic biomass, primary production, POC export at 150 m and prokaryotic phytoplankton. Steinberg *et al.* (2012) also report an increase in mesozooplankton biomass during 1994 – 2010. Interestingly, the increase in 150 m export was not reflected in export at 300 m (Lomas *et al.*, 2010b), indicating the doubling of carbon attenuation in the mesopelagic, along with the increase in apparent oxygen utilization (AOU). Steinberg *et al.* (2008) addressed the changes in AOU and hypothesized that increased attenuation may be related to the plankton community composition and metabolic activities. They also suggest that the shift in the North Atlantic Oscillation from positive to neutral may have played a role in triggering increased productivities due to the increase in deep mixing frequencies. These findings address the need for the model to estimate the changes in the ecosystem structure with respect to possible future environmental pressures.

An interesting result of the detritus consumer addition (M-ZOO) was the change in flow paths of detritus (see Section 3.3.3). Due to the major carbon flow shift from “slow detritus to DOC” to “slow detritus to detritus consumers”, some of the carbon is not actually

converted to the dissolved organic form, but is stored in the particulate form inside the zooplankton biomass. It is counterintuitive that the addition of detritus feeders did not increase recycling in terms of carbon. However, increased nitrogen flow to the NH_4 pool (Figure 20b) indicates an increased recycling of nitrogen, decoupled from carbon flow. This resulted in a minor increase in prokaryotic and minor decrease in eukaryotic production. The reasoning of the prokaryotic response lies in the predefined nutrient quotas and excretion flow in the model. By definition in NAGEM, zooplankton carbon excretion is directly converted to DOC. However, 50% of the nitrogen excretion is converted to DON, and the remaining 50% is directly converted to NH_4. In fact, an increase of ~3 times in the total excretion flux to NH_4 was simulated. Since the prokaryotes (especially *Prochlorococcus*) are heavily dependent on NH_4 and less on PO_4 for growth, additional source of nitrogen promoted prokaryotic production, and caused a decrease in eukaryotic (AG 4 and 5) production.

These modifications did not have a major impact on the total productivity of the system. However, with the addition of the detritus consumers, we were able to quantify the effect of N recycling through an additional model state variable, and its impact to the community structure. Through zooplankton feeding and excretion, N was further decoupled from C from the "Detritus" form to DIN form. With the M-ZOO simulations, zooplankton excretion was the source of the changes in C/N partitioning compared to the M-REF simulations. However, there may as well be other perturbations that may deviate the marine systems from their current C/N/P dynamics, which emphasize the importance of C/N/P decoupling between the trophic levels. If the impact of global warming, increase in water column stability and the changes in community structure on carbon export in future predictions to be represented correctly, such details in model structures may play a vital role in future predictions.

Following the results of M-ZOO simulations and the response of prokaryotes to the additional NH_4 source (see Section 3.3.3), the importance of C/N/P decoupling was mimicked further with the nutrient addition sensitivity analyses. Unequal response of the two sites' primary productivity and community compositions to N and P additions emphasize the importance of defining detailed structures in the global models to predict spatial and temporal responses to external sources such as increasing atmospheric depositions of N and P due to anthropogenic activities (Prospero *et al.*, 1996; Duce *et al.*, 2008; Zamora *et al.*, 2013), dust depositions (Neuer *et al.*, 2004), N-fixation (Hansell *et al.*,

2004; Capone *et al.*, 2005) and even further adding detail to the model by representing iron dynamics to represent the response to iron addition (Okin *et al.*, 2011). Together with the internal sources discussed in Section 3.4.1, representing the ecosystem responses in community levels in terms of production and export discussed in Section 3.4.3, global models may better predict temporal and spatial dynamics of the global carbon cycle.

3.4.3. Effect of plankton community on carbon export

The observed variability in dominant phytoplankton groups were successfully represented by our simulations (see Section 3.3.1.1). Phytoplankton functional type seasonal and spatial distributions in the simulations revealed that they have implications on the magnitude and variability of the carbon export. It was recently understood that the herbivorous and the microbial food web is tightly coupled. Traditionally thought to be lost in recycling (Pomeroy, 1974; Azam *et al.*, 1983), Richardson and Jackson (2007) showed that the contribution of picoplankton to export at depth was proportional to their production, demonstrating the importance of aggregation. In fact, Lomas and Moran (2011) found pigments associated with pico- and nanoplankton in the sediment traps at depths between 150 m and 300 m. They estimated for BATS that *Synechococcus*, *Prochlorococcus* and nano-eukaryotes aggregates contributed 2–13% (5±4%), 1–20% (5±7%), and 6–43% (23±14%) of the total POC export flux measured by sediment traps, respectively, which were likely to be exported through gravitational settling of aggregates. As for the gravitational settling, both Brew *et al.* (2009) and Lomas and Moran (2011) give physical aggregation and settling, zooplankton grazing on aggregates and fecal pellet formation, and/or interaction between free cells and settling aggregates/fecal pellets as the possible mechanisms. The community separation, and the presence of detritus aggregation in our model becomes very useful at this point. The partitioning of the planktonic biomass is reflected in the transfer of carbon to detritus that is exported out of the EZ. We have shown the percentage contribution of each plankton group to detritus at 200 m (Section 3.3.1.3). Regarding the variability in the contribution of different communities to export, our results have shown that the eukaryotic contribution is greater during winter/spring months, and the prokaryotic contribution is greater in summer/fall. The effect of the aggregation of slow sinking particles (formed by mortality of plankton and unassimilated grazing) to form fast sinking detritus is clearly seen in Figure 19. Even at 200 m, the contribution of prokaryotes to sinking detritus (~20%) is mostly the aggregated fast detritus that settled from the upper layers (0 - 100 m). These results are in agreement with the ranges given in Lomas and

Moran (2011), and highlight the importance of the picoplankton contribution to export as mentioned in Richardson and Jackson (2007). Above all, it is striking to observe in the model data that the microzooplankton contribution to sinking particulate matter reached values as high as ~70%, a significant value which shows the indirect contribution of picoplankton through grazing and in turn aggregation to particle export.

3.5. Conclusions

Initially, the productivity and the resulting anomalies can be partly controlled by the difference in physical structure of both sites was hypothesized, as was pointed out by Helmke *et al*. (2010). In all of the simulations (M-REF, M-ZOO and M-REM), BATS showed more variability in production and export compared to ESTOC. The anomalies in mixing, productivity and export were related, and the strength of the physical forcing and the settling and recycling time scales were quatified. Deep mixing events lead to the enhanced supply of inorganic nutrients which trigger high productivity and biomass/POM formation, and in turn export production. It is also the physical dynamics in connection with nutrient dynamics that lead to the variability in community composition. BATS with its stronger hydrodynamic forcing could transfer particles out of the EZ faster than ESTOC, whereas at ESTOC, the less dynamic nature lead to the increased retention times in particle settling and enhanced recycling. The observed differences in export ratios between BATS and ESTOC can be partially attributed to the different physical regimes. To pursue our initial hypothesis further, pathways to increase this difference were introduced with (1) increasing recycling through detritus feeding by zooplankton (M-ZOO simulation) and (2) increasing bacterial remineralization effect (M-REM simulation). Both stations responded, such that export ratios at BATS and ESTOC nearly halved, and as a result BATS' export ratio became 17% higher than ESTOC, pointing out the importance of the physics and the recycling mechanism at both sites maintaining particle export. This difference was 7% before the additions emphasizing that removal mechanisms are more effective at ESTOC due to its stable water column structure.

The inclusion of separate algal communities in the model mimicked their contribution to export, and their role in defining the strength and timing of the realized export rates. Different responses of the algal communities to physics and the environmental limitations revealed that community specific carbon export algorithms may introduce seasonal to interannual variabilities to export which may have been missed by simpler modelling

approaches. Prokaryotes and pico- nanoeukaryotes each contributed to carbon export as much as 20%. Our sensitivity analyses showed the importance of detritus grazing and bacterial remineralization on export rates. Stable water column and longer residence times at ESTOC enhanced the recycling pressure applied through detritus consumers and increased bacterial remineralization, such that ESTOC detritus was removed by 10 % more compared to BATS, although the same configuration was applied. A decline in in export ratios up to ~50% through combined detritus consumption by zooplankton and increased bacterial activities proved how sensitive these two stations are to recycling processes.

The experiments yield various responses of the community structure to separate additions of N and P to the system. The model dynamics allowed an increase in NH_4 concentrations in the EZ when zooplankton were allowed to consume detritus. This resulted in shifts to prokaryotic production from eukaryotic production because prokaryotes were set to be highly dependent on N for growth. These changes were mimicked further when NH_4 and PO_4 were separately added from the surface layer representing a hypothetical external nutrient intrusion to the system. Prokaryotes responded more to N additions and eukaryotes, on the contrary, responded to P addition. Although very experimental, these applications show how important it is to include detailed community structures with detailed trophic decoupling of C/N/P elements in the models. In order to answer the questions of global warming and future predictions of carbon export, models should be able to address the complex interactions within the community structure.

The complex link between physics, nutrient dynamics and de-coupling, community structure and carbon export point out that we need better understanding of these mechanisms, and they should be included in the models by novel algorithms. The importance of particle sinking in relation to regional physics point out the need for a reliable particle sinking mechanism in the models. Complex community links should be related to carbon export. For example, formation of episodic high concentration of labile particles by diatom blooms especially in winter months, and their faster attenuation in the mesopelagic (Helmke *et al*., 2010; Henson *et al*., 2012) may further explain the gap in export rates. The importance of particle aggregation for the sinking of the pico-and nanoplankton was stated by Richardson and Jackson (2007). Aggregation of particles has been shown to be essential in initiating particle export in modeling studies (Gehlen *et al*., 2006). Extending this mechanism to allow further interactions with the physical dynamics (Kriest and Evans, 1999; Kriest, 2002; Aumont and Bopp, 2006, Aumont *et al*., 2015) may allow improved representation of the

relationship between export and intense mixing events at BATS and stability at ESTOC. In parallel to physical aggregation, with the inclusion of dense and fast sinking fecal pellet formation (Lampitt *et al*., 1993), the direct contribution of micro- and mesozooplankton to fast sinking detritus would be resolved, and this way, both the physical and biological aggregation processes are represented in the model. The community link may also be important when mineral ballasting (Armstrong *et al*., 2001; Klaas and Archer, 2002) is incorporated in the model. Its use was adopted in global modeling studies (Gehlen *et al*, 2006; Yool *et al*., 2011) and Gehlen *et al*. (2006) have shown the possible effects of ballasting at greater depths in the oceans, with high particle fluxes occurring down the bathypelagos due to the combined effect of aggregate formation and mineral ballasting. The effect of recycling through microzooplankton grazing is already described in this study, but active transport of organic matter (Steinberg *et al*., 2000) is still missing. The importance of differences in the mesozooplankton community and active transport between both stations is still a process that remains to be resolved when investigating the difference between both stations.

The model has major advantages in resolving the processes stated above. With its multiple functional type representations, modifications to algorithms regarding subgroups of the model compartments will require less effort. Therefore, effects such as ballasting, aggregation and vertical migration may be seamlessly added to the related functional types, and the effect on export and productivity be evaluated. Another advantage of NAGEM is that performance in two similar and contrasting sites (BATS & ESTOC) has been tested and the success of their dynamics demonstrated. The effects of the proposed algorithm modifications can be assessed easily due to the large time-series data sets available at both of these stations. With its 1D structure, the response of modifications can be evaluated quickly, disregarding time restrictions of the 3D computations, and ultimately, it is hoped that the improvements in numerical representations of carbon export can be incorporated into 3D models.

CHAPTER

4. MODEL IMPLEMENTATION TO PAP SITE & RESULTS OF LOWER TROPHIC MODEL DYNAMICS

This chapter is dedicated to the implementation of NAGEM to PAP site in the North Atlantic, where the information given here are the supplementary material for the PAP site results shown in Chapter 5. The model results related to export at PAP is extensively discussed in Chapter 5, along with the comparison to BATS and ESTOC. Including the PAP site lower trophic ecosystem dynamics would have been out of context in Chapter 5, where Chapter 5's main purpose is to discuss the model algorithms. Chapter 3 on the other hand was solely dedicated to the BATS and ESTOC dynamics. In that regard, this short chapter introduces the PAP site model dynamics and their comparison with the observations. Background information such as primary production and chlorophyll seasonal evolutions, dominant algal groups and nutrient dynamics will be presented in this chapter.

4.1. Results-data presentation & discussion

The PAP site is located in the far north at the southeast of the Subpolar Gyre (49 ^{o} N–16.5 ^{o} W). For this reason, it depicts much different physical and ecosystem dynamics than the subtropical counterparts. For instance the depths of the winter convective mixing (Figure 2) (> 400 m) is much deeper than BATS and ESTOC. Inorganic nutrient concentrations are higher (Figure 3, Figure 4, Figure 5), and light exposure needed for growth is lower (Figure 8). These driving mechanisms are the key elements that dictate different ecosystem character at PAP site compared to BATS and ESTOC.

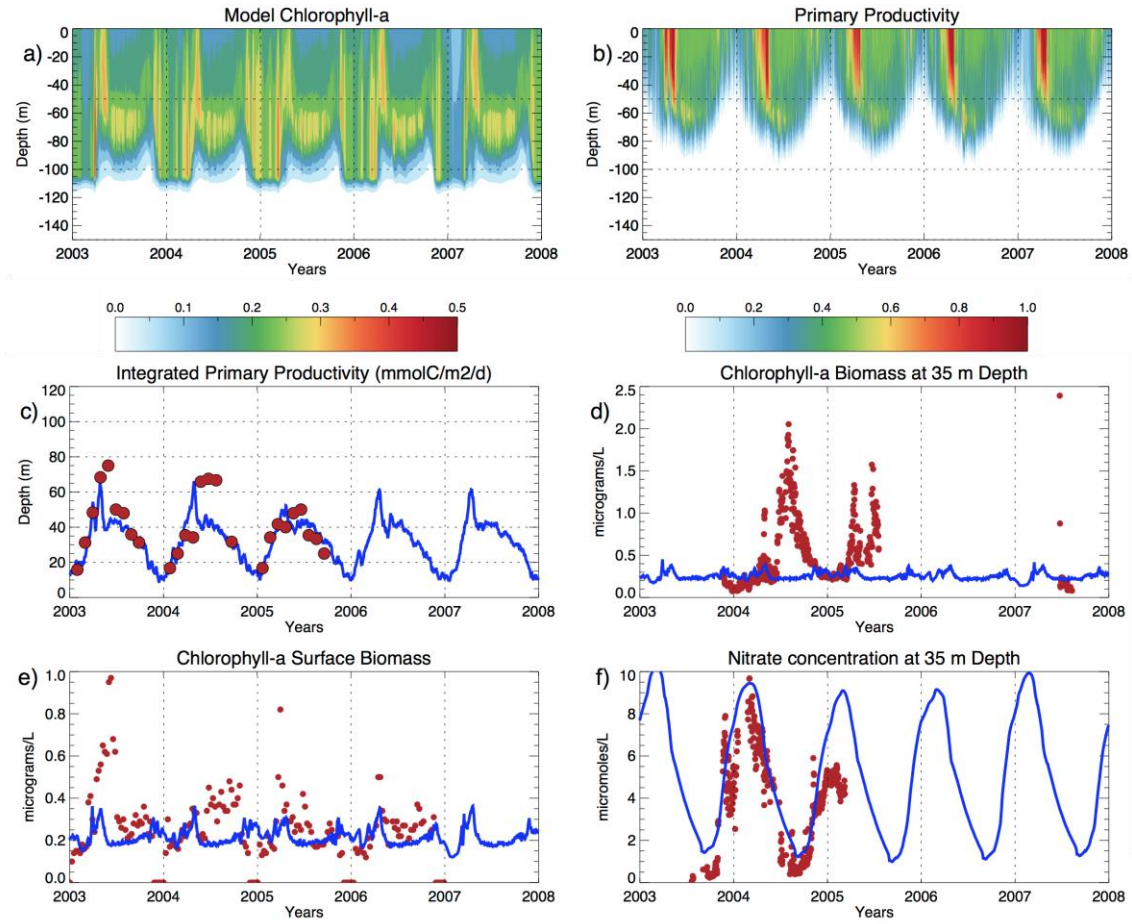

Figure 23) PAP site model results compared to the available observations. Hovmoeller plots of a) Model chlorophyll-a (mg m^{-3}), b) Model primary production (µmoles C m^{-3} d^{-1}). c). Integrated primary productivity (mmoles C m^{-2} d^{-1}. c). Red markers indicate satellite observations. d) Model chlorophyll compared to mooring station chlorophyll sensor (red markers) at 35 m depth (mg m^{-3}). e) Model surface chlorophyll compared to satellite data (mg m^{-3}) (red markers). f) Model nitrate compared to mooring station nitrate sensor (red markers) at 35 m depth (mg m^{-3}). See text for the source of observational data.

Enhanced chlorophyll concentrations at BATS and ESTOC were already present in December/January each year (Figure 10). This was supported by the increased primary production (Figure 12) due to winter convective mixing and supply of new nutrients. PAP site as well witness intense winter convective mixing events much deeper than BATS and ESTOC. However, the chlorophyll concentrations and the primary productivity (Figure 23a,b,c) did not immediately respond to mixing and enhanced nutrient concentrations (Figure 23f and Figure 24). Although phytoplankton were not nutrient limited, as shown by high concentrations throughout the water column, their growth was suppressed by the light limitation implied by deep mixing and general low light availability at higher latitudes. During the simulated period, PAP site received around less than $1/5^{th}$ of exposure compared to BATS (Figure 8). Thus, the initial bloom time was simulated to be later in the year,

around late winter, with peaks in May, although the new nutrient input the EZ had already begun late November. In December – February period, BATS and PAP site already reached the peaks in primary production. NAGEM primary production results were compared to the monthly mean values calculated by remote sensing data given in Hartman *et al.* (2010), where the model results in good match with the given values. In fact, the relatively lower bloom peak in 2005 was also captured by NAGEM, proving its capability to simulate both seasonal and interannual differences in production. Hartman *et al.* (2010) addresses the decrease to lower nutrient supply due to the combined effect of the changes in convective mixing and lateral interactions. NAGEM does not take lateral interactions into account, but the weak convective mixing for 2005 was included in the simulations.

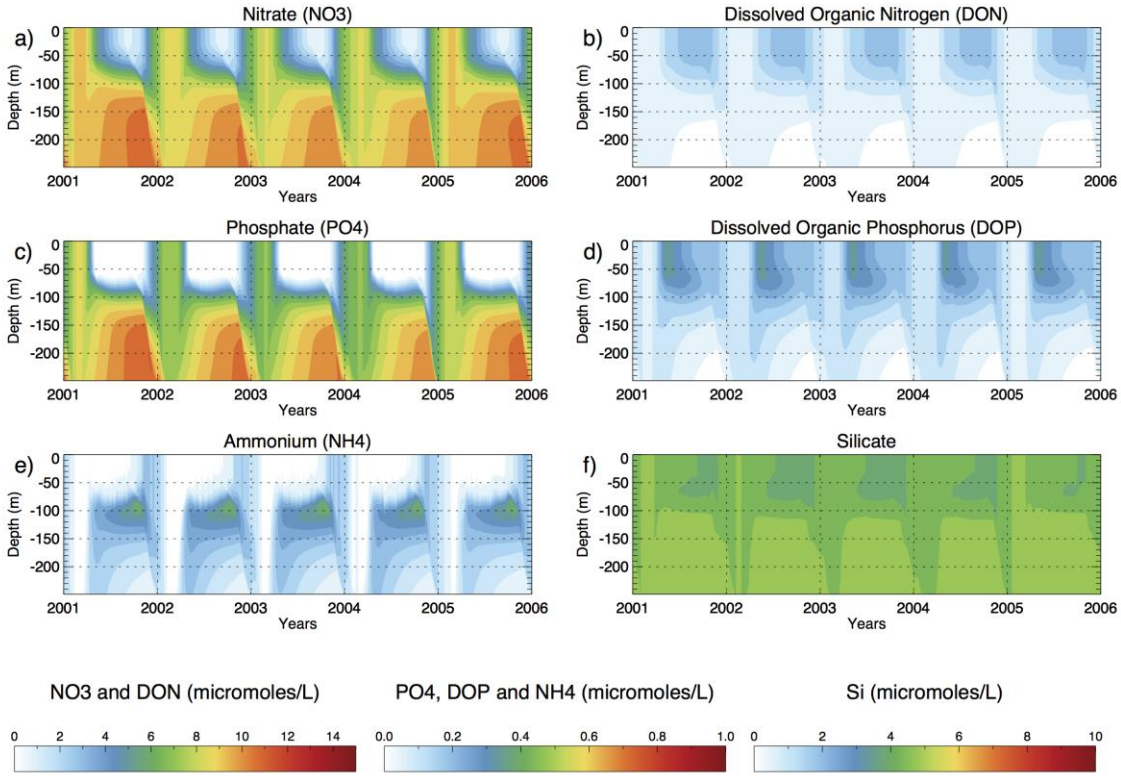

Figure 24) Hovmoeller plots of simulated inorganic nutrients at PAP site (µmoles L^{-1}).

PAP mooring site fluorometer data (Figure 23d) was used for the model chlorophyll to observation comparisons. Data was retrieved from www.eurosites.eu/info. The model results have a god match with the observations in winter periods, where productivity is low and the water column is homogenized due to convective mixing. However, there is high discrepancy with the observed data at 35 m and the corresponding model data in summer. Model predicts chlorophyll concentrations ~0.25 mg m^{-3}, whereas observed values were as high as 2 mg m^{-}

^{3}. Although chlorophyll calculations from fluorometer measurements are subject to uncertainty derived from changes in taxa, size and photo-quenching due to the changes in the ambient light field, such high discrepancy suggest that model partly fails to capture the deep chlorophyll maximum. This could have been due to NAGEM locating the DCM at a different depth. Notice that NAGEM locates DCM at ~70 m in summer periods, but still the chlorophyll concentrations were below 0.5 mg m^{-3}. To extend the model vs observation comparisons, 8-day composite level 3 SeaWiFS data were used. The model vs observed data match better in case of surface comparisons, but still, model summertime chlorophyll results were lower by ~50 – 100 %.

Simulated inorganic nutrients (Figure 24) indicate seasonal signal in nutrient concentrations in the EZ, where both nitrate and phosphate concentrations were homogeneously distributed throughout the water column in winter periods. The nutrient depletion starts in-line with the increased production in late spring. Figure 24f shows the good match between the nitrate sensor data and the results in terms of both timing and magnitude. The model estimates N:P ratio of 25 averaged throughout the simulated period in the upper 0 – 100 m. This is in contradiction with the reported N-limitation for the Porcupine Bank (Martin *et al.*, 1998), where they estimate a N:P ratio of 15. Nitrate was also depleted in summer bottle samples taken from PAP site (www.eurosites.info/pap). Again, around 6 – 10^{o} latitude south, Leblanc *et al.* (2005) report a possible silicate limitation on the diatom spring bloom. PAP simulations in this study fail to represent either N or Si limitation. The seasonal succession of the simulated phytoplankton is given in Figure 25. Compared to the subtropics (Figure 13), the larger sized phytoplankton were relatively dominant throughout the simulated period. Picoeukaryotes had the highest biomass for all seasons, except occasional diatom blooms in winter periods. Simulations resulted in relatively low biomasses of prokaryotes.

Overall, the model resulted in relatively good results, considering the fact that NAGEM was heavily tuned for BATS and ESTOC. The model's response to mixing dynamics were reflected in the timing of the bloom initiation and peaks in magnitude in agreement with the observations. The discrepancies between the modeled and observed chlorophyll values could be due to the empirical formulation of the chlorophyll:carbon ratio used in the model and its tendency to represent environments of high light availability. Incorporation of prognostic chlorophyll state variable (Geider *et al.*, 1997) could resolve this issue in future versions of this model, so that chlorophyll:carbon ratio have better adaptable capacities. Nevertheless,

the model primary production at PAP site (138.4 gC m^{-2} y^{-1}) is in good agreement with the range (116 – 143 gC m^{-2} y^{-1}) given in Hartman *et al.* (2010).

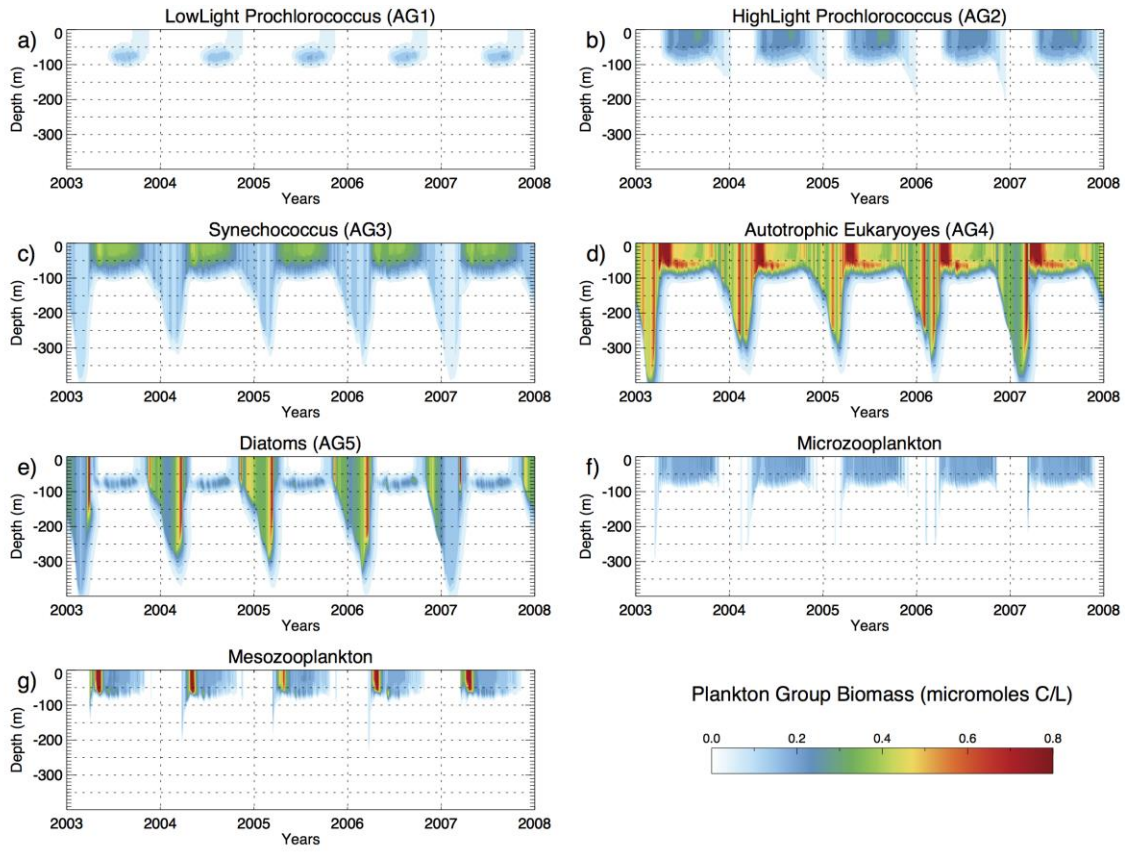

Figure 25) Hovmoller plots of simulated plankton community distributions at PAP site (µmoles C L^{-1} d^{-1}). **a)** LL *Prochlorococcus*, **b)** HL *Prochlorococcus*, **c)** *Synechococcus*, **d)** Autotrophic eukaryotes, **e)** Diatoms, **f)** Microzooplankton, **g)** Mesozooplankton.

The key result of the PAP site simulations is the change in the plankton biomasses relative to each other compared to BATS and ESTOC stations. For example, simulated contribution of diatoms to total plankton biomass in winter period at BATS and ESTOC were <10%, and mesozooplankton contributed <0.5% In the case of PAP, diatom contribution to total annual biomass was 21%, with mesozooplankton contribution of 6%. From a primary production point of view, the 5 – 10 % increase in larger size classes can be irrelevant. However, the relative productivities of larger size classes will have major implications on carbon export. The effect of community composition on the formation and sequestration carbon export is extensively discussed in Chapter 5, and such effect was shown to be a major element in defining the variability and magnitude of export. The model's response to physics and differentiation of various characteristics among different regions, and in turn its productivity and the formation of size classes may answer some of the discrepancies in carbon export simulated by global models. The parameterization at this stage, acknowledging the

mentioned discrepancies mentioned above, especially those regarding the nutrient dynamics, the model provide a reliable tool to be used in algorithm comparative studies described in Chapter 5. However, for future studies, the parameterization used here should be revisited to better simulate the nutrient and chlorophyll dynamics. For the purpose of this thesis, the PAP model is acceptable at this stage, because it manages to get reliable productivities, and differentiate communities among regions of different physical and ecological backgrounds.

CHAPTER

5. CARBON EXPORT ALGORITHM ADVANCEMENT IN MODELS: A COMPARATIVE CASE STUDY OF PARTICLE FORMATION AND SEQUESTRATION IN THE NORTH ATLANTIC

5.1. Introduction

The biological carbon pump (BCP) is the transport of organic carbon into the ocean interior due to the interactions of biology, physics and gravity. In other words, the process of inorganic carbon fixation from the atmosphere into organic carbon during photosynthesis, and its transformation by food web processes, mixing, transport and settling are together referred to as the "biological carbon pump" (Ducklow *et al.*, 2001). The, BCP plays an important role in distributing carbon and nutrients in the oceans and controls atmospheric carbon dioxide (CO2) levels (Volk and Hoffert, 1985). The role of the BCP in modulating atmospheric CO2 levels necessitates the proper representation of carbon sequestration in global climate models. Since the beginning of the industrial era, atmospheric carbon dioxide has increased exponentially from 277 parts per million (ppm) (Joos and Spahni, 2008) to 400.72 ppm in April 2015 and to 404.08 ppm in April 2016 (Dlugokencky and Tans, 2016), an increase an order of magnitude higher than any change estimated for the past 22,000 years.

It is estimated that the oceans fix 40 – 50 GT C yr^{-1} by primary production, roughly an equal amount to that of terrestrial primary production (Falkowski *et al.*, 1998, Field *et al.*, 1998). Of this fixed carbon, through BCP processes, 5 – 15 GT C yr^{-1} (Kwon and Primeau, 2006; Boyd and Trull, 2007; Henson *et al.*, 2011; Sanders et al., 2014) are transferred below the euphotic zone and ~0.1 GT C y^{-1} settle to the deep reaches of the oceans (Sarmiento and Gruber, 2006). In fact, In the absence of the BCP, the atmospheric CO2 concentration would be 200 ppm higher than todays observed levels (Parekh *et al.*, 2006). Therefore,

understanding the dynamics of the BCP has become a priority for present and future marine studies (Sanders *et al.*, 2014).

The definition of the BCP, as the oceans biologically driven sequestration of carbon (Hain *et al.*, 2014), can be simple. However, each process that contributes to sequestration has many sub-processes and numerous dependents. Many of these processes are physically and biologically controlled and are highly restricted by environmental constraints, and their magnitude and attenuation with depth will vary greatly within different regions and seasons (Buesseler and Boyd, 2009). Understanding of these dynamics is hindered by the limited observational data. At this point, models emerge as a tool to fill these gaps, and improved predictions of the strength and magnitude of the BCP has the potential to enable better representation of the global carbon cycle and aid improved climate predictions.

Numerical models transfer empirical knowledge into quantitative descriptions and as such provide tools that can be used to improve understanding of ecosystem dynamics, but the empirical definitions are derived from only a small number of datasets and lack the functionality representing different locations and past and future conditions. Unfortunately, the algorithms used by the modelling community have not evolved much from the classical NPZD models till recent years, and models mainly drive carbon attenuation at depth using the Martin curve (Martin *et al.*, 1987). Lately, more complex and detailed definitions of processes, and numerous state variables have been added to marine ecosystem models, such as multiple plankton functional types (PFTs) and explicit bacteria (Blackford *et al.*, 2004; Hood *et al.*, 2006; Vichi *et al.*, 2007), complex definitions of zooplankton (Mitra 2006), advance particle dynamics of aggregation and settling (Kriest 2002; Aumont *et al.*, 2015) and mineral ballast interactions (Armstrong *et al.*, 2002; Gehlen *et al.*, 2006; Yool *et al.*, 2011). Adding certain complexities to the models is necessary for improved representations of the global carbon cycle. However, such efforts may also introduce the problem of dysfunctionality to the models (Anderson and Mitra, 2010). Incorporating new compartments to the models with the aim of increasing complexity requires the introduction of an increasing number of parameters, and those parameters have to be tuned in order to fit the observations. New parameterization/functions may also lead to a correct answer for the wrong reason, meaning the predictive capacities of more complex models would be less than those simple models (Hood *et al.*, 2006).

In this chapter, I focus on the carbon attenuation specific model use of various settling behaviors of particles, and their remineralization through the water column, physical and biological aggregation, mineral ballast effect and the diel vertical migration of zooplankton. I aim to (1) describe the effect, use and success of each individual algorithm on sequestration, and (2) try to explain the observed carbon export at various time series stations using the newly incorporated algorithms. NAGEM was applied to describe two time-series stations in the Subtropical North Atlantic: BATS (Bermuda Atlantic Time-series Study 31.7º N–64.2º W) and ESTOC (European Station for Time series in the Ocean, Canary Islands, 29.16º N–15.5º W). These stations are reported to have similar primary productivity with major differences in carbon export magnitude (Neuer *et al.*, 2002; Helmke *et al.*, 2010). The success of the algorithms used will be based on the model's predictive capacity of the carbon export gap observed at BATS and ESTOC. To test the model's adaptive capacity and the response of the algorithms to different environments, the model has also been applied to the PAP site (Porcupine Abyssal Plain 49º N–16.5º W), which is located below the Subpolar North Atlantic a physically and biologically a different region compared to the Subtropical North Atlantic. Extensive model vs observation comparisons supported by statistical analyses of the results were done. A successful set of algorithms and their use may target existing global ecosystem models, and with their incorporation to the 3D models, the scientific community may benefit from improved predictive capabilities of global ecosystem models.

5.2.Methods

The model adopted for this study, NAGEM (North Atlantic Generic Ecosystem Model) is a 1D lower trophic pelagic ecosystem model designed for the North Atlantic (see Chapter 3) [NA1]. This section introduces the NA1 model setup, the theoretical background, formulation and parameterization of the modifications done on NA1. For the validation of the model formulations and parameterizations at BATS and ESTOC sites, the reader is referred to Chapter 3.

5.2.1. The reference model setup

NA1 incorporates 3 simulations. These are (1) 2 zooplankton version, (2) 3 zooplankton version (includes detritus feeders) and (3) a modified version based on 3 zooplankton version. The starting simulation, on which was bases for the rest of the simulations for this study is the 2nd version which includes 3 zooplankton, and was referred to it as "ORIG" from this point on. ORIG includes 5 algal groups (AG) representing different size classes and process rates. AG's are classified as prokaryotes (3 subgroups), autotrophic eukaryotes and large diatoms. Prokaryotes are divided into low light adapted *Prochlorococcus*, high light adapted *Prochlorococcus* and *Synechococcus*. The schematic description of the model compartments and currency flow are shown in Figure 26. The ORIG and the following simulations share the following lower trophic model equations, unless stated otherwise for a specific run. For a detailed description and the theoretical background of the equations, see Section 3.2.

Algae growth and grazing follow:

$$\frac{\partial AG_i}{\partial t} + w\frac{\partial AG_i}{\partial z} - \frac{\partial}{\partial z}Kv\frac{\partial AG_i}{\partial z} = \left[min\left(\mu_{ll_i}, \mu_{nul_i}\right)\right]AG_i - m_i AG_i - I_{AG_i}Z \quad \text{for i=1,5} \tag{5.1}$$

$$\frac{\partial Z_{micro}}{\partial t} = \sum_{i=1}^{4} \lambda\, I_{AG_i} Z_{micro} - I_{Z_{micro}} Z_{meso} - exc_{micro} Z_{micro} - m_{Z_{micro}} Z_{micro} \tag{5.2}$$

$$\frac{\partial Z_{meso}}{\partial t} = \lambda\, I_{AG_5} Z_{meso} + \lambda\, I_{Z_{micro}} Z_{meso} - exc_{meso} Z_{meso} - m_{Z_{meso}} Z_{meso} \tag{5.3}$$

$$I_{AG_i} = g_{AG_i}\, \Lambda\, [AG_i]\left(1 - e^{-\Lambda\,(AG_i)}\right) \tag{5.4}$$

$$I_{Z_{micro}} = g_{Z_{micro}}\, \Lambda\, [Z_{micro}]\left(1 - e^{-\Lambda\,(Z_{micro})}\right) \tag{5.5}$$

where the terms on the LHS of Eq.(5.1) represent the changes in algal group AG in time *t* at any location. *z* is depth, *w* is vertical advection and *Kv* is the vertical diffusive flux. The RHS terms are the biological source and sink terms which include light- (μ_{ll_i}) and nutrient- (μ_{nul_i}) limited growth rates that are temperature corrected for each time step, natural mortality (mi) and losses due to grazing activity (I_{AG_i}) applied by micro- and mesozooplankton. $g_{AG,Z}$ denotes maximum grazing rate on each AG and microzooplankton. The terms *exc* and *m* denote excretion and natural mortality rates. λ denotes zooplankton

assimilation efficiency and Λ represents the Ivlev (1955) coefficient for zooplankton grazing.

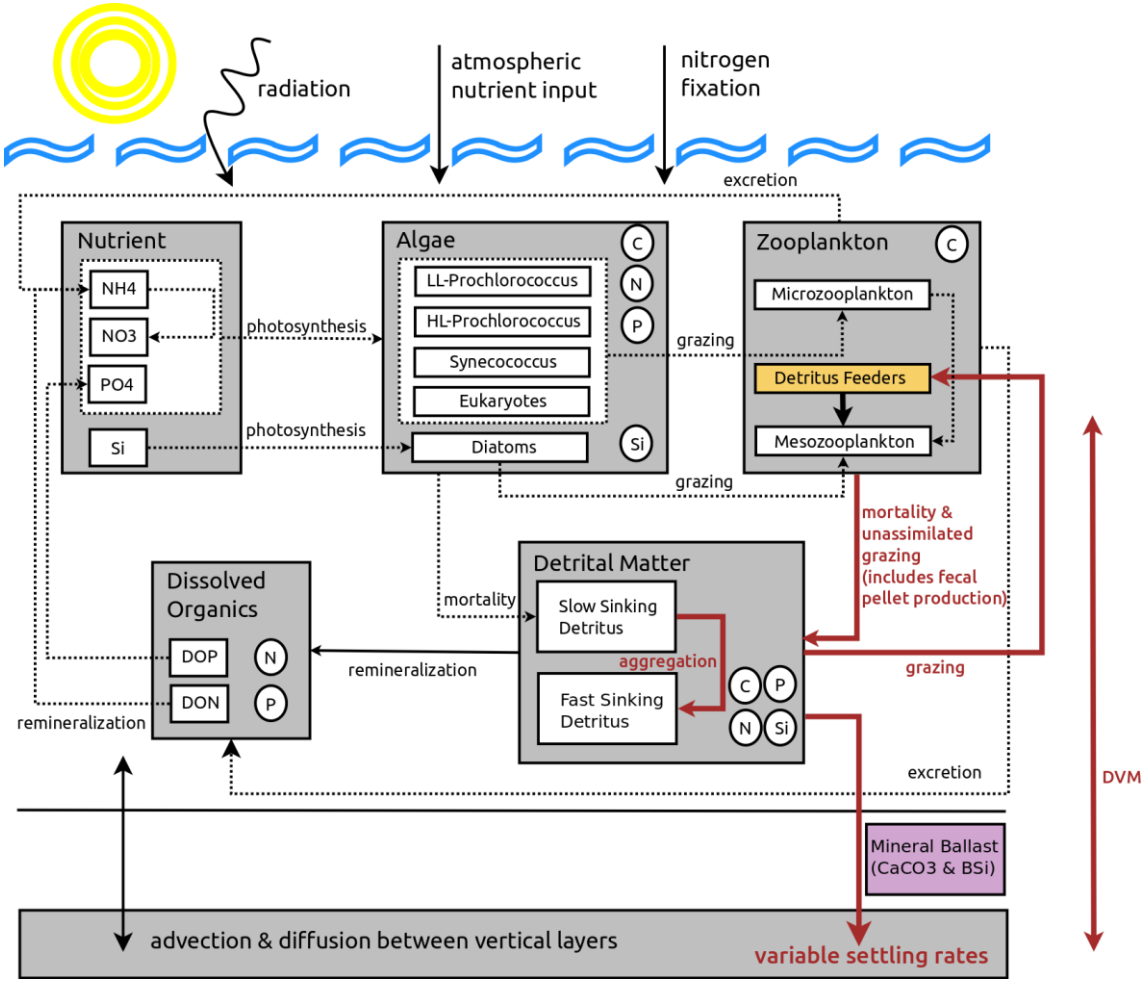

Figure 26) Structure of NAGEM and the added algorithms. Boxes indicate trophic levels, and internal compartments are indicated within. The small circles within the trophic levels indicate the internal nutrient compositions. Arrows represent the direction of transfer between the state variables. Abbreviations used are: C - carbon, N - nitrogen, P - phosphate, Si - silicate, DON - dissolved organic nitrogen, and DOP - dissolved organic phosphorus. The original setup from NA1 paper are given in grey color scale. Additional state variables are given in colored boxes such as Detritus Consumers and mineral ballast state variables. Additional or modified flows between state variables representing scenarios in this study are given in red arrows.

Each AG has separate cellular carbon, nitrogen, phosphorus ratios. AG5 has an extra silicate compartment. Separate growth rates for nitrogen, phosphorus and silicate are estimated through calculating uptake rates of nutrients in reference to cellular nutrient contents. Variable chlorophyll *a* to carbon ratios for each AG are also included in the model. Carbon content, irradiance and growth rates are coupled to estimate chlorophyll *a* to carbon ratios for each AG at each time step. Nutrient state equations are:

$$\frac{\partial NO_3^-}{\partial t} = -\sum_{i=1}^{5} \rho_{NO_3^- i} + nitr + \delta(z)[FN + Nfix] \qquad \begin{matrix}\delta(z=0)=1\\ \delta(z>0)=0\end{matrix} \quad (5.6)$$

$$\frac{\partial NH_4^+}{\partial t} = -\sum_{i=1}^{5} \rho_{NH_4^+ i} - nitr + 0.5exc_{micro} Z_{micro} \left(\frac{N}{C}\right)_{Z_{micro}} + 0.5exc_{meso} Z_{meso} \left(\frac{N}{C}\right)_{Z_{meso}} + c_a DON \quad (5.7)$$

$$\frac{\partial PO_4^{3-}}{\partial t} = -\sum_{i=1}^{5} \rho_{PO_4^{3-} i} + c_p DOP \quad (5.8)$$

$$\frac{\partial Si}{\partial t} = -\rho_{Si_5} + c_{Si} DetSi \quad (5.9)$$

where, ρ denote the nutrient and AG specific uptake rates, *nitr* represent the nitrification of ammonium to nitrate, *FN* and *Nfix* are extra sources of nitrogen from the surface boundary layer in the form of atmospheric (aeolian) deposition of nitrate and nitrogen fixation respectively. N/C terms denote the internal zooplankton nitrogen:carbon ratios. C_x terms represent the remineralization rates applied to DON, DOP and detrital silicon.

The uptake rates for nutrients are calculated via a Monod function applied to the ambient nutrient concentrations. All nutrients follow the same equation, phosphate is given as an example here:

$$\rho_{PO_4^{3-} i}(z,t) = \mu_{mt_i}(z,t) AGP_i \left[\frac{PO_4^{3-}}{K_{sPO_4^{3-} i} + PO_4^{3-}}\right] \quad (5.10)$$

where $\mu_{mt_i}(z,t)$ is the temperature dependent specific growth rate of each AG, and $K_{sPO_4^{3-}}$is the half saturation constant for phosphate uptake. Note that internal P content (AGP) is included in the equations. μ_{mt_i} (temperature (*T*) corrected growth rate using specific growth relationship given by Eppley (1972), determines the maximum growth rate, μ_i, an AG can achieve under nutrient saturated conditions as:

$$\mu_{mti}(z,t) = \mu_{mi}(z,t)exp^{0.0633(T(z)-27)} \tag{5.11}$$

$$\mu_i(z,t) = \mu_{mt_i}(z,t)\left[1 - \frac{K_{QN_i}}{QN_{max_i}}\right]^{-1}\left[1 - \frac{K_{QP_i}}{QP_{max_i}}\right]^{-1}\left[1 - \frac{K_{QSi_5}}{QSi_{max_5}}\right]^{-1} \tag{5.12}$$

where $QN, QP\ and\ QSi$ are the algal group internal nitrogen to carbon ratios ($AGN_i{:}\,AG_i$), phosphorus to carbon ratios ($AGP_i{:}\,AG_i$) and silicate to carbon ratio ($AGSi_5{:}\,AG_5$). Higher maximum growth rates were assigned for AG's compared to Salihoglu and Hoffman (2007) and Salihoglu *et al.* (2008) to reach the observed productivity at BATS and ESTOC (Table 2). A *max* subscript denotes the maximum attainable nutrient to carbon ratios. K_{QN_i}, K_{QP_i} and K_{QSi_5} denote the minimum allowed nutrient to carbon ratios, where the zero growth rate occurs. Following the maximum growth rate under temperature corrected conditions, the actual nutrient limited growth rate (μ_{nul_i}) is calculated by the actual nutrient to carbon ratios (Q):

$$\mu_{nul_i}(z,t) = \mu_i(z,t)\left[1 - \frac{K_{QN_i}}{Q_{N_i}(z,t)}\right]\left[1 - \frac{K_{QP_i}}{Q_{P_i}(z,t)}\right]\left[1 - \frac{K_{QSi_5}}{Q_{Si_5}(z,t)}\right] \tag{5.13}$$

DOM dynamics are included in NAGEM, and breakdown of detritus and DOM by bacteria is parameterized implicitly as a function of temperature, following:

$$\frac{\partial DON}{\partial t} = 0.5exc_{micro}Z_{micro}\left(\frac{N}{C}\right)_{Z_{micro}} + 0.5exc_{meso}Z_{meso}\left(\frac{N}{C}\right)_{Z_{meso}} + c_{DON}DetSlow_N + c_{DON}DetFast_N - c_aDON \tag{5.14}$$

DOP state equations are exactly the same, except all excreted P are sent to the DOP pool, rather than distributing half to the inorganic PO_4^{3-} pool. Suspended and slow sinking particles under the "Slow Sinking Detritus" state variable in NAGEM. This compartment is labile and since it's sinking speed is slow, it is prone to high rates of recycling within the surface layers. Aggregation leads to the formation of the Fast Detritus compartment. Slow and fast sinking detritus are defined by their sinking and remineralization rates. Breakdown

of detritus is parameterized through remineralization to DON and DOP. Detritus equations are:

$$\frac{\partial Det_{slow}}{\partial t} + \left(w + sink_{slow}^{det}\right)\frac{\partial Det_{slow}}{\partial z} - \frac{\partial}{\partial z}Kv\frac{\partial Det_{slow}}{\partial z} = \sum_{i=1}^{4}\left[m_i AG_i + (1-\lambda)\, I_{AG_i} Z_{micro}\right] + m_5 AG_5 + m_{Z_{micro}} Z_{micro} + (1-\lambda)(\, I_{AG_5} + I_{Z_{micro}} + I_{Z_{det}})Z_{meso} + m_{Z_{meso}} Z_{meso} + m_{Z_{det}} Z_{det} + (1-\lambda)\, I_{Z_{det}} Z_{det} - I_{Z_{det}} Z_{det} - c_c Det_{slow} - aggDet_{slow} \quad (5.15)$$

$$\frac{\partial Det_{fast}}{\partial t} + \left(w + sink_{fast}^{det}\right)\frac{\partial Det_{fast}}{\partial z} - \frac{\partial}{\partial z}Kv\frac{\partial Det_{fast}}{\partial z} = aggDet_{fast} - c_c Det_{fast} \quad (5.16)$$

5.2.2. Model implementation and the data used

NAGEM was applied to three time-series stations in the North Atlantic: BATS (Bermuda Atlantic Time-series Study 31.7º N–64.2º W), ESTOC (European Station for Time series in the Ocean, Canary Islands, 29.16º N–15.5º W), and PAP site (Porcupine Abyssal Plain 49º N–16.5º W). The simulation periods were chosen according to the observation availability for model evaluation. Thus, BATS and ESTOC simulations cover the years 1996 – 2000, and PAP simulations cover 2003 – 2008. Model depth for every simulation extends down to 3000 m depth, with 1 meter resolution vertical levels. 1 hour time step was chosen for the temporal progress.

The ecosystem model is not coupled to any other physics model. This approach was chosen in order to get the most precise physics available from the observations, and eliminate the discrepancies resulting in physics from an external simulation. The state variables are homogenously mixed within the mixed layer depth (MLD), where MLD's were estimated from the temperature forcing fields. MLD was assigned as the depth that is 0.5ºC colder from the surface temperature following the criteria from Spall *et al.* (2000). Although the state equations include advection terms, the model only uses MLD mixing and vertical

diffusion for the displacement of the state variables. Temperature fields are also used to force the ecosystem processes that are dependent on temperature. Regarding the ecosystem part, primary productivity is driven by the irradiation applied from the surface layer, where the model has its own internal dynamics to calculate the radiation at depth. No lateral boundary conditions or relaxation fields for temperature or any other state variables were used, but the inorganic nutrients; nitrate (NO_3), phosphate (PO_4) and silicate (Si), are forced from the bottom layer (3000 m), and at 250 m for BATS and ESTOC, and at 400 m for PAP station. The nutrient forcing at intermediate depths are set in order to capture the variability in nutrient levels due to mesoscale events or lateral interactions to compensate for the events that we were not able to capture with the MLD's applied from the temperature fields. The depths are set such that the forcing is applied below the MLD's throughout the simulations. Apart from nutrient forcing at depth, nitrate is forced from the surface layer to represent the input from atmosphere and N_2 fixation only at BATS. This routine was neglected at ESTOC simulations due to the less importance at that site (Neuer *et al.*, 2002).

Temperature forcing data were taken from monthly-bimonthly field observations at BATS (www.bats.bios.edu). Further details can be seen in Lomas *et al.* (2013). For ESTOC and PAP, temperature data was retrieved from ARGO database (Cabanes *et al.*, 2013). Data were linearly interpolated at depth to match the 1m resolution vertical levels of the model and 1 hour resolution in time. In a similar fashion, "surface net solar radiation" variable from ECMWF ERA-INTERIM (Dee *et al.*, 2011) reanalysis data was retrieved and converted to µmol quanta m^{-2} s^{-1} and interpolated to 1 hour interval in time. The state equations were solved numerically using the Crank-Nicholson scheme (Crank, 1956). Nitrate, phosphate and silicate bottom boundary (3000 m) conditions were taken from World Ocean Atlas 2013 climatology (WOA) (Garcia *et al.*, 2014) and linearly interpolated to 1 hour intervals. The intermediate nutrient forcing data is retrieved from BATS website, from the PLOCAN database (http://data.plocan.eu/thredds/) for ESTOC and WOA'13 for PAP. Initial conditions for January 1st, 1996 for BATS and ESTOC, were retrieved from cruise data in the upper layers where data is available and from WOA'13 January climatology for the deeper layers. For PAP site, only WOA'13 data is used for initialization. A higher vertical diffusion (K_v = 1 cm^2s^{-1}) is applied within the MLD compared to the rest of the water column (K_v = 0.01 cm^2s^{-1}) (See Section 3.2.2 for discussion on the values used). A 10 year repeated 1996 for BATS and ESTOC, 2003 for PAP site spin-up runs were carried on for the model output storage.

Model and observation comparisons for carbon export are based on the sediment trap data taken from the BATS website and the PANGEA (Neuer *et al.*, 2002; Torres Valdés *et al.*, 2014) database. The euphotic zone ecosystem model result comparisons and discussions were given in Section 3.3.1, and those data were retrieved from BATS website, PLOCAN database, EUROSITES (www.eurosites.info/pap.php) website, and were extensively discussed in Neuer *et al.* (2007), Hartman *et al.* (2010) and Lomas *et al.* (2013). Plots is the results section include direct comparisons with the observed data. For those plots, model depth coinciding with the observation depth were directly plotted without any modification/adjustment. Model vs observed data (primary production and carbon export at various depths) statistics were calculated and outputs were summarized using Taylor plots (Taylor, 2001). Taylor plots include correlations, % biases, and normalized standard deviations (NSTD) where standard deviations of each variable was normalized to that variable's observed standard deviation. For the statistics, the model output points were averaged by 5 consecutive days in time and 10 meters at depth for the primary production comparisons locating the observation depth, and again, 5 consecutive days in time and exact depth were used for the carbon export comparisons.

5.2.3. Modifications of carbon sequestration algorithms

In order to understand the effects of different algorithms and parameterizations, some of the terms in the equations were either modified or new terms were added.

The algorithm modifications in this study cover:

- Depth dependent sinking rates
- Physical aggregation (aggregation sensitive to turbulence shear)
- Biological aggregation (fecal pellet production)
- Mineral ballasting
- Community specific remineralization and sinking rates
- and diel vertical migration (DVM)

5.2.3.1. Variable sinking rates

All of the scenarios with specific modifications follow the same governing equations listed in Section 3.2.4. NA1 adopted single settling rates of 5 m s^{-1} and 24 m s^{-1} for DetSlow and DetFast respectively. That formulation is represented in this study as ORIG scenario. The detritus in the "depth dependent sinking rate" scenarios in this paper adopt an increasing settling rate as they descend, following:

$$sink^{det} = sink_{min}^{det} + \left(sink_{max}^{det} - sink_{min}^{det}\right) max\left(0, \frac{z - z_{MLD}}{2000}\right) \qquad (5.17)$$

where $sink^{det}$, sinking speed of detritus at each level, $sink_{max}^{det}, sink_{min}^{det}$, minimum and maximum threshold speed values, z, depth and z_{MLD}, mixed layer depth. Particles begin to increase their sinking rates below the MLD. Sinking rates are constant below 2000 m at their maximum thresholds. This routine was taken from Gehlen *et al.* (2006). Sensitivity analyses on the settling rates of the slow and fast sinking detritus are given with the STL abbreviations, under scenario names STL1-6. STL1, STL2 and STL3 focus on the settling rate of "Slow" detritus, and STL4, STL5 and STL6 focus on the "Fast" detritus settling rate. Prescribed settling rates are listed in Table 7, where speeds range between 2 – 7 m d^{-1} for slow detritus, and 15 – 40 m d^{-1} for the fast detritus. The results of the scenarios are compared to the ORIG simulation which incorporates single settling rates of 5 and 24 m d^{-1}.

Table 7) Variable settling speeds (m d^{-1}) applied on the "Slow Detritus" and "Fast Detritus" compartments in the STL scenarios.

	ORIG	**STL1**	**STL2**	**STL3**	**STL4**	**STL5**	**STL6**
SlowDet minimum	5	2	4	6	2	2	2
SlowDet maximum	5	7	7	7	7	7	7
FastDet minimum	24	15	15	15	25	35	20
FastDet maximum	24	40	40	40	40	40	30

In addition to STL scenarios, rather than using variable single settling rates for each detritus, a community based set of settling rates was introduced, because source and size of the particles determine a wide range (5 – 2700 m d^{-1}) of sinking rates (Turner, 2002 and references therein). Richardson and Jackson (2007) emphasize the role of aggregation on particle settling rates, and even small phytoplankton can contribute to export, given enough time for aggregation. To evaluate the response of carbon export to variable settling rates

originating from different sources of the lower trophic system, we introduced separate "slow" and "fast" sinking settling rates for each AG and zooplankton. The settling rates are chosen based on their defined size, and the matching settling rates in Richardson and Jackson (2007). Intermediate values were assigned for the "slow" settling rates. Higher values were assigned for the aggregated detritus, or the fecal pellets from zooplankton. The assigned settling rates are listed in Table 8. For each time-step and depth, a weighted average of settling rates are calculated using each plankton's contribution to detritus, detritus from previous time-step, and their unique settling speeds to calculate a unique settling rate for each depth formulated as following:

$$sink^{det}_{slow\_calc} = \frac{\left(sink^{det}_{slow_{previous}} Det_{slow} + \sum_{i=0}^{8} det_{prod_i} * \ biomass_i * \ sink^{det}_{slow_i}\right)}{\left(Det_{slow} + \sum_{i=0}^{8} det_{prod_i} * \ biomass_i\right)} \quad 18a$$

$$sink^{det}_{fast\_calc} = \frac{(sink^{det}_{fast_{previous}} Det_{fast} + agg * Det_{slow} * sink^{det}_{fast_i} + \sum fec * Zoo * sink^{det}_{fast_i})}{(Det_{fast} + agg * Det_{slow} + \sum fec * Zoo)} \quad 18b$$

where $sink^{det}_{slow\_calc}$ and $sink^{det}_{fast\_calc}$ are the calculated settling rates, $sink^{det}_{slow_{previous}}$ and $sink^{det}_{fast_{previous}}$ are settling rates from previous time-step, det_{prod_i} is the contribution of each state variable to detritus production and fec is the fecal pellet production coefficient (see Section 5.2.3.2). The simulation that adopts this approach is referred to as COMSTL.

Table 8) Assigned settling speeds (m d^{-1}) applied for each phytoplankton and zooplankton to determine an average settling speeds for DetSlow and DetFast. These values are first introduced to COMSTL scenario. Those other scenarios that use these values are given in text.

	AG1	**AG2**	**AG3**	**AG4**	**AG5**	**Z_{micro}**	**Z_{meso}**	**Z_{det}**
SlowDet minimum	1.5	1.5	1.5	3.5	6	5	10	5
FastDet minimum	10	10	10	20	35	28	55	28

5.2.3.2. Aggregation

Aggregation and direct sedimentation of phytoplankton out of the euphotic zone is regarded as important elements of the biological carbon pump. Through aggregation, particle properties change along with their interactions with the marine environment (Jackson and

Burd, 1998), and combination of small and slowly settling particles into larger and faster aggregates can increase the efficiency of removal of organic matter from the ocean surface. Aggregation can occur through both physical and biological means. The physical aggregation occurs via combination of the particle concentrations, their density, stickiness, size and shape, fluid shear and differential settling (Jackson, 1990; Alldredge and Jackson, 1995; Simon *et al.* 2002; Burd and Jackson, 2009), whereas biological aggregation occurs when particles are ingested by animals and released back to the marine environment in the form of fecal pellets (Simon *et al.* 2002, Kiørboe *et al.* 2003).

ORIG, followed by COMSTL simulation include simple physical aggregation, where at each time-step a constant proportion of the Slow Detritus is converted to Fast Detritus (Eq 5.15 and 5.16). The formation of fecal pellet is not represented in these scenarios. Both processes were attempted to be included, and were further improved for the variability in physical aggregation. Additions and modifications were kept as simple as possible to address feasibility to 3D model but at the same time effectiveness of the approaches would be our priority. Jackson (1990) defines physical aggregation is the combination of particle collusion by laminar or turbulent shear (particles of different velocities collide) and differential settling (faster particles collect smaller particles as they sink). In simulations here, to account for the turbulent shear, faster aggregation rate (0.05 d^{-1}) within the MLD, and slower below (0.005 d^{-1}) were introduced. The values used are the lower and higher ends given in Jackson and Burd (1998). This routine is added on the COMSTL simulation and referred to as AGG in the results. In the case of biological aggregation, that is the formation of fecal pellets by zooplankton, sources to DetSlow and DetFast were modified. The ORIG simulation channels all the mortality loss terms of zooplankton to DetSlow, which by definition, sinks slower and remineralize faster. To account for the production of fast sinking and relatively protected particulate organic matter (fecal pellets), a user defined proportion of the zooplankton mortality is directly channeled to DetFast, which sink faster and is less prone to recycling. The *fec* multiplier is shown in Eq 5.18. The ratios given were 0.0, 0.25 and 0.5 for microzooplankton, detritus consumers and mesozooplankton respectively. The routine is added on the COMSTL simulation, and hence called FEC. FECAGG simulation includes both changes from AGG and FEC simulations.

5.2.3.3. Mineral ballast effect

The effect of mineral ballast on POC flux was proposed to be critical in carbon reaching deep sea floor, where mineral ballast mechanism was hypothesized control the carbon flux in the deep ocean by protecting the sinking matter from oxidation or by increasing their sinking speed (Armstrong, Francois, Klaas and Archer etal 2002). Among the minerals: $CaCO_3$, BSi and lithogenic material, $CaCO_3$ was considered to be the mineral of strong correlation with sinking POC. To introduce a mineral ballast effect on sinking organic matter, by the definition, the model requires the presence of Bsi and $CaCO_3$. NAGEM already includes Bsi in the form of Detritus Silicate produced by diatoms. Unfortunately, NAGEM does not resolve explicit *coccolithophores*. To represent their presence, an implicit *coccolithophore* implementation was adopted following Dunne *et al.* (2007) and Yool *et al.* (2011). We have introduced the production of $CaCO_3$ by AG4 (picoeukaryotes, closest size range to *coccolithophores*) mortality and the amount ingested and released by zooplankton. Production of $CaCO_3$ follows the DetSlow formulation (Eq 5.15) with parts relevant to AG4 and zooplankton (with proportion to the ingested AG4), multiplied by the *rain* ratio. The assigned *rain* ratio is 0.035 (after Dunne *et al.* 2007). Thus, the $CaCO_3$ production follow:

$$\begin{aligned}\frac{\partial CaCO_3}{\partial t} + \left(w + sink_{fast}^{det}\right)\frac{\partial CaCO_3}{\partial z} - \frac{\partial}{\partial z}Kv\frac{\partial CaCO_3}{\partial z} \\ = rain \\ * \left[mAG4 + \left(\frac{I_{AG4}}{I_{total_{micro}}}\right)mZ_{micro}\right. \\ \left. + \left(\frac{I_{AG4}}{I_{total_{micro}}}\right)\left(\frac{I_{Z_{micro}}}{I_{total_{meso}}}\right)mZ_{meso}\right] - c_{caco3}CaCO_3\end{aligned} \tag{5.19}$$

where;

c_{caco3} stand for the dissolution rate for the $CaCO_3$. Due to the supersaturation concentration of carbonate ion in surface waters $CaCO_3$ has a very low dissolution rate in the model (1/100 of carbon) since our sites fall within the lysocline depth given in Yool *et al.* (2011).

The protected ratio of DetFast is calculated by:

$$Bal_{CaCO3}(z) = CaCO_3(z)\left(\frac{M_{CaCO_3}}{M_{C_{org}}}\right)f_{CaCO_3} \tag{5.20a}$$

$$Bal_{Si}(z) = Det_{Si}(z)\left(\frac{M_{Det_{si}}}{M_{C_{org}}}\right)f_{Det_{si}} \tag{5.20b}$$

$$\frac{\partial Det_{fast}}{\partial t} + \cdots = \cdots + \left[1 - \left(\frac{\left(Bal_{CaCO3}(z) + Bal_{Si}(z)\right)}{DetFast}\right)\right] c_c DetFast + \cdots \qquad (5.20c)$$

where;

Eq20c is the ballast protected version of Eq 5.16. $Bal_{CaCO3}(z)$ and $Bal_{Si}(z)$ are the $CaCO_3$ and BSi protected proportions of DetFast at each depth. M_{CaCO_3}, $M_{Det_{si}}$ and $M_{C_{org}}$ are the mass:mole ratios; 100.086 ($gCaCO_3$ $molC^{-1}$), 60.084 ($gBSi$ $molSi^{-1}$) and 12.011 (gC $molC^{-1}$) respectively. f_{CaCO_3} and $f_{Det_{si}}$ are protection ratios, the values were taken from Klass and Archer (2002), 0.083 and 0.023 respectively. Yool *et al.* (2011) implicitly sends the protected detritus directly to the level below. However, DetFast was resolved explicitly, but with DetFast high settling rates, Eq20c ensures that the protected proportion is transferred to the layer below. The ballast formulation is built on COMSTL simulation and hence referred to as BAL simulation. BAL simulation therefore does not include any aggregation. Aggregation activated ballast simulation is called ALL, standing for including all of the modifications (COMSTL, FECAGG and BAL) up until this point.

5.2.3.4. Community specific remineralization rates

The response of the sinking organic material to the ecosystem structure has been an argument in various studies (Francois *et al.*, 2002; Helmke *et al.*, 2010; Henson *et al.*, 2012). The authors argue that different communities produce sinking materials that are either easily broken through remineralization, or densely packed that are less prone to recycling. To support this view, they give, at high latitudes, export ratio is high, suggesting that large plankton, mainly diatoms, may produce particles that sink fast (this was adopted in COMSTL), but are easily broken due to inefficient packing. Conversely, at low latitudes, small phytoplankton produce particles that sink slower (adopted in COMSTL), thus recycled continuously, leading to particles densely packed that are effectively protected from breakdown.

NA1 emphasized the importance of remineralization mechanism in defining carbon export at depth. Application and differentiation of separate remineralization rates may dictate deviations from the carbon export curve resulting from single remineralization rates. This approach may resolve different remineralization rates in various oceanic regions with different community structure. Similar to Eq 5.18, both DetSlow and DetFast

remineralization rates at each depth and time are weight averaged from various sources of detritus. The settling rates in Eq 5.18 are replaced by the corresponding remineralization rates given in Table 9, such that diatoms and grazed diatoms have higher remineralization rates, and small phytoplankton lower the remineralization rates by their contribution to the aggregated part with low values. These changes are built on the ALL scenario, named here and after REM scenario.

5.2.3.5. Diel vertical migration

Diel vertical migration (DVM) is another mechanism which zooplankton contribute significantly to the total carbon flux at depth (Longhurst and Harrison, 1988; Dam *et al.*, 1995). Zooplankton with this mechanism actively export the organic material to depth via vertical migration, via the gut flux (Angel, 1989), carbon dioxide respiration (Longhurst *et al.*, 1990), DOC excretion (Steinberg *et al.*, 2000) and mortality at depth (Zhang and Dam, 1997). Within the DVM cycle, migrating zooplankton ingest food near the surface and carry the food downward to egest and metabolize, or to be passed on to the consumers of zooplankton.

Table 9) Assigned remineralization rates (d^{-1}) applied for each phytoplankton and zooplankton to determine an average rate for DetSlow and DetFast. Aggregated detritus represent the weights assigned to the aggregation process, so that each plankton can contribute to sinking detritus. AG weight are missing in DetFast values because their contribution is to only aggregated detritus. DetFast has a direct source only from fecal pellet production.

	AG1	**AG2**	**AG3**	**AG4**	**AG5**	**Z_{micro}**	**Z_{meso}**	**Z_{det}**
DetSlow minimum	0.18	0.18	0.18	0.22	0.4	0.2	0.22	0.2
DetFast minimum	-	-	-	-	-	0.16	0.16	0.16
Aggregated Det	0.04	0.04	0.04	0.26	0.4	0.22	0.3	0.2

To represent DVM effect, a light intensity switch was introduced, where in the daylight hours, model mesozooplankton descend to layers that have 1‰ of the surface radiation, and in the night time, they ascend to the upper layers following the food abundance proportionally. Their feeding is mostly stalled in the day since there is not enough available food at depths below the EZ. Estimated swimming speeds of migrating copepods were given between 50 – 200 m h^{-1} (Wiebe *et al.*, 1992). Considering the effective swimming range of mesozooplankton due to light availability (0 – 300m), the depth range can be covered in 1 hour by zooplankton, which is an equal time frame to NAGEM's time step. Thus, NAGEM

dictates an immediate relocation of mesozooplankton up and down the water column given the light signal of day and night. This way, mesozooplankton are not assigned a swimming speed for the numerical solver to handle. Instabilities that may arise from such high swimming speeds (200 m h^{-1}) was eliminated by the approach that was used. Diel vertical migration is applied onto the REM simulation with DVM abbreviation.

5.3.Results

The comparison of model and observed carbon export at depth related to STL and COMSTL scenarios are shown in Figure 27 and Figure 28 and the statistics listed in Table 10. Before the discussion on the export rates, it is important to mention the model primary production and its relevance to the observed values. Unrealistic primary production would result in unrealistic carbon export at depth. Therefore, the model should produce reliable productivities before any attempt on the extensive carbon export analyses.

The model derived annual primary production range between 430 – 450 mg C m^{-2} d^{-1} (13.0 – 13.6 moles C m^{-2} y^{-1}) at BATS and 357 – 381 mg C m^{-2} d^{-1} (10.9 – 11.6 moles C m^{-2} y^{-1}) at ESTOC for the STL scenarios. Given the reported primary production values of 13.33 moles C m^{-2} y^{-1} (Menzel and Ryther, 1960), 12.83 moles C m^{-2} y^{-1} (Steinberg *et al*, 2001), 13.08 moles C m^{-2} y^{-1} (Lomas *et al*, 2013), 11.56 moles C m^{-2} y^{-1} (Helmke *et al*, 2010) at BATS and 13.66 moles C m^{-2} y^{-1} (Davenport *et al*, 2002) and 13.38 moles C m^{-2} y^{-1} (Helmke *et al*, 2010) at ESTOC, all of the BATS results are within the range of the observed values. ESTOC results are slightly less than the observed values, but this issue was reported in NA1 and existed regardless of the changes applied here. In fact, statistics show that the model & observation data correlations are ~ 0.8 and ~ 0.53 for BATS and ESTOC, and normalized standard deviations are ~ 0.72 for BATS and between 0.52 – 0.64 for ESTOC for all of the STL simulations. For model derived chlorophyll a values, statistics yield model – observation correlations of ~ 0.73 and 0.52, and normalized standard deviations of ~ 0.68 and ~ 0.88 for BATS and ESTOC respectively. These statistics conclude that the settling rate modifications had minor implications on the upper water column lower trophic dynamics. Since the model has an acceptable range of primary production results, analyses can be carried on with the carbon export rates, where significant changes were observed. Figure 27 summarizes these changes perfectly. At each shown depth range, carbon export rates deviated from the ORIG simulation without any exception. The response of the model was highly robust to the changes in related sinking rates, such that changes in DetSlow

sinking rate (STL1, 4, 5,and 6) affected the surface layers more (Figure 27a,b,c,e,f,g and j), those that relate with DetFast were effective mostly in deeper layers (Figure 27d, e, h, i and j).

Profile plots (Figure 27e and j) successfully emphasize the effective locations of the modifications on DetSlow and DetFast. Having the slowest settling rates of DetSlow, STL1, STL4, STL5 and STL6, all piled together at depths above 200 m when averaged annually. On the contrary, with relatively higher DetSlow settling rates, STL2, STL3 and ORIG scenarios had nearly double the carbon export reaching as deep as 300 m. Modifications on the "DetFast" settling rates effected the deeper layer carbon export more. With elevated "DetFast" settling rates, STL4 and STL5 scenarios deviated from the rest, especially at depths below 300 m. Direct comparison with the observations emphasize these as well. Export at 150 m depths (Figure 27a and f) show a cluster with relatively lower values fixed around 20 – 30 mg C m^{-2} d^{-1} range from the STL1, STL4 and STL5 scenarios, and scenarios STL2, STL3 and ORIG with as high as 60 – 70 mg C m^{-2} d^{-1} range for the summer period. Carbon export for the winter mixing period are generally elevated for all of the scenarios, with again STL3 having the highest peaks in export. Similar patterns were also valid for 200 m depth (Figure 27b and g) with STL1 having the lowest export and STL3 having the highest. As the particles descend through the mesopelagic, the gap between the scenarios decreased at 300 m (Figure 27c), and increase again shifting to the STL4 and STL5 scenarios. The gap became much more evident as the particles descended lower than 500 m depth range (Figure 27d, h and i). Scenarios with the lower "DetFast" range (STL1, STL2, STL3 and ORIG) pile together, and STL4 and especially STL5 becoming dominant in export. This kind of a shift was expected because, due to their prescribed sinking speeds, "DetSlow" was more abundant in the upper 300 meters, and with having higher sinking rates, "DetFast" could escape the upper water column, becoming more abundant in the deeper layers. Therefore, any attempt in modifying their individual settling rates effected the related depth range in the water column. Starting from the STL1 scenario, prescribed "DetSlow" 2 m d^{-1} settling rate was doubled and tripled in STL2 and STL3 scenarios with a common upper limit of 7 m d^{-1}. ORIG simulation had single a speed of 5 m d^{-1}. Carbon export at 200 m at BATS increased by 54 % and 122 %, and at ESTOC by 59 % and 147 % within STL2 and STL3 simulations respectively. Likewise at depth, BATS export at 500 m increased by 97 % and 179 % in STL4 and STL5 scenarios. ESTOC response at 500 m was no different. Export increased by 88 % and 158 % respectively. The response increases with depth. For example at 900 m at ESTOC, export increased by 106 % and 206 % in STL4 and STL5 scenarios.

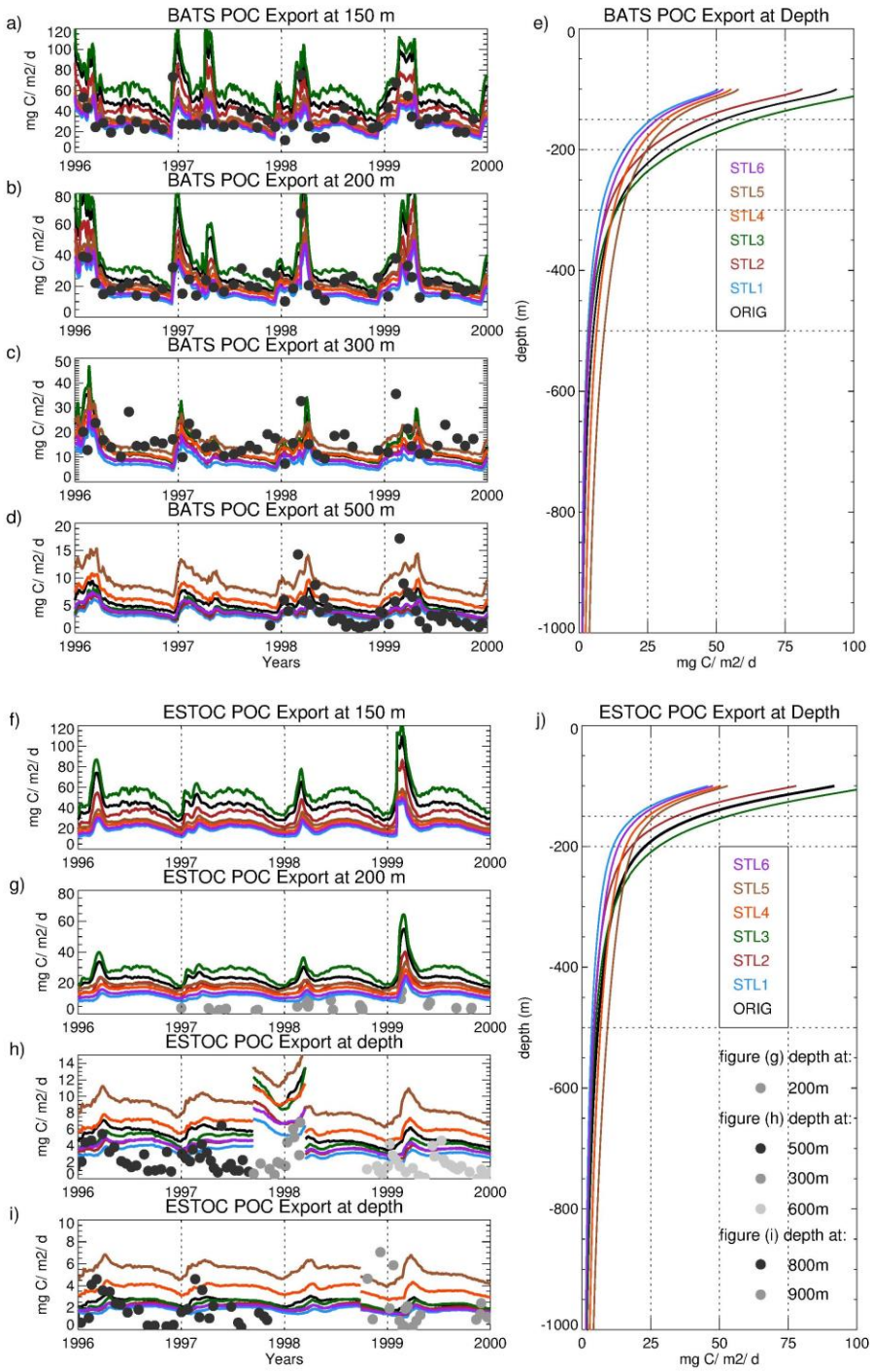

Figure 27) STL1-6 carbon export (mg C m^{-2} d^{-1}) at depth for BATS (Figures a - e) and ESTOC (Figures f - j). Simulated carbon export is compared to the observed carbon export data taken from Torres Valdés *et al.* (2014) and references therein, at depths **a)** 150 m, **b)** 200 m, **c)** 300 m, **d)** 500 m for BATS, and **f)** 150 m, **g)** 200 m, **h)** 500, 300, and 600 m, **i)** 800 and 900 m for ESTOC. Simulated annually averaged water column carbon export (mg C m^{-2} d^{-1}) are given in **e)** for BATS and **j)** for ESTOC. For the ESTOC comparisons, observations are grey color coded with the corresponding simulated carbon export matching that depth. Black solid lines denote the ORIG simulation, and the STL 1 – 6 scenarios are color coded. Color codes for the simulations and the observations are given in the legend in the figures.

Table 10) Summarized statistics of the STL scenarios for BATS and ESTOC simulations. Standard deviations are given in the normalized form (norm std.) such that each variables model standard deviation is normalized to the observation standard deviation resulting in standard deviation value of "1" for a perfect match with the observations. Model to observation correlations (r) are also given. Primary productions (PP) are given in depth integrated form (mg C m^{-2} d^{-1}). Carbon export (exp.) are listed for various depths matching the observation depths given in "mg C m^{-2} d^{-1}".

		ORIG		STL1		STL2		STL3	
		mean	**NSTD**	**mean**	**NSTD**	**mean**	**NSTD**	**mean**	**NSTD**
BATS	PP	429.6	0.703	450.0	0.733	445.2	0.728	430.8	0.708
	150 m	53.3	1.067	26.7	0.478	44.3	0.796	64.2	1.065
	200 m	31.2	1.546	16.6	0.714	25.5	1.191	36.9	1.627
	300 m	13.5	0.786	8.1	0.431	10.5	0.643	13.9	0.885
	500 m	5.3	0.328	3.3	0.173	3.7	0.198	4.3	0.245
ESTOC	PP	362.4	0.596	379.2	0.518	381.6	0.569	357.6	0.642
	200 m	23.2	2.150	11.4	0.409	18.1	1.277	28.2	2.553
	300 m	11.6	0.496	6.7	0.328	8.7	0.424	11.8	0.568
	500 m	5.8	0.339	3.6	0.282	4.2	0.318	5.0	0.392
	600 m	4.4	0.518	2.8	0.300	3.3	0.354	3.8	0.482
	800 m	2.7	0.185	1.9	0.165	2.2	0.185	2.5	0.220
	900 m	2.1	0.174	1.6	0.128	1.8	0.145	2.1	0.172
		ORIG		**STL1**		**STL2**		**STL3**	
		r	**% bias**	**r**	**% bias**	**r**	**% bias**	**r**	**% bias**
BATS	PP	0.806	0.3	0.809	5.0	0.807	4.0	0.805	0.5
	150 m	0.479	71.5	0.424	-13.6	0.460	42.5	0.453	106.2
	200 m	0.481	46.4	0.412	-22.4	0.462	19.4	0.480	72.3
	300 m	0.190	-8.9	0.187	-45.3	0.170	-28.9	0.178	-6.1
	500 m	0.493	30.8	0.249	-20.1	0.256	-8.3	0.304	4.7
ESTOC	PP	0.529	-2.7	0.524	0.5	0.522	2.0	0.530	-3.4
	200 m	0.644	354.3	0.510	118.0	0.584	253.2	0.586	451.8
	300 m	0.465	256.2	-0.548	99.9	-0.460	157.8	-0.124	241.8
	500 m	0.229	141.4	-0.419	46.8	-0.358	75.2	-0.206	106.1
	600 m	-0.052	173.5	-0.113	76.4	-0.122	106.7	-0.069	137.8
	800 m	0.363	44.7	-0.494	0.2	-0.407	17.4	-0.203	33.95
	900 m	-0.405	5.63	-0.011	-25.1	-0.035	-13.1	-0.130	-1.84

Table 10 continued

		STL4		STL5		STL6	
		mean	**NSTD**	**mean**	**NSTD**	**mean**	**NSTD**
BATS	PP	444.0	0.722	440.4	0.715	447.6	0.728
	150 m	31.8	0.528	34.9	0.580	28.8	0.504
	200 m	21.6	0.788	24.9	0.859	18.7	0.752
	300 m	12.7	0.523	16.0	0.614	9.8	0.473
	500 m	6.5	0.336	9.2	0.530	4.1	0.220
ESTOC	PP	373.2	0.514	368.4	0.512	376.8	0.517
	200 m	16.1	0.531	18.8	0.697	13.3	0.463
	300 m	11.0	0.309	13.8	0.456	8.2	0.272
	500 m	6.8	0.332	9.3	0.437	4.4	0.241
	600 m	5.5	0.546	7.8	0.855	3.4	0.32
	800 m	3.9	0.232	5.6	0.335	2.1	0.130
	900 m	3.3	0.230	4.9	0.420	1.7	0.116
		STL4		**STL5**		**STL6**	
		r	**% bias**	**r**	**% bias**	**r**	**% bias**
BATS	PP	0.808	3.6	0.808	2.7	0.809	4.4
	150 m	0.415	2.9	0.418	12.7	0.424	-6.6
	200 m	0.406	0.9	0.407	15.7	0.414	-12.8
	300 m	0.217	-15.2	0.241	6.32	0.202	-34.4
	500 m	0.445	61.1	0.555	130.3	0.404	0.8
ESTOC	PP	0.526	-1.1	0.527	-2.2	0.524	-0.3
	200 m	0.681	205.5	0.744	257.2	0.637	153.9
	300 m	0.008	239.3	0.535	337.5	-0.252	151.9
	500 m	-0.057	180.9	0.315	284.7	-0.218	81.1
	600 m	-0.028	245.9	-0.003	383.7	-0.095	111.4
	800 m	0.019	109.6	0.457	206.8	-0.216	14.3
	900 m	-0.286	62.8	-0.410	150.0	-0.200	-15.6

When the model performances are compared, BATS simulations perform much better. Although with minor exceptions, BATS % biases were within the ± 50% range, with many reaching a no major bias range (Table 10). In the ESTOC case, biases as high as 354 % were simulated, with most of the biases outside the ± 100% range. Correlations and normalized standard deviations were no different. Normalized standard deviations were low and were mostly packed below 0.75. BATS export correlations performed much better, with all positive values and within the 0.2 – 0.5 band, with most of the normalized standard deviations located within the 0.5 – 1 range.

STL simulations suggest that the carbon export is very sensitive to changes in settling rates. However, none to very low variability were achieved in these changes, where most of the changes were observed in % biases. This suggest that the model is very robust with the settling rates. The robustness of the model to settling rates also suggest that plankton specification in settling rates may introduce high variability to carbon export with different settling rate ranges. COMSTL simulation adopt community specific settling rates for this reason. Major changes were simulated coinciding with the winter mixing periods at both BATS and ESTOC (Figure 28). The simulated carbon export were already higher in winter mixing periods in STL6 scenarios, but the results were exacerbated with the addition of community specific settling rates. Winter export within 150 – 300 m nearly doubled in both BATS and ESTOC. On the contrary, slight decrease in export rates, especially at deeper layer were observed. These changes were the reflections of the high sinking rates of diatom and mesozooplankton and relatively lower rates assigned for the small phytoplankton. Within the same station, community settling rates can change the magnitude of export relative to the single settling rates (STL6) scenario, and hence increase the variability among different seasons. However, the striking result of the COMSTL simulation lies within its capacity to differentiate export at different locations. Figure 29a and b are BATS and ESTOC which are located at the subtropics and Figure 29c is PAP station, which is located north in the transition region to subpolar North Atlantic. Therefore, PAP station has different physical dynamics, atmospheric forcing, nutrient concentrations and as a result of those, different community structure. As was discussed in detail in Chapter 4, PAP diatom and mesozooplankton biomasses are relatively much higher compared to its subtropical counterparts, leading to faster export and higher export efficiency out of the EZ. In fact, with COMSTL modifications, export at 150, 200 and 300 m at BATS increased by 47%, 21% and 3.6%, and at ESTOC by 55%, 38% and 14%, whereas these values were as high as 156%, 212% and 264% respectively.

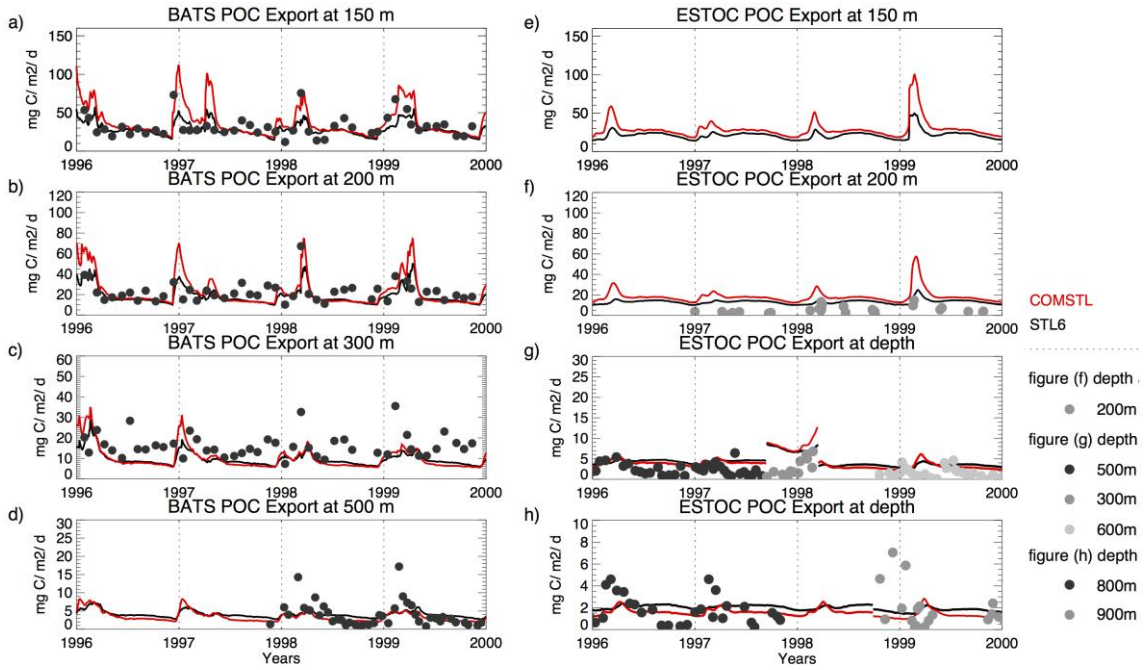

Figure 28) COMSTL carbon export (mg C m^{-2} d^{-1}) at depth for BATS (Figures a - d) and ESTOC (Figures e - h). Black line denotes STL6, and the red line denote COMSTL simulations. The definitions of the observations are given in Figure 27.

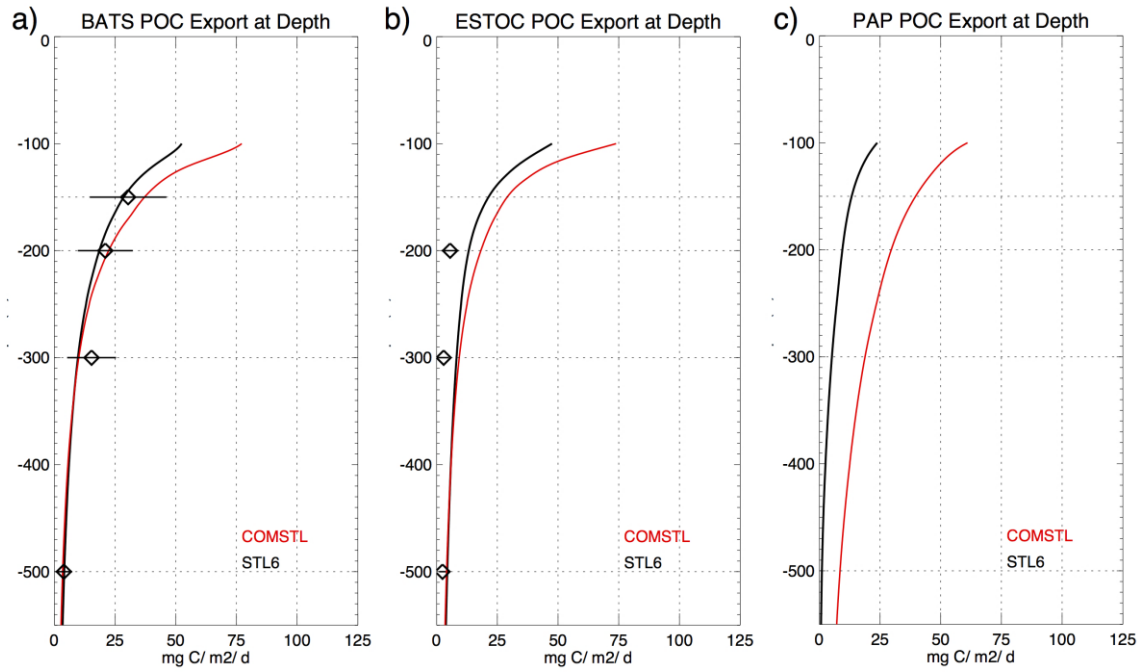

Figure 29) Comparison of COMSTL and STL6 scenario's annual averaged carbon export (mg C m^{-2} d^{-1}) profile at **a)** BATS, **b)** ESTOC and **c)** PAP. Diamonds in figure a and b indicate the averaged available sediment trap data at the corresponding depth and lines crossing the diamonds indicate the extent of observation standard deviations.

The AGG, FEC, FECAGG and COMSTL (for comparison) results for particle export at depth and observations are given in Figure 30 and statistics are given in Table 11. These

aggregation scenarios are based on the COMSTL scenario. The model derived annual primary production range between 427 – 434 mg C m^{-2} d^{-1} for these 4 scenarios suggesting a none to a very minor change compared to the annual primary productivities achieved in COMSTL scenario. Weaker primary production at ESTOC compared to BATS still holds. Since the changes were minor in primary production at both sides, the model results fall in the reliable range when compared to the observations at both sides. BATS model and observed primary production data correlations were high (~0.8), and ~ 20% increase in ESTOC correlations (from 0.52 to ~0.63) were seen for all four simulations compared to STL scenarios. Normalized primary productivity standard deviations range around 0.69 - 0.71 at BATS and 0.53 – 0.57 at ESTOC.

Similar to the STL scenarios, major changes were observed in carbon export, and their related statistics. STL simulations resulted in very weak correlations with the observations. COMSTL simulation had minor improvements on these. Just like COMSTL did on STL6, aggregation scenarios exacerbated the variability in export. Wintertime AGG export at BATS and ESTOC and at all depths were higher compared to COMSTL. The AGG simulation was most effective in the presence of turbulence, represented as the mixed layer in NAGEM. Deeper and prolonged mixing triggered higher aggregation flux to DetFast which in turn resulted in higher export rate compared to stable water column periods. FEC, on the other hand, was zooplankton biomass triggered, thus, the changes achieved with FEC did not always coincide with AGG simulation, especially in winter periods, i.e Figure 30g winter 1998. The true effect of aggregation is realized when both physics and biology is combined in FECAGG. BATS 150 m export witnessed as high as ~50% increase, and the increase was as high as ~100% at 200 m.

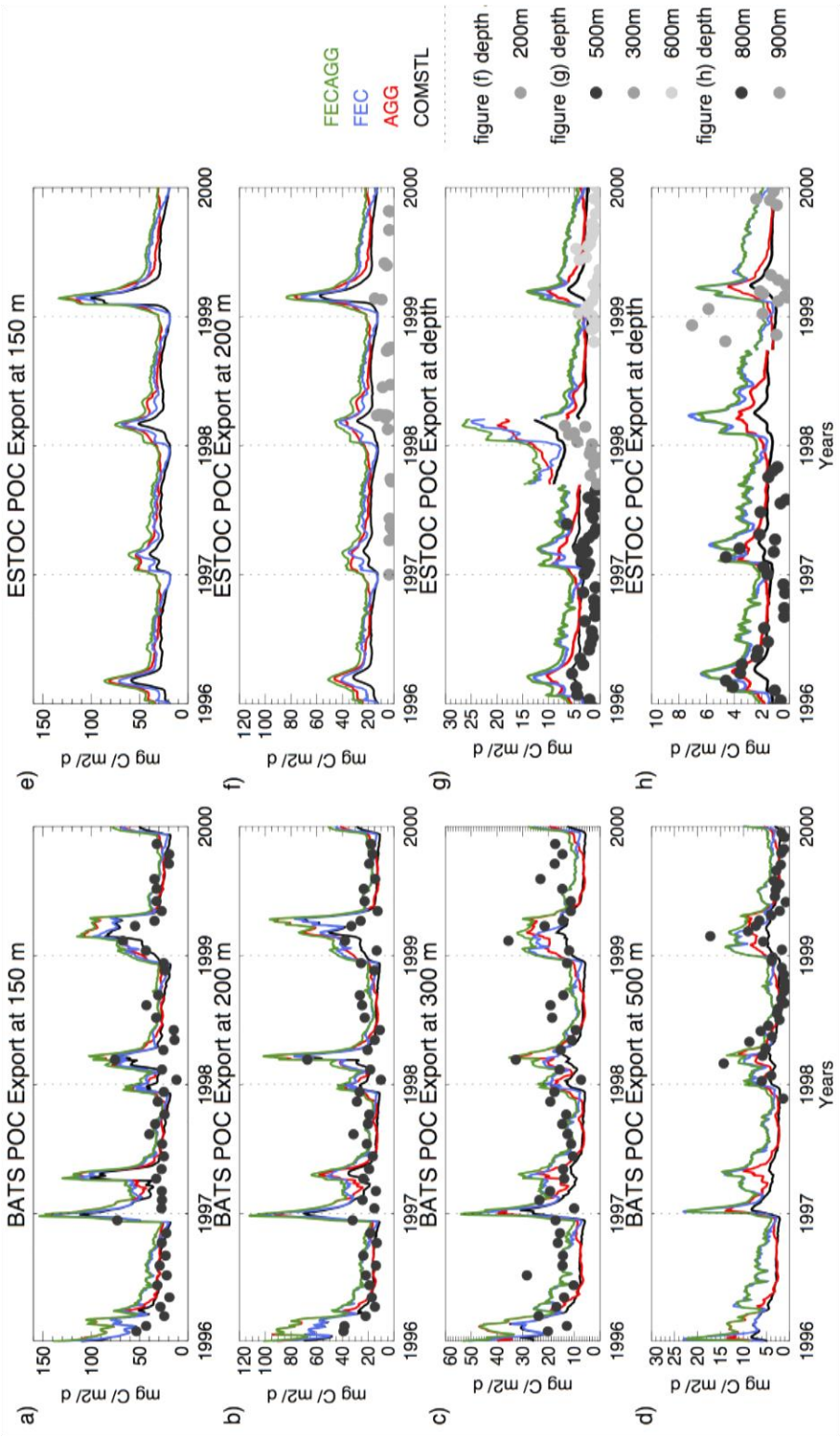

Figure 30) AGG, FEC and FECAGG carbon export (mg C m^{-2} d^{-1}) for BATS (Figures a - d) and ESTOC (Figures e - h), at depths **a)** 150 m, **b)** 200 m, **c)** 300 m, **d)** 500 m for BATS, and **f)** 150 m, **g)** 200 m, **h)** 500, 300, and 600 m, **i)** 800 and 900 m for ESTOC. Color codes for the simulations and the observations are given in the legend in the figures.

Table 11) Summarized statistics of the COMSTL, AGG, FEC, FECAGG, BAL, ALL and REM scenarios for BATS and ESTOC simulations. Standard deviations are given in the normalized form (norm std.) such that each variables model standard deviation is normalized to the observation standard deviation resulting in standard deviation value of "1" for a perfect match with the observations. Model to observation correlations (r) are also given. Primary productions (PP) are given in depth integrated form (mg C m^{-2} d^{-1}). Carbon export are listed for various depths matching the observation depths given in "mg C m^{-2} d^{-1}".

		COMSTL		AGG		FEC		FECAGG	
		mean	**NSTD**	**mean**	**NSTD**	**mean**	**NSTD**	**mean**	**NSTD**
BATS	PP	434.16	0,71	433.92	0,71	428.88	0,70	427.8	0,70
	150 m	37,13	1,13	45,64	1,58	44,75	1,22	51,74	1,52
	200 m	22,35	1,33	28,61	1,93	29,16	1,33	34,22	1,83
	300 m	10,05	0,74	13,56	1,22	15,23	0,82	17,91	1,13
	500 m	3,42	0,28	4,77	0,66	6,41	0,69	7,31	0,79
ESTOC	PP	366.72	0,53	363.6	0,56	359.88	0,53	355.56	0,56
	200 m	18,21	2,63	24,67	3,96	23,90	3,27	29,11	4,12
	300 m	9,30	0,53	12,98	1,65	14,00	2,42	16,72	2,48
	500 m	4,10	0,41	5,73	1,12	7,17	1,31	8,16	1,28
	600 m	2,95	0,65	4,10	1,27	5,43	1,86	6,06	1,70
	800 m	1,66	0,21	2,25	0,51	3,31	0,75	3,56	0,67
	900 m	1,29	0,26	1,73	0,47	2,65	0,73	2,81	0,66
		COMSTL		**AGG**		**FEC**		**FECAGG**	
		r	**% bias**	**r**	**% bias**	**r**	**% bias**	**r**	**% bias**
BATS	PP	0,81	1,36	0,81	1,29	0,81	0,12	0,81	-0,14
	150 m	0,45	20,11	0,49	47,59	0,42	42,66	0,48	66,31
	200 m	0,45	5,00	0,48	34,49	0,42	33,35	0,47	58,64
	300 m	0,16	-32,18	0,17	-8,56	0,19	-1,55	0,19	17,92
	500 m	0,59	-21,42	0,62	12,90	0,59	42,30	0,65	66,77
ESTOC	PP	0,63	-2,08	0,64	-2,71	0,63	-3,82	0,64	-4,71
	200 m	0,68	276,72	0,68	389,85	0,71	397,62	0,69	484,09
	300 m	0,48	182,46	0,82	371,46	0,70	353,39	0,80	485,92
	500 m	0,36	68,63	0,59	136,11	0,36	187,27	0,55	230,83
	600 m	-0,18	82,92	-0,12	147,78	-0,05	238,02	-0,03	276,43
	800 m	0,49	-9,94	0,75	25,61	0,52	73,89	0,64	89,92
	900 m	-0,36	-29,73	-0,41	3,30	-0,46	46,55	-0,43	54,18

Table 11 continued

		BAL		ALL		REM	
		mean	**NSTD**	**mean**	**NSTD**	**mean**	**NSTD**
BATS	PP	430.44	0,70	423.48	0,69	423.84	0,69
	150 m	38,88	1,17	53,43	1,58	52,79	1,60
	200 m	23,49	1,40	35,36	1,94	35,25	1,91
	300 m	10,90	0,80	18,75	1,24	19,33	1,14
	500 m	4,08	0,41	7,96	0,96	8,69	0,96
ESTOC	PP	362.76	0,53	350.76	0,56	350.76	0,57
	200 m	19,15	2,78	30,05	4,30	30,37	4,30
	300 m	9,98	0,60	17,39	2,59	18,71	2,57
	500 m	4,60	0,53	8,64	1,44	9,87	1,43
	600 m	3,42	0,89	6,51	1,97	7,58	1,80
	800 m	2,09	0,35	3,99	0,84	4,77	0,80
	900 m	1,72	0,47	3,24	0,90	3,90	0,79
		BAL		**ALL**		**REM**	
		r	**% bias**	**r**	**% bias**	**r**	**% bias**
BATS	PP	0,81	0,49	0,81	-1,15	0,81	-1,06
	150 m	0,44	25,81	0,48	71,92	0,48	69,64
	200 m	0,44	10,43	0,46	64,17	0,46	63,12
	300 m	0,17	-26,35	0,20	23,64	0,20	26,55
	500 m	0,57	-5,65	0,65	81,75	0,65	102,53
ESTOC	PP	0,63	-3,10	0,64	-5,91	0,65	-5,88
	200 m	0,69	297,68	0,70	505,86	0,70	508,10
	300 m	0,52	198,05	0,81	501,08	0,83	557,68
	500 m	0,41	89,15	0,57	250,64	0,59	303,38
	600 m	-0,13	111,64	-0,01	302,52	0,01	364,76
	800 m	0,59	13,88	0,67	113,14	0,69	156,92
	900 m	-0,37	-1,46	-0,40	83,13	-0,44	110,13

Besides visual improvements, statistical improvements in carbon export at both stations were also clear (Table 11). Statistical evaluation of BATS show controversial results at the surface (150 – 200 m) and in deep (300 – 500 m). The addition AGG simulation increased the NSTD at the surface. COMSTL resulted in good agreement with the observations at these depths (1.13 – 1.33), but changes with AGG and FECAGG resulted in higher estimates (1.52 – 1.93). However, the changes improved the export in deeper layers. The jumps at depths 300 and 500 m were from 0.74 and 0.28 to 1.22 – 0.66 in AGG and 1.13 – 0.79 in FECAGG respectively. Correlations maintained their average values in COMSTL, AGG and FECAGG simulations (0.45±0.03 at 150 – 200 m), as well as the low correlations at 300 m (0.17±0.02). Interestingly, correlations at BATS 500 m are high (0.62±0.03). As expected, % biases increased from 20% to 66% at 150 m, and from 5% to 58% in FECAGG scenario. Similar to the surface, at 300 m, % biases increased from -32% to 17.92, and at 500 m from -21% to 67%. Interestingly, AGG scenario export within 0 – 1000 m increased compared to COMSTL (Table 12), where below, AGG witnessed a decrease. This decrease was only valid for the AGG simulation. FEC and FECAGG simulation export all increased throughout the water column, FECAGG receiving the highest change.

Similar to BATS, ESTOC received increased export rates within 0 – 1000 m depth range between 31.4 – 39.8, and a decrease below (between -5 and -16). The increase in export was more pronounced in the mesopelagic (as high as 100%) in FECAGG simulation for both of the simulations, as expected due to faster sinking rates assigned for fecal pellets in COMSTL. Increased export was also followed by increased NSTD's for AGG, FEC and FECAGG at ESTOC. ESTOC export at 300 – 800 m had significant improvements in correlations with AGG and FECAGG simulations, suggesting that just like at BATS, aggregation was necessary to capture variability. However, % biases were not subject any improvements. In fact, increases of 2-3 fold %biases were simulated with AGG and FECAGG. Although added variability and higher correlations suggest improvements in model statistics, the actual output in terms of magnitude got worse.

Table 12) Annually averaged primary production and export rates (mg C m^{-2} d^{-1}) at certain depths from COMSTL simulations, and percent changes achieved in AGG, FEC, FECAGG, BAL, ALL, REM and DVM simulations for BATS, ESTOC and PAP.

Model Result	mg C m^{-2} d^{-1}	**% Change Compared to COMSTL**						
BATS	**COMSTL**	**AGG**	**FEC**	**FECAGG**	**BAL**	**ALL**	**REM**	**DVM**
Prim. Prod.	434.16	~0.00	~ -0.01	~ -0.01	~ -0.00	~ -0.02	~ -0.02	~ -0.02
Exp 150 m	37.13	22.9	20.5	39.4	4.7	43.9	42.2	39.5
Exp 200 m	22.35	28.0	30.4	53.1	5.1	58.2	57.7	51.8
Exp 300 m	10.05	35.0	51.5	78.2	8.5	86.6	92.4	125.5
Exp 500 m	3.42	39.6	87.7	114.1	19.3	132.9	154.5	191.4
Exp 1000 m	0.75	30.7	127.1	143.6	79.9	227.8	267.8	303.4
Exp 2000 m	0.36	-7.3	87.3	82.4	179.1	279.4	299.4	258.3
Exp 3000 m	0.34	-16.6	64.1	53.7	214.3	290.6	294.4	214.9
Model Result	mg C m^{-2} d^{-1}	**% Change Compared to COMSTL**						
ESTOC	**COMSTL**	**AGG**	**FEC**	**FECAGG**	**BAL**	**ALL**	**REM**	**DVM**
Prim. Prod.	366.72	~ -0.00	~ -0.02	~ -0.03	~ -0.01	~ -0.04	~ -0.04	~ -0.04
Exp 150 m	29.03	31.6	21.6	47.7	3.6	51.6	49.3	57.9
Exp 200 m	18.20	35.5	31.3	59.9	5.2	65.0	66.8	80.0
Exp 300 m	9.30	39.6	50.6	79.8	7.3	87.0	101.1	168.7
Exp 500 m	4.10	39.8	75.0	99.2	12.2	110.8	140.9	197.8
Exp 1000 m	1.02	31.4	111.4	120.7	41.6	162.9	217.7	286.2
Exp 2000 m	0.36	-5.2	90.6	81.1	125.1	219.1	250.8	230.0
Exp 3000 m	0.35	-16.06	62.7	51.7	140.0	208.0	215.8	144.9
Model Result	mg C m^{-2} d^{-1}	**% Change Compared to COMSTL**						
PAP	**COMSTL**	**AGG**	**FEC**	**FECAGG**	**BAL**	**ALL**	**REM**	**DVM**
Prim. Prod.	374.78	0.2	-0.3	0.2	-1.2	-1.3	0.6	-0.3
Exp 150 m	39.63	24.2	39.8	60.0	4.2	63.5	49.8	30.3
Exp 200 m	29.61	27.7	46.8	70.5	4.3	74.4	59.0	32.8
Exp 300 m	18.80	31.2	58.3	85.8	5.7	91.4	74.9	101.1
Exp 500 m	8.50	32.9	83.9	113.9	12.1	125.5	106.6	114.9
Exp 1000 m	2.13	28.4	137.8	168.4	49.4	214.8	190.2	181.7
Exp 2000 m	0.54	3.4	142.8	161.4	203.4	354.9	340.	274.8
Exp 3000 m	0.37	-13.9	87.0	86.2	314.8	386.7	383.3	291.3

The standalone mineral ballast simulations (BAL) were not effective as the aggregation simulations (Figure 31) in the upper layers. Both BATS and ESTOC export within 150 – 300 m % change compared to COMSTL were below 10 % (Table 12). The situation also holds for the ALL simulations, where BAL simulation added <10% change on FECAGG simulation. Similar NSTD values were simulated with the COMSTL simulation in BAL, with similar % biases compared to COMSTL. The true effect of BAL simulations were initiated below 300 m, where BATS export at 500 m, and ESTOC export at 500 m and below increased in magnitude starting with the winter followed by the spring increase in export. The actual % change in BAL simulations were located at 3000 m (Table 12). Compared to FECAGG increase of 51.7 and 86.2 % at BATS and ESTOC respectively, BAL simulations resulted in 140 and 314 %. The increases in export at depth were not regular, as mentioned, seasonal changes were observed, an expected result due to the dominance of diatoms and picoeukaryotes ($CaCO_3$ source) in winter/spring periods in NAGEM simulations. Although minor, correlation improvements (increasing with depth) were simulated at ESTOC (BATS data lack below 500 m for comparison).

Figure 32 compares the combination of community settling rates, aggregation and ballasting (ALL) with the community specific remineralization rates (REM). Similar to BAL compared to COMSTL, REM compared to ALL was ineffective at the surface. Both BATS and ESTOC % changes at 150 and 200 m were very similar to ALL simulations. The export rates in REM start to deviate from ALL at 300 m and below with an increase in magnitude. Although minor, the changes were mainly located in summer periods, suggesting that low remineralization rates set for the picoplankton were effective in these periods. At 500 m and below, the difference in REM and ALL is distinct (Figure 32). Minor improvements were achieved in ALL correlations compared to FECAGG, and in REM compared to ALL. However, % biases are very high at ESTOC. BATS export at depth % biases are within 26 – 102 % range, but the biases at ESTOC are as high as 500 %, suggesting that 3-5 fold difference in export ratios between BATS and ESTOC were completely missed with these simulations.

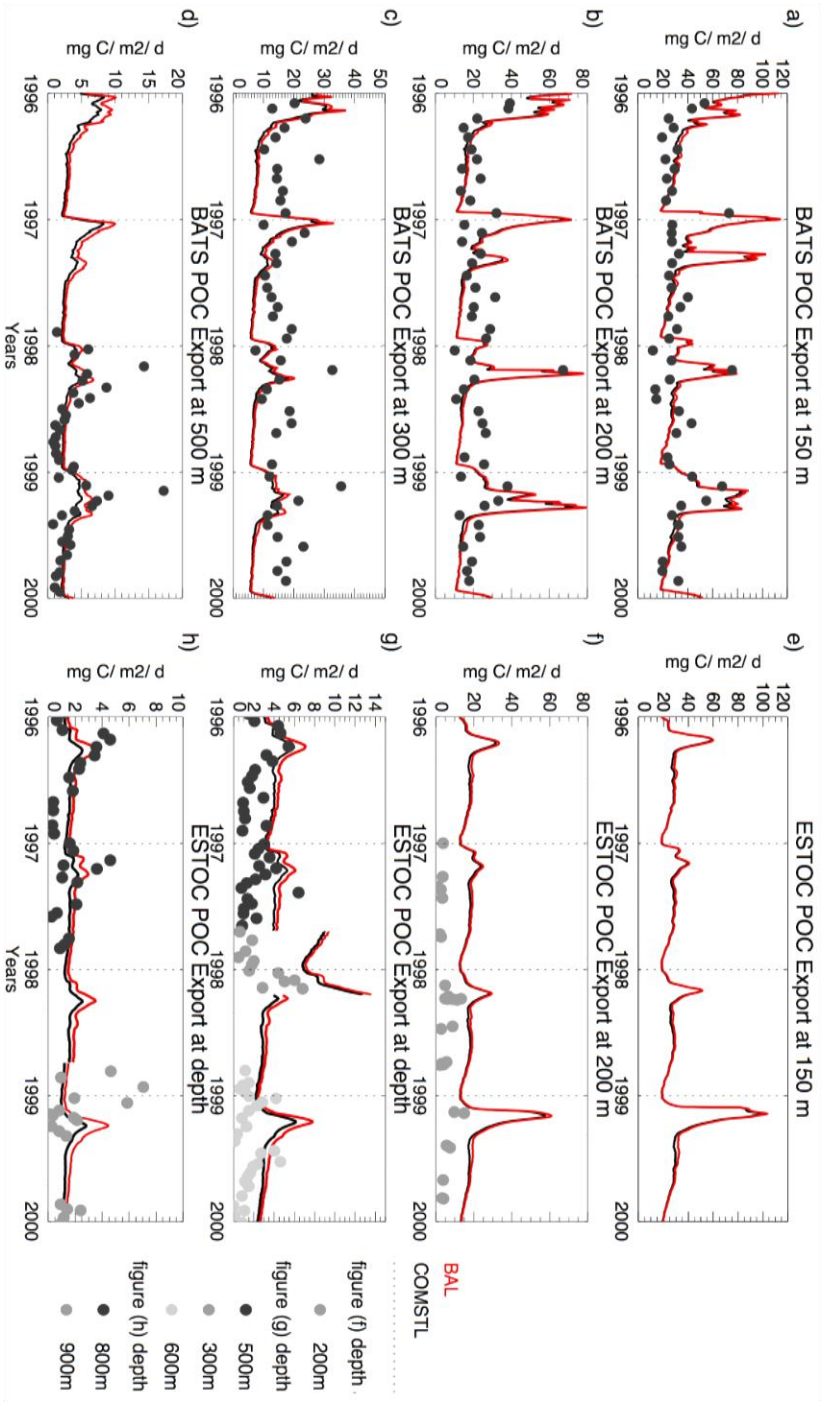

Figure 31) COMSTL and BAL carbon export (mg C m^{-2} d^{-1}) for BATS (Figures a - d) and ESTOC (Figures e - h), at depths **a)** 150 m, **b)** 200 m, **c)** 300 m, **d)** 500 m for BATS, and **f)** 150 m, **g)** 200 m, **h)** 500, 300, and 600 m, **i)** 800 and 900 m for ESTOC. Color codes for the simulations and the observations are given in the legend in the figures

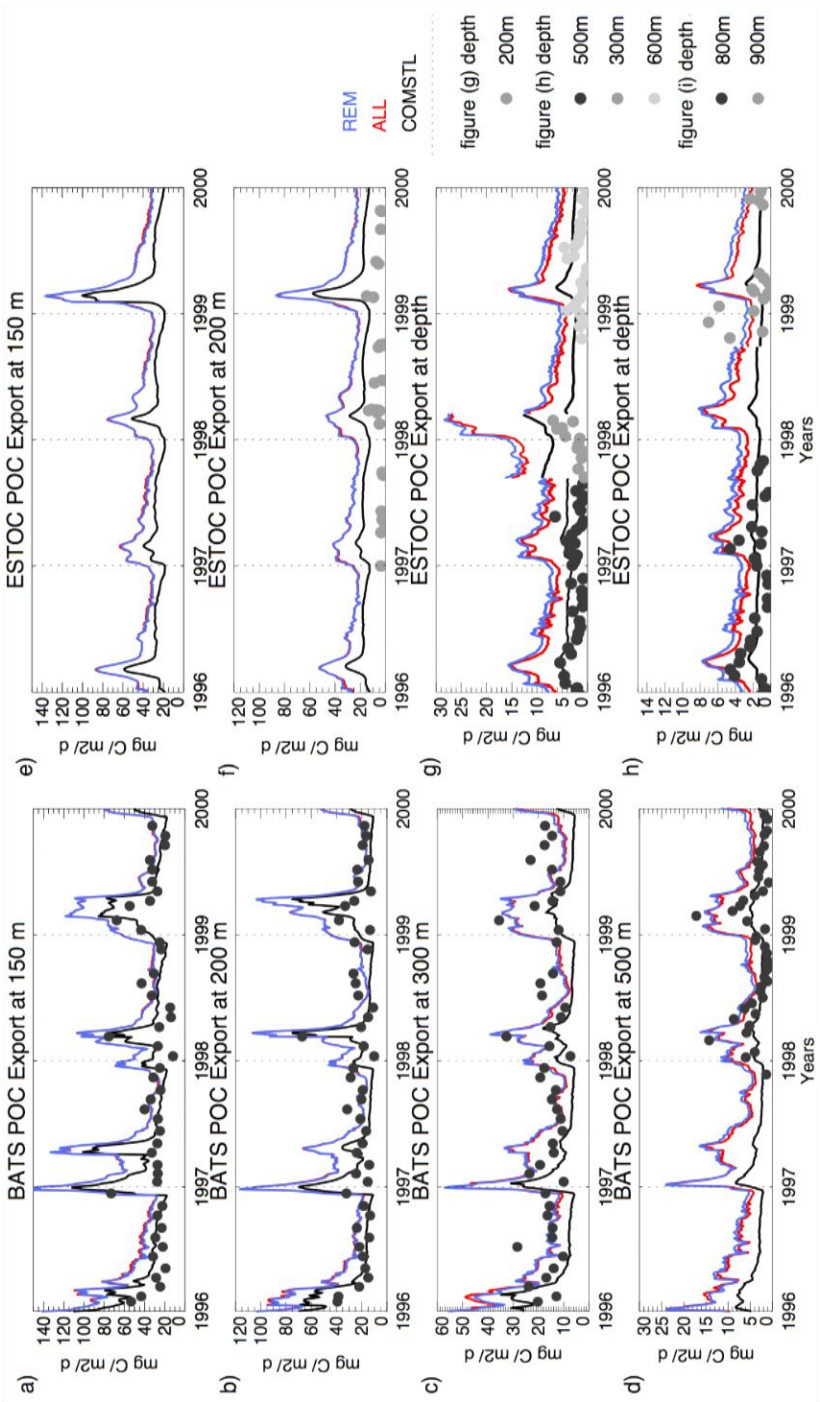

Figure 32) COMSTL, ALL and REM carbon export (mg C m^{-2} d^{-1}) for BATS (Figures a - d) and ESTOC (Figures e - h), at depths **a)** 150 m, **b)** 200 m, **c)** 300 m, **d)** 500 m for BATS, and **f)** 150 m, **g)** 200 m, **h)** 500, 300, and 600 m, **i)** 800 and 900 m for ESTOC. Color codes for the simulations and the observations are given in the legend in the figures.

Plankton state variables in NAGEM are prone to advection and diffusion for the vertical displacement. A unique addition to REM simulation was applied, where mesozooplankton follow the radiation at the surface to swim down below the EZ in day, and follow the prey availability in the night, swimming to the surface. The parameterization and code adjustment is given in Section 5.2.3.5, and PAP site result is given as an example biomass distribution (Figure 33). The plot is daily averaged, so that both daytime and nighttime mesozooplankton are visible in the plot, where a narrow band of biomass between 200 – 300 m were simulated. The implications show the intense and immediate transport of biomass on export. From the 0 – 100 m depth band, zooplankton biomass bypasses > 200 m within a period of 1 hour, where in the other simulations, a particle with an average sinking rate of 20 m d^{-1} would take 10 days to cover that range, and be degraded by detritus consumers and bacteria. Due to the active transport of particles, detritus is completely protected from degradation bypassing 200 m depth into the mesopelagic. The jumps in export rate at 300 m is evident in Table 12, where significant increase in % change is simulated. The depths below 300 m are thus affected by the intense change responding accordingly.

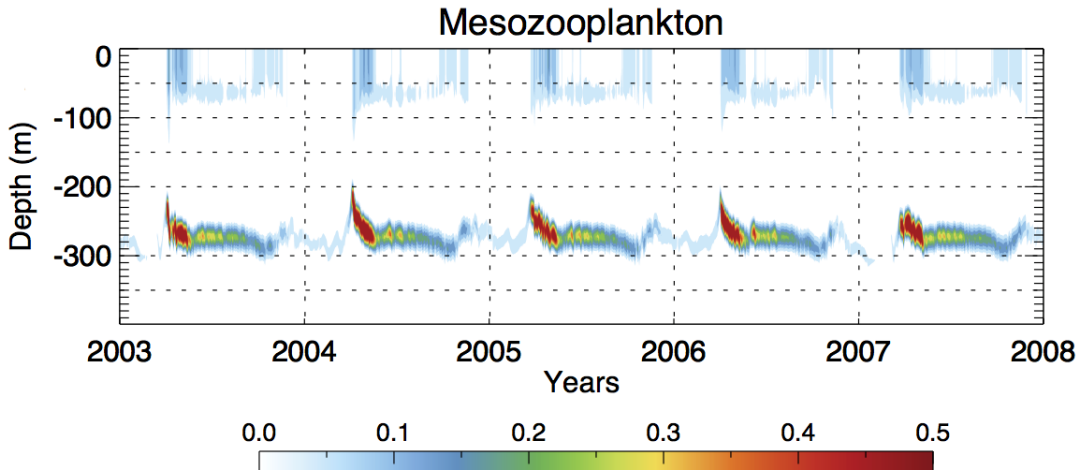

Figure 33) DVM simulation daily averaged (µmol C m^{-3}) mesozooplankton biomass simulated at PAP site. Since the plot is daily averaged, mesozooplankton appear to co-locate at the surface and at depth, whereas simulations at each time-step (1 hour) distribute biomass accordingly.

The same set of simulations were also incorporated to PAP site in order to investigate the response of the algorithms to a colder, vertically more dynamic environment with a different community structure. The adoption of the community specific settling rates were already discussed in Section 5.2.3.1. Clear response was achieved with highly efficient export rates compared to STL6 due to the presence of faster sinking detritus from diatoms and

mesozooplankton. The remaining simulation's export rates are given in Figure 34, and % changes achieved compared to COMSTL simulation in Table 12.

The annually averaged primary production achieved in COMSTL simulation was 374 mg C m^{-2} d^{-1}, and the remaining scenarios resulted in similar productivities. At all depths, annually averaged carbon export is higher at PAP site compared to the subtropics. The gap between PAP export and the export at subtropics increases down in the water column, where at 300 and 500 m, export at PAP is nearly double of BATS and ESTOC.

Carbon export at PAP site is also very seasonal, with high peaks coinciding the end of the deep mixing period and beginning of the spring bloom, with a decreased pattern in the following months (Figure 34). Unfortunately, sediment trap data was unavailable for a mesopelagic export rate comparison with the subtropical counterparts, but sediment trap records are available in the abyss (3000 m) to compare deep model export predictions. The evident result from the simulations is that only ballast related simulations (BAL, ALL, REM and DVM) achieved to predict export rates closer to the observations, where the remaining failed. Just like in BATS and ESTOC, DVM simulation had a jump in % change at 300 m (more than 3-fold).

5.4.Discussions

Improved representation of carbon sequestration is a major focus of global carbon cycle studies, and the need for advanced algorithms of carbon export in models is recognized in recent decades (Sanders et al., 2014). The necessity of including detailed components of the BCP in ecosystem models, lies in BCP's importance in regulating the global carbon cycle. Sanders *et al.*, (2014) discuss the interconnected processes of the BCP and the importance of these processes, which include primary production, microbial loop, particle aggregation and sinking, remineralization, grazing, vertical migration and transport of materials in the North Atlantic and the necessity of the inclusion of these processes in models. Those processes are represented in ecosystem models by simple to complex definitions, and in this chapter, it was attempted to represent those procedures with the aim of evaluating their use and success.

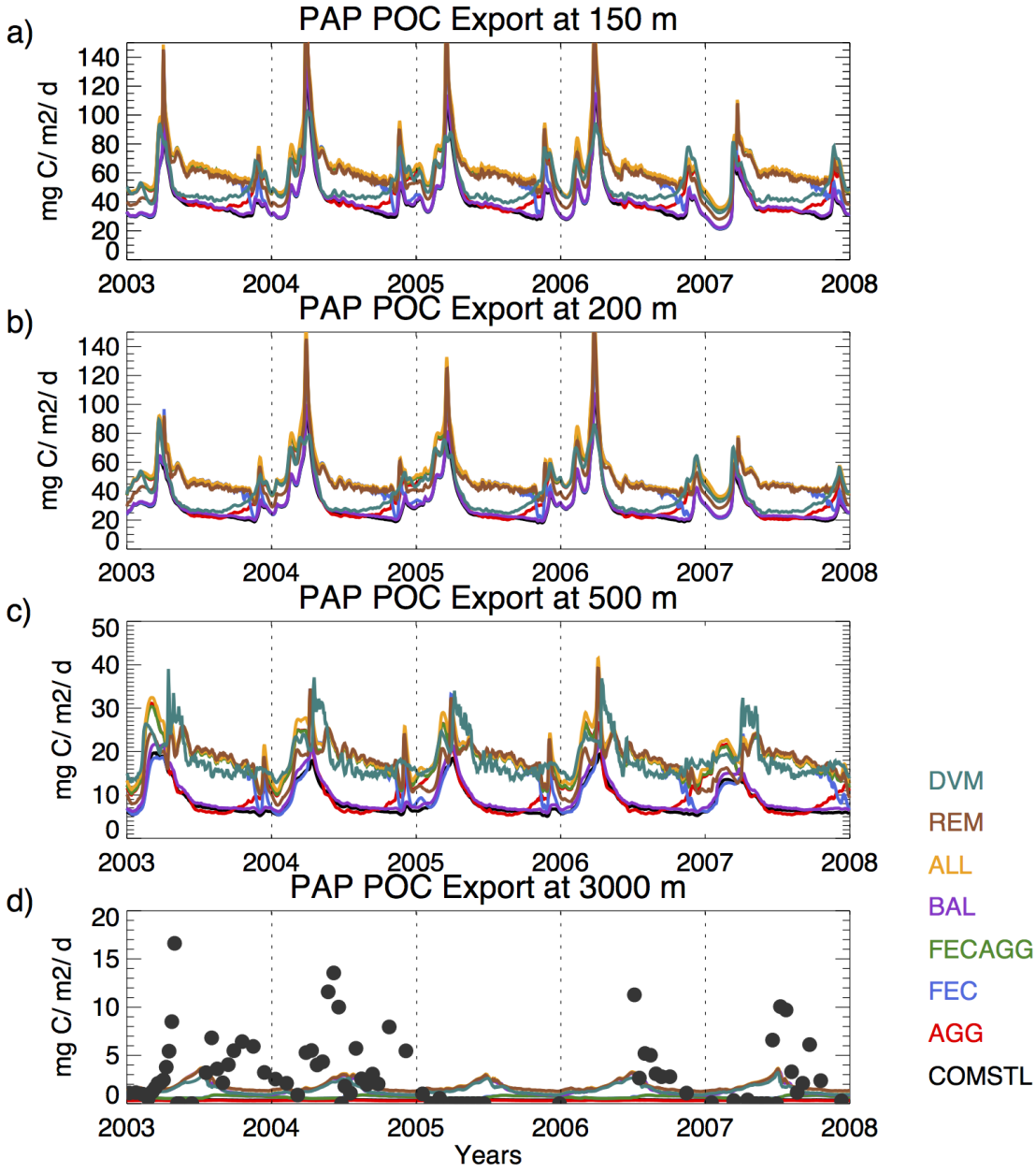

Figure 34) PAP site response to algorithms. Simulated carbon export (mg C m^{-2} d^{-1}) at depth for PAP station. Simulations are color coded as given in the plot.

5.4.1. On variable settling rates

Before the discussions on various details of carbon sequestration in models, it is important to understand the extent of the common term used in every model that resolve the vertical dimension of the particles, the "particle settling rate". No matter how complex the models define various processes in the surface ocean, settling rates drive carbon sequestration down the mesopelagic and below. In most of the models, however, definition of the settling rates is too simple, even the most complex ones assign a single settling rate for each particle state

variable. Evaluation of this simplification was the aim of the STL and COMSTL scenarios (Section 5.2.3.1). There are various attempts to resolve sinking rates with additional complexity, such as increasing speeds along depth (Berelson, 2002; Fischer and Karakaş, 2009; Aumont *et al.*, 2015), immediate transfer to deeper layers defining implicit particle sinking Yool *et al.* (2011), to prognostic definitions of settling rates in 1D models (Kriest and Evans, 1999 and 2000; Kriest, 2002) and 3D models (Gehlen *et al.*, 2006; Karakaş *et al.*, 2009, Aumont *et al.*, 2015) resolving continuous particle sizes and sinking speeds. However, the nature of the particles, including size, density, source and content, and even temperature (Giesecke *et al.*, 2010), does not provide an easy and robust choice of settling rates, in fact, the choice has to be made from a numerous list with a wide range of settling rates. Studies on the subject yield various values ranging from 0.1 – 10 m d^{-1} for individual cells (Smayda, 1970) to aggregate size with 74 ± 25 m d^{-1} (Alldredge and Gotschalk, 1988), 50 - 100 m d^{-1} (Deuser *et al.*, 1981), 100 – 150 m d^{-1} (Billett *et al.*, 1993), 49 ± 25 m d^{-1} and 270 ± 150 m d^{-1} (McDonnell *et al.*, 2015), 10 – 100 m d^{-1} (McDonnell and Buesseler, 2010), 5 – 2700 m d^{-1} (Turner, 2002 and references therein). Turner (2015) and references therein extended the list of Turner (2002) focus more on the mineral ballast effect, giving a range of 33 – 900 m d^{-1}.

The STL scenarios cover multiple ranges of settling rates, in compliance with the observations. The numerical restrictions of the model allowed to assign an upper threshold to the highest sinking rate of 50 m d^{-1}. Compared to the observations, 50 m d^{-1} is low and considering the size range of the modeled particles, a realistic upper threshold would have been ~100 - 150 m d^{-1}, and this study acknowledges that it was unable to maintain that. Such high values could have been achieved by decreasing the model time-step, which would increase the computing power needs, and considering the number of sensitivity analyses required for this study, an attempt to decrease the time-step would have been unfeasible. Therefore, STL scenarios covered 20 – 50 m d^{-1} for DetFast, and 2 – 7 m d^{-1} for DetSlow. Even with this narrow band of settling rates, the model response to changes was striking.

The response of carbon export to changes in settling rates was very robust. The whole carbon export time-series (Figure 27) shifted up and down without any change in variability. Furthermore, the effect was linear and changes in DetSlow settling rate effect the upper water column (0 – 300 m), and changes in DetFast effect the deeper layers, mostly visible in Figure 27d, h, and i. Figure 27e and j indicate the accumulation of DetSlow and DetFast in separate parts of the water column. The scenarios with high DetSlow sinking rates were

grouped away from the rest in the upper layers, those with high DetFast sinking rates deviated below 200 m, especially, STL5 had a clear response with higher sequestration within the mesopelagic. However, these changes did not add or improve any variability in the results, but were very effective in modifying the % biases, such that % biases ranged between 0.2 % to 354 % in STL scenarios. The STL scenario's indifference to variability is shown in Figure 35a and b using Taylor plots (Taylor, 2001). Both BATS and ESTOC STL simulations had no effect in improving the correlations with the observations, where results specific to a certain depth were all grouped together at similar correlation lines. There were some changes in NSTD's for individual depths due to the changes in export magnitude, but without the correlation support, it would be inconclusive to judge the STL simulations' success.

The robustness of the model's response to sinking rates dictate that, carefully picked and accurate settling should be chosen for this term, since ultimately, as mentioned above, carbon export will be dependent on and most probably be determined by the settling rates defined. Since most of the models only have single/few sinking particles, such a robust term will have major implications on export. The choice will still be vitally important with models of multiple detritus compartments, because after all, models usually tolerate a few detritus state variables at most. There are attempts to improve this by assigning variable settling rates dependent on various parameters. Increasing sinking rate with depth can be an option (Berelson, 2002; Fischer and Karakaş, 2009; Aumont *et al.*, 2015) (already included this in STL scenarios), which is a simplification of the mineral ballast and/or differential settling.

Much more complex definitions of prognostic sinking rates were adopted by several models (Kriest and Evans, 1999 and 2000; Kriest, 2002; Gehlen *et al.*, 2006; Karakaş *et al.*, 2009, Aumont *et al.*, 2015). At each time-step and depth, these models calculate the realized sinking rates derived from the aggregate mass and number concentrations. The approach by definition definitely introduces variability to the system, in fact Gehlen *et al.* (2006) state that the routine was superior to the other available carbon export parameterizations, referencing the importance of aggregation (discussed below). However, complexity increases the number of parameters to be used, and in a system that is too sensitive (0.2 – 354% bias range achieved in STL1-6), complexity does not eliminate the necessity of accurately defined settling rates.

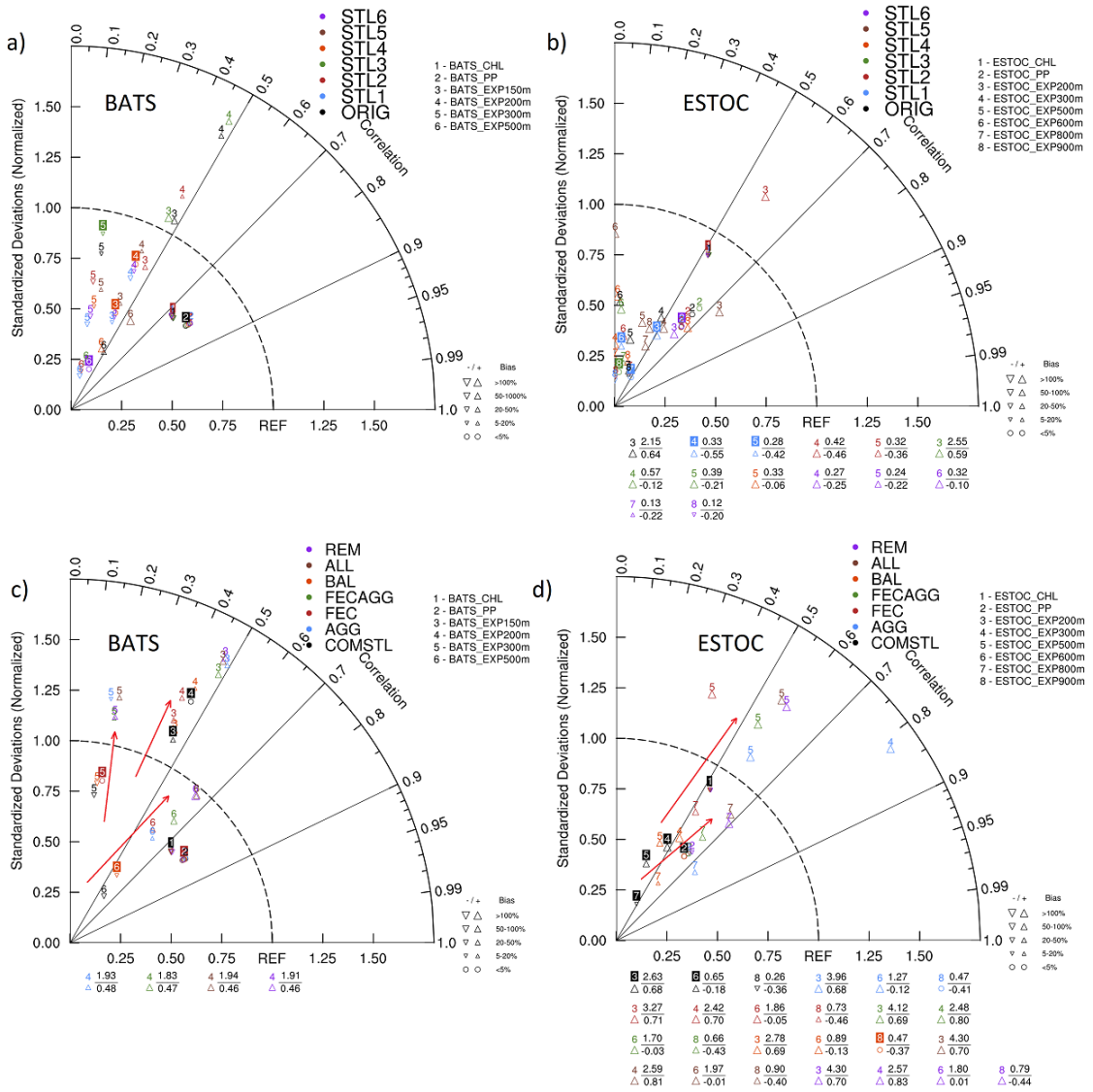

Figure 35) Model statistics shown on a Taylor diagram. The x- and y-axis denote the standard deviations of the model data normalized to standard deviations of the observed data. The REF on the x-axis is the observed data standard deviation. The radial axis represents the model data to observed data correlation coefficients (r). Statistically, the success of model in representing the observations increases towards the REF point on the x-axis, with 1-to-1 standard deviation and with the r equal to 1. Percent biases are also represented with triangles. Upper triangles indicate that model has a positive bias, and down triangles indicate negative bias. The percent intervals are represented with the triangle size. Model data standard deviations outside the x- and y-axis range are shown below the diagram. A color coding was set for the scenarios. The compared parameters, chlorophyll a, primary production and the export at various depths are represented by numbers on the figures **a)** BATS STL scenarios, **b)** ESTOC STL scenarios, **c)** BATS algorithms and **d)** ESTOC algorithms. The improvements achieved with the addition of the algorithms compared to STL scenarios are given in arrows in figures c and d.

The model's use of settling rates, and its ultimate estimate of carbon export are coupled information, in fact, these are highly coupled to each other, in which the settling rates determine the time it takes particles to cover the specified depths in the model vertical domain. While particles descend, they are prone to remineralization, and the amount of biogenic carbon that reach the deep is a result of the speed of sequestration and the strength of the attenuation. Therefore, defining the settling rates emerges as the vital tool not for informative purposes to address the model results, but the tool to be the dictating element to determine the results. For this reason, this study investigates the use of settling rates further by defining separate settling rates for different plankton size classes as given in Richardson and Jackson (2007) in COMSTL scenario. The COMSTL scenario was designed to assign realistic community specific initial settling rates given in Richardson and Jackson (2007), and detritus were allowed to aggregate to detritus with higher settling rates given in Table 8. This way, the model was able handle settling rates higher than 50 m d^{-1}, acknowledging that those high settling rates would be trimmed down to relatively lower values by the contribution of the smaller particles. Nevertheless, the experiment was a success. Exacerbated export rates were captured in winter periods due to the presence of enhanced diatom and mesozooplankton concentrations. The real value of defining community specific settling rates lies in its capacity to differentiate various locations in the ocean with different physical community backgrounds. NAGEM predicted (as expected) proportionally higher diatom and mesozooplankton biomass for the northern station, PAP site. Martin *et al.* (2011) tracked a spring diatom bloom in the Iceland Basin, and reported that diatoms had efficiently contributed to the export, even through the mesopelagic indicating a high export efficiency. Henson *et al* (2012) also argue that export efficiency was high in higher latitudes, and agree that diatoms could lead to a higher initial export efficiency. This was also the point of Helmke *et al.* (2010) that could partially explain the higher export efficiency at BATS compared to ESTOC. Indeed, both BATS and ESTOC carbon export (Figure 28) show pulses of increases coinciding with the deep winter mixing events due to the presence of diatoms, but overall, the change was confined to the winter period. Since both BATS and ESTOC had high biomass contributions from small phytoplankton, the enhanced export was discontinuous from the late winter and early spring. For this reason, the export was exacerbated relatively more in winter at PAP, visible in Figure 29 because PAP site can sustain higher diatom biomasses for longer periods in a year. Supporting Martin *et al.* (2011) and Henson *et al.* (2012), the model estimated much higher export efficiencies, as high as a 250% increase in export at 300 m depth. Martin *et al.* (2011) report that 25 – 43 % of 100 m export reached 750 m, whereas at the PAP site 100 m export that reached 750 m depth increased from 0.8% to 6.5% with COMSTL, suggesting that through the added variability

to settling behavior of particles, models can adopt to various environments and can predict variability without the necessity of tuning the lower trophic level model dynamics.

5.4.2. On physical and biological aggregation

Following the response of particle export to variable settling rates, it is important to investigate the detailed formation of the aggregates that eventually become the source of the deep transport. Diatom blooms and mesozooplankton pellets of high export efficiency has been addressed before (Smayda 1970; Steele and Frost, 1977; Eppley and Peterson, 1979), but the contribution of small phytoplankton to carbon export proportional to their productivity (Richardson and Jackson, 2007) is a recent issue gathering attention. Rather than the variable initial settling rates (applied in COMSTL), it is the similar higher settling rates achieved by most of the phytoplankton of different size classes through aggregation summarize the value of results from Richardson and Jackson (2007). Individual small cells are too small to sink rapidly due to the viscosity of seawater (Smayda, 1970). Higher sinking rates (Turner, 2015) are achieved through physical (McCave, 1984; Jackson and Burd, 1998; Burd and Jackson, 2009) and/or biological (Beaulieu, 2002; Turner, 2015) aggregation. Thus, the use of simplified size classes (suspended, slow and fast sinking detritus) by the modellers (Fasham *et al.*, 1990; Blackford *et al.*, 2004; Vichi *et al.*, 2007) was preferred, which was also adopted in NAGEM. As discussed in various parts of this study, the detritus was divided into slow and fast sinking compartments connected with the "aggregation" process. In fact NAGEM was designed such that DetSlow is mostly recycled in the epipelagic and DetFast contributes mostly to the deep carbon flux. This scheme agrees with the findings of Riley *et al.* (2012), where they emphasize the contribution of small particles to total export and their ultimate full recycling in the mesopelagic, and separates large particles and their contribution to deep export. Separation of detritus and simple aggregation process were already included in NAGEM in a simple form (ORIG and COMSTL). Sensitivity analyses were carried out with the aim of perturbing the aggregation process by introducing dependency on turbulence (AGG) and added direct aggregation to DetFast through fecal pellet formation. Eventually, seasonal variability of NAGEM increased (Figure 30). The response was clear at depths below the MLD. The pulses of enhanced export due to mixing in the upper layer does not linger below the MLD in COMSTL scenario (see BATS results at 500 m and ESTOC results at 800 and 900 m). With the introduction of turbulence dependent high aggregation rates, even at 900 m, pulses of high export were visible at ESTOC, in much better agreement with the observations. Improved

standard deviation and higher correlation values achieved for BATS (at 300 and 500 m) and ESTOC (500 and 800 m) with the AGG simulation (Figure 30). The response of export to fecal pellet formation, due to the presence of mesozooplankton in the following seasons, and increases in export at all seasons were achieved (Figure 30) due to the presence of fecal pellets and was not restricted to winter as AGG. Without any exception, carbon export increased at all depth and at all seasons. This shows how effective the fecal pellet formation is for carbon export. For the Sargasso Sea for example, fecal pellet contribution to total POC flux was given between 0.4 – 89 % at various depths (Goldthwait and Steinberg, 2008; Shatova *et al*., 2012; Steinberg *et al*., 2012). Higher settling rates were achieved by faster formation of aggregates. This also holds for the AGG simulation.

5.4.3. On mineral ballasting

Because of POC's similar densities (Francois *et al.*, 2002) to seawater, particles need a supporting mechanism to overcome viscosity (De La Rocha and Passow, 2007). Referencing to the results to deep sediment trap observations (Armstrong *et al.*, 2002; Francois *et al.*, 2002; Klaas and Archer., 2002), the incorporation of opal, calcite and lithogenic material into sinking aggregates can increase POC density to achieve a faster sinking mechanism, and provide further support to withstand degradation while descending. Sanders *et al.* (2010) have found evidence of biomineral ballasting in the EZ. Le Moigne *et al.* (2012) have highlighted the possible diminishing effect of mineral ballast on the remineralization of POC by microozooplankton, whereas Plough *et al.* (2008) and Iversen and Plough (2010) concluded that mineral ballast increased the sinking speeds of aggregates and marine snow, with calcite ballasting more effective than opal and they found no significant effect on the rate of decomposition. Henson *et al.* (2012) suggest that transfer efficiency of particles is strongly negatively correlated with opal export flux, and uncorrelated with calcium carbonate export flux. They argue that the ecosystem structure rather plays a role in determining export and transfer efficiencies, in agreement with the "packaging effect" Francois *et al.* (2002) proposed, where in these author's view, particles in high latitudes have high export ratios due to faster sinking mechanism (applied in NAGEM - COMSTL), but also are labile in nature, thus prone to faster removal in the mesopelagic, compared to the tropical/subtropical counterparts. The importance of the community structure in setting the transfer efficiency is also the conclusion given by Lam *et al.* (2011). A counter idea was also proposed by Passow and De La Rocha (2006) and De La Rocha *et al.* (2008), where

POC itself act as the glue mechanism that collect biominerals as it descends, resulting in high correlations. Nevertheless, mineral ballasting effect is still a debate, but it has been argued by many authors, used by various modeling studies and since the mechanisms of how biominerals and POC interact is still unclear (De La Rocha and Passow, 2007), adding mineral ballasting mechanism to NAGEM was necessary.

After the addition of community specific settling rates, it was technically not possible to implement biomineral affected settling rates to the model. Examples of increasing settling rates in response to the biomineral presence was included in Gehlen *et al.* (2006), later on, Aumont *et al* (2015) removed the ballasting routine from the same model, due to the lack of clear relationship between sinking speeds and mineral composition of particles addressing Lee *et al.* (2009), but they also acknowledged that, rather than increasing settling rates due to density differences, organic matter protection by the inorganic matrix may explain efficiency of organic matter settling. For technical purposes, and possible protection effect implied by minerals, this study kept a protective mechanism in BAL. The problem encountered was that Dunne *et al.* (2007) concluded that the rain ratio in the North Atlantic was by average systematically low (0.02). The rain ratio of 0.035 was applied in NAGEM, the highest Dunne *et al.* (2007) give. This is still a low value, especially compared to 0.1 in the equator. For this reason, especially at the surface, the ballast mechanism in NAGEM was basically ineffective (Figure 31). Minor increases in export simulated at depths below 300 m, and these were mainly located in winter/spring periods (results follow the presence of implicit $CaCO_3$ formation by AG4). Interestingly, simulations including the mineral ballast effect (BAL, ALL and REM) resulted in considerable export at 3000 m shown in PAP site (Figure 34). Although an increase in export at 3000 m was observed, it was not enough to estimate the observations, where observations were 3 – 5 times higher than NAGEM predicted. This can be partly due to the low settling rates (<50 m d^{-1}) NAGEM was restricted to, but it was still a valuable exercise to see the effect of mineral ballast as deep as 3000 m. The potential effect of mineral ballasting at deep oceans were already reported (Thomalla *et al.*, 2008). In their global modelling study, Gehlen *et al.* (2006) also conclude that mineral ballast was effective in the deep ocean, whereas aggregation was the main driving mechanism to initiate export at the surface. NAGEM results agree with these finding, where aggregation routines indeed enhanced export as shallow as 150 m (Figure 30). It was also valuable to see that given the mineral ballast theory is true, models can easily be adopted, and given the results in PAP site, and in a location with high rain ratio, mineral ballast effect can dominate the export in the deep oceans.

5.4.4. On community specific remineralization rates

Since NAGEM responded (although limited) to changes in remineralization due to the presence of mineral ballast, the hypothesis of community structure and its relation to export and transfer efficiency (Francois *et al.*, 2002; Henson *et al.*, 2012) would be the next thing to evaluate. Similar to COMSTL (community dependent settling rates), community dependent remineralization rate approach was added following COMSTL formulation in REM. BATS and ESTOC response to the changes were similar (Figure 32). Simulations suggest that both stations respond with very minor decrease in export rates at 150 m to an almost equal export compared to ALL simulation at 200 m. Below this depth, REM simulation overcame ALL, with again minor increase in export below. Reasoning was the mere fact of the dominant community compositions. Located in the subtropics, both stations had relatively low diatom and thus mesozooplankton biomass. Since the assigned remineralization rates were low for the small phytoplankton by the so called "packaging effect (Francois *et al.*, 2002)", just like the ballasting simulations, sinking POC was partially protected from degradation by bacteria. On the contrary, the opposite case holds for the PAP site simulations (Figure 34). Again the changes were minor, but this time REM simulation export was lower than ALL at 200 m including the summer period. The actual change was simulated in winter, with ~20% decrease in export at 500 m coinciding February/March each year (Figure 34), whereas this change for the winter period at BATS and ESTOC was negligible or non-existent. Just like pointed out in Henson *et al.* (2012), diatom dominated export (which was highly export efficient simulated in COMSTL) was more prone to degradation in the mesopelagic. However, the additional higher/lower remineralization rates dictated by the community structure were not as decisive as pointed out in the references above. The community dominated settling rates resulted in much more profound effects. This can be due to the formulation design and the capabilities of the model: (1) settling rates are direct inputs to export, such that the to achieve export, detritus concentrations are directly multiplied by the settling rates. This multiplication makes the effect immediate and explicit to environmental constraints such as temperature. (2) Unlike settling rates, remineralization is temperature dependent. Colder environments, such as PAP or deep oceans, will be less prone to changes in remineralization rates. (3) Community dependent detritus consumption by zooplankton was absent in REM simulation, which can be an important factor if applied (Lampitt *et al.*, 1993; Steinberg *et al.*, 1995). (4) Above all, due to the formulation restrictions, at each vertical level, community specific settling and remineralization rates were weight averaged, which narrowed down the higher and lower ends to intermediate values if all plankton were

present with similar biomasses. To overcome this, separate detritus should be assigned for each community, which in the case of NAGEM, it would add extra 14 state variables. To include in total 16 detritus state variables is beyond the scope of this work, and it would most probably be too expensive for a 3D model, but if the true effect of community structure on settling rates and remineralization rates to be evaluated, it is strongly recommended for the modeling community to investigate opportunities in setting a cluster of community specific detritus state variables.

5.4.5. Lessons learned and future work

Figure 36 and Figure 37 summarize the changes in annually averaged profiles of carbon export with the additions of each algorithm. Surface profiles (100 – 500 m) suggest that, community settling rates increased export rates for all simulations. The attained change was mostly confined to the upper 300 m range in the subtropics, but the effect was still pronounced below 1000 m for the PAP station (Table 12). This suggested a high export efficiency in the high latitudes due to the presence of large phytoplankton such as diatoms, and followed by mesozooplankton with their production of fast sinking fecal pellets. This indicates that, once the model dynamics adopt to environments with different physical and biological structures, the difference in export ratios can be exacerbated with community specific additions to the sinking carbon sources.

The relative changes in export ratios and the transfer efficiencies among different latitudes were quite different (Table 13). After community related settling modifications, export ratios increased by only 24 – 41 % at BATS and ESTOC, whereas this change was 220 % at PAP site, indicating the dominance of the faster sinking detritus in the epipelagic. The increase in export ratios both at BATS and ESTOC, although they are abundant in cyanobacteria that produce slow sinking detritus, is due to the assigned settling rates. STL6 simulation assigns 2 - 7 m d^{-1} settling rates for DetSlow, whereas with the averaging applied in COMSTL, DetSlow reached ~ 4 m d^{-1} settling rates. However, the actual slow down of settling rates were achieved at depth, such that the transfer efficiencies decreased by ~45 % due to the decreased settling rates of DetFast. For the PAP site on the contrary, increased export ratios were followed by increased, as high as ~440 %, transfer efficiencies, due to the calculated higher sinking rates. These changes were achieved only by assigning variable sinking rates to communities, and it should be underlined that no site specific tuning was made. Common

parameterization can achieve global differentiation in export characteristics due to community specification. This information is importantt since, most of the recent models adopt plankton functional type approach (Hood *et al.*, 2006), suggesting that multiple phytoplankton and zooplankton is already present, and can form the base for settling rate specification.

The increase in carbon export due to turbulence controlled aggregation (AGG) was pronounced more in the surface to upper mesopelagic layers, since this region was turbulence dependent (MLD's) which allowed to enhance aggregation rates. Enhanced aggregation triggered faster sinking particles, eventually, increasing the sinking rate, and the export ratios (Table 13). Realize that physical aggregation had minor effect on the transfer efficiencies. As expected, fecal pellet formation aided the increase achieved in AGG simulations, where FECAGG simulation suggested for all of the stations, physical and biological aggregation can create mechanism of high export. Overall, faster sequestration was achieved with the inclusion of multiple aggregation mechanisms.

Table 13) Summary of the changes in simulated export ratios (carbon export/integrated PP) and transfer efficiency (export at 1000 m/export at 200 m). STL6 was used as the reference scenario. The % changes in COMSTL (community settling rates) column are calculated by the changes simulated compared to STL6. The remaining % changes are individually calculated by the changes simulated compared to COMSTL.

		% change from STL6	% change from COMSTL						
	Export Ratio (STL6)	COMSTL	AGG	FEC	FECAGG	BAL	ALL	REM	DVM
BATS	0.041	24.3	28.1	32.1	55.4	7.0	62.2	61.5	45.9
ESTOC	0.035	41.4	36.7	33.8	64.9	6.3	72.6	74.4	79.0
PAP	0.025	220.4	27.4	47.3	70.8	5.6	76.8	58.0	33.2
		% change from STL6	% change from COMSTL						
	Transfer Eff. (STL6)	COMSTL	AGG	FEC	FECAGG	BAL	ALL	REM	DVM
BATS	6.3	-46,5	2.5	74.1	59.1	71.2	107.2	133.3	165.7
ESTOC	10.8	-47,9	3.0	61.1	38.0	34.5	59.3	90.4	114.6
PAP	1.3	439.5	0.6	62.0	57.4	43.2	80.5	82.5	112.2

On the contrary to the aggregation routines, ballast additions were ineffective at the surface (~5 -7% changes in export ratios, but the true effect can be seen in the deep layers of the mesopelagic and below (Figure 37). Especially at PAP site, ballast mechanism allowed an increase by 3-fold at 3000 m depth, in fact ballast activated simulations were the only ones to simulate close values to the observations. The effect of aggregation as the driving mechanism of export, and the possible influence of ballast mechanism in the deep ocean was also mentioned in the global modeling study of Gehlen *et al.*, 2006. However, the ballast theory is still a debate as discussed above, but if the theory is valid, the model response suggest that mineral ballasting can be a conclusive element in determining the export in deep ocean, which models should definitely include.

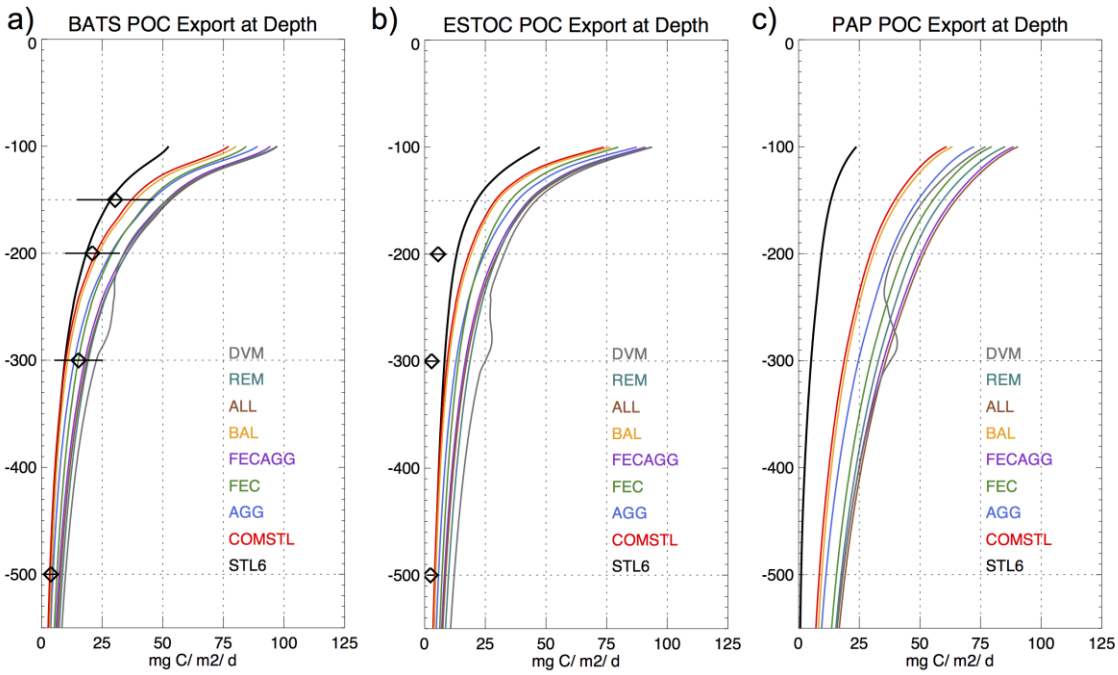

Figure 36) Carbon export profiles (mg C m^{-2} d^{-1}) of all the algorithm built on STL6 simulation depicting upper 100 – 550 m. a) BATS, b) ESTOC and c) PAP site.

The community specific remineralization rates were not as effective as the community settling rates additions (see Section 5.2.3.4, 5.3 and 5.4.4). However, decrease in export rates in REM compared to ALL simulation was more pronounced in PAP site (diatom dominated) (Table 12), suggesting that community specific settling rates can be effective in determining the transfer efficiency of regions of different physics. Both COMSTL and REM simulations suggest that, community differentiation can be vitally important in determining export and transfer efficiencies, and can simulate differences in export rates for different regions in the ocean without any site specific modifications in the parameters used. This issue definitely addresses a benefit for the 3D global models. However, the downside is, true

representation can only be achieved by setting explicit detritus for each community, which would be very expensive. In this study, the contribution from each community was averaged, which buffered the possible extreme values assigned to diatoms and mesozooplankton.

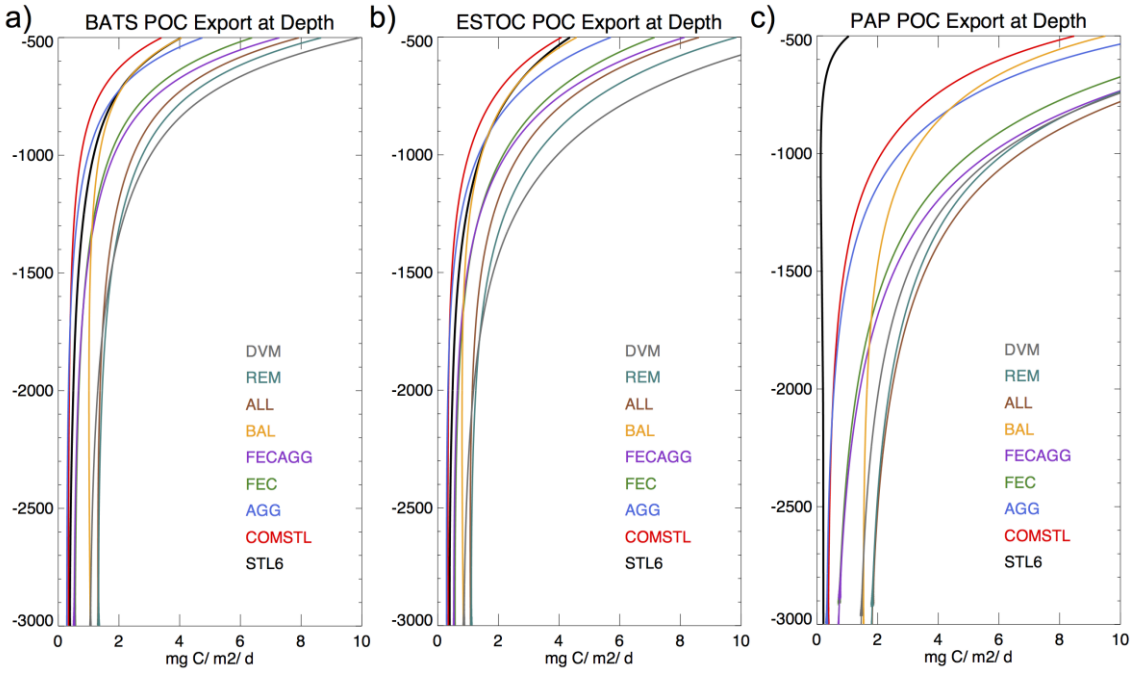

Figure 37) Carbon export profiles (mg C m^{-2} d^{-1}) of all the algorithm built on STL6 simulation depicting 500 – 3000 m. a) BATS, b) ESTOC and c) PAP site.

DVM analyses provided important results, shown in Figure 36, where it was the only simulation NAGEM predicted a deviation from the Martin curve. The rest of the simulations can be fitted to the Martin curve by adjusting the "b" exponent. This situation was not valid for DVM, where all sites predicted a "bump" within 200 – 350 m in export. Not only modeling studies use Martin curve. Many observational studies base their assumptions by extrapolating the limited number of measurements at depth to fit the Martin curve. Unlike ballast theory, DVM is a fact. It has been tracked simultaneously by acoustic studies, and the process is fast (Jiang *et al.*, 2007). The differentiation in export profiles (Figure 36) suggest the use of DVM, even in global models should be investigated.

Overall, simulations suggest that the model response to settling rate changes was very robust. On the other hand, additions of community dependent (fecal pellet production, remineralization rates, ballast effect, vertical migration) and physics dependent

(aggregation) changes were vital to achieve variability observed in the sediment trap records. Changes in settling rates alone (STL simulations) fail to capture such variability in export. The lack of added variability of settling rates alone, and the variability achieved with community and physics dependent algorithms were perfectly summarized by the arrows shown in Figure 35, and listed in Table 10 and Table 11. Better standard deviations and correlations were achieved with the added variability by the simulations. However, although very valuable to show and quantify the effect of each algorithms for future modeling purposes, the results failed to simulate the 3 – 5 fold gap in export rates at BATS and ESTOC. The improvements in the correlations, especially at ESTOC, suggest that such additions were necessary to simulate better export, but the model bias in export at ESTOC suggest that the removal mechanisms in the model should be further investigated. In this study, the model was restricted to a common parameterization to address multiple sites, which global models do as well. This can be a reason of the gap because model parameters were picked to achieve productivity and export in both subtropics and transition to polar regions, which may miss the true character of ESTOC. However, a common parameterization is important to evaluate the model dynamics in order to address global models. On the other hand, the high response of the model to changes is still very optimistic, because with the use of realistic parameters, measured *in-situ,* or in laboratory conditions representing ESTOC, tuning specific to ESTOC can lead to much better model representations. For example, in terms of community structure, the community specific remineralization rates in this study lacked site specific values, and with better model representations (detritus for each state variable) and better tuned remineralization rates, ESTOC export can be predicted with higher accuracy. Since model results in much higher export rates at ESTOC, better tuned removal mechanisms addressing community composition can decrease the export to observed values.

5.5. Conclusions

This chapter extends the modeling framework (NAGEM) that was introduced in Chapter 3, with the purpose of evaluating the use, the effect and the success of model algorithms addressing community structure, settling rates, physical and biological aggregation, mineral ballasting and diel vertical migration. The success of NAGEM in the subtropical North Atlantic was extensively discussed in Chapter 3, and proved to be a useful tool to investigate the underlying mechanisms leading to the observed primary production and export rates at BATS and ESTOC. In this study, the modeling framework extends to north and adopts PAP

site for the comparison of the model algorithms between the subtropics and subpolar transition zone, forming a comparative study carbon export between locations with different physical and biological backgrounds. For this reason, this study focuses more on the dynamics initiated in the EZ extending down to the mesopelagic and below.

Results suggest that NAGEM carbon export was very sensitive to the changes in the settling rates of particles. Since the use of settling rates is common to every modeling study that investigate carbon sequestration, this holds for all modeling systems that incorporate settling rates, and the use of this parameter in global carbon cycle estimations make the choice of this parameter a vital issue. Even with minor changes from 20 m d^{-1} to 30 m d^{-1}, model bias increases considerably, whereas in nature, particles can settle with speeds of several hundreds of meters per day. Moreover, most of the models simplify the particles as a bulk matter and assign single settling rates for each detritus, where in most cases, the number of detritus state variables do not go beyond three. Thus, together with the model's robustness and the simplification of settling rates, the model export flux was bound to witness biases in the deep ocean that can rarely be controlled, and completely lack the variability the oceans achieve. For this reason, in order to increase variability, a size based settling rates to the community composition was assigned in NAGEM, totaling in 16 in number of settling rates chosen. The model variability boasted, and the responses were clearly visible among different seasons, and more importantly, export efficiencies rapidly changed and model adopted to low vs high latitude dynamics. Such that, PAP export efficiency was exacerbated without any changes on the lower trophic growth parameters, simply due to the fact that PAP site sustains higher diatom and mesozooplankton biomass with higher settling rates.

The problem with the settling rates arises, because, constant and single settling rates oversimplify the dynamic and complex interconnected processes linking the primary production and the formation of settling particles. The lack of variability in model processes result in the lack of variability in simulated export rates, and in turn the model will over or underestimate (with high biases) the export within the different regions in the oceans. To investigate the variability, and possibly overcome some of the discrepancies in export that models simulate, turbulence dependent physical aggregation, and zooplankton type and growth dependent fecal pellet production was added. Furthermore, protection against degradation for particles in the presence of biominerals, and further extended the community composition support to variable remineralization rates was also added. The final approach was to include the active transport applied through diel vertical migration of

mesozooplankton. All of the processes above, some minor some major increased the variability of export, and model export at BATS and ESTOC fitted better with the observed export.

The magnitude of carbon export was highly responsive to aggregation, where the effect was dominant and initiated at the surface layers, following the seasonality of the strength of the turbulence and resulting zooplankton community structure, whereas, mineral ballasting was very effective in the deepest reaches of the oceans, such that only ballast enabled simulations achieved to represent the carbon export at 3000 m observed at PAP site. If mineral ballast theory is true, the models for this reason should include the process. The response of model carbon flux was immediate with the application of DVM, such that within a matter of hours, model mesozooplankton transferred the grazed organic carbon into the mesopelagic, forming a "bump" in the export profiles. This is a major result, because, enabling the DVM effect, the model predicted profiles that cannot be fit to the commonly used Martin curve (Martin, *et al.,* 1987). The profiles achieved in DVM simulations contradict with the extrapolations applied to estimate carbon export in observational studies, and suggest that DVM effect should be considered in estimating carbon export in the mesopelagic.

Model results, in-line with the points above, emphasize the importance of classification of particle state variables. This study investigated community specific settling rates, physical aggregation, fecal pellet formation and DVM effect due to the presence of separate sized particulate matter. Results suggest that small and slow sinking particles were responsible for recycling supporting primary production, and furthermore forming the link between primary production and large and fast sinking particles, where ultimately, fast particles were responsible for deep carbon export to the abyss. Therefore, representing the complex interactions between these components was vital to understand the dynamics of carbon export, which was the end product of all these processes.

Results also address, probably the key results of this study, again in-line with the particle size and behavior classification, that emphasizing community compositions on carbon export is a must. Apart from the community specific settling rates, this study investigated the community specific remineralization rates. Due to the reasons discussed in various sections, the variability and response of carbon flux was less pronounced compared to

variable settling rates. However, with the proper representation of size classes, specifically, each community produce explicit separate detritus with different settling and remineralization behavior, the model performance would possibly be highly effected. This thesis acknowledges that such addition can be costly and would require carefully selected rates for each detritus. However, additions can address the differences observed in carbon export in various regions of the oceans, and possibly can explain the 3 -5 fold gap in export observed at BATS and ESTOC consisting of similar productivities.

With the added and investigated algorithms, the true answer why BATS and ESTOC having the similar productivities can end up having a major gap in export was still missing. The removal mechanisms in NAGEM should be investigated further, and this study addresses the necessity of using realistic remineralization and settling rates with different community sources. Using community structure, differences in export efficiency in high vs low latitudes mentioned in Henson *et al.* (2012) were simulated, but it was not possible to simulate the high removal of particles leading to low transfer efficiency. Increasing the number of detritus state variables with community composition support and carefully picked and supported by experimental studies remineralization rates can improve the model carbon export, because although in general the model response was low, PAP site responded more to community specific remineralization rates as suggested by Henson *et al.* (2012).

To conclude, although the question still remains to be answered, the gap in export rates measured at BATS and ESTOC, this study quantified the model dynamics and response to various carbon export algorithms used in models. Each algorithm added unique response to export, where each addition enhanced model variability which is vitally important for global studies. The key result was the use of community related formation, behavior, settling and removal of particles. Supported with the experimental studies, inclusion of multiple particles with community links can enhance the model performance.

CHAPTER

6. THESIS CONCLUSION

This thesis aimed to investigate the components and structure of, and controls on the biological carbon pump in the North Atlantic, and its representation in ecosystem models. The effects of specific algorithms addressing the formation and transport of carbon in the deep reaches of the oceans were evaluated.

The first part of the thesis introduces NAGEM, a 1D lower trophic pelagic ecosystem model designed for the purposes of this study, and its implementation to the time-series stations (BATS and ESTOC) in the subtropical North Atlantic. Through the comparison of model results with the extensive dataset from BATS and ESTOC, NAGEM was evaluated for its capability in reproducing the primary production with separating multiple plankton functional types and their dominance in different seasons and depths, capturing the correct nutrient dependence of phytoplankton and its recycling, and finally the mechanisms leading to particle export. After the evaluation of the model dynamics, NAGEM was used to investigate the controls on carbon export at both sites, and the possible reasons of the observed 3 – 4 fold gap in export rates between BATS and ESTOC.

The second part of the thesis focuses more on the use of various model algorithms, and their success in regulating particle export and its capability to adopt to various locations with different physical and ecosystem backgrounds. For this purpose, BATS and ESTOC sediment trap data were used to evaluate different algorithms incorporated to NAGEM. In addition to the subtropical stations, NAGEM was also applied to the PAP site in the North

Atlantic to investigate the response of the algorithms to different physical and ecosystem backgrounds.

6.1. NAGEM evaluation and the controls on export at BATS and ESTOC

NAGEM was evaluated in representing the lower trophic dynamics of BATS and ESTOC, where it captures the magnitude of primary production, and the start of bloom. The model results agreed with the distribution of the community structure at BATS, simulating picoeukaryote dominance in winter/spring bloom, and the cyanobacteria dominance in summer months, with occasional diatom blooms at the onset of winter mixing. The ESTOC community structure was similar to that simulated at BATS, but data were not available to validate the model. Results suggest that new nutrient input to the euphotic zone by deep mixing events in winter/spring trigger eukaryotic growth, where picoeukaryotes and diatoms contribute to the winter/spring bloom at both BATS and ESTOC. As the time progresses towards summer, the water column stabilizes, triggering nutrient depletion in the EZ, where phytoplankton growth is then controlled by the recycled nutrients, favoring cyanobacteria due to their high capacity to survive low nutrient conditions.

BATS and ESTOC results indicate that primary production and carbon export was directly coupled to the variability in the water column hydrography. Periods of intense mixing and high supply of new nutrients into the EZ were followed by high carbon export compared to months with stable water column structure. Inorganic nutrient concentrations at BATS are significantly lower than at ESTOC; but BATS with a deeper MLD' and more frequent mixing events can sustain similar primary productivity levels compared to ESTOC. Although these two stations can sustain similar primary productivity, BATS carbon export ratio at 200 m is significantly (3 - 4 fold) higher than at ESTOC, suggesting certain processes that lead to lower export production and higher flux attenuation at ESTOC. Finding out why this happens was one of the main goals of this study.

The sensitivity analyses showed the importance of detritus grazing and bacterial remineralization on export rates. Stable water column and longer residence times at ESTOC enhanced the recycling pressure applied through detritus consumers and increased bacterial remineralization, such that ESTOC detritus was removed by 10% more compared to BATS,

although the same configuration was applied. A decline in export ratios up to ~50% through combined detritus consumption by zooplankton and increased bacterial activities proved how sensitive these two stations are to recycling processes.

The investigation of the dynamics of carbon export show the importance the small phytoplankton's role in contributing to the carbon export. NAGEM results show seasonality in the origin of carbon export, such that the phytoplankton contribution to carbon export was mostly through diatoms and picoeukaryotes (~20% contribution to total export) during winter/spring periods. A shift in dominance of algal communities from larger phytoplankton to small phytoplankton in summer months result in cyanobacteria contribution to export as high as 20% of the total export. This result points to the importance of aggregation processes in regulating carbon export, and support the fact that small phytoplankton regardless of their small size can contribute to export. Overall, model results show that zooplankton were the dominant contributors to export, but recall that zooplankton mortality was used as the closure term in the model, which contributes to the model's results of high export rates through zooplankton.

Apart from carbon export dynamics, model results also revealed various responses of the community structure to separate additions of N and P to the system. The response of the community structure to decoupled additions of inorganic nutrients was highlighted in simulations when zooplankton were allowed to consume detritus. The model simulated higher NH_4 input to the inorganic nutrient pool due to the additional flow path of excretion created by adding an extra zooplankton state variable to the model. Higher N availability favored prokaryotic production over eukaryotic production because prokaryotes were set to be highly dependent on N for growth. To test the effect of separate additions of nutrients, NH_4 and PO_4 were separately added to the surface layer representing a hypothetical external nutrient intrusion to the system. Prokaryotes responded more to N additions and eukaryotes, on the contrary, responded more to P addition. Although very experimental, these applications show how important it is to include detailed community structures with detailed trophic decoupling of C/N/P elements in the models. In order to answer the questions of global warming and future predictions of carbon export, models should be able to address the complex interactions within the plankton community structure.

6.2.Evaluation of carbon export algorithms

Following the extensive evaluation of NAGEM model dynamics and its success in reproducing the lower trophic system and the resulting carbon export in the subtropical North Atlantic, the study was extended to make a model algorithm testing framework such that the model parameterization that includes the detritus consumption by zooplankton was chosen to be the reference run for the algorithm incorporation. The purpose was to evaluate the use, effect and success of model algorithms addressing community structure, settling rates, physical and biological aggregation, mineral ballasting and diel vertical migration. The comparative modeling framework was extended to the north to include the PAP site to evaluate the model algorithms between the subtropics and subpolar transition zone. This provided the opportunity to understand the response of the algorithms to locations with different physical and biological settings.

Results suggest that NAGEM carbon export was very sensitive to the changes in the settling rates of particles. Since the use of settling rates is common to every modeling study that investigates carbon sequestration, the situation holds for all modeling systems that incorporate settling rates, and the use of this parameter in global carbon cycle estimations make the choice of this parameter a vital issue. Dramatic changes were achieved in carbon export rates, even with minor modifications on settling rates of particles. In marine ecosystems, particles can settle with speeds from a few to several hundreds of meters per day. Because of this variability in nature, and because it is such a sensitive parameter in models, settling rates should be chosen with care given particular environmental conditions. However, most of the models simplify the particles as a bulk matter and assign single settling rates for each detritus type. Together with the model's robustness and the simplification of settling rates, the model export flux is bound to simulate biases in export to the deep oceans, which can rarely be controlled, and would completely lack the actual variability observed in nature. For this reason, in order to increase variability, size based settling rates as a function of the community composition were incorporated in NAGEM. The model variability increased, and the responses were clearly visible among different seasons, and more importantly, export efficiencies rapidly changed. Thus, the model was sensitive to low vs high latitude dynamics, such that export efficiency at PAP increased without any changes on lower trophic growth parameters, simply due to the fact that the PAP site sustains higher diatom and mesozooplankton biomass with higher settling rates.

To investigate the variability, and to overcome some of the discrepancies in export that the models simulate, turbulence dependent physical aggregation, and zooplankton type and growth dependent fecal pellet production were added to the model. Furthermore, protection against degradation for particles in the presence of biominerals was incorporated, and remineralization rates were modified to give specific rates for each plankton community. The final approach was to include the active transport by diel vertical migration of mesozooplankton. These processes, some minor and some major, increased the variability of export, and modelled export at BATS and ESTOC better matched the observed export.

The magnitude of carbon export was highly responsive to aggregation, where the effect was dominant and initiated at the surface layers, following the seasonality of the strength of the turbulence and resulting zooplankton community structure. On the other hand, mineral ballasting was very effective in the deepest reaches of the oceans, such that only ballast enabled simulations achieved the carbon export at 3000 m observed at the PAP site. To make a final conclusion on mineral ballasting, the presence of such mechanism should be supported by experimental and observational studies. The response of the model led carbon flux was immediate with the application of DVM (Diel Vertical Migration), such that within a matter of hours, model led mesozooplankton transferred the grazed organic carbon into the mesopelagic, forming a "bump" in the export profiles. This is a major result, because, enabling the DVM effect, the model predicted profiles that cannot be fit to the commonly used Martin curve (Martin, *et al.,* 1987). The profiles achieved in DVM simulations contradict extrapolations applied to estimate carbon export in observational studies, and suggest that the DVM effect should be considered in estimating carbon export in the mesopelagic.

Small and slow sinking particles were responsible for recycling, supporting primary production, and furthermore forming the link between primary production and large and fast sinking particles, but ultimately, fast particles were responsible for deep carbon export to the abyss. Therefore, representing the complex interactions between these components is critical to understanding the dynamics of carbon export, which is the end product of all these processes. The particle size and behavior classification of plankton community structure on carbon export was shown to be very important. Its use in ecosystem models could increase variability and fix the biases resulting in between the observations and the model that fail to represent such differentiation. Community specification was represented in two ways. (1) community specific settling rates, and (2) remineralization rates. The variability in settling

rates increased variability in carbon export. The effect of variable remineralization rates on carbon export magnitude and variability was relatively weaker. This could be due to the averaging applied when the model determines the final remineralization rates at each time step and depth. This issue addresses the need to explicitly define separate detritus state variables specific to each plankton type. Such definition requires proper representation of size classes related to community specific settling and remineralization rates. This way the model performance would possibly be highly affected, and could be used to explain observed and modeled discrepancies of carbon export.

Even with the added algorithms, the model was unable to answer why BATS and ESTOC, with similar primary productivity, can end up having a major difference in export rates. The removal mechanisms in NAGEM should be investigated further, and this study emphasizes the need to use realistic remineralization and settling rates with different plankton community sources. With detailed community structure separation of settling rates, the model was able to simulate the differences in export efficiency in high vs low latitudes, but was unable to simulate the high removal of particles leading to low transfer efficiency, especially in the higher latitudes. By increasing the number of detritus state variables with community composition support, carefully chosen and supported by experimental studies, remineralization rates can improve the modelled carbon export.

6.3. The overall model performance

Modelled depth integrated annual mean primary productivity agreed well with reported observations and reproduced observed high productivity values in winter and early spring at both stations, including multiple blooms and abnormal highs in primary productivity. The model was less capable once the comparisons were scaled down to specific time periods. Including higher resolution physics may improve the results. Also recall that the 1D model structure does not include lateral interactions, which can be a major source of model discrepancy. The general model use of inorganic nutrients is successful in a way that nutrient depletion in the EZ was captured, and the nutrient availability was reflected on the phytoplankton community structure which introduced broader implications on productivity and export. The model was successful to estimate P-limitation at BATS and N-limitation at ESTOC which is supported by observations. However, it failed to simulate an N-limited environment at the PAP site. The model parameterization should be revisited in that case. The general phytoplankton community distributions were also successfully simulated such

that larger phytoplankton were dominant in nutrient abundant winter/spring months, and smaller, more competitive phytoplankton were dominant in nutrient scarce summer months. Regional community differences were also captured so that the PAP site sustained a higher large phytoplankton biomass. The correct community setup in model simulations was a major achievement because the structure was used to link productivity to carbon export variability. However, the community structure should be supported more with the available observations because only the BATS site had enough coverage field observations for a detailed model vs observation comparison.

Although the estimated model productivity was supported by the observations, the results still show the model's lack in capturing the 3-4 fold difference in export ratios. The experience gained from this study, such as the link between community and carbon export should be exploited more with detailed community specific particle formation and attenuation to introduce temporal and regional variabilities. In reference to these findings, the model performance was acceptable for this study. Ultimately, every model has their strengths and weaknesses, and NAGEM also had its own as discussed in many sections of this study. Some of the 1-to-1 comparisons were very successful, for some variables, it was necessary to do a temporal and spatial averaging. The model skill was evaluated using statistical calculations of correlations, standard deviations and biases, with achieved improvements relative to the initial simulations after the algorithm was modified for some parameters, if it was not statistically highly successful. However, the model was detailed enough to raise questions for further future work, especially with the presence of community structure. With a less detailed state variable and parameterization setup, it would have been impossible to emphasize the temporal and spatial differentiation in carbon export resulting from the community structure. The model was also detailed enough to evaluate the effects of particle aggregation, mineral ballasting and even diel vertical migration. To conclude, NAGEM was simple enough for application to various time series stations, and with its 1D structure, easy enough for algorithm evaluations, but at the same time detailed enough to investigate specific processes and their detailed representations used in various other models. With the algorithm additions, NAGEM was able to simulate many processes in a common parameterization that are used separately by other models and thus was able to model success and the algorithm use in models. The expertize gained here can be used in 3D models with investigating the global carbon cycle.

REFERENCES

Alldredge, A.L., Jackson, G.A., 1995. Aggregation in marine systems. Deep-Sea Research II 42, 1–7.

Alldredge, A.L., Silver, M.W., 1988. Characteristics, dynamics and significance of marine snow. Progress in Oceanography 20, 41–82.

Álvarez-Salgado, X. A., Arístegui, J., Barton, E. D., Hansell, D. A., 2007. Contribution of upwelling filaments to offshore carbon export in the subtropical Northeast Atlantic Ocean. *Limnology and Oceanography*, *52*(3), 1287–1292. http://doi.org/10.4319/lo.2007.52.3.1287.

Anderson, T.R., Mitra, A., 2010. Dysfunctionality in ecosystem models: an underrated pitfall? Progress in Oceanography, 84 (1-2). 66-68.

Angel, M.V., 1989. Does mesopelagic biology a!ect the vertical #ux? In: Berger, W.H., Smetacek, V.S., Wefer, G. (Eds.), Productivity of the Oceans: Present and Past. Wiley, New York, pp. 155-173.

Armstrong, R. A., Lee, C., Hedges, J. I., Honjo, S., Wakeham, S. G. (2001). A new, mechanistic model for organic carbon fluxes in the ocean based on the quantitative association of POC with ballast minerals. *Deep Sea Research Part II: Topical Studies in Oceanography*, *49*(1-3), 219–236. http://doi.org/10.1016/S0967-0645(01)00101-1.

Aumont, O., Ethé, C., Tagliabue, A., Bopp, L., Gehlen, M., 2015. PISCES-v2: an ocean biogeochemical model for carbon and ecosystem studies, Geosci. Model Dev., 8, 2465-2513, doi:10.5194/gmd-8-2465-2015.

Aumont, O., Bopp, L., 2006. Globalizing results from ocean in-situ iron fertilization studies, Global Biogeochem. Cy., 20, GB2017, doi:10.1029/2005GB002591.

Azam, F., Fenchel, T., Field, J. G., Gray, J. S., Meyer-Reil, L. A., Thingstad, F., 1983. The ecological role of water column microbes in the sea, Mar. Ecol., 10, 257–263.

Azam, F., Hodson, R. E., 1977. Size distribution and activity of marine microheterotrophs. Limnology and Oceanography, 22(3):492–501.

Banse, K., 1990. New views on the degradation and disposition of organic particles as collected by sediment traps in the open sea. *Deep Sea Research Part A. Oceanographic Research Papers*, *37*(7), 1177–1195. http://doi.org/10.1016/0198-0149(90)90058-4.

Benitez-Nelson, C., 2000. The biogeochemical cycling of phosphorus in marine systems. Earth-Science Review 51, 109–135.

Berelson, W.M., 2002. Particle settling rates increase with depth in the ocean. Deep- Sea Research II 49, 237–251.

Bertilsson, S., Berglund, O., Karl, D.M., Chisholm, S.W., 2003. Elemental composition of marine *Prochlorococcus* and *Synechococcus*: implications for the ecological stoichiometry of the sea. Limnology and Oceanography 48, 1721–1731.

Betts, R. A., Jones, C. D., Knight, J. R., Keeling, R. F., Kennedy, J. J., 2016. El Nino and a record CO2 rise. Nature Climate Change 6, 806 – 810.

Billett, D.S.M., Lampitt, R.S., Rice, A.L., Mantoura, R.F.C., 1983. Seasonal sedimentation of phytoplankton to the deep-sea benthos. Nature 302, 520–522.

Bissett, W. P., Walsh, J. J., Dieterle, D. A., Carder, K. L., 1999. Carbon cycling in the upper waters of the Sargasso Sea: II. Numerical simulation of apparent and inherent optical properties. Deep-Sea Research I 46 (2), 271-317.

Blackford, J.C., Allen, J.I., Gilbert, F.J., 2004. Ecosystem dynamics at six contrasting sites: a generic modelling study. J. Mar. Syst. (52): 191-215.

Boyd, P.W., Trull, T.W., 2007. Understanding the export of biogenic particles in oceanic waters: Is there consensus? Prog. Oceanogr. 72(4): 276-312.

Brew, H. S., Moran, S. B., Lomas, M.W., Burd, A. B., 2009. Plankton community composition, organic carbon and thorium-234 parti- cle size distributions, and particle export in the Sargasso Sea, J. Mar. Res., 67, 845–868.

Brix, H., Gruber, N., Karl, D. M., Bates, N. R., 2006. On the relationships between primary, net community, and export production in subtropical gyres. *Deep-Sea Research Part II: Topical Studies in Oceanography*, *53*(5-7), 698–717. http://doi.org/10.1016/j.dsr2.2006.01.024.

Bronk, D.A., 2002. Dynamics of DON. In: Hansell, D.A., Carlson, C.A. (Eds.), Biogeochemistry of Marine Dissolved Organic Matter. Academic Press, New York, pp. 153–250.

Brzezinski, M. A., Nelson, D. M., 1996. Chronic substrate limitation of silicic acid uptake rates in the western Sargasso Sea. Deep Sea Research Part II: Topical Studies in Oceanography, 43(2-3):437–453.

Burd, A.B., Jackson, G.A., 2009. Particle aggregation. Annual Review of Marine Science 1, 65–90. http://dx.doi.org/10.1146/annurev.marine.010908. 163904.

Buesseler, K. O., Boyd, P. W., 2009. Shedding light on processes that control particle export and flux attenuation in the twilight zone of the open ocean. Limnology and Oceanography, 54(4), 1210–1232. http://doi.org/10.4319/lo.2009.54.4.1210.

Cabanes, C., Grouazel, A., Von Schuckmann, K., Hamon, M., Turpin, V., Coatanoan, C., Paris, F., Guinehut, S., Boone, C., Ferry, N., De Boyer Montégut, C., Carval, T., Reverdin, G., Pouliquen, S., Le Traon, P. Y., 2013. The CORA dataset: Validation and diagnostics of in-situ ocean temperature and salinity measurements. Ocean Science, 9(1):1–18.

Capone, D. G., Burns, J. A., Montoya, J. P., Subramaniam, A., Mahaffey, C., Gunderson, T., Michaes, A. F., Carpenter, E. J. (2005). Nitrogen fixation by Trichodesmium spp.: An important source of new nitrogen to the tropical and subtropical North Atlantic Ocean. *Global Biogeochemical Cycles*, *19*(2), 1–17. http://doi.org/10.1029/2004GB002331

Carlson, C.A., 2002. Production and removal processes. In: Hansell, D.A., Carlson, C.A. (Eds.), Biogeochemistry of Marine Dissolved Organic Matter. Academic Press, New York, pp. 91–151.

Caron, D., Dam, H., Kremer, P., Lessard, E., Madin, L., Malone, T., Napp, J., Peele, E., Roman, M., Youngbluth, M., 1995. The contribution of microorganisms to particulate carbon and nitrogen in surface waters of the Sargasso Sea near Bermuda. Deep Sea Research Part I: Oceanographic Research Papers, 42(6):943–972.

Casey, J. R., Aucan, J. P., Goldberg, S. R., Lomas, M. W., 2013. Changes in partitioning of carbon amongst photosynthetic pico- and nano-plankton groups in the Sargasso Sea in response to changes in the North Atlantic Oscillation. Deep-Sea Research Part II: Topical Studies in Oceanography, 93:58–70.

Casey, J. R., Lomas, M. W., Mandecki, J., Walker, D. E., 2007. *Prochlorococcus* contributes to new poduction in the Sargasso Sea deep chlorophyll maximum. Geophysical Research Letters, 34(10):1–5.

Cavender-Bares, K. K., Karl, D. M., Chisholm, S. W., 2001. Nutrient gradients in the western North Atlantic Ocean: Relationship to microbial community structure and comparison to patterns in the Pacific Ocean. Deep-Sea Research Part I: Oceanographic Research Papers, 48(11):2373–2395.

Chelton, D.B., Schlax, M.G., Samelson, R.M., de Szoeke, R.A. 2007. Global observations of large oceanic eddies. Geophysical Research Letters 0094- 8276. 34 (15) p:L15606.

Cianca, A., Godoy, J. M., Martin, J. M., Perez-Marrero, J., Rueda, M. J., Llinás, O., Neuer, S., 2012. Interannual variability of chlorophyll and the influence of low-frequency climate modes in the North Atlantic subtropical gyre. *Global Biogeochemical Cycles*, *26*(2), 1–11. http://doi.org/10.1029/2010GB004022.

Cianca, A., Helmke, P., Mouriño, B., Rueda, M. J., Llinás, O., Neuer, S., 2007. Decadal analysis of hydrography and in situ nutrient budgets in the western and eastern North Atlantic subtropical gyre. Journal of Geophysical Research: Oceans, 112(7), 1–18. http://doi.org/10.1029/2006JC003788.

Cotner, J. B., Ammerman, J. W., Peele, E. R., Bentzen, E., 1997. Phosphoruslimited bacterioplankton growth in the Sargasso Sea. Aquatic Microbial Ecology, 13(2):141–149.

Crank, J., 1956. The Mathematics of Diffusion. Oxford University Press, Oxford.

Dadou, I., Evans, G., Garcon, V., 2004. Using JGOFS in situ and ocean color data to compare biogeochemical models and estimate their parameters in the subtropical North Atlantic Ocean. Journal of Marine Research 62 (4), 565–594.

Dam, H.G., Zhang, X., Butler, M., Roman, M.R., 1995. Mesozooplankton grazing and metabolism at the equator in the central Pacific: implications for carbon and nitrogen fluxes. Deep-Sea Research II 42 (2–3), 735–756.

Davenport, R., Neuer, S., Helmke, P., Perez-Marrero, J., Llinas, O. 2002. Primary productivity in the northern Canary Islands region as inferred from SeaWiFS imagery. *Deep Sea Research Part II: Topical Studies in Oceanography*, *49*(17), 3481–3496. http://doi.org/10.1016/S0967-0645(02)00095-4.

De Boyer Montégut, C., Madec, G., Fischer, A. S., Lazar, A., Iudicone, D., 2004. Mixed layer depth over the global ocean: An examination of profile data and a profile-based climatology. Journal of Geophysical Research C: Oceans, 109(12):1– 20.

De La Rocha, C.L., Nowald, N., Passow, U., 2008. Interactions between diatom aggregates, minerals, particulate organic carbon, and dissolved organic matter: further implications for the ballast hypothesis. Global Biogeochemical Cycles 22, GB4005. http://dx.doi.org/10.1029/2007GB003156.

De La Rocha, C.L., Passow, U., 2007. Factors influencing the sinking of POC and the efficiency of the biological carbon pump. Deep-Sea Research Part II-Topical Studies in Oceanography 54 (5–7), 639–658. http://dx.doi.org/10.1016/ j.dsr2.2007.01.004.

Dee, D. P., Uppala, S. M., Simmons, A. J., Berrisford, P., Poli, P., Kobayashi, S., Andrae, U., Balmaseda, M. A., Balsamo, G., Bauer, P., Bechtold, P., Beljaars, A. C. M., van de Berg, L., Bidlot, J., Bormann, N., Delsol, C., Dragani, R., Fuentes, M., Geer, A. J., Haimberger, L., Healy, S. B., Hersbach, H., Hólm, E. V., Isaksen, L., Kållberg, P., Köhler, M., Matricardi, M., Mcnally, A. P., Monge-Sanz, B. M., Morcrette, J. J., Park, B. K., Peubey, C., de Rosnay, P., Tavolato, C., Thépaut, J. N., Vitart, F., 2011. The ERA-Interim reanalysis: Configuration and performance of the data assimilation system. Quarterly Journal of the Royal Meteorological Society, 137(656):553–597.

Deuser, W.G., Ross, E.H., Anderson, R.F., 1981. Seasonality in the supply of sediment to the deep Sargasso Sea and implications for the rapid transfer of matter to the deep ocean. Deep-Sea Research 28A, 495–505.

Dlugokencky, E., Tans, P., 2016. Trends in atmospheric carbon dioxide, National Oceanic & Atmospheric Administration, Earth System Research Laboratory (NOAA/ESRL), available at: http://www.esrl.noaa.gov/gmd/ccgg/trends, last access: 6 June 2016.

Droop, M. R., 1973. Some thoughts on nutrient limitation in algae. Journal of Phycology 9 (3), 264-272.

Ducklow, H.W., Steinberg, D.K., Buesseler, K.O., 2001. Upper ocean carbon export and the biological carbon pump. Oceanography 14(4): 50-58.

Dunne, J.P., Sarmiento, J.L., Gnanadesikan, A., 2007. A synthesis of global particle export from the surface ocean and cycling through the ocean interior and on the seafloor. Global Biogeochemical Cycles 21, GB4006. http://dx.doi.org/10.1029/ 2006GB002907.

DuRand, M. D., Olson, R. J., Chisholm, S. W., 2001. Phytoplankton population dynamicsat the BermudaAtlantic Time-series stationin the Sargasso Sea. Deep-Sea Research Part II: Topical Studies in Oceanography, 48(8-9):1983–2003.

Emerson, S., Mecking, S., Abell, J., 2001. The biological pump in the subtropical North Pacific Ocean: Nutrient sources, Redifield ratio, and recent changes. *Global Biogeochemical Cycles*, *15*(3), 535–554.

Emerson, S., Quay, P., Karl, D., Winn, C., Tupas, L., Landry, M., 1997. Experimental determination of the organic carbon flux from open-ocean surface waters, *389*(6654), 951–954. http://doi.org/10.1038/40111.

Eppley, R. W., Peterson, B. J., 1979. Particulate organic matter flux and planktonic new production in the deep ocean, Nature, 282, 677–680.

Eppley, R.W., 1972. Temperature and phytoplankton growth in the sea. Fishery Bulletin 70, 1063–1085

Falkowski, P.G., Barber R.T., Smetacek, V., 1998. Biogeochemical controls and feedback on ocan primary production. Science 281: 200-206.

Fanning, K. A., 1992. Nutrient provinces in the sea: Concentration ratios, reaction rate ratios, and ideal covariation. Journal of Geophysical Research, 97(C4):5693.

Fasham, M.J.R., 2003. Ocean Biogeochemistry: The Role of the Ocean Carbon Cycle in Global Change, Springer, Berlin Heidenberg, pp 31-32 (Chapter 2).

Fernández-Castro, B., Anderson, L., Marañón, E., Neuer, S., Ausín, B., GonzáezDávila, M., Santana-Casiano, J. M., Cianca, a., Santana, R., Llinás, O., Rueda, M. J., Mouriño-Carballido, B., 2012. Regional differences in modelled net production and shallow remineralization in the North Atlantic subtropical gyre. Biogeosciences, 9(8):2831–2846.

Field, C. B., Behrenfeld, M. J., Randerson, J. T., 1998. Primary production of the biosphere: integrating terrestrial and oceanic components. Science 281: 237-40.

Fischer, G., Karakaş, G., 2009. Sinking rates and ballast composition of particles in the Atlantic ocean: implications for the organic carbon fluxes to the deep ocean. Biogeosciences 6, 85–102.

Flynn, K.J., Davidson, K., Leftley, J.W., 1994. Carbon–nitrogen relations at whole-cell and free-amino-acid levels during batch growth of *Isochrysis galbana* (prymnesiophyceae) under conditions of alternating light and dark. Marine Biology 118 (2), 229–237.

François, R., Honjo, S., Krishfield, R., Manganini, S., 2002. Factors controlling the flux of organic carbon to the bathypelagic zone of the ocean. Global Biogeochemical Cycles 16 (4), 1087. http://dx.doi.org/10.1029/2001GB001722.

Garcia, H. E., Locarnini, R. A., Boyer, T. P., Antonov, J. I., Baranova, O. K., Zweng, M. M., Reagan, J. R., Johnson, D. R., 2014. World Ocean Atlas 2013, Volume 4: Dissolved Inorganic Nutrients (phosphate, nitrate, silicate). S. Levitus, Ed., A. Mishonov Technical Ed.; NOAA Atlas NESDIS 76, 25 pp.

Gehlen, M., Bopp, L., Emprin, N., Aumont, O., Heinze, C., Ragueneau, O., 2006. Reconciling surface ocean productivity, export fluxes and sediment composition in a global biogeochemical ocean model. *Biogeosciences Discussions*, *3*(3), 803–836. http://doi.org/10.5194/bgd-3-803-2006.

Geider, R.J., La Roche, J., 2002. Redfield revisited: variability in the N:P ratio of phytoplankton and its biochemical basis. European Journal of Phycology 37, 1–17.

Geider, R.J., MacIntyre, H.L., Kana, T.M., 1998. A dynamic regulatory model of phytoplanktonic acclimation to light, nutrients, and temperature. Limnology and Oceanography 43 (4), 679–694.

Geider, R.J., MacIntyre, H.L., Kana, T.M., 1997. A dynamical model of phytoplankton growth and acclimation: responses of the balanced growth rate and chlorophyll a:carbon ratio to light, nutrient-limitation and temperature. Marine Ecology Progress Series 148, 187–200.

Giering, S. L. C., Sanders, R., Lampitt, R. S., Anderson, T. R., Tamburini, C., Boutrif, M., … Mayor, D. J., 2014. Reconciliation of the carbon budget in the ocean's twilight zone. *Nature*, *507*(7493), 480–483. http://doi.org/10.1038/nature13123.

Giesecke, R., González, H.E., Bathmann, U., 2010. The role of the chaetognath Sagitta gazellae in the vertical carbon flux of the Southern Ocean. Polar Biology 33, 293– 304.

Goericke, R., 1998. Response of phytoplankton community structure and taxonspecific growth rates to seasonally varying physical forcing in the Sargasso Sea off Bermuda. Limnology and Oceanography, 43(5):921–935.

Gonzalez, H. E., Smetacek, V., 1994. The possible role of the cyclopoid copepod Oithona in retarding vertical flux of zooplankton faecal material. Marine Ecology Progress Series, 113(1982):233–246.

Hain, M.P., Sigman, D.M., Haug, G.H., 2014. The Biological Pump in the Past. Treatise on Geochemistry, 2nd Edition. pp: 485–517.

Hansell, D. A., Bates, N. R., Olson, D. B., 2004. Excess nitrate and nitrogen fixation in the North Atlantic Ocean. *Marine Chemistry*, *84*(3-4), 243–265. http://doi.org/10.1016/j.marchem.2003.08.004.

Harrison, W.G., Harris, L.R., Irwin, B.D., 1996. The kinetics of nitrogen utilization in the oceanic mixed layer: nitrate and ammonium interactions at nanomolar concentrations. Limnology and Oceanography 41 (1), 16–32.

Hartman, S.E., Larkin, K.E., Lampitt, R.S., Lankhorst, M., Hydes, D.J., 2010. Seasonal and inter-annual biogeochemical variations in the Porcupine Abyssal Plain 2003-2005 associated with winter mixing and surface circulation. Deep-Sea Research II 57 (15), 1303–1312.

Helmke, P., Neuer, S., Lomas, M.W., Conte, M., Freudenthal, T., 2010. Cross-basin differences in particulate organic carbon export and flux attenuation in the subtropical North Atlantic gyre. Deep Sea Research I 57: 213-227.

Henson, S.A., Sanders, R., Madsen, E., 2012. Global patterns in efficiency of particulate organic carbon export and transfer to the deep ocean. Global Biogeochemical Cycles, 26, GB1028, doi:10.1029/2011GB004099.

Henson, S. A., Sanders, R., Madsen, E., Morris, P. J., Le Moigne, F., Quartly, G. D., 2011. A reduced estimate of the strength of the ocean's biological carbon pump, Geophysical Research Letters, 38.

Ho, T.Y., Quigg, A., Finkel, Z.V., Milligan, A.J., Wyman, K., Falkowski, P.G., Morel, F.M.M., 2003. Elemental composition of some eukaryotic marine phytoplankton. Journal of Phycology 39, 1145–1159.

Hood, R.R., Laws, E.A. *et al.*, 2006. Pelagic functional group modelling: Progress, challenges and prospects. Deep Sea Res.II, 53(5-7): 459-512.

Hood, R.R., Bates, N.R., Capone, D.G., Olson, D.B., 2001. Modeling the effects of nitrogen fixation on carbon and nitrogen fluxes at BATS. Deep-Sea Research II 48 (8–9), 1609–1648.

Hutchins, D.A., Bruland, K.W., 1995. Fe, Zn, Mn and N transfer between size classes in a coastal phytoplankton community: trace metal and major nutrient recycling compared. Journal of Marine Research 53 (2), 297–313.

IPCC, 2014: Summary for Policymakers. In: Climate Change 2014: Impacts, Adaptation, and Vulnerability. Part A: Global and Sectoral Aspects. Contribution of Working Group II to the Fifth Assessment Report of the Intergovernmental Panel on Climate Change [Field, C.B., V.R. Barros, D.J. Dokken, K.J. Mach, M.D. Mastrandrea, T.E. Bilir, M. Chatterjee, K.L. Ebi, Y.O. Estrada, R.C. Genova, B. Girma, E.S. Kissel, A.N. Levy, S. MacCracken, P.R. Mastrandrea, and L.L. White (eds.)]. Cambridge University Press, Cambridge, United Kingdom and New York, NY, USA, pp. 1-32.

Iversen, M.H., Ploug, H., 2010. Ballast minerals and the sinking carbon flux in the ocean: carbon-specific respiration rates and sinking velocity of marine snow aggregates. Biogeosciences 7, 2613–2624.

Ivlev, V.S., 1955. Experimental Ecology of the Feeding of Fishes. Yale University Press, New Haven (translated from Russian by D. Scott).

Jackson, G.A., Burd, A.B., 1998. Aggregation in the marine environment: a critical review. Environmental Science and Technology 32, 2805–2814.

Jackson, G.A., 1990. A model of the formation of marine algal flocs by physical coagulation processes. Deep Sea Research Part A, Oceanographic Research Papers 37 (8), 1197–1211.

Jenkins, W. J., 1998. Studying subtropical thermocline ventilation and circulation using tritium and 3 He. *Journal of Geophysical Research*, *103*(C8), 15817. http://doi.org/10.1029/98JC00141

Jenkins, W. J., Goldman, J. C., 1985. Seasonal oxygen cycling and primary production in the Sargasso Sea. *Journal of Marine Research*, *43*, 465–491. http://doi.org/10.1357/002224085788438702.

Jiang, S.N., Dickey, T.D., Steinberg, D.K., Madin, L.P., 2007. Temporal variability of zooplankton biomass from ADCP backscatter time series data at the Bermuda Testbed Mooring site. Deep-Sea Research I 54, 608–636.

Joos, F., Spahni, R., 2008. Rates of change in natural and anthropogenic radiative forcing over the past 20,000 years. *Proceedings of the National Academy of Sciences*, *105*(5), 1425–1430. http://doi.org/10.1073/pnas.0707386105.

Jumars, P. A., Penry, D. L., Baross, J. A., Perry, M. J., Frost, B. W., 1989. Closing the microbial loop: dissolved carbon pathway to heterotrophic bacteria from incomplete ingestion, digestion and absorption in animals. Deep Sea Research Part A. Oceanographic Research Papers, 36(4):483–495.

Kana, T.M., Glibert, P.M., 1987. Effect of irradiances up to 2000 μ Em^{-2} s^{-1} on marine *Synechococcus* WH7803. I. Growth, pigmentation, and cell composition. Deep-Sea Research 34 (4A), 479–495.

Karakaş, G., Nowald, N., Schäfer-Neth, C., Iversen, M., Barkmann, W., Fischer, G., Marchesiello, P., Schlitzer, R., 2009. Impact of particle aggregation on vertical fluxes of organic matter. Progress in Oceanography 83, 331–341.

Karl, D.M., Bjorkman, K.M., 2002. Dynamics of DOP. In: Hansell, D.A., Carlson, C.A. (Eds.), Biogeochemistry of Marine Dissolved Organic Matter. Academic Press, New York, pp. 250–367.

Kiørboe, T., Tang, K., Grossart, H.-P., Ploug, H., 2003. Dynamics of microbial communities on marine snow aggregates: colonization, growth, detachment, and grazing mortality of attached bacteria. Applied and Environmental Microbiology 69, 3036–3047.

Klaas, C., 2002. Association of sinking organic matter with various types of mineral ballast in the deep sea: Implications for the rain ratio. *Global Biogeochemical Cycles*, *16*(4). http://doi.org/10.1029/2001GB001765.

Krause, J. W., Nelson, D. M., Lomas, M. W., 2009. Biogeochemical responses to late-winter storms in the Sargasso Sea, II: Increased rates of biogenic silica production and export. *Deep-Sea*

Research Part I: Oceanographic Research Papers, *56*(6), 861–874. http://doi.org/10.1016/j.dsr.2009.01.002.

Kriest, I., 2002. Different parameterizations of marine snow in a 1D-model and their influence on representation of marine snow, nitrogen budget and sedimentation. Deep Sea Research I 49: 2133-2162.

Kriest, I. and Evans, G. T.: A vertically resolved model for phyto- plankton aggregation, Proc. Indian Acad. Sci. Earth Planet. Sci., 109, 453–469, 2000.

Kriest, I., Evans, G. T., 1999. Representing phytoplankton aggregates in biogeochemical models. *Deep-Sea Research Part I: Oceanographic Research Papers*, *46*(11), 1841–1859. http://doi.org/10.1016/S0967-0637(99)00032-1.

Kwon, E. Y., F. Primeau., 2006. Optimization and sensitivity study of a biogeochemistry ocean model using an implicit solver and in situ phosphate data. Global Biogeochemical Cycles 20.

Lam, P.J., Doney, S.C., Bishop, J.K.B., 2011. The dynamic ocean biological pump: insights from a global compilation of particulate organic carbon, CaCO3, and opal concentration profiles from the mesopelagic. Global Biogeochemical Cycles 25 (3), GB3009, 10.1029/2010gb003868.

Lampitt, R.S., Salter, I., de Cuevas, B.A., Hartman, S., Larkin, K.E., Pebody, C.A., 2010. Long-term variability of downward particle flux in the deep northeast Atlantic: Causes and trends. Deep Sea Research II 57: 1346-1361.

Lampitt, R.S., Bett, B.J., Kiriakoulis, K., Popova, E.E., Ragueneau, O., Vangriesheim, A., Wolff, G.A., 2001. Material supply to the abyssal seafloor in the Northeast Atlantic. Progress in Oceanography 50, 27–63.

Lampitt, R. S., Hillier, W. R., Challenor, P. G., 1993. Seasonal and diel variation in the open ocean concentration of marine snow aggregates. *Nature*, *362*(6422), 737–739. http://doi.org/10.1038/362737a0

Lampitt, R. S., Noji, T., von Bodungen, B., 1990. What happens to zooplankton faecal pellets? Implications for material flux. Marine Biology, 104(1):15–23.

Landry, M.R., Kirshtein, J., Constantinou, J., 1996. Abundances and distributions of picoplankton populations in the central equatorial Pacific from 12ºN to 12ºS, 140ºW. Deep-Sea Research II 43 (4–6), 871–890.

Landry, M.R., Kirshtein, J., Constantinou, J., 1995. A refined dilution technique for measuring the community grazing impact of microzooplankton, with experimental tests in the central equatorial Pacific. Marine Ecology Progress Series 120 (1–3), 53–63.

Laws, E.A., Falkowski, P.G., Smith, W.O., Ducklow, H., McCarthy, J.J., 2000. Temperature effects on export production in the open ocean. Global Biogeochemical Cycles 14, 1231–1246.

Laws, E.A., Bannister, T.T., 1980. Nutrient- and light-limited growth of Thalassiosira fluviatilis in continious culture, with implications for phytoplankton growth in the ocean. Limnology and Oceanography 25 (3), 457–473.

Le Moigne, F. A. C., Sanders, R. J., Villa-Alfageme, M., Martin, A. P., Pabortsava, K., Planquette, H., Morris, P. J., Thomalla, S. J., 2012. On the proportion of ballast versus non-ballast associated carbon export in the surface ocean. Geophysical Research Letters, 39(15-16):L15610.

Le Quéré, C., Moriarty, R., Andrew, R. M., Canadell, J. G., Sitch, S., Korsbakken, J. I., … Zeng, N., 2015. Global Carbon Budget 2015. *Earth System Science Data*, *7*(2), 349–396. http://doi.org/10.5194/essd-7-349-2015.

Leblanc, K., A. Leynaert, C. Fernandez I., P. Rimmelin, T. Moutin, P. Raimbault, J. Ras, and B. Que´guiner (2005), A seasonal study of diatom dynamics in the North Atlantic during the POMME experiment (2001): Evidence for Si limitation of the spring bloom, J. Geophys. Res., 110, C07S14, doi:10.1029/2004JC002621.

Ledwell, J.R., Watson, A.J., Law, C.S., 1998. Mixing of a tracer in the pycnocline. Journal of Geophysical Research 103 (C10), 21499–21529.

Lee, C., Peterson, M. L., Wakeman, S. G., Armstrong, R. A., Cochran, J. K., Miquel, J. M., Fowler, S. W., Hirschberg, D., Beck, A., and Xue, J.: Particulate organic matter and ballast fluxes measured using time-series and settling velocity sediment traps in the northwestern Mediterranean Sea, Deep-Sea Res. Pt. II, 56, 1420–1436, 2009.

Leonard, C.L., McClain, C.R., Murtugudde, R., Hofmann, E.E., Harding, L.W.J., 1999. An iron-based ecosystem model of the central equatorial Pacific. Journal of Geophysical Research 104 (C1), 1325–1341.

Leonardos, N., Geider, R.J., 2004. Effects of nitrate: phosphate supply ratio and irradiance on the C:N:P stoichiometry of *Chaetocerosmuelleri*. European Journal of Phycology 39, 173–180.

Lima, I. D., Doney, S. C., 2004. A three-dimensional, multinutrient, and sizestructured ecosystem model for the North Atlantic. Global Biogeochemical Cycles, 18(3).

Lomas, M. W., Bates, N. R., Johnson, R. J., Knap, A. H., Steinberg, D. K., Carlson, C. A., 2013. Two decades and counting: 24-years of sustained open ocean biogeochemical measurements in the Sargasso Sea. Deep-Sea Research Part II: Topical Studies in Oceanography, 93:16–32.

Lomas, M. W., Moran, S. B., 2011. Evidence for aggregation and export of cyanobacteria and nano-eukaryotes from the Sargasso Sea euphotic zone, Biogeosciences, 8, 203-216, doi:10.5194/bg-8-203-2011.

Lomas, M.W., Burke, A.L., Lomas, D.A., Bell, D.W., Shen, C., Dyhrman, S.T., Ammerman, J. W., 2010. Sargasso Sea phosphorus biogeochemistry: an important role for dissolved organic phosphorus (DOP). Biogeosciences, 7(2):695–710.

Lomas, M. W., Steinberg, D. K., Dickey, T., Carlson, C. A., Nelson, N. B., Condon, R. H., Bates, N. R., 2010b. Increased ocean carbon export in the Sargasso Sea is countered by its enhanced mesopelagic attenuation. *Biogeosciences*, *7*, 57–70. http://doi.org/10.5194/bgd-6-9547-2009

Lomas, M. W., Bates, N. R., 2004. Potential controls on interannual partitioning of organic carbon during the winter/spring phytoplankton bloom at the Bermuda Atlantic time-series study (BATS) site. Deep-Sea Research Part I: Oceanographic Research Papers, 51(11):1619–1636.

Longhurst, A.R., Bedo, A., Harrison, W.G., Head, E.J.H., Sameoto, D.D., 1990. Vertical flux of respiratory carbon by oceanic diel migrant biota. Deep Sea Research 37, 685–694.

Longhurst, A.R., Harrison, W.G., 1989. The biological pump: profiles of plankton production and consumption in the ocean. Progress in Oceanography 22, 47– 123.

Madin, L. P., Horgan, E. F., Steinberg, D. K., 2001. Zooplankton at the Bermuda Atlantic Time-series Study (BATS) station: Diel, seasonal and interannual variation in biomass, 1994-1998. Deep-Sea Research Part II: Topical Studies in Oceanography, 48(8-9):2063–2082.

Marañón, E., Fernández, A., Mouriño-Carballido, B., Martínez-García, S., Tiera, E., Cermeño, P., Chouciño, P., Huete-Ortega, M., Fernández, E., Calvo-Díaz, A., Morán, X. A. G., Bode, A., Moreno-Ostos, E., Varela, M., Patey, M., Achterberg, E., 2010. Degree of oligotrophy controls the response of microbial plankton to Saharan dust. Limnology and Oceanography, 55(6):2339–2352.

Martin, P., R. S. Lampitt, M. Jane Perry, R. Sanders, C. Lee, and E. D'Asaro (2011), Export and mesopelagic particle flux during a North Atlantic spring diatom bloom, Deep Sea Res., Part I, 58(4), 338–349, doi:10.1016/j.dsr.2011.01.006.

Martin, J.H., Knauer, G.A., Karl, D.M., Broenkow, W.W., 1987. VERTEX: carbon cycling in the northeast Pacific. Deep-Sea Res., (34): 267-285.

Martiny, A. C., Kathuria, S., and Berube, P. M., 2009. Widespread metabolic potential for nitrite and nitrate assimilation among *Prochlorococcus* ecotypes. *Proceedings of the National Academy of Sciences of the United States of America*, *106*(26), 10787–10792. http://doi.org/10.1073/pnas.0902532106.

Mather, R. L., Reynolds, S. E., Wolff, G. A., Williams, R. G., Torres-Valdes, S., Woodward, E. M. S., Landolfi, A., Pan, X., Sanders, R., Achterberg, E. P., 2008. Phosphorus cycling in the North and South Atlantic Ocean subtropical gyres. Nature Geoscience, 1(7):439–443.

McDonnell, A. M. P., P. W. Boyd, and K. O. Buesseler (2015), Effects of sinking velocities and microbial respiration rates on the attenuation of particulate carbon fluxes through the mesopelagic zone, Global Biogeochem. Cycles, 29, 175–193, doi:10.1002/ 2014GB004935.

McDonnell AMP, Buesseler KO. 2010. Variability in the average sinking velocity ofmarine particles. Limnol. Oceanogr. 55:2085–96.

McGillicuddy, D. J., Jr., Anderson, L. A., Doney, S. C., Maltrud, M. E., 2003. Eddy-driven sources and sinks of nutrients in the upper ocean: Results from a 0.1? resolution model of the North Atlantic, Global Biogeochem. Cycles, 17(2), 1035, doi:10.1029/2002GB001987.

McGillicuddy Jr., D. J., R. Johnson, D. A. Siegel, A. F. Michaels, N. R. Bates, and A. H. Knap (1999), Mesoscale variations of biogeochemical properties in the Sargasso Sea, J. Geophys. Res., 104(C6), 13381–13394, doi:10.1029/1999JC900021.

McGillicuddy Jr., D.J., Robinson, A.R., Siegel, D.A., Jannasch, H.W., Johnson, R., Dickey, T.D., McNeil, J., Michaels, A.F., Knap, A.H., 1998. Influence of mesoscale eddies on new production in the Sargasso Sea. Nature 394, 263-266.

McGillicuddy, D.J., Robinson, A.R., 1997. Eddy induced nutrient supply and new production in the Sargasso Sea. Deep-Sea Research I 44, 1427-1450.

Menzel, D. and Ryther, J., 1959. The annual cycle of primary production in the sargasso sea off bermuda. Deep Sea Research, 6:351 – 367.

Michaels, A.F., Knap, A.H., 1996. Overview of the U.S. JGOFS BATS and Hydrostation S program. Deep-Sea Research 43 (2-3), 157-198.

Michaels, A.F., Knap, A.H., Dow, R.L., Gundersen, K., Johnson, R.J., Sorensen, J., Close, A., Knauer, G.A., Lohrenz, S.E., Asper, V.A., Tuel, M., Bidigare, R.R., 1994. Seasonal patterns of ocean biogeochemistry at the U.S. JGOFS Bermuda Atlantic Time-series Study site. Deep-Sea Research 41, 1013-1038.

Mitra, A., 2006. A multi-nutrient model fort he description of stochiometric modulation of predation in micro and mesozooplankton. Journal of Plankton Res. 28(6): 597-611.

Moore, L. R., Post, A. F., Rocap, G., Chisholm, S. W., 2002. Utilization of different nitrogen sources by the marine cyanobacteria *Prochlorococcus* and *Synechococcus*. Limnology and Oceanography, 47(4):989–996.

Moore, L.R., Goericke, R., Chisholm, S.W., 1995. Comparative physiology of *Synechococcus* and *Prochlorococcus*: influence of light and temperature on growth, pigments, fluorescence and absorptive properties. Marine Ecology Progress Series 116 (1–3), 259–275.

Moran XAG. (2007). Annual cycle of picophytoplankton photosynthesis and growth rates in a temperate coastalecosystem: a major contribution to carbon fluxes. Aquat Microb Ecol 49: 267–279.

Mouriño-Carballido, B., Neuer, S., 2008. Regional differences in the role of eddy pumping in the north atlantic subtropical gyre: Historical conundrums revisited. Oceanography, 21 (2):52–61, http://dx.doi.org/10.5670/oceanog.2008.53.

Nelson, D.M., Treguer, P., Brzezinski, M.A., Leynaert, A., Queaguiner, B., 1995. Production and dissolution of biogenic silica in the ocean: revised global estimates, comparison with regional data and relationship to biogenic sedimentation. Global Biogeochemical Cycles 9, 359–372.

Nelson, D.M., Treguer, P., 1992. Role of silicon as a limiting nutrient to antarctic diatoms: evidence from kinetic studies in the Ross Sea ice-edge zone. Marine Ecology Progress Series 80, 255–264.

Neuer, S., Cianca, A., Helmke, P., Freudenthal, T., Davenport, R., Meggers, H., Knoll, M., Santana-Casiano, J. M., González-Davila, M., Rueda, M. J., Llinás, O., 2007. Biogeochemistry and

hydrography in the eastern subtropical North Atlantic gyre. Results from the European time-series station ESTOC. Progress in Oceanography, 72(1):1–29.

Neuer, S., R. Davenport, T. Freudenthal, G. Wefer, O. Llinás, M.-J. Rueda, D. K. Steinberg, and D. M. Karl, 2002a. Differences in the biological carbon pump at three subtropical ocean sites, Geophys. Res. Lett., 29(18), 1885, doi:10.1029/2002GL015393.

Neuer, S., R. Davenport, T. Freudenthal, G. Wefer, O. Llinás, M.-J. Rueda, D. K. Steinberg, and D. M. Karl, 2002b. Differences in the biological carbon pump at three subtropical ocean sites, Geophys. Res. Lett., 29(18), 1885, doi:10.1029/2002GL015393.

Oschlies, A., 2002. Can eddies make ocean deserts bloom?, *16*(4). http://doi.org/10.1029/2001GB001830

Oschlies, A., Koeve, W., Garcon, V., 2000. An eddy-permitting coupled physical-biological model of the North Atlantic 2. Ecosystem dynamics and comparison with satellite and JGOFS local studies data. *Global Biogeochemical Cycles*, *14*(1), 499–523. http://doi.org/10.1029/1999GB900080

Oschlies, A., Garcon, V., 1998. Eddy-induced enhancement of primary production in a model of the North Atlantic Ocean. *Nature*, *394*(July), 266–269. http://doi.org/10.1038/28373

Owens, S. A., Buesseler, K. O., Lamborg, C. H., Valdes, J., Lomas, M. W., Johnson, R. J., Steinberg, D. K., Siegel, D. A., 2013. A new time series of particle export from neutrally buoyant sediments traps at the Bermuda Atlantic Time-series Study site. Deep-Sea Research Part I: Oceanographic Research Papers, 72:34–47.

Parekh, P., Dutkiewicz, S., Follows, M.J., Ito, T., 2006. Atmospheric carbon dioxide in a less dusty world. Geophys. Res. Lett., (33): L03610.

Parpais, J., Marie, D., Partensky, F., Morin, P., Vaulot, D., 1996. Effect of phosphorus starvation on the cell cycle of the photosynthetic prokaryote *Prochlorococcus*. Marine Ecology Progress Series 132, 265–274.

Partensky, F., Hoepffner, N., Li, W.K.W., Ulloa, O., Vaulot, D., 1993. Photoacclimation of *Prochlorococcus* sp. (Prochlorophyta) strains isolated from the North Atlantic and the Mediterranean Sea. Plant Physiology 101 (1), 285–296.

Passow, U., De La Rocha, C., 2006. The accumulation of mineral ballast on organic aggregates. Global Biogeochemical Cycles 20, GB1013. http://dx.doi.org/ 10.1029/2005GB002579.

Pelegrí, J. L., Arístegui, J., Cana, L., González-Dávila, M., Hernández-Guerra, A., Hernández-León, S., Marrero-Díaz, A., Montero, M. F., Sangrá, P., Santana-Casiano, M., 2005. Coupling between the open ocean and the coastal upwelling region off northwest Africa: Water recirculation and offshore pumping of organic matter. *Journal of Marine Systems*, *54*(1-4 SPEC. ISS.), 3–37. http://doi.org/10.1016/j.jmarsys.2004.07.003.

Ploug, H., Iversen, M.H., Koski, M., Buitenhuis, E.T., 2008. Production, oxygen respiration rates, and sinking velocity of copepod fecal pellets: direct measurements of ballasting by opal and calcite. Limnology and Oceanography 53, 469–476.

Pomeroy, L. R., 1974. The Ocean's Food Web, A Changing Paradigm. BioScience, 24(9):499–504.

Poulsen, L. K., Moldrup, M., Berge, T., Hansen, P. J., 2011. Feeding on copepod fecal pellets: a new trophic role of dinoflagellates as detritivores. Marine Ecology Progress Series, 441:65–78.

Poulsen, L. K., Iversen, M. H., 2008. Degradation of copepod fecal pellets: Key role of protozooplankton. Marine Ecology Progress Series, 367:1–13.

Poulsen, L. K., Kiørboe, T., 2006. Vertical flux and degradation rates of copepod fecal pellets in a zooplankton community dominated by small copepods. Marine Ecology Progress Series, 323:195–204.

Prospero, J. M., Barrett, K., Church, T., Dentener, F., Duce, R. A., Galloway, J. N., Levy II, H., Moody, J., Quinn, P. (1996). Atmospheric deposition of nutrients to the North Atlantic Basin. *Biogeochemistry*, *35*(1), 27–73. http://doi.org/10.1007/BF02179824

Pulido-Villena, E., Wagener, T., Guieu, C., 2008. Bacterial response to dust pulses in the western Mediterranean: Implications for carbon cycling in the oligotropic ocean. Global Biogeochemical Cycles, 22(1):1–12.

Richardson, T., Jackson, G., 2007. Small phytoplankton and carbon export from the surface ocean, Science, 315, 838–840.

Roman, M.R., Adolf, H.A., Landry, M.R., Madin, L.P., Steinberg, D.K., Zhang, X., 2002. Estimates of oceanic mesozooplankton production: a comparison using the Bermuda and Hawaii time-series data. Deep-Sea Research II 49, 175–192.

Roman, M.R., Gauzens, A.L., 1997. Copepod grazing in the equatorial Pacific. Limnology and Oceanography 42 (4), 623–634.

Sakshaug, E., Andresen, K., Kiefer, D.A., 1989. A steady state description of growth and light absorption in the marine planktonic diatom *Skeletonema costatum*. Limnology and Oceanography 34 (1), 198–205.

Salihoglu, B., Garçon, V., Oschlies, a., Lomas, M., 2008. Influence of nutrient utilization and remineralization stoichiometry on phytoplankton species and carbon export: A modeling study at BATS. Deep Sea Research Part I: Oceanographic Research Papers, 55(1):73–107.

Salihoglu, B., Hofmann, E. E., 2007. Simulations of phytoplankton species and carbon production in the equatorial Pacific Ocean 1. Model configuration and ecosystem dynamics. Journal of Marine Research, 65(2):219–273.

Salihoglu, B., 2005. Modeling the effects of physical and biogeochemical processes on phytoplankton species and carbon production in the equatorial Pacific Ocean. PhD thesis, Old Dominion University.

Sanders, R., Henson, S. A., Koski, M., De La Rocha, C. L., Painter, S. C., Poulton, A. J., … Martin, A. P., 2014. The Biological Carbon Pump in the North Atlantic. Progress in Oceanography Elsevier, 2014, 129 (PB), pp. 200-218. http://doi.org/10.1016/j.pocean.2014.05.005.

Sarmiento, J. L., N. Gruber., 2006. Ocean Biogeochemical Dynamics. Princeton University Press.

Siegel, D. A., McGillicuddy, D.J., Fields, E.A., 1999. Mesoscale eddies, satellite altimetry, and new production in the Sargasso Sea. Journal of Geophysical Research 104, 13359-13379.

Simon, M., Grossart, H.P., Schweitzer, B., Ploug, H., 2002. Microbial ecology of organic aggregates in aquatic ecosystems. Aquatic Microbial Ecology 28 (2), 175–211.

Smayda, T.J., 1970. The suspension and sinking of phytoplankton in the sea. Oceanography and Marine Biology: an Annual Review 8, 353–414.

Spall, M. A., Weller, R. A., Furey, P. W., 2000. Modeling the three-dimensional upper ocean heat budget and subduction rate during the Subduction Experiment. Journal of Geophysical Research, 105(C11):26151.

Spitzer, W. S., Jenkins, W. J., 1989. Rates of vertical mixing, gas exchange and new production: Estimates from seasonal gas cycles in the upper ocean near Bermuda. *Journal of Marine Research*, *47*(1), 169–196. http://doi.org/10.1357/002224089785076370.

Steele, J., Frost, B., 1977. The structure of plankton communities, Phi- los. Trans. R. Soc. Lond. Ser. B-Biol. Sci., 280, 485–534.

Steinberg, D. K., Lomas, M. W., Cope, J. S., 2012. Long-term increase in mesozooplankton biomass in the Sargasso Sea: Linkage to climate and implications for food web dynamics and biogeochemical cycling. *Global Biogeochemical Cycles*, *26*(1), 1–16. http://doi.org/10.1029/2010GB004026

Steinberg, D. K., Van Mooy, B. A. S., Buesseler, K. O., Boyd, P. W., Kobari, T., Karl, D. M., 2008. Bacterial vs. zooplankton control of sinking particle flux in the ocean's twilight zone. *Limnology and Oceanography*, *53*(4), 1327–1338. http://doi.org/10.4319/lo.2008.53.4.1327.

Steinberg, D. K., Carlson, C. A., Bates, N. R., Johnson, R. J., Michaels, A. F., Knap, A. H., 2001. Overview of the US JGOFS Bermuda Atlantic Time-series Study (BATS): A decade-scale look at ocean biology and biogeochemistry. DeepSea Research Part II: Topical Studies in Oceanography, 48(8-9):1405–1447.

Steinberg, D.K., Carlson, C.A., Bates, N.R., Goldthwait, S.A., Madin, L.P., Michaels, A.F., 2000. Zooplankton vertical migration and the active transport of dissolved organic and inorganic carbon in the Sargasso Sea. Deep-Sea Research I 47, 137–158.

Strom, S. L., Benner, R., Ziegler, S., Dagg, M. J., 1997. Planktonic grazers are a potentially important source of marine dissolved organic carbon. Limnology and Oceanography, 42(6):1364–1374.

Sweeney, E. N., McGillicuddy, D. J., Buesseler, K. O., 2003. Biogeochemical impacts due to mesoscale eddy activity in the Sargasso Sea as measured at the Bermuda Atlantic Time-series Study (BATS). *Deep-Sea Research Part II: Topical Studies in Oceanography*, *50*(22-26), 3017–3039. http://doi.org/10.1016/j.dsr2.2003.07.008.

Svensen, C., Wexels Riser, C., Reigstad, M., Seuthe, L., 2012. Degradation of copepod faecal pellets in the upper layer: role of microbial community and calanus finmarchicus. Marine Ecology Progress Series, 462:39–49.

Sunda, W.G., Huntsman, S.A., 1995. Iron uptake and growth limitation in oceanic and coastal phytoplankton. Marine Chemistry 50, 189–206.

Takahashi, T., S. C. Sutherland, R. Wanninkhof, C. Sweeney, R. A. Feely, D. W. Chipman, B. Hales, G. Friederich, F. Chavez, A. Watson, D. C. E. Bakker, U. Schuster, N. Metzl, H. Yoshikawa-Inoue, M. Ishii, T. Midorikawa, Y. Nojiri, C. Sabine, J. Olafsson, Th. S. Arnarson, B. Tilbrook, T. Johannessen, A. Olsen, Richard Bellerby, A. Körtzinger, T. Steinhoff, M. Hoppema, H. J. W. de Baar, C. S. Wong, Bruno Delille, N. R. Bates, 2009. Climatological mean and decadal changes in surface ocean pCO2, and net sea-air CO2 flux over the global oceans. Deep-Sea Res. II, 56, 554-577.

Takeda, S., 1998. Influence of iron availability, on nutrient consumption ratio of diatoms in oceanic waters. Nature 393, 774–777.

Taylor, K. E., 2001. Summarizing multiple aspects of model performance in a single diagram. *Journal of Geophysical Research*, *106*(D7), 7183. http://doi.org/10.1029/2000JD900719.

Thomalla, S.J., Poulton, A.J., Sanders, R., Turnewitsch, R., Holligan, P.M., Lucas, M.I., 2008. Variable export fluxes and efficiencies for calcite, opal and organic carbon in the Atlantic Ocean: a ballast effect in action? Global Biogechemical Cycles 22. http://dx.doi.org/10.1029/2007GB002982.

Timmermans, K.R., *et al.*, 2005. Physiological responses of three species of marine pico-phytoplankton to ammonium, phos- phate, iron and light limitation. Journal of Sea Research 53, 109–120.

Torres Valdés, S., Painter, S. C., Martin, A. P., Sanders, R., Felden, J., 2014. Data compilation of fluxes of sedimenting material from sediment traps in the Atlantic Ocean, Earth Syst. Sci. Data, 6, 123-145, doi:10.5194/essd-6-123-2014.

Turner, J. T., 2015. Zooplankton fecal pellets, marine snow, phytodetritus and the ocean's biological pump, Progress in Oceanography, Volume 130, Pages 205-248, ISSN 0079-6611, http://dx.doi.org/10.1016/j.pocean.2014.08.005.

Turner, J. T., 2002. Zooplankton fecal pellets, marine snow and sinking phytoplankton blooms. Aquatic Microbial Ecology, 27:57–102.

Verity, P.G., Stoecker, D.K., Sieracki, M.E., Nelson, J.R., 1996. Microzooplankton grazing of primary production at 140ºW in the equatorial Pacific. Deep-Sea Research II 43 (4–6), 1227–1256.

Vichi, M., Pinardi, N., Masina, S., 2006. A generalized model of pelagic biogeochemistry for the global ocean ecosystem: Part I. Theory J. Mar. Syst. 64, 89–109, doi:10.1016/j. jmarsys.2006.03.006.

Viitasalo, M., Rosenberg, M., Heiskanen, A. S., Koski, M., 1999. Sedimentation of copepod fecal material in the coastal northern Baltic Sea: Where did all the pellets go? Limnology and Oceanography, 44(6):1388–1399.

Volk, T., Hoffert M. I., 1985. Ocean carbon pumps: Analysis of relative strengths and efficiencies in ocean-drive atmospheric CO2 changes. Geophys. Mono., 32, 99-110.

Weaver, P.P.E., Wynn, R.B., Kenyon, N.H., Evans, J.M., 2000. Continental margin sedimentation, with special reference to the north-east Atlantic margin. Sedimentology 47, 239–256.

Wexels Riser, C., Reigstad, M., Wassmann, P., Arashkevich, E., Falk-Petersen, S., 2006. Export or retention? Copepod abundance, faecal pellet production and vertical flux in the marginal ice zone through snap shots from the northern Barents Sea. Polar Biology, 30(6):719–730.

White M, Mohn C, Orren MJ (1998) Nutrient distributions across the Porcupine Bank. ICES J Mar Sci 55:1082–1094.

Wiebe PH, Copley NJ, Boyd SH (1992) Coarse-scale horizon- tal patchiness and vertical migration of zooplankton in Gulf Stream warm-core ring 82-H. Deep-Sea Res (Suppl 1) 39:S247–S278.

Williams, R. G., Follows, M. J., 1998. The Ekman transfer of nutrients and maintenance of new production over the North Atlantic. *Deep Sea Research Part I: Oceanographic Research Papers*, *45*(2-3), 461–489. http://doi.org/10.1016/S0967-0637(97)00094-0

Wu, J., Sunda, W., Boyle, E. A., Karl, D. M., 2000. Phosphate depletion in the western North Atlantic Ocean. Science, 289(5480):759–762.

Yool, A., Popova, E. E., Anderson, T. R., 2011. MEDUSA-1.0: a new intermediate complexity plankton ecosystem model fort he global domain. Geosci. Model. Dev. 4: 381-417.

Zamora, L. M., Prospero, J. M., Hansell, D. A., and Trapp, J. M., 2013. Atmospheric P deposition to the subtropical North Atlantic: Sources, properties, and relationship to N deposition. *Journal of Geophysical Research Atmospheres*, *118*(3), 1546–1562. http://doi.org/10.1002/jgrd.50187

Zhang, C., Zou, J., 1997. Nutrient uptake kinetics and growth under nutrient limitation of Pseudonitzschia. Oceanologia et Limnologia Sinica 28, 599–603.

CURRICULUM VITAE

e-mail: caglar.yumruktepe@nersc.no

ReseachGate: http://www.researchgate.net/profile/Caglar_Yumruktepe

---

Research Interests

I have 9 years research experience in the field of coupled (hydrodynamic-ecosystem) numerical ocean modelling which spans model development, model configuration and model validation. My work has focused on the application of coupled numerical models to problems concerning:

- Primary production, nutrient cycles and nutrient limitation
- The marine carbon cycle and the biological carbon pump
- Interactions between plankton functional types
- Transport and dispersion of riverine and wastewater inflows
- Atmospheric deposition on the marine environment

Professional Experience

Research scientist at NERSC (Nansen Environmental and Remote Sensing Center), Bergen, Norway since July 2016 as an employee of the Copernicus Arctic MFC project and the PARADIGM project funded through Bjerknes Center in Bergen, Norway.

The main aims of the job are:

- Work with development and validation of the biogeochemical module of the Northeast Atlantic and Arctic Ocean component of the European Copernicus marine forecasting service.
- Analysis of the model results with respect to the influence of environmental forcing

---

Education

Doctor of Philosophy, Oceanography (will be completed in December 2016)
Middle East Technical University, Institute of Marine Sciences, Turkey
(February 2011 – December 2016)

Title: Development and application of new model algorithms of the biological carbon pump in the North Atlantic, a study on particulate export, sinking and decomposition

Master of Science, Physical Oceanography
Middle East Technical University, Institute of Marine Sciences, Turkey
(September 2008 – February 2011)

Title: Investigation of primary production and nutrient cycles in the Cilician Basin

Bachelor of Science, Environmental Engineering

Middle East Technical University, Faculty of Engineering, Turkey
(September 2003 – June 2008)

Research Projects

- **EU FP7 EURO-BASIN (Basin Scale Analysis, Synthesis and Integration)**

Responsible for WP 2.4: 'Ecosystem modelling algorithm advancements' which aims to improve numerical representations of the global carbon cycle in order to better understand climatic stress on the marine environment (2012-2014).

- ***Scientific and Technological Research Council (TUBITAK) Funded Projects:***

(i) Dynamics and bacterial and primary production potential of distinct ecosystems composed of upwelling regions, shelf and offshore waters in the Eastern Mediterranean, reflections on higher trophic levels

Responsible for the development and Implementation of a 1D ecosystem model in the Rhodes and the Cilician Basins, Eastern Mediterranean (July 2012-present).

(ii) Urban Wastewater Management Along Coastal Areas of Turkey: Reidentification of Hot Spots & Sensitive Areas, Determination of Assimilation Capacities by Monitoring and Modelling and Development of Sustainable Urban Wastewater Investment Plans

Implementation of a Delft3D circulation and ecosystem model in the Cilician Basin, Eastern Mediterranean, identification of limiting nutrients, quantification of primary production, and investigation of coastal pollution and nutrient cycles (2008 – 2011).

Publications

Yumruktepe, V.Ç., Salihoğlu, B., Neuer, S. A numerical study of controls on productivity and carbon export rates at BATS and ESTOC (in preparation)

Yumruktepe, V.Ç., Salihoğlu, B., Neuer, S. Carbon export algorithm advancement in models: a case study at the Subtropical North Atlantic (in preparation)

Yumruktepe, V.Ç., Salihoğlu, B., Tuğrul, S. Impact of coastal discharges on the ecosystem dynamics in the oligotrophic Cilician Basin, Northeast Mediterranean, and implications for environmental management. (in preparation)

Presentations

Yumruktepe, V. Ç., Salihoğlu, B. (2016) Comparison of productivity, plankton types and carbon export mechanisms in two different regimes of Subtropical North Atlantic: a modeling study, poster presentation, **AGU**, New Orleans, USA, 2016

Yumruktepe, V.Ç., Salihoğlu, B. (2015) Carbon export algorithm advancements in models, poster presentation, **EGU**, Vienna, Austria, April, 2015

Ibello, V., **Yumruktepe, V.Ç.**, Butenschon, M., Salihoğlu, B., (2015) Key processes influencing particle carbon flux: a modelling study, **ASLO Aquatic Sciences Meeting,** Granada, Spain, Feb 2015.

Yumruktepe, V.Ç., Salihoğlu, B., Kıdeyş, A.E. (2013) Response of ocean carbon export to different model algorithms, poster presentation, **EGU**, Vienna, Austria, April, 2013

Yumruktepe, V.Ç., Salihoğlu, B. (2013) Carbon export algorithm advancements in models, oral and poster presentations, **IMBER-IMBIZO conference: The future of marine biogeochemistry, ecosystems and societies**, Goa, India, Jan 2013.

Yumruktepe, V.Ç., Salihoğlu, B., Oğuz, İ.T., Tuğrul, S. (2010) Eco-hydrodynamic modelling of eutrophication and nutrient cycles using Delft3D model for the Cilician Basin, oral and poster presentations, **39. CIESM Congress,** Venice, Italy, May 2010

Awards and Fellowships

Ph.D. researcher grant: Scientific and Technological Research Council of Turkey (TUBITAK): for successful Ph.D. progress towards science priority areas (Nov 2013 - onwards)

POGO-SCOR Visiting Fellowship: awarded to carry out short term research at NOC, Southampton and participate in a 1 month North Atlantic cruise on RRS James Cook (summer 2013) Responsible for *in-situ* nitrogen uptake measurements at various light levels and incorporation of the resulting uptake rates in ecosystem models

TUBITAK travel grant: Award to attend IMBER-IMBIZO III conference in Goa, India (Jan 2013)

TUBITAK PhD fellowship (2011-2013)

TUBITAK Masters research fellowship (2008-2011)

Technical skills and experience

Computer Skills

Scientific computing and modeling:

- Advanced knowledge of Coupled Delft3D model
- Advanced knowledge of Coupled HYCOM-ECOSMO
- Working knowledge of NEMO-ERSEM
- Theoretical knowledge of NEMO-MEDUSA and NEMO-PISCES

Languages: Fortran (advanced), Matlab and IDL (advanced)

Platforms: Linux (Debian/Ubuntu, Redhat/Fedora) and Microsoft OS's at advanced level

Software: Data processing, analysis, and plotting (advanced: IDL, NCL, Matlab, beginner: python and related software)

Office and typesetting tools (MS Office, OpenOffice, LaTeX)

Advanced visual manipulation and design (the Gimp, Freehand)

Research cruise ship time

RV Bilim2 / Middle East Technical University – 31 days oceanographic survey experience in the Mediterranean

RRS James Cook / National Oceanography Center – NERC UK – 20 days PAP site cruise in the N Atlantic

On board instrumentation and operations

Practical experience of CTD sampling, dissolved oxygen, turbidity, and fluorescence measurement; oxygen titration; bottle sampling at depth; colorimetric, titrimetric and gravimetric measurements

---

Professional Training

- ICTP International summer school on ocean climate modelling: Physical and biogeochemical dynamics of semi-enclosed seas. Ankara, Turkey, 2015
- IMBER CLIMECO3 International summer school: A View Towards Integrated Earth System Models. Human-nature Interactions in the Marine World. Ankara, Turkey, 2012
- EUROBASIN open workshop: Measuring zooplankton vital rates. Hamburg, Germany, 2012
- MEECE International summer school: Marine Ecosystem Evolution in a Changing Environment. Ankara, Turkey, 2011
- Advanced course on the structure and application of Delft3D model. Delft,Holland, 2011
- Introductory course on the structure and application of Delft3D model. Mersin,Turkey, 2009

Community Involvement / Administrative Activity

I have been directly involved in communicating my research to policy makers, and in facilitating its uptake by end-users. The Delft 3D model I configured during my Masters programme was ultimately transferred to the Ministry of Environment and TUBITAK, allowing them to take action to protect the marine environment. To assist this process, I prepared a technical manual, organized training and provided ongoing support.

Certification: valid ENG11 (UK), safety at sea certification (UK)

Languages: Turkish (native), English (fluent)

References

Dr. Annette Samuelsen – Nansen Environmental and Remote Sensing Center
Thormøhlens gate 47 N-5006, Bergen, Norway

annette.samuelsen@nersc.no
tel: +47 45254927

Dr. Barış Salihoğlu – METU Institute of Marine Sciences
ODTÜ Deniz Bilimleri Enstitüsü PK28 33731 Erdemli / Mersin / Turkey

baris@ims.metu.ed
u.tr tel: +90 324
5213434

Dr. Adrian Martin – National Oceanography Center Southampton
Waterfront Campus, European Way, Southampton, Hampshire SO14 3ZH, United Kingdom

adrian.martin@noc.ac.uk
tel : +44 02380 596342 – 26342